APPLICATION OF NUCLEAR MAGNETIC RESONANCE SPECTROSCOPY FOR THE DETECTION OF METABOLIC CHANGES IN BLOOD CELLS WITH DEFECTIVE DNA REPAIR

Dissertation

zur Erlangung des Doktorgrades

der Naturwissenschaften

vorgelegt beim Fachbereich Biochemie, Chemie und Pharmazie

der Johann Wolfgang Goethe -Universität

in Frankfurt am Main

von Gaelle Vanderstichelen

aus Soignies

Frankfurt Am Main

26 July 2021

ABSTRACT

The DNA damage response (DDR) is a vast network of molecules that preserves genome integrity and allow the faithful transmission of genetic information in human cells. While the usual response to the detection of DNA lesions in cells involves the control of cell-cycle checkpoints, repair proteins or apoptosis, alterations of the repair processes can lead to cellular dysfunction, diseases, or cancer. Besides, cancer patients with DDR alterations often show poor survival and chemoresistance. Despite the progress made in recent years in identifying genes and proteins involved in DDR and their roles in cellular physiology and pathology, the question of the involvement of DDR in metabolism remains unclear. It remains to study the metabolites associated with specific repair pathways or alterations and to investigate whether differences exist depending on cellular origin. The identification of DDR-related metabolic pathways and of the pathways that cause metabolic reprogramming in DDR-deficient cells may produce new targets for the development of new therapies.

In this thesis, nuclear magnetic resonance spectroscopy (NMR) was used to assess the metabolic consequence of the loss of two central DNA repair proteins with importance in diseases context, ATM and RNase H2, in haematological cells. An increase in intracellular taurine was found in RNase H2- and ATM-deficient cells compared to wild-type cells for these genes and in cells after exposition to a source of DNA damage. The rise in taurine does not appear to result from an increase in its biosynthesis from cysteine, but more likely from other cellular processes such as degradation pathways.

Overall, evidence for metabolic reprogramming in haematological cells with faults in DNA repair resulting from ATM or RNase H2 deficiencies or upon exposition to a source of DNA damage is presented in this study.

ZUSAMMENFASSUNG

Die DNA-Schadensreaktion (DDR; englischer Fachbegriff für die Gesamtheit aller zellulären Mechanismen, die nach einem DNA-Schaden aktiviert werden) ist ein riesiges Netzwerk von Molekülen, das die Integrität des Genoms bewahrt und die getreue Weitergabe der genetischen Information in menschlichen Zellen ermöglicht. Während die übliche Reaktion auf die Erkennung von DNA-Schädigungen in Zellen die Steuerung von Zellzyklus-Checkpoints, Reparaturproteinen oder Apoptose beinhaltet, können Veränderungen der Reparaturprozesse zu zellulärer Dysfunktion, Krankheiten oder Krebs führen. Außerdem zeigen Krebspatienten mit DDR-Veränderungen oft ein schlechtes Überleben und Chemoresistenz.

Trotz der Fortschritte, die in den letzten Jahren bei der Identifizierung von Genen und Proteinen, die an der DDR beteiligt sind, und ihrer Rolle in der zellulären Physiologie und Pathologie gemacht wurden, bleibt die Frage nach der Beteiligung der DDR am Metabolismus unklar. Daher ist es wichtig, die Metabolite zu untersuchen, die mit spezifischen Reparaturwegen oder Veränderungen assoziiert sind, und zu untersuchen, ob Unterschiede in Abhängigkeit von der zellulären Herkunft bestehen. Die Identifizierung von DDR-bezogenen Stoffwechselwegen und der Wege, die eine metabolische Umprogrammierung in DDR-defizienten Zellen bewirken, könnte neue Ziele für die Entwicklung neuer Therapien liefern.

In dieser Arbeit wurde die Kernspinresonanzspektroskopie (NMR), eine Technik, die die Analyse der metabolischen Zusammensetzung einer Probe ohne vorherige Trennung oder Behandlungen und die Identifizierung unbekannter Metaboliten ermöglicht, verwendet, um die metabolischen Folgen zu bewerten und mögliche metabolische Biomarker von DNA-Schädigungen nach dem Verlust von ATM und Ribonuklease H2 (RNase H2) in hämatologischen Zelllinien und Primärzellen der chronischen lymphatischen Leukämie zu

identifizieren. ATM und Ribonuklease H2 sind zwei zentrale DNA-Reparaturproteine im Kontext von Krankheiten. Während das ATM-Protein eine Serin/Threonin-Proteinkinase ist, die als Reaktion auf DNA-Doppelstrangbrüche (DDSB) aktiviert wird und Zellzyklusarrest, DNA-Reparatur oder Apoptose einleitet, ist RNase H2 ein Enzym, das für die Entfernung von RNA aus RNA-DNA-Hybriden, die während der Replikation gebildet werden, durch den Ribonukleotid-Exzisions-Reparatur-Weg (RER) verantwortlich ist. Darüber hinaus wurde in diesem Projekt untersucht, wie Störungen in der DDR, die aus der Exposition gegenüber einer externen Quelle von DNA-Schädigungen resultieren, den Stoffwechsel der Blutzellen beeinflussen. Schließlich wurden Tracer basierende Stoffwechselstudien durchgeführt, um den Fluss von ^{13}C-isotopisch markierten Vorläufern in verschiedene Stoffwechselwege und den Einbau der Markierung an bestimmten atomaren Positionen in Stoffwechselintermediaten zu untersuchen. Insgesamt zielte diese Arbeit darauf ab, detaillierte mechanistische Informationen zu erhalten und metabolische Veränderungen im Kontext von DDR-Veränderungen in Blutzellen zu untersuchen.

In der Praxis wurden NMR-Spektren mit Bruker NMR-Spektrometern erzeugt, verarbeitet und mit der MetaboLab-Software in MATLAB (MathWorks, USA) analysiert. Die Zuordnung der Metabolite erfolgte mit der Software Chenomx (Chenomx Inc., Kanada) und der Human Metabolome Database (HMDB).

Zunächst ergab die Analyse der metabolischen Profile von ATM- und RNase H2-defizienten Zellen Blutzellen einschließlich CII, Multiple Myelom und lymphoblastischen Zelllinien höhere intrazelluläre Taurinspiegel in allen DDR-defizienten Zelllinien im Vergleich zur Kontrolle und legte eine Verbindung zwischen Taurin und der DDR nahe. Im Fall von ATM schien es also, dass Taurin als Reaktion auf DNA-Schädigungen nach dem Verlust der ATM-Kinase-Aktivität erhöht war. Der Anstieg von Taurin wurde auch in WT-Blutzellen nach

Exposition gegenüber einer DNA-Schadensquelle gefunden und deutete darauf hin, dass Taurin als Reaktion auf DNA- Schädigungen erhöht werden könnte.

Auf der anderen Seite zeigte die Analyse des extrazellulären Gehalts verschiedener Zelllinien Variationen im Glukose-, Laktat- und Glutaminspiegel zwischen WT- und DDR-defizienten Zellen. Da jedoch einige Diskrepanzen zwischen den Zelllinien bestanden, blieb zu untersuchen, ob Veränderungen im Glukose- und Glutamin-Stoffwechsel auch bei Abwesenheit effizienter DNA-Reparaturmechanismen bestehen. Daher wurden auf Tracer basierende NMR-Ansätze unter Verwendung von ^{13}C-Glukose und Glutamin durchgeführt, um Veränderungen des Glukose- und Glutaminflusses in isogenen Zelllinien zu überwachen. Ziel war es, die Auswirkung des Verlusts von ATM oder RNase H in Zellen auf den Glukose- und Glutamin-Stoffwechsel besser zu verstehen.

Leukämie-CII-ATM- und Multiple Myelom RNASEH2-KO-JJN3-Zelllinien wurden als Modell für ATM- bzw. RNase H2-Mangel verwendet und mit ihrem WT-Äquivalent verglichen. Nach 24 Stunden Inkubation mit [U-^{13}C]-Glukose zeigte sich, dass alle Zelllinien Glukose verbraucht hatten, die durch Glykolyse zu Pyruvat metabolisiert wurde. Pyruvat wurde dann weiter in Laktat oder Alanin umgewandelt oder gelangte in den Krebszyklus. In den HSQC-Spektren von CII- und JJN3-Zellen schienen daher Kohlenstoffe in mehreren Stoffwechselintermediaten ^{13}C-markiert zu sein. Obwohl Unterschiede im Glukosefluss zwischen den Leukämie- und Multiplen Myelom-Zelllinien bestanden, waren die Prozentsätze der ^{13}C-Markierung zwischen WT- und DDR-defizienten Zellen ähnlich. Daher schien es nicht, dass das Fehlen eines effizienten DNA-Reparaturweges im CII- und JJN3-Zellmodell eine Veränderung des Glukosestoffwechsels verursacht hatte.

Nach 24 Stunden Inkubation mit [3-^{13}C]-Glutamin verstoffwechselten alle Zellen Glutamin durch Glutaminolyse, wie durch den ^{13}C-Markierungseinbau in Glutamat, α-Ketoglutarat und

andere Kreb-Zyklus-Zwischenprodukte nachgewiesen wurde. Oder die Zellen metabolisierten Glutamin nach der Umwandlung in Glutamat direkt zu Glutathion und Prolin. Die HSQC-Analysen zeigten, dass in DDR-defizienten Zellen mehr Glutamin den TCA-Zyklus durchläuft. Außerdem hatten Zellen, denen ATM oder RNase H2 fehlte, weniger Glutamin zu Glutathion metabolisiert als ihre WT-Gegenstücke. Obwohl diese Ergebnisse statistisch nicht signifikant waren, werden sie teilweise durch frühere Studien unterstützt, die eine signifikante Reduktion der Glutathion-Synthetase, dem Enzym, das den letzten Schritt der Glutathion-Synthese katalysiert, in AT-defizienten Zellen zeigten. Insgesamt gab es signifikante Unterschiede zwischen CII- und JJN3-Zelllinien, aber nicht zwischen DDR-defizienten und WT-Zellen, was darauf hindeutet, dass es keine Unterschiede zwischen dem Glutamin-Stoffwechsel von WT- und Zellen mit defizientem ATM oder RNase H2 gibt.

Interessanterweise zeigte jedoch der Vergleich der ^{13}C-Anteile in Metaboliten sowohl aus [U-^{13}C]-Glukose- als auch aus [3-^{13}C]-Glutamin-Markierungsexperimenten eine höhere ^{13}C-Rate in Metaboliten nach Inkubation mit Glutamin als mit Glukose in allen untersuchten Zellen. Dies impliziert, dass Glutamin das primäre Kohlenstoffsubstrat für den TCA-Zyklus in den untersuchten Zelllinien ist und bestätigt teilweise, was zuvor beim Multiplen Myelom gezeigt wurde.

Später in diesem Projekt wurden die Quelle und die Mechanismen hinter dem Taurinanstieg in DDR-defizienten Zellen untersucht. Nachdem sichergestellt wurde, dass das Zellkulturmedium oder das FBS kein Taurin enthielt, das von den Zellen aufgenommen werden könnte, wurde eine Tracer-basierte Analyse mit isotopisch markierten Vorläufern durchgeführt, um zu untersuchen, ob Taurin in DDR-defizienten Zellen aus dem Taurin-Syntheseweg stammen könnte. Da Taurin aus Methionin oder Cystein über die Cysteinsulfinsäure-Decarboxylase (CSAD) synthetisiert werden kann, wurden 2D-HSQC-Spektren nach 24-

stündiger Inkubation von WT- und Zellen mit defizientem ATM oder RNase H2 in Zellkulturmedien mit [^{13}C3]-Cystein oder [U-^{13}C]-Methionin erhalten. Ziel war es, zu untersuchen, ob in diesen Zellen Taurin aus Cystein und/oder Methionin gebildet werden kann. Nach 24-stündiger Inkubation mit [^{13}C3] Cystein schien Cystein nur zu Glutathion metabolisiert zu werden, wie der ^{13}C-Markierungseinbau in C12 und C^{13} zeigte. Taurin schien nicht aus Cystein synthetisiert zu werden, wie durch das Fehlen des ^{13}C-Markierungseinbaus in Taurin und Hypotaurin in allen WT- oder DDR-defizienten Zelllinien gezeigt wurde. Diese Ergebnisse legen nahe, dass keine der Zellen unabhängig von ihrem DDR-Veränderungsstatus Taurin aus Cystein synthetisiert.

In ähnlicher Weise deutet das Fehlen des ^{13}C-Markierungseinbaus in Homocystein, Cystathionin und α-Ketobuttersäure nach Inkubation der Zellen mit [U-^{13}C]-Methionin auf eine fehlende Cysteinsynthese aus Methionin hin. Daher wurde nach den Experimenten mit markiertem Cystein und Methionin ausgeschlossen, dass Taurin in den untersuchten Blutzellen aus seiner Biosynthese stammt. Es könnte sein, dass B-Zellen und Plasmazellen nicht in der Lage sind, Taurin zu synthetisieren, was durch die niedrigen RNA-Expressionsniveaus von CSAD unterstützt wird, die in Blutzellen im Vergleich zu anderen Zelltypen gefunden wurden. Dennoch sind zusätzliche Experimente erforderlich, um die CSAD-Expression auf Proteinebene und die Aktivität zu bewerten und das Fehlen der Taurinsynthese in diesen Zellen weiter zu bestätigen.

Der Rest dieses Projekts konzentrierte sich auf die Untersuchung, ob Taurin durch Abbauprozesse wie Autophagie oder Ubiquitin-Proteasom-Weg entstehen könnte, wobei ein Inhibitor der Autophagie, Bafilomycin (BAF), und ein Inhibitor des Proteasoms (MG132) in isogenen Zelllinien verwendet wurden. Bemerkenswerterweise zeigten alle Zelllinien, mit Ausnahme der Myelomzellen, reduzierte intrazelluläre Taurinspiegel nach Autophagie- oder

Proteasominhibition. Diese Ergebnisse deuten darauf hin, dass Abbauprozesse teilweise die Ursache für den in DDR-defizienten Zellen beobachteten Taurinanstieg sein könnten und könnten der erste Beweis dafür sein, dass hämatologische Zellen Abbauprozesse nutzen, um Taurin zu gewinnen.

Da man vermutet, dass sowohl die DNA-Schadensreaktion als auch Taurin mit der Redox-Homöostase verbunden sind, wurden schließlich Messungen reaktiver Sauerstoffspezies in CII WT und ATM-defizienten leukämischen Zelllinien durchgeführt. Angesichts der antioxidativen Eigenschaften von Taurin wurde die Hypothese aufgestellt, dass die höheren Taurinwerte, die in ATM-defizienten CII-Zellen gefunden wurden, mit dem hohen Grad an oxidativem Stress zusammenhängen könnten, der in Zellen mit einem defekten DNA-Reparaturweg gefunden wird. Daher war das Ziel, eine mögliche Korrelation zwischen den ROS-Spiegeln und den höheren Taurinspiegeln, die in CII-ATM gemessen wurden, zu untersuchen. Die Ergebnisse zeigten keine Unterschiede in den Gesamt-ROS-Werten von CII WT und ATM, aber CII ATM zeigte höhere mitochondriale ROS-Werte. Obwohl diese vorläufigen Ergebnisse die Idee eines Zusammenhangs zwischen den hohen Taurinspiegeln, die in CII ATM beobachtet wurden, und dem oxidativen Stress in diesen Zellen bestärkten, sind weitere Experimente erforderlich, um diese Hypothese zu untermauern.

Insgesamt konnte in dieser Arbeit gezeigt werden, dass defekte ATM- und RNaseH2-initiierte Reparaturmechanismen eine metabolische Neuverdrahtung in humanen hämatologischen Zellen verursachen. Das wichtigste Ergebnis war der höhere intrazelluläre Taurinspiegel, der in Zellen ohne ATM oder RNaseH2 gefunden wurde, die als Modelle für DDR-Veränderungen verwendet wurden, wo Abbauprozesse wahrscheinlich als Taurinquelle fungieren. Obwohl der Anstieg der intrazellulären Taurinspiegel spezifisch für den Verlust von ATM und RNase H2 sein könnte, könnte das gleiche Phänomen auch bei anderen Arten von DNA-

Reparaturveränderungen auftreten. Daher bietet diese Studie neue Einblicke in den Crosstalk zwischen der DDR und den metabolischen Netzwerken. Weitere Untersuchungen sollten daraufabzielen, die metabolische Rolle der verschiedenen kritischen Proteine in den DNA-Reparatur- Wegen zu erforschen. Die Entdeckung neuer Assoziationen zwischen diesen beiden komplexenNetzwerken könnte dazu beitragen, neue Therapien zu entwickeln oder bestehende Therapien bei DDR-bezogenen Krankheiten oder Krebserkrankungen mit defekter DNA-Reparatur zu verbessern.

TABLE OF CONTENTS

LIST OF FIGURES

LIST OF TABLES

LIST OF ABBREVIATIONS

1D	One-dimensional
2D	Two-dimensional
AA	Amino acids
Acetyl-CoA	Acetyl coenzyme A
ADP	Adenosine diphosphate
AGS	Aicardi–Goutieres syndrome
Akt	Protein kinase B
ALL	Acute lymphoblastic leukaemia
AML	Acute myeloid leukaemia
AMPK	AMP kinase
ANOVA	Analysis of variance
ASNS	Asparagine synthetase
AT	Ataxia-telangiectasia
ATM	Ataxia-telangiectasia mutated
ATP	Adenosine triphosphate
ATR	Ataxia telangiectasia and Rad3 related
BAF	Bafilomycin
Bax	Bcl2-associated X protein
BER	Base-excision repair
BRCA	Breast cancer
CAFs	Cancer-associated fibroblasts
CDO	Cysteine dioxygenase

CHK	Checkpoint kinase
CDK	Cyclin-dependent kinase
CLL	Chronic lymphocytic leukaemia
CRISPR	Clustered regularly interspaced short palindromic repeats
CSAD	Cysteine sulfinic acid decarboxylase
CSD	Cystathionine γ-lyase
CTL	Control
Da	Dalton
DCFH-DA	2',7'-Dichlorodihydrofluorescein Diacetate
DDR	DNA damage response
DSBs	Double-strand breaks
DMSO	Dimethyl sulfoxide
DNA	Deoxyribonucleic acid
DNA-PKcs	DNA-dependent protein kinase catalytic subunit
EBV	Epstein-Barr virus
Exo1	Exonuclease 1
FACs	Fluorescence-activated cell sorting
FAD	Flavin adenine dinucleotide
FAO	Fatty acid oxidation
FAT	Focal adhesion targeting
FBS	Foetal bovine serum
FDR	False discovery rate
FEN1	Flap endonuclease 1
FID	Free induction decay

G6PD	Glucose-6-phosphate dehydrogenase
GAD	Glutamate decarboxylase
GCS	Gamma-glutamylcysteine synthetase
GFP	Green fluorescent protein
GGC	γ-glutamylcysteine
GLS	Glutaminase
GLUT	Glucose transporter
GSH	Glutathione
GSS	Glutathione synthetase
GSSG	Glutathione disulfide
H2AX	H2A histone family member X
HATs	Histone acetyltransferases
HBD	Hybrid binding domain
HBSS	Hank's Balanced Salt Solution
HDH	Hypotaurine dehydrogenase
HL	Hodgkin lymphoma
HMDB	Human Metabolome Database
HPLC	High-performance liquid chromatography
HR	Homologous recombination
HRP	Horseradish peroxidase
HSQC	Heteronuclear single quantum coherence
IR	Ionising radiation
KO	Knock-out
LCLs	Lymphoblastoid cells lines

LOH	Loss of heterozygosity
MACS	Magnetic-activated cell sorting
MCL	Mantle cell lymphomas
MDM2	Mouse double minute 2 homolog
Mitosox	Mitochondrial superoxide
MM	Multiple myeloma
MMR	Mismatch repair
MRN	MRE11/RAD50/NBS1
MS	Mass spectrometry
mTORC1	Mammalian target of rapamycin complex 1
MTS	Mitochondrial targeting sequence
NAD+	Nicotine adenine dinucleotide oxidised
NADH	Nicotine adenine dinucleotide reduced
NADP+	Nicotinamide adenine dinucleotide phosphate
NADPH	Reduced nicotinamide adenine dinucleotide phosphate
NER	Nucleotide-excision repair
NHEJ	Non-homologous end-joining
NMR	Nuclear magnetic resonance
NOESY	Nuclear Overhauser effect spectroscopy
Nox1	NADPH oxidase 1
Noxes	NAD(P)H oxidases
NRF2	Nuclear factor E2-related factor 2
NS	Number of scans
NUS	Non-uniform sampling

OCR	Oxygen consumption rate
OXPHOS	Oxidative phosphorylation
P53	Tumour protein 53
PAG	DL-Propargylglycine
PAR	Poly ADP ribose
PARP1	Poly(ADP-ribose) polymerase 1
PARPi	PARP inhibitors
PBMCs	Peripheral blood mononuclear cells
PBS	Phosphate buffer saline
PC	Pyruvate carboxylase
PDH	Pyruvate dehydrogenase
PFG	Pulsed field gradient
PI3K	Phosphatidylinositol 3-kinase
PIKK	Phosphatidylinositol 3-kinase-like kinases
ppm	Parts per million
PPP	Pentose phosphate pathway
PRPP	5-phosphoribosyl-1-pyrophosphate
PRR	Post replication repair
Puma	p53-upregulated modulator of apoptosis
RER	Ribonucleotide excision repair
RF	Radio frequency
RNA	Ribonucleic acid
RNase H1 or H2	Ribonuclease H1 or H2
RNases H	Ribonucleases H

ROS	Reactive oxygen species
RPMI	Roswell Park Memorial Institute medium
SAM	S-adenosylmethionine
SDS	Sodium dodecyl sulphate
Ser	Serine
sh	Short hairpin
SIRT	Sirtuin
SMC1	Structural maintenance of chromosomes 1
SSBs	Single-strand break
stdev	Standard deviation
SUMO	Small ubiquitin-like modifier
TAUT	Taurine transporter
TCA	Tricarboxylic acid
TCI	Triple resonance cryoprobe
TD	Data points
TET2	Ten-eleven translocation methylcytosine dioxygenase 2
TFEB	Transcriptional factor EB
TMS	Tetramethylsilane
TMSP	Trimethylsilyl propanoic acid
T-PLL	T-cell prolymphocytic leukaemia
tRNA	Transfer RNA
TSA	Total spectral area
TUG1	Taurine upregulated gene 1
Ub	Ubiquitin

UDP	Uridine diphosphate
UPS	Ubiquitin-proteasome system
UV	Ultraviolet
VATPase	Vacuolar-type ATPase
WT	Wild type
XRCC1	X-Ray Repair Cross Complementing
γH2AX	Phosphorylation of histone H2AX

Chapter 1 Introduction

1.1. The DNA damage response

Every day, each human cell is subject to thousands of DNA lesions [1]. The type of DNA lesion will depend on the origin of damage, divided into two categories: (I) endogenous damage that occurs after endogenous cellular processes, such as replication errors, metabolism, and oxidative stress. (II) exogenous damage caused by external factors, including ultraviolet (UV) and ionising radiation (IR), chemicals or chemotherapeutic drugs [2]. Fortunately, cells have evolved mechanisms for the detection and the repair of DNA lesions, united under the term of DNA damage response (DDR), to preserve genomic integrity and prevent the transmission of heritable genetic mutations. The typical DDR involves the detection of damage by sensors, the diffusion of the signal to transducers and the recruitment of repair molecules at the site of DNA damage so that the proper cellular response by the downstream effectors ensues. The type of DNA damage sensors and repair mechanisms are various and depend on the DNA lesion, as reviewed in [1,3,4].

The DDR is mainly controlled by three members of the phosphatidylinositol 3-kinase-like kinases (PIKK) family: ataxia telangiectasia mutated (ATM), ATM and Rad3 related (ATR), and DNA dependent protein kinase (DNA-PK). The type of damage governs the activation of either of these kinases, which will phosphorylate and activate various downstream targets to trigger repair pathways and cell cycle arrest, as reviewed in [5]. Among DDR pathways, the base excision repair (BER) allows the repair of damaged DNA bases, including oxidised, deaminated and alkylated bases, abasic sites, and single-strand breaks [6]. Nucleotide excision repair (NER) exists to remove bulky DNA lesions, including DNA adducts and DNA interstrand cross-links, such as those produced by exposure to UV radiation and chemical agents [7]. Misincorporated nucleotides occurring during replication are detected and excised by the mismatch repair (MM) pathway, which is also responsible for repairing insertion-deletion mismatches in DNA [8].

Finally, homologous recombination (HR) and non-homologous end-joining (NHEJ) are the two major pathways for repairing DNA double-strand breaks (DSBs) [9]. Examples of DNA damage and the associated repair pathways and cellular responses are depicted in Figure 1-1. Ultimately, the DDR ensures the arrest of the cell cycle for DNA reparations or the initiation of apoptosis when the DNA lesions cannot be repaired [10]. Faulty repair processes can result in an increased sensitivity to DNA damaging agents and can cause diseases, including cancers [11]. Therefore, the study of the DDR is not only crucial to explain how cells protect their DNA against threats but also to examine the consequence of faulty DDR in a pathological context.

This thesis describes some key proteins implicated in DNA repair and fundamental cellular processes associated with the DDR, focusing on DNA double-strand break and the nucleotide excision repair pathways.

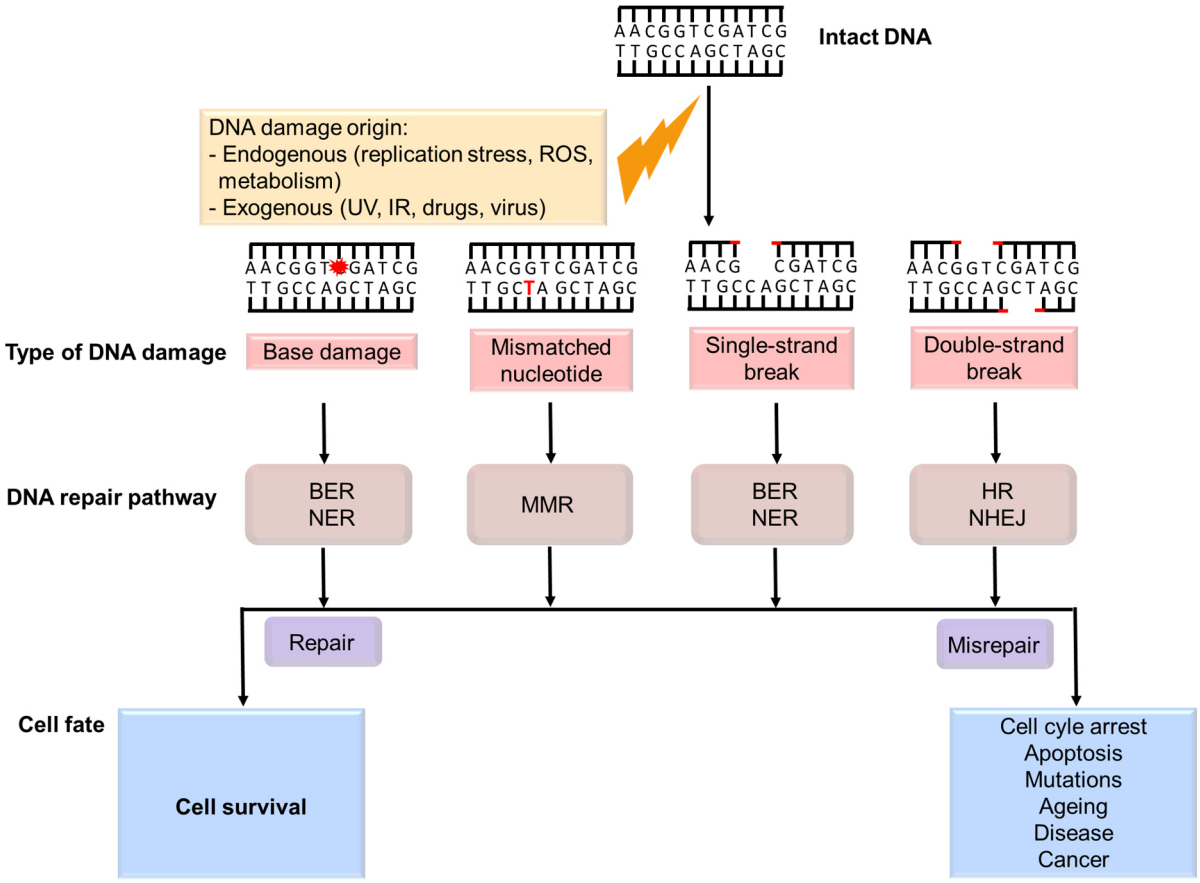

Figure 1-1: Schematic representation of DNA damage and associated DNA repair pathways and cellular responses

The sources of DNA damage can be endogenous or exogenous. They can cause a variety of DNA lesions such as base damage, mismatched nucleotides, single or double-strand break. In response, cells have evolved repair mechanisms, including, base-excision repair (BER), nucleotide-excision repair (NER), mismatch repair (MMR), homologous recombination (HR), and non-homologous end-joining (NHEJ). If lesions are repaired, cells will be able to survive; otherwise, they will enter apoptosis or accumulate chromosomic instability. Adapted from Aziz *et al.* [4]

1.1.1. Ataxia–telangiectasia mutated and the DNA double-strand breaks repair

1.1.1.1. The ATM gene and protein

The ataxia-telangiectasia mutated (*ATM)* gene, located on chromosome 11q22-q23 [6], was first identified and described by Savitsky *et al.* [12]. Mutations of that gene are responsible for the neurodegenerative disorder ataxia-telangiectasia (AT) characterised by immunodeficiency, cerebellar degeneration, increased risk of cancer, and radiation sensitivity [14]. The *ATM* gene encodes a 350 kDa serine-threonine protein kinase, ATM[15] and belongs to the PIKK family. Therefore, ATM contains a catalytic domain homologous to the phosphatidylinositol 3-kinase (PI3K) at the C-terminus together with FAT and FATC motifs [16]. On the other hand, the N-terminus comprises a binding site for ATM target proteins, including, p53, BRCA1 and SMC1 [17] (Figure 1-2).

In cells, the ATM protein is mainly found in the nucleus, although around 20% is also present in the cytoplasm [18]. In the inactive state, ATM forms a noncovalent dimer. The autophosphorylation of the ATM dimer induces a change in the kinase structure that will cause the conversion of ATM into an active covalent dimer [19] or monomers [20]. Besides, upon ATM activation, the protein interaction domain in N-terminus becomes accessible [17].

1.1.1.2. Role of ATM in double-strand breaks signalling

The ATM kinase plays an essential role in the DNA double-strand breaks (DSBs) signalling and repair where it protects genome integrity by initiating cell cycle arrest, DNA repair or apoptosis, reviewed in [21,22]. DNA double-strand breaks for which both complementary DNA strands are damaged can be caused by exposure of cells to DNA damaging agents, including ionising radiation, certain drugs, or chemotherapeutic agents. DSBs can also occur in the

context of endogenous events such as DNA replication, when processing replication forks, during mitotic, meiotic and oxidative stress [23]. Near-simultaneous excision of neighbouring lesions in opposing DNA strands during BER can also generate DSBs [24]. Programmed DSBs and their consecutive repair, on the other hand, are crucial to generate biological diversity, including DSBs produced during meiotic recombination, V(D)J recombination in T and B lymphocytes or immunoglobulin class-switch recombination in B-lymphocytes reviewed in [25].

It is estimated that 10-50 DSBs occur per cell every day [26]. While this number can seem relatively low compared to the total of DNA lesions occurring in our cells per day, DSBs are the most toxic lesions in cells. They can cause genome rearrangements if not repaired or misrepaired, including mutations, insertions, deletions or chromosomal loss, translocations, and fusions. The failure to properly repair DSBs can also result in loss of heterozygosity (LOH) of tumour suppressor genes [27], and genome instability [28], characteristics commonly found among tumours, or cell death if left unrepaired [23]. Therefore detection and repair of DSBs are critical for maintaining genome stability and preventing the onset of cancer [1].

In mammalian cells, the MRE11/RAD50/NBS1 (MRN) complex is the central sensor for DSBs. Upon DSBs recognition, MRN binds to the broken ends and tethers them together [29]. The ATM protein partially activated in response to DSB is recruited at the break site where it binds to NBS1 in the MRN complex [30], causing its full activation by autophosphorylation on Ser367, Ser1983 and Ser1981 [20] and acetylation at Lys3016 by the acetyltransferase TIP60 [31]. Activated ATM monomers phosphorylate and activate various substrates with roles in DNA repair, cell checkpoint activation, transcription or apoptosis, as reviewed by Kastan *et al.* [32]. Among ATM targets, the histone H2AX is phosphorylated on ser139 after binding to active ATM monomers, changing its conformation into its active form γH2AX [33]. γH2AX acts as a recruitment platform for many other repair proteins, including 53 BP1, BRCA1, and MDC1 [34].

ATM also controls the stabilisation and activation of the tumour suppressor protein p53 [35,36]. Under normal conditions, p53 is maintained at

low levels through its interaction with the mouse double minute 2 homolog (MDM2), causing its constant ubiquitylation and degradation by the proteasome complex. On DSB, active ATM phosphorylates p53 and MDM2, making it impossible to bind to p53 [37]. Similarly, CHK2 also phosphorylates the p53 transactivation domain that usually binds to MDM2 to suppress MDM2 negative control [38]. As a result, p53 survives in cells and forms tetramers that bind to DNA and control the expression of genes involved in DNA repair machinery, cell cycle or apoptosis [39].

Active ATM also controls crucial cell cycle checkpoints. ATM phosphorylates CHK2 [40] and Artemis [41], leading to activation of S-phase cell cycle checkpoint or G2/M checkpoint activation, respectively. Also, due to p53 activation by ATM, p21 is upregulated and cause cyclin-dependent kinase (CDK) inhibition. It mediates cell cycle arrest, as reviewed by Karimian et al. [42]. Altogether ATM and its substrates prevent the transmission of erroneous DNA by initiating cell cycle arrest until the repair is complete. However, when the damage accumulates or is too severe, the ATM–Chk2–p53 apoptotic-signalling pathway is initiated and leads to the activation of pro-apoptotic genes under the control of p53, including Bax (Bcl2-associated X protein), Puma (p53-upregulated modulator of apoptosis) or the FAS receptor. As a result, controlled cell death is initiated, reviewed in [43].

1.1.1.3. DSB repair pathway choice

Multiple pathways exist in mammalian cells to repair double-strand breaks, the two crucial ones being non-homologous end joining and homologous recombination. NHEJ is a cell cycle independent process consisting of the direct ligation of the broken DNA ends without requiring long sequence homologies [44]. When the DNA ends are clean with complementary and not

damaged bases, repair by NHEJ occurs accurately. However, unprecise joining by NHEJ can cause small insertions or deletions, giving it a reputation of error-prone pathway [45]. Homologous recombination (HR), on the other hand, is highly accurate but is cell-cycle dependent as it requires a homologous template to restore the damaged segment of DNA, ideally the intact sister chromatid in mitotic cells or a homologous chromosome in meiotic cells [46]. Both HR and NHEJ pathways are summarised in Figure 1-3.

The first pathway, NHEJ, is initiated by DSB recognition and subsequent binding of the Ku70/Ku80 complex to broken DNA ends [47]. Then, Ku70/Ku80 recruits other components of the NHEJ machinery, including the DNA-dependent protein kinase catalytic subunit (DNA PKcs). Together, Ku70/Ku80 and DNA PKcs form a holoenzyme called DNA-dependent protein kinase (DNA PK) [48]. DNA PK recruits other downstream target proteins, including Artemis. Artemis is activated by phosphorylation at the catalytic site of DNA PK and, through its exonuclease activity, trims the ssDNA overhangs from the break. It results in blunt ends on both strands of the DSB that can be ligated [49]. Various DNA ends are generated at the break. Besides, DSBs are often dirty breaks with overhangs that are not immediately ready for ligation. Therefore, the NHEJ machinery has many other components to process DNA ends, including DNA polymerases μ/λ and polynucleotide kinase, reviewed in [50]. Ultimately, clean DNA ends will be ligated by the XRCC4-XLF-DNA ligase IV complex [51].

In HR, the MRN complex binding to the loose ends on either side of the break initiates the recruitment and successive binding of the CtlP protein to NBS1 [52]. Next, a two-phase process, DNA-end resection, occurs, resulting in the trimming of portions of DNA at the 5' ends of the break. During the first step, called 5' to 3' end resection, MRN complexed with CtlP moves away from the break over 100-200 base pairs. Through the endonucleolytic activity of MRe11, the MRN complex makes a nick in the single DNA strand that has its 5' extremity facing the broken ends. During long-range resection, the exonuclease activity of Mre11 in the CtIP/MRN

complex removes the nucleotides in a 3' to 5' direction from the nick towards the DNA break [53]. In parallel, other proteins, including exonuclease 1 (Exo1), DNA helicase/nuclease 2 (DNA2) and the Bloom helicase (BLM), are recruited to facilitate long-range resection [54]. In the end, ~1000 bp 3' single-stranded DNA (ssDNA) overhangs are produced on either side of the break [55]. The resulting 3' ssDNA are coated by Replication Protein A (RPA) for stabilisation and to prevent their degradation from nucleases [56]. With the help of various other proteins, including Breast Cancer 2 (BRCA2) protein, RAD 51 will then replace RPA to form RAD51-ssDNA nucleofilaments on the 3' ends [57]. RAD51 nucleofilaments initiate a homology search on the sister chromatid to find DNA sequences complementary to the 3' overhang. Once found, RAD51 catalyses the opening of the strand on the sister chromatid (homologous chromosome) and insert the broken 3' overhang DNA section complementary to the intact sister chromatid. This process called DNA strand invasion results in displacement loop (D-loop) formation between the 3' ssDNA overhang and the sister chromatid [58]. Then, new DNA will be synthesised by a DNA polymerase on the invading 3' strand until complete strand extension [46]. Finally, distinct pathways exist to resolve the junctions formed after DNA synthesis into either non-crossover or crossover products [59]. In the context of DSBs repair, given the aim of HR to restore the broken DNA sequence to its origin, non-crossover products are usually generated.

The choice of the DSB repair pathway is tightly regulated and depends on cell type, cell cycle stage and lesion context so that the repair process is optimal, reviewed in [60]. In proliferative humans cells, the most commonly used pathway to repair DSBs is NHEJ [61]. It is because NHEJ is supposed to be faster and occurs at any stage of the cell cycle, unlike homologous recombination that can only take place in the presence of a homologous template. Therefore, cells control the expression and activity of constituents of the HR pathway to ensure recombination only occurs during the S-G2 phase of the cell cycle, when a sister chromatid is present [62]. The MRN complex, in addition to its central role in DSBs signalling and detection,

also plays an essential role in repair pathway choice and initiation between NHEJ [63] and HR [64]. Hence, initiation of DNA end resection is another critical mechanism in cells to decide on the DSB repair pathway and prevent inappropriate recombination, review in [65]. Proteins may also play a role in promoting one or the other DSBs repair pathway. For instance, active ATM is known to regulate the two major pathways of DSBs repair; ATM initiates homologous recombination [66] while it antagonises toxic NHEJ by removing NHEJ proteins Ku and DNA-PKcs at the site of DSB [67].

1.1.1.4. Implication of ATM in oxidative stress

Apart from its role in DSBs repair, ATM acts as a redox sensor. Under oxidative stress, ATM is activated and converted into an active disulfide-crosslinked dimer. In particular, the cysteine 2991 in the FATC domain is critical for ATM pathway activation through ROS as its oxidation causes the formation of a disulfide bond that activates the dimer [19,68]. ATM pathway activation through ROS is independent of DSBs and differs from the activation trough the MRN complex. Although downstream targets overlap between active ATM dimers and monomers, some of the substrates are specific for ATM activation through oxidative stress. In brief, ATM restores redox homeostasis by activating antioxidant enzymes [69], the pentose phosphate pathway (PPP) [70], autophagy [71] and by controlling mitochondrial [72], peroxisome [73] and protein [74] homeostasis. Figure 1-2 depicts the two ways of ATM activation.

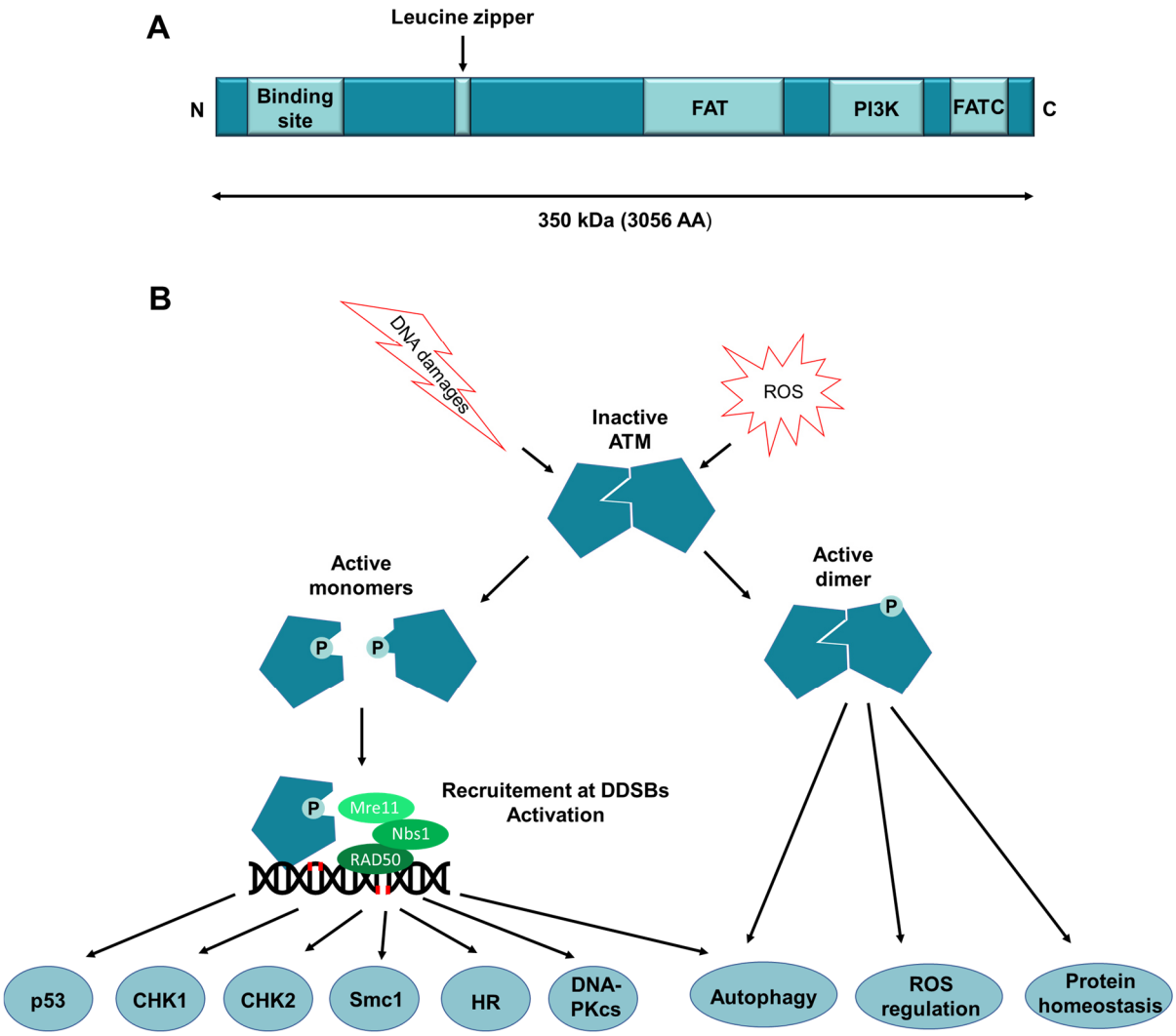

Figure 1-2: ATM protein and activation

Schematic representation of the human ATM protein and activation. A. ATM protein. The ATM protein is a serine-threonine kinase (350 kDa) comprising a catalytic domain PI3K, FAT and FATC domains, and a N-terminal substrate-binding site. B. Activation of the ATM protein. ATM forms a noncovalent dimer in the inactive state. The ATM protein in its monomer form can be activated and recruited at the site of DSBs by the MRN complex. ATM will activate a variety of downstream targets to protect genome integrity. When exposed to ROS, ATM is converted into an active dimer and restore homeostasis in cells.

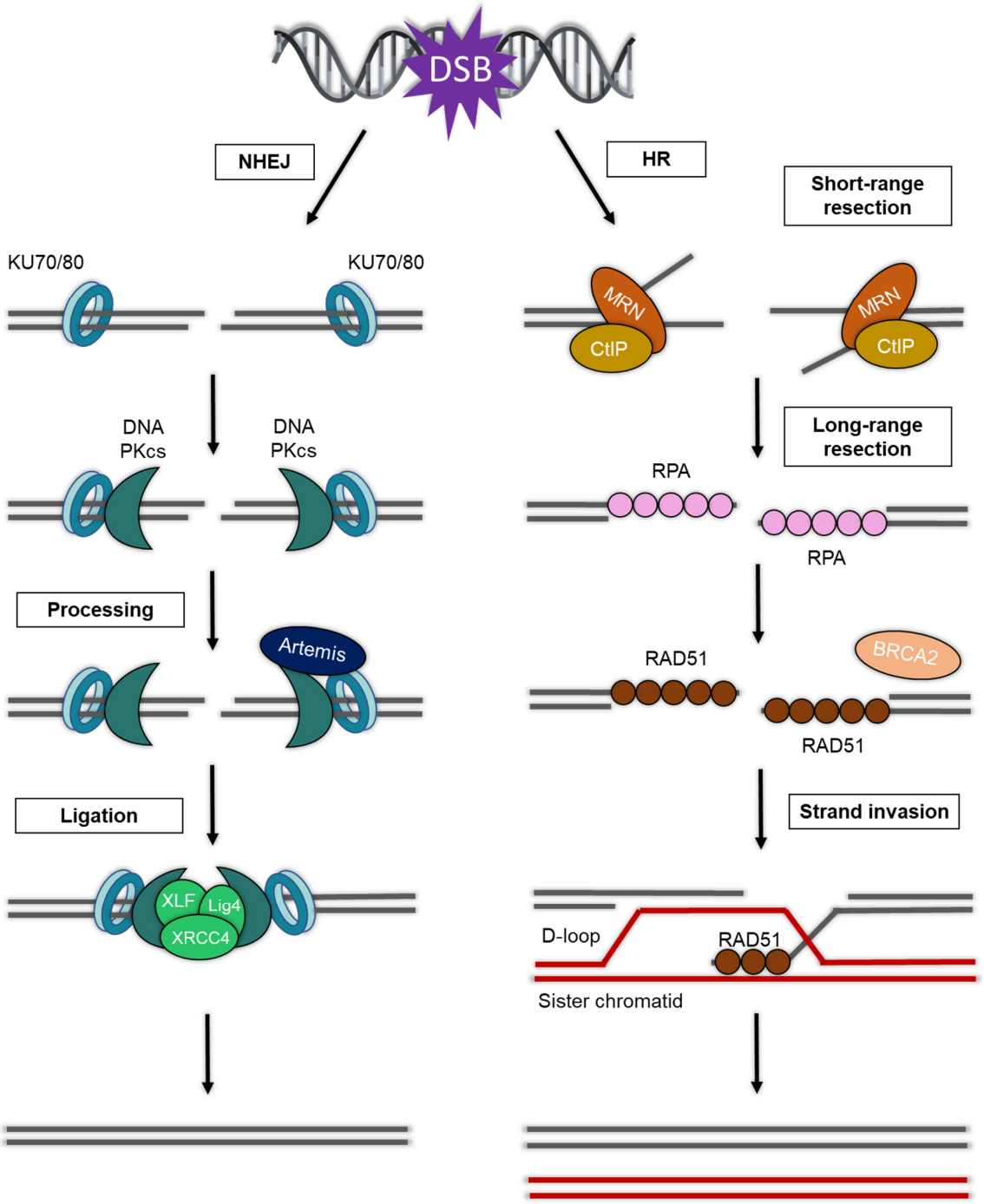

Figure 1-3: The NHEJ and the HR pathways

Schematic representation of non-homologous end joining and homologous recombination. NHEJ is initiated by the recognition and binding of Ku70/80 heterodimer on broken DNA ends. DNA PKcs is recruited at the site of the break. Dirty DNA ends will be processed by an enzyme such as the nuclease Artemis before ligation by the XRCC4-XLF-DNA ligase IV complex. During HR, the recruitment and binding of CtIP protein to the MRN complex initiates DNA end resection. ssDNA overhangs are produced on either side of the break and are coated by RPA. Then RAD51, with the help of BRAC2, replaces RPA and initiates homology search and DNA strand invasion. Adapted from Brandsma *et al.* [75].

1.1.2. Ribonuclease H and the ribonucleotide excision repair pathway

Ribonucleases H (RNases H) were discovered in calf thymus by Stein and Hausen [76]. These enzymes initiate the ribonucleotide excision repair (RER) to remove mistakenly incorporated ribonucleotides from RNA/DNA hybrids formed during replication [77].

In humans, more than a million ribonucleotides are estimated to be wrongly incorporated in DNA per replication cycle which is partly explained by the higher intracellular concentration of ribonucleotides over deoxyribonucleotides. The misincorporation of ribonucleotides is problematic as it modifies the DNA structure locally and makes it more sensitive to strand breakage [78]. In human cells, structural damage is prevented through two types of ribonuclease proteins that differ in their structure and substrate specificity, RNase H1 and RNase H2.

RNase H1 is a monomeric protein formed of 286 amino acids (AA) that possesses a mitochondrial targeting sequence (MTS) together with a hybrid binding domain (HBD) in the N-terminal region and a catalytic domain in the C-terminal region [79]. RNase H2 has three subunits indispensable to its activity: one catalytic, RNase H2A (299 AA) and two regulatory units, RNase H2B (312 AA) and RNase H2C (164 AA) [80]. Both RNase H1 and H2 can catalyse the degradation of four or more ribonucleotides and R-loops, but RNase H2 only can cleave a single ribonucleotide in a RNA/DNA hybrid [81–84]. The mechanism for the nucleotide excision repair described by Sparks *et al.* [83], depicted in Figure 1-4, is initiated with RNase H2 incision in the DNA, on the 5' side of the ribonucleotide. The RNAse H2 cleavage activity leaves a single-stranded DNA break bordered by a 3' hydroxyl (3'OH) group and a 5' phosphate (5'PO4). The polymerase δ or ε will synthesise the DNA through strand displacement synthesis, creating a flap structure containing the ribonucleotide which will be removed through the action

of the flap endonuclease FEN1/Exo1. The last step consists in the ligation of the single-strand nick via DNA ligase I.

Although the RNase H2 is the primary source of RNase activity in humans, ribonucleases one and two, mutually help genome maintenance and are essential for survival [77,84]. Defects in RNase H result in chromosomal instability and increase spontaneous DNA damage. In the most severe cases, mutations of RNase H2 can cause Aicardi–Goutieres syndrome (AGS), an autoimmune disease affecting mostly the central nervous system, the immune system and the skin [85,86].

Over the last 50 years, progress has been made in understanding the role of ribonucleases in the DNA damage response. In their review, Feng *et al.* [87] suggest that due to its structure and ability to bind to other proteins, RNase H2 could have different cellular functions besides its enzymatic activity. Therefore, more research should be done to give more insight into the role of RNase H2 in health and disease.

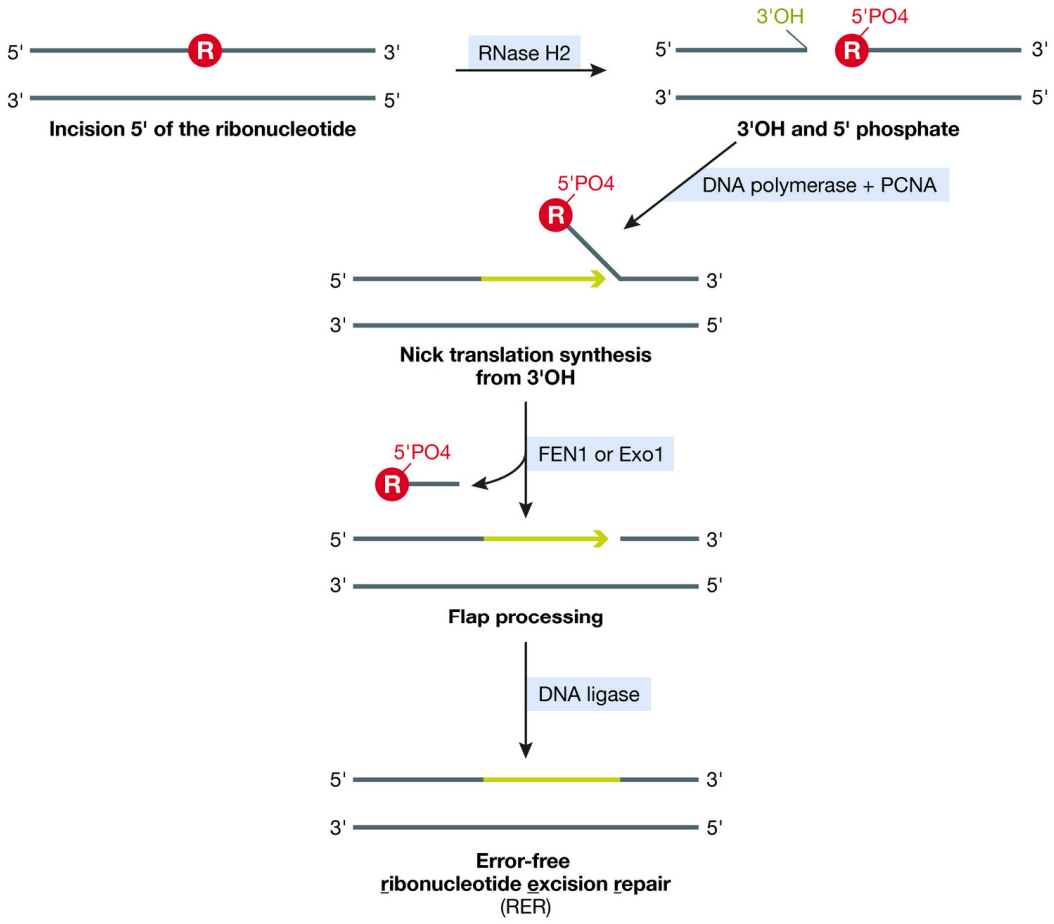

Figure 1-4: Ribonucleotide excision repair mediated by RNase H2

Schematic representation of the nucleotide excision repair pathway mediated by RNase H2. The first step is the incision of the 5' side ribonucleotide bound to DNA that leaves a single-stranded DNA break bordered by a 3' hydroxyl (3'OH) group and a 5' phosphate (5'PO4). Pol δ or ε synthesise DNA through strand displacement synthesis. A flap structure is created and removed by FEN1/Exo1. Finally, DNA ligase I ligates the single-strand nick. From Kellner *et al.* [86]

1.1.3. The DNA-damage response in diseases

As mentioned previously, the DNA damage response is crucial to insure DNA stability, the transmission of correct genetic information in cells and survival. Given the extent of the DDR, there are multiple consequences to the alterations of cell cycle checkpoints and DNA repair genes. Notably, there are a variety of DNA-repair diseases that can arise from an inherited defect in the DDR, including neuromuscular and neurodegenerative disorders, premature ageing and immune dysfunction, reviewed in [1,88]. For instance, the Ataxia-telangiectasia and Aicardi–Goutieres syndromes mentioned above are caused by mutations in ATM [14] or RNaseH2 [85], respectively.

Alteration of fundamental repair pathways has also been shown to be associated with cancer predisposition, reviewed in [89]. For instance, patients with xeroderma pigmentosum, characterised by a defect in the NER exhibit predisposition to skin cancer due to the cell's inability to repair UV-induced DNA lesions [90,91]. Also, patients with pathogenic ATM mutations have an increased chance of developing breast [92], pancreatic [93], prostate [94]and other cancers reviewed in [95]. On the other hand, defaults in the human *BRCA1* or *BRCA2* genes that code for BRCA proteins involved in the HR pathway, increase the risk of developing breast, ovarian cancers [96] or certain leukaemia and lymphoma [97]. Also, the polymorphisms of DDR genes such as RAD51 or XRCC3, XRCC1 have been associated with increased risk of developing haematological malignancies, including acute myeloid leukaemia (AML) [98,99], acute lymphoblastic leukaemia (ALL) [100,101] and Hodgkin lymphoma (HL) [102], reviewed in [103].

At the cellular level, mutations in DNA-repair genes can cause the gene not to be expressed or compel the production of aberrant proteins [104]. The failure to arrest the cell cycle at control checkpoints and to repair DNA lesions, yet critical to prevent unrepaired DNA from being transmitted will cause DNA-damage accumulation. The build-up of DNA errors and the

genomic instability that results from DDR-dysregulations can then promote tumorigenesis and the development of malignancies [105,106]. Hence, most cancer cells exerts mutations or epigenetic silencing of DDR factors [1]. The modifications in the DDR or DNA-repair genes may result from the application of selective pressures in the tumour microenvironment to select for cells with high genomic instability that can adapt quickly to confer growth and survival advantage [107–111]. Among DDR genes and proteins, ATM has been reported to be defective in a multitude of tumours, mostly in haematological malignancies, including chronic lymphocytic leukaemia (CLL) [112], T-cell prolymphocytic leukaemia (T-PLL) [113], mantle cell lymphomas (MCL) [114], and, Hodgkin lymphoma (HL) [115], reviewed in [116], and in pancreatic [93], colorectal [117], and breast cancers [118]and are associated with poor outcome and chemoresistance. Genetic aberrations of ATM are the consequence of 11q deletion and/or ATM mutation and can lead to a complete loss of ATM protein and its kinase activity. ATM mutations can also cause the production of a mutant ATM protein conserving some kinase activity or of a regular ATM protein at lower levels in cells [116,119]. Other common DDR defects in haematological malignancies include alterations in TP53 [120], RNase H2 [121]or TET2 [122].

The loss of DDR abilities also influences the cell response to DNA damaging therapies. Indeed, most of the chemotherapy drugs operate by inducing DNA damage that compromise cell viability, so the treatment's response will depend on the ability of cells to repair these damage efficiently before they become toxic [123]. The best example comes from the resistance to chemotherapy and radiotherapy observed in cancer cells when specific DNA repair pathways are upregulated, reviewed in [124,125]. However, it's possible to targets these cells specifically by inhibiting the upregulated pathway using different inhibitors, reviewed in [89]. On the other hand, the inactivation of specific DDR pathways can cause the cells to be more sensitive to cytotoxic treatments, DNA damaging therapies or DDR inhibitors [123,126]. That explains the enhanced sensitivity to ionising radiation observed in cells that have lost ATM, the master regulator of

the repair of IR-induced DSBs [127]. Besides, the complete loss of one of the repair pathways can cause cells to be highly dependent on compensatory DDR components and pathways. The identification and targeting of these dependencies by DDR inhibitors are the basic principles of the synthetic lethality strategy. This approach is based on the assumption that cell death is only induced when two pathways are altered together but not separately and was described for the first time by Hartwell *et al.* [128]. The advantage of this approach is that it targets specifically DDR-deficient cells, given normal cells with fully functional repair pathways will not be affected by the treatment. For instance, poly(ADP-ribose) polymerase 1 (PARP1) inhibition has shown efficiency to kill BRCA-mutated cells defective in HR without affecting the viability of normal cells [129,130]. PARP is involved in the single-strand break (SSBs) repair. Thus, its inhibition causes SSBs to persist and subsequently become converted to single-ended DSBs by replication forks. These structures are dependent on HR for repair, which is why HR-deficient BRCA-mutated cells are sensitive to PARP inhibitors. PARP inhibitors (PARPi) can also be used to target HR deficiency caused by ATM-loss [131], defects in CHK2 and others reviewed in [132]. Other examples of synthetic approaches consist of inhibiting ATM, ATR or checkpoints kinases [89,123].

The non-toxic aspect of the synthetic lethality is attractive for clinical application, as demonstrated by the number of ongoing clinical trials. The most promising treatment appeared to be the usage of PARP inhibitors alone or in combination with chemotherapy or radiotherapy. Some are already used in the clinic , including Olaparib (AZD2281) commercialised under the name of Lynparza and mainly used in the treatment of ovarian, breast and prostate cancers [133]. Others such as veliparib demonstrated promising activity for the treatment of leukaemia and lymphoma in a clinical trial (clinicaltrials.gov, NCT01139970).

Given the number of interconnections between the components of the DDR, it is probable that other examples of synthetic lethality will be discovered and exploited in therapies in the near

future. In this sense, the search for new biomarkers of the DDR defect could help the discovery of exploitable weaknesses in patients. Hence, new effective DDR inhibitors could be developed for use alone or in combination with chemotherapy or radiotherapy.

1.1.4. Metabolism and the response to DNA damage

In recent years, evidence has been obtained suggesting the response to DNA damage, in addition to being involved in DNA repair and participating in cell survival, also influences cell metabolism which includes break down, catabolic and synthesis, anabolic reactions. The links between the DDR components and metabolism are made at different levels, reviewed in [134,135], and relate to (I) chromatin rearrangements and DNA structure, (II) metabolic rewiring and upregulation of nucleotide biosynthesis, (III) redox homeostasis (IV) recycling of the DDR components through clearance pathways.

This section reviews the associations between DNA damage and repair mechanisms with metabolism as well as multiple DNA damage sensors and signal transducers in the DDR implicated in metabolism.

1.1.4.1. Metabolic intermediates controlling DNA structure and remodelling

In the nucleus, the chromatin structure is dictated by DNA methylation and histone posttranslational modifications. The folding of the chromatin directly influences the accessibility of molecules to the DNA, including DDR molecules that need to bind to the DNA. [136,137]. Most importantly, the chromatin modulations will directly influence the choice of the DNA-repair pathway [138,139]. Metabolic intermediates are the source of molecules added to the DNA or histone, explaining how metabolism influences the DNA folding and the repair pathways [140,141]. Therefore, the availability of nutrients and metabolic intermediates will affect the DDR. To this end, the S-adenosylmethionine (SAM) pathway provides most of the methyl-groups for DNA, and histone methylation and its activity will influence DNA gene expression and folding [142,143]. Besides, the metabolites acetyl-CoA and acetate are essential for delivering

the acetyl-groups required for histone acetylation by the histone acetyltransferases (HATs) [144–146]. Fumarate and succinate, through inactivation of particular histone demethylase activity, promote DNA repair [147,148]. Other metabolites such as NAD+, FAD or α-ketoglutarate can also serve as substrates for enzymes involved in histone posttranslational modifications, reviewed in [140].

1.1.4.2. Metabolic rewiring upon DNA repair and damage

Metabolic rewiring is the strategy cells have found to stimulate DNA repair and reduce the risk of mutations. Generally, in response to genotoxic stress, cells increase nucleotide synthesis, activate catabolic processes that generate ATP and reduce the energy-consuming anabolic reactions [135].

In cells, salvage pathways can generate nucleotides, but they can also be synthesised *de novo* for DNA synthesis and repair [149]. Numerous metabolic pathways participate in the biosynthesis of purines and pyrimidines. The most important one, the pentose-phosphate pathway (PPP) is initiated by the dehydrogenation of glucose-6-phosphate (G6P) during glycolysis by glucose-6-phosphate dehydrogenase (G6PD). The PPP will produce metabolite intermediates, including the ribose-5-phosphate used to generate 5-phosphoribosyl-1-pyrophosphate (PRPP) for nucleotide synthesis and produce NADPH from NAD+. On the other hand, the amino acid glutamine has a significant influence on the *de novo* synthesis of nucleotides since it is used for the pyrimidine and purine ring construct [150]. Therefore glutamine can regulate nucleotide production when DNA damage occurs in cells [151]. Other metabolites such as aspartate, PPP intermediates, and derivatives of the serine/glycine pathway and one-carbon metabolism are donors of nitrogen and carbon, necessary for nucleotide synthesis [149]. Besides, while the cell

cycle is arrested for allowing DNA repair, metabolic pathways essential for cell-cycle progression are paused.

Among DNA repair transducers participating in metabolic rewiring, ATM has been shown to enhance nucleotide synthesis via the PPP through its activation of the glucose-6-phosphate dehydrogenase (G6PD) [70,152,153]. On the other hand, Sun *et al.* [154] showed that active ATM could phosphorylate GLUT1 to be expressed in the plasma membrane in cancer-associated fibroblasts (CAFs).

Another key protein in the DDR, the tumour suppressor p53 influence the metabolic response upon DNA damage and repair. p53 is linked with various metabolic processes, including glucose uptake [155,156], glycolysis [157], mitochondrial respiration [158], PPP [159], lipid metabolism [160], and glutamine metabolism [161,162], reviewed in [163]. Notably, the different isoforms in the sirtuins (SIRT) family of proteins involved in the regulation of DNA repair [164] and chromatin structure [165] also play a role in various metabolic pathway , including glucose [166], glutamine [167], and lipid metabolism [168], reviewed in [169]. Finally, when DNA lesions occur in cells, PARP1 is activated and recruited at the site of DNA damage. PARP1 will synthesise poly ADP ribose (PAR) chains through a process called PARylation to signal the lesion and recruit DNA repair molecules [170]. Given PARylation consumes NAD+ and ATP, PARP repair activity will cause a reduction in intracellular levels of these metabolites which results in AMP kinase (AMPK) activation [171], an essential regulator of cellular energy homeostasis [172]. In its activated form, AMPK can lower ATP-consuming biosynthetic processes and increase ATP-producing pathways such as fatty acid oxidation (FAO) or oxidative phosphorylation (OXPHOS) [173].

1.1.4.3. The DDR in the regulation of oxidative stress

The DDR plays a crucial role in the regulation of oxidative stress, which arises when the reactive oxygen species (ROS) exceed the antioxidant defences. In cells, ROS can be increased because of aerobic metabolism or the activity of the NAD(P)H oxidases (Noxes) [174,175]. The hydroxyl radical ROS can react with the nucleotides or the deoxyribose through mechanisms reviewed in [176]. The oxidised nucleotides will usually be removed via the BER pathway in cells. On the contrary, ROS-induced DNA damage can degenerate and cause SSBs. If left unrepaired by the NER or BER, the SSBs can alter the replication fork, causing DNA replication stress, chromosome instability and the appearance of DSBs [177,178]. Oxidative stress can also damage DNA repair proteins [179] or generate DNA lesions indirectly through lipid peroxidation [180]. The increase in ROS levels can also be caused by DNA damage itself [181]. One of the proposed mechanisms for the rise in DNA damage-induced ROS involves the histone H2AX which in its phosphorylated form, γH2AX accumulates at the site of DSBs where it is required for DNA repair proteins assembly [182,183]. Most specifically, DNA damage causes ROS production via the H2AX-Nox1/Rac1 pathway [184].

Metabolic pathways exist in cells to detoxify and prevent ROS accumulation. The most important one involves the synthesis of the ROS scavenger glutathione (GSH) [185]. In the cytoplasm, the cysteine is used with glutamate to produce glutathione [186]. On the other hand, NADPH synthesised from NADP+ during the PPP can be used for the reduction of glutathione in its oxidised form glutathione disulfide (GSSG) by the glutathione reductase to regenerate GSH. Therefore both GSH and NADPH are essential for redox homeostasis [187].

Among the DDR molecules, some play a role in the oxidative stress response. For instance, the ATM protein apart from its role as a ROS sensor already mentioned above (1.1.1), can initiate an antioxidant response by phosphorylating Hsp27 and promoting its binding with

G6PD, enhancing its enzymatic activity, thus PPP [70]. Besides, the tumour suppressor BRCA1, an ATM substrate was shown to regulate the transcription factor nuclear factor E2-related factor 2 (NRF2) which controls the expression of antioxidant defence genes such as those required for glutathione synthesis [188,189]. Another ATM target, p53 also demonstrated its ability to regulate the transcription of various antioxidant genes [190]. Besides, PARP1 is a DNA damage sensor involved in the regulation of the response to ROS-induced DNA damage. While PARP1/2 promotes cell survival under moderate oxidative stress, it induces cell death through massive PARylation when the ROS levels are too high [191]. PARP1 also participates in the elimination of oxidised histones through its interaction with the proteasome [192]. Finally, members of the sirtuins family were also shown to regulate oxidative stress, reviewed in [193]. Altogether, the illustrated links between DNA repair molecules and regulators of ROS levels further evidence the role of DDR in redox homeostasis. Nonetheless, it is important to stress that, while high ROS levels cause oxidative stress and can damage the DNA, a small amount of ROS is essential to activate various signalling pathways, including antioxidant pathways, reviewed in [194].

1.1.4.4. Role of the clearance pathways in the DDR

Degradation processes are other catabolic pathways with critical importance in response to various cellular stress such as nutrient deprivation, oxidative stress, and DNA damage. In cells, the two main degradation pathways are the autophagy, and the ubiquitin (Ub)-proteasome system (UPS).

The UPS is responsible for the breakdown of intracellular proteins. In this pathway, proteins are first conjugated with multiple molecules of ubiquitin and then transferred to the catalytic core, which consists of a protease complex, the proteasome to be degraded [195]. The UPS, through its selective protein degradation, regulates many cellular processes, including the DDR.

Indeed, UPS through various interactions regulates DNA repair proteins, including those involved in the NER, post replication repair (PRR) and HR pathways [196]. In particular, the proteasome controls the repair mechanisms by degrading repair proteins once DNA lesions have been repaired and helping towards disassembly of the repair complex [197]. Also, ubiquitin signalling towards the UPS can control the activity of DNA repair proteins, including the tumour suppressor p53. Under normal conditions, p53 is continuously ubiquitinylated through the action of ubiquitin ligases, mainly by MDM2 which ensures it is maintained at a low level through consecutive proteasomal degradation for cellular growth and homeostasis. DNA damage will cause the inhibition of the ubiquitination process, resulting in p53 release and accumulation [198,199]. The UPS is also of critical importance in promoting the response to DSBs by modifying the proteins of this pathway by ubiquitin and SUMO (small ubiquitin-like modifier) [200]. Most importantly, the UPS regulates the response to IR as it causes inhibition of the proteasome and therefore substrate degradation [201,202].

Autophagy is a mechanism through which cells can degrade and recycle unnecessary or dysfunctional cellular constituents. During autophagy proteins, organelles, or macromolecules are isolated in vesicles called autophagosomes which after their fusion with lysosomes will be degraded by the action of hydrolases [203,204]. As a result, autophagy releases amino acids and other metabolites that can be used for *de novo* synthesis of cellular constituents or to produce energy via the different metabolic pathways, both crucial for genome stability and survival [205]. Many DNA damage and repair pathways activate autophagy, suggesting a close link between these processes. For example, autophagy activation can be induced after initiation of the transcription of p53 target genes [206] or PARylation by PARP1 [207]. Autophagy also plays a significant role in the DSBs repair pathway by recycling DNA repair factors [208]. Also, ATM can increase or decrease autophagic activity depending on its concentration [209]. The activation of autophagy by ATM occurs following the activation of its downstream targets, including

AMPK resulting in the suppression of MTORC1, which is an autophagy inhibitor [210,211]. Besides, in response to DNA damage, ATR/Chk1 signalling has also been shown to cause mTORC1 inhibition and activate autophagy [212]. Another role of autophagy called mitophagy is to assist in a reduction of the DNA damage induced by ROS by the degradation of faulty mitochondria [213]. The process of mitophagy is partially dependent on ATM [71]. There is also evidence that autophagy degrades damaged chromosomes and genome fragments following exposure to a source of DNA damage, reviewed in [205].

It is important to stress that autophagy as for metabolism and the DDR, is often altered in human pathologies and can play an active role in cancer progression, ageing or neurodegeneration. For this reason, this degradation pathway appeared as an attractive therapeutic target with many compounds aiming at autophagy modulation being investigated on clinical trials or already in the market [203,204]. Among autophagy inhibitor, bafilomycin A1 is an antibiotic which blocks the V-ATPase enzyme, essential for lysosome acidification and hydrolase activity. In addition to its inhibitory function, bafilomycin has been shown to modulate metabolism by increasing glycolysis activity and decreasing cell cycle and glutaminolysis intermediates [214]. Proteasome activity can also be chemically inhibited. MG132, a widely used proteasome inhibitor, for instance, is a peptide aldehyde which inhibits proteasome by binding to its β subunits [215–217]. In the clinic, the proteasome inhibitor Bortezomib, commercialised under the name Velcade® is used in the treatment of multiple myeloma and relapsed mantle-cell lymphoma and is under clinical trial for other types of haematological malignancies including leukaemia, as reviewed in [218]. Little is known about the effect of proteasome inhibition on metabolism, but previous publications suggested treatment with MG132 induced ROS formation and reduction of intracellular glutathione levels in vitro [219–221]. Given the metabolic changes observed after treatment with BAF and MG132, it might

be worth studying the effect of these inhibitors in DDR-deficient cells known for their altered metabolism.

1.1.4.1. Effect of DNA damage and defect on metabolism - The case of ATM

Further evidence for the implication of the DDR in metabolism is supported by metabolic reprogramming that occurs during DNA repair-deficiency disorder rand most notably in cancer cells, given that many genes and proteins involved in DNA-repair with a dual role in cell metabolism are mutated in tumour cells [134]. Also, the tremendous genomic instability in tumour cells increases the chance for metabolic rewiring to take place. In general, defective DNA repair leads to perturbation of energy metabolism, especially in cancer cells [222]. Especially, given that glucose and glutamine are essential for nucleotide synthesis, many DDR-deficiencies are translated into metabolic perturbations of these two metabolic pathways, reviewed in [185]. This section aims at describing some effects of DDR deficiency on metabolism with a focus on the metabolic response to the loss of ATM.

ATM is involved in various metabolic pathways and modifications of its gene expression, or its kinase structure and activity can seriously affect the metabolism. Many of these metabolic variations are the result of the absence of ATM-mediated p53 activation. First, ATM loss and A-T phenotype are associated with glucose metabolism modification. This result in A-T patients loss of affinity for insulin receptors which caused hyperglycaemia, glucose intolerance and insulin resistance [223]. In the skeletal muscles of ATM −/− mice, the ATM deficiency causes a loss of insulin-stimulated Akt phosphorylation resulting in a reduction of glucose transport, while ATM +/− mice with a functional ATM allele show a normal insulin-stimulated glucose transport similar to the WT [224]. In their paper, Armata *et al.* [225] suggest the insulin resistance is

caused by the absence of p53 Ser18 phosphorylation by ATM. The lack of insulin-stimulated Akt phosphorylation was further evidenced in *ATM*−/− cells and in mouse muscle cells after ATM inhibition with KU-55933 and was accompanied by an absence of GLUT4 translocation to the cell surface [226]. Besides, loss of ATM caused an increase in G6PD activity, is explained by the suppression of p53 inhibitory effect of G6P and the PPP [152].

High intracellular ROS and oxidative stress are other common features in ATM-defective cells [227–229]. ATM-deficient cells have increased ROS due to defects in NRF2 activity and consecutive increased sensitivity to pro-oxidants [230,231]. The mitochondrial disorder characterised by perturbation of mitochondrial production and structure, observed in AT patients, was suspected to be at the origin of the increase in ROS [232,233]. Besides, Valentin-Vega *et al.* [72] showed that ATM loss was associated with mitophagy failure, leading to an intracellular build-up of faulty mitochondria and an associated increase in mitochondrial ROS. It is also possible that the high ROS levels associated with ATM-deficiencies are the consequence of the lower expression of glutathione synthetase (GSS), the second enzyme in glutathione synthesis pathway, reported in A-T [234]. Interestingly, apart from mitophagy ATM loss has demonstrated to cause perturbation of autophagy [72,209,235].

It was also suggested that ATM-deficient cells exhibit an altered glutamine metabolism leading to more sensitivity to glutamine deprivation while several genes of the glutamine pathway including asparagine synthetase (ASNS) and glutamate decarboxylase (GAD) were downregulated in these cells [234]. Hence in a publication from Galicia-Vázquez *et al.* [236], del11q CLL lymphocytes deficient for ATM showed a difference in the glutamine metabolism which resulted in enhance ammonia uptake, glutamine synthetase expression and sensitivity towards glutaminase (GLS1) inhibition compared to their wild-type counterparts.

Finally, the loss of ATM is associated with a metabolic syndrome, characterised by "insulin resistance, adiposity, blood pressure, circulating cholesterol and lipid levels, and atherosclerosis" [237].

Overall, the DDR is linked with metabolism in many ways, likely to occur at levels yet to be discovered. Researching the interactions between these two critical cellular processes is essential because it could give new insight into their mechanism of actions. Also, it could allow the discovery of new metabolic biomarkers associated with repair pathway defects and DNA damage that could be targeted therapeutically. However, it should be borne in mind that the metabolic rewiring occurring after DNA damage or DNA repair activation and defect might be cell type- and context-dependent.

1.2. Taurine, an enigmatic metabolite

Given the number of molecules involved in the metabolic pathways, it is expected that not all have been fully described. Among them, taurine is suspected of having many undefined functions.

Taurine also called taurine 2-aminoethanesulfonic acid, was isolated for the first time from ox bile. It is one of the four common sulfur-containing amino acids, the others being methionine, cysteine, and, homocysteine [238]. Taurine has an amine group but no carboxyl, though it is sometimes classified as an AA although with a sulfonic acid group [239]. It is the most abundant amino acid found in mammals. However, depending on the situation, it is considered an essential amino acid or not [240]. In humans, it is an essential amino acid, some cellular type being able to synthesise it and another not [240,241]. Most of the taurine found in tissues originates from the diet, especially animal products. The rest of the time taurine is synthesised from methionine and cysteine [240].

The first step of taurine synthesis pathway consists of the oxidation of cysteine, directly or after its conversion from methionine to cysteine sulfinic acid by the enzyme cysteine dioxygenase (CDO). Then follows a decarboxylation of cysteine sulfinic acid by the rate-limiting enzyme of taurine synthesis, cysteine sulfinic acid decarboxylase (CSAD) resulting in hypotaurine production. The last step is the oxidation of hypotaurine to taurine by the hypotaurine dehydrogenase (HDH) [241]. Glutamate can also be added to cysteine by the gamma-glutamylcysteine synthetase (GCS) to form γ-glutamylcysteine (GGC). Glycine can then be combined with GGC by glutathione synthase to form glutathione [186] (Figure 1-5).

Contrary to methionine and cysteine, it is widely accepted that taurine is not incorporated into proteins. Until recently, the only evidence of the incorporation of taurine into macromolecules has been reported in a publication from Suzuki *et al*. [242] who showed taurine could be

incorporated post-transcriptionally into human mitochondrial tRNAs to produce 5-taurinomethyluridine and 5-taurinomethyl-2-thiouridine. Then, in their latest study, Olson *et al*. [243] demonstrated taurine can also be covalently linked with tubulin, the precursor for the formation of microtubules. Although these observations were done in avian erythrocytes, the same mechanism probably occurs in human. Altogether, these discoveries suggest that taurine could be incorporated into other types of molecules and should be the subject of further research.

The import of taurine is regulated by the TAUT transporter, which depends on the amino acid concentration[244]. Although taurine is often found in free form in cells, it has many cellular functions. The most recognised role of taurine is the formation of bile acids conjugates [240]. Besides, taurine by maintaining stable intracellular chloride levels helps stabilise cell membrane, membrane potential and the pH [245]. A different cytoprotective role of taurine concerns the regulation of oxidative stress. Taurine supplementation was shown to reduce ROS levels in the liver [246] and muscles [247,248] as well as in the brain [249]. However, the mechanism of action of taurine as an antioxidant remains uncertain. Taurine was also reported to increase the autophagic flux in mouse adipocytes [250]. The same was observed in Leydig cells, besides reducing oxidative stress and apoptosis [251]. Finally, taurine has an important role for neutrophils function and has been shown to be decreased in aged neutrophils compared to active ones [252].

There is also evidence for the involvement of taurine in cancer. Indeed, high levels of taurine have been found in some cancers and can be used as a tumour biomarker. For instance, higher levels of taurine were measured in the urine of patients with bladder cancer [253], in the colorectal biopsy of patients with colorectal cancer [254], in plasma of patients with oesophageal tumour [255], in human breast and prostate cancer tissues [256,257] when compared to the control. Nonetheless, the role of taurine in cancer and carcinogenesis remains poorly understood. One could think it

could be correlated with the high oxidative stress and genotoxic stress found in cancer cells, but this question will need to be further addressed.

On the other hand, the taurine upregulated gene 1 (TUG1) which belongs to the long non-coding RNAs (lncRNAs) family known to control gene expression, has an important role in cancer [258]. TUG1 was identified for the first time after being shown to be upregulated after taurine treatment during retinal development [259]. TUG1 has been shown to control the expression of a variety of target genes, either by activation or suppression. Hence, in cancer, TUG1 can either promote tumour cell proliferation and be associated with poor prognosis or prevent cancer progression. Also, depending on the context TUG1 can act as chemo protectant [260,261] or on the contrary, can confer resistance to chemotherapies [262–264]. The role of TUG1 as a cancer promoter or suppressor will depend on the type of cancer as reviewed by Baliou *et al.* [265]. Moreover, TUG1, through its role in mitochondrial bioenergetics [266], glycolysis [267], and insulin secretion [268], is involved in cell metabolism. Finally, the promoter of TUG1 contains binding sites and is a transcriptional target for the DDR protein, p53 [269].

Overall, while taurine seems to have various roles in the cell, its mechanism of action is not always well described. Therefore, future research should aim at a better understanding of these processes and exploring other functions of taurine. Given the role of taurine target TUG1 in metabolism and the fact that p53 can bind to its promoter, it would be interesting to study the role of taurine in both the context of metabolic reprogramming and DNA repair in cells.

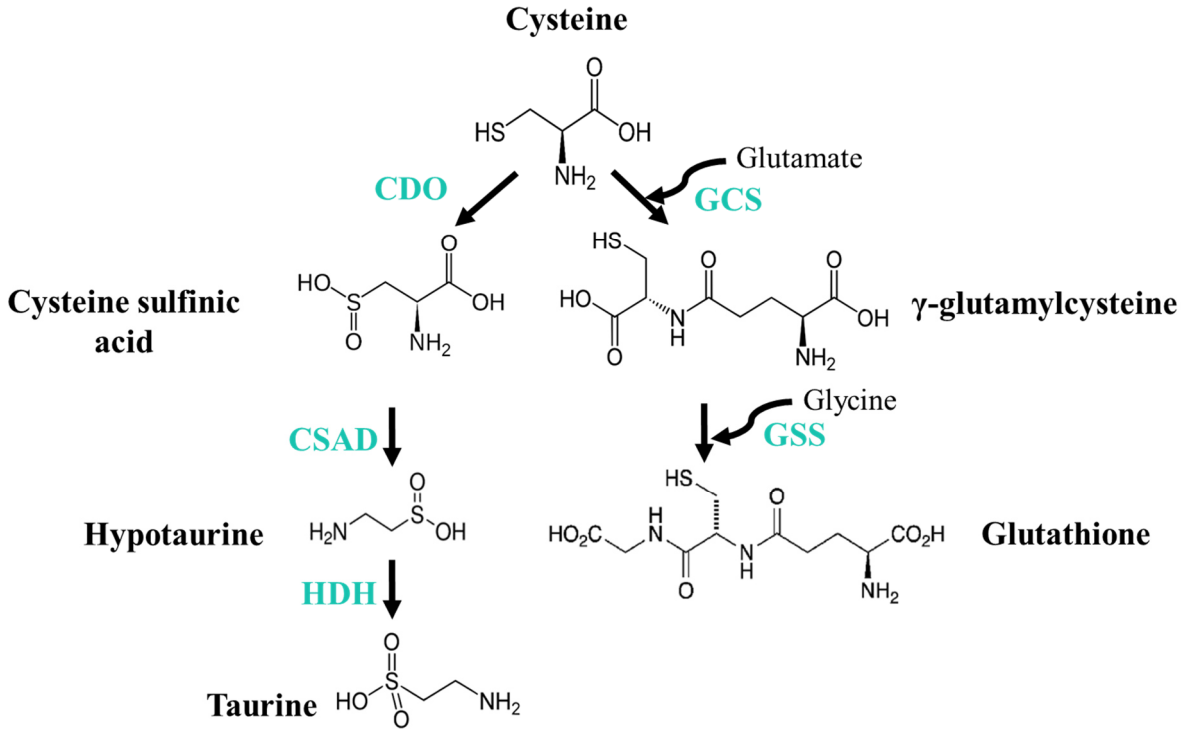

Figure 1-5: Taurine and glutathione synthesis from cysteine.

For taurine synthesis, cysteine is oxidised to cysteine sulfinic acid by the cysteine dioxygenase (CDO). Cysteine sulfinic acid is then decarboxylated to hypotaurine via the cysteine sulphinic acid decarboxylase (CSAD). In the end, hypotaurine is oxidised by the hypotaurine dehydrogenase (HDH) to form taurine. Glutathione synthesis occurs via two steps. The first step consists in the addition of glutamate to cysteine by the gamma-glutamylcysteine synthetase (GCS) to give γ-glutamylcysteine. Glycine can then be combined with GGC by glutathione synthase (GSS) to form glutathione.

1.3. NMR in metabolic studies

A multitude of chemical reactions is taking place every day in living cells. Together these reactions are referred to as the metabolism. Metabolomics and metabolic studies explore metabolic pathways involving metabolites, small molecules below 1500 Dalton. Metabolites can be endogenous, synthesised in cells, such as sugars, lipids, vitamins, or amino acids or exogenous, like drugs or nutrients from the diet.

The identification and quantification of metabolites present in a living organism can help to understand its cellular processes and physiological status. In response to stimuli, including drugs, pathologies or genetic alterations, modifications of metabolic pathways are most likely to occur. Hence biomarkers for cellular dysfunctions or toxic response can be detected [270–272].

When it comes to metabolic profiling, nuclear magnetic resonance (NMR) spectroscopy and mass spectrometry (MS) are the most widely used analytical platforms as they allow the simultaneous analysis of multiple metabolites in a sample. Both techniques have different strengths and weaknesses as reviewed in [273], and the choice of the method will depend on the aim of the experiment. Although NMR is less sensitive than mass spectrometry, it allows the analysis of the metabolic composition of a sample without any preceding separation or treatments and identification of structures of unknown metabolites. Moreover, it is highly reproducible, quantitative and non-destructive [273,274].

1.3.1. NMR basic principles

NMR spectroscopy is based on the magnetic properties of nuclei and enables the identification of molecular structures. In brief, NMR spectroscopy consists of the excitation of nuclei in a magnetic field by applying radiofrequency pulses to induce resonance. The resulting resonant current will be recorded and converted into an NMR signal that contains information about the chemical environment of the nuclei.

The angular momentum is defined as the propensity of a rotating object to stay in motion around a fixed point or axis. In the nuclei, neutrons and protons exhibit an analogous but intrinsic angular momentum called spin (*S*). The spin can be represented as a vector passing through the centre of a particle, in the direction of the rotation axis. The total spin of a nucleus is the vector sum of spins of nucleons. It is characterised by a nuclear spin quantum number (*I*) which may take integer or half-integer values. When the number of nucleons is even in a nucleus, spins from proton and neutron will pair up. In other words, a nucleon's spin will be oriented in the opposite direction of another, and the total spin will be equal to zero (*I*=0). In the situation were nuclei have an odd number of nucleons, the total spin will take values multiple of ½. In NMR, the most frequently studied nuclei have half-integer quantum number, i.e., ^{1}H, ^{13}C, ^{15}N, ^{19}F, and ^{31}P [275,276].

Nuclei with a non-zero spin can act like tiny magnets and interact with an external magnetic field, thus have a magnetic moment. The spin magnetic moment is calculated from the spin angular momentum and the gyromagnetic ratio, a constant characteristic of each nucleus, as followed:

Equation 1-1

$$\mu = \gamma S$$

where μ is the spin magnetic moment, γ is the gyromagnetic ratio and, S is the angular magnetic moment.

In the absence of an external magnetic field, spins of ½ nuclei are oriented randomly. When placed in an external magnetic field (B_0), spins will orient parallel (α) or anti-parallel (β) to the field, two states with different energy levels. Spins in the lower energy state α can absorb energy and move to the more energetic state β (Figure 1-6A). The energy necessary to trigger the transition between the two states should equal the differences in energy (ΔE) between the two states, calculated as followed:

Equation 1-2

$$\Delta E = \frac{\gamma h B_0}{2\pi}$$

Where ΔE is the energy difference between the two states, γ is the gyromagnetic ratio, h is the Planck's constant and B_0 the external magnetic field.

At equilibrium, the numbers of spins in the lower energy state will be slightly in excess following the Boltzmann distribution probability and depend on the type of nuclei, on the magnetic field strength and the temperature:

Equation 1-3

$$\frac{N\beta}{N\alpha} = e^{-\Delta E/kT}$$

Where Nα and Nβ are the number of spins at lower and upper energy state, ΔE is the energy difference; k is Boltzmann's constant (1.3805 x 10^{-23} J/Kelvin), and T is the temperature (K) [277,278].

The excess of spins in the α state will cause the creation of a net magnetisation. The net magnetisation is represented by a vector oriented along the direction of the magnetic field and with a size proportional to the number of spins (Figure 1-6B). When a radio frequency (RF) pulse with a frequency equal to ΔE is applied, a resonance emerges causing the net magnetisation to move towards the direction of the applied RF pulse. The transverse magnetisation will start precessing around the external magnetic field at a frequency called the

Larmor frequency (Figure 1-6C). The precession will generate a second magnetic field that can be measured by a receiver coil. After the pulse, the transverse magnetisation will return to equilibrium. This process is called relaxation and involved the spin-spin and spin-lattice relaxations. Spin-lattice or longitudinal relaxation defines the return of the magnetisation to his equilibrium in the direction of the magnetic field. The relaxation time *T1* defines the time for the magnetisation to reach back the equilibrium. This parameter is crucial for NMR experiments as the return to equilibrium is essential to avoid saturation of the signal. In NMR, full relaxation is enabled by sufficient interscan delay, the time between two consecutive pulses. On the other hand, spin-spin or transverse relaxation, *T2* characterises the decay of the transverse magnetisation perpendicular to the external magnetic field and determines the spectral line width [279,280].

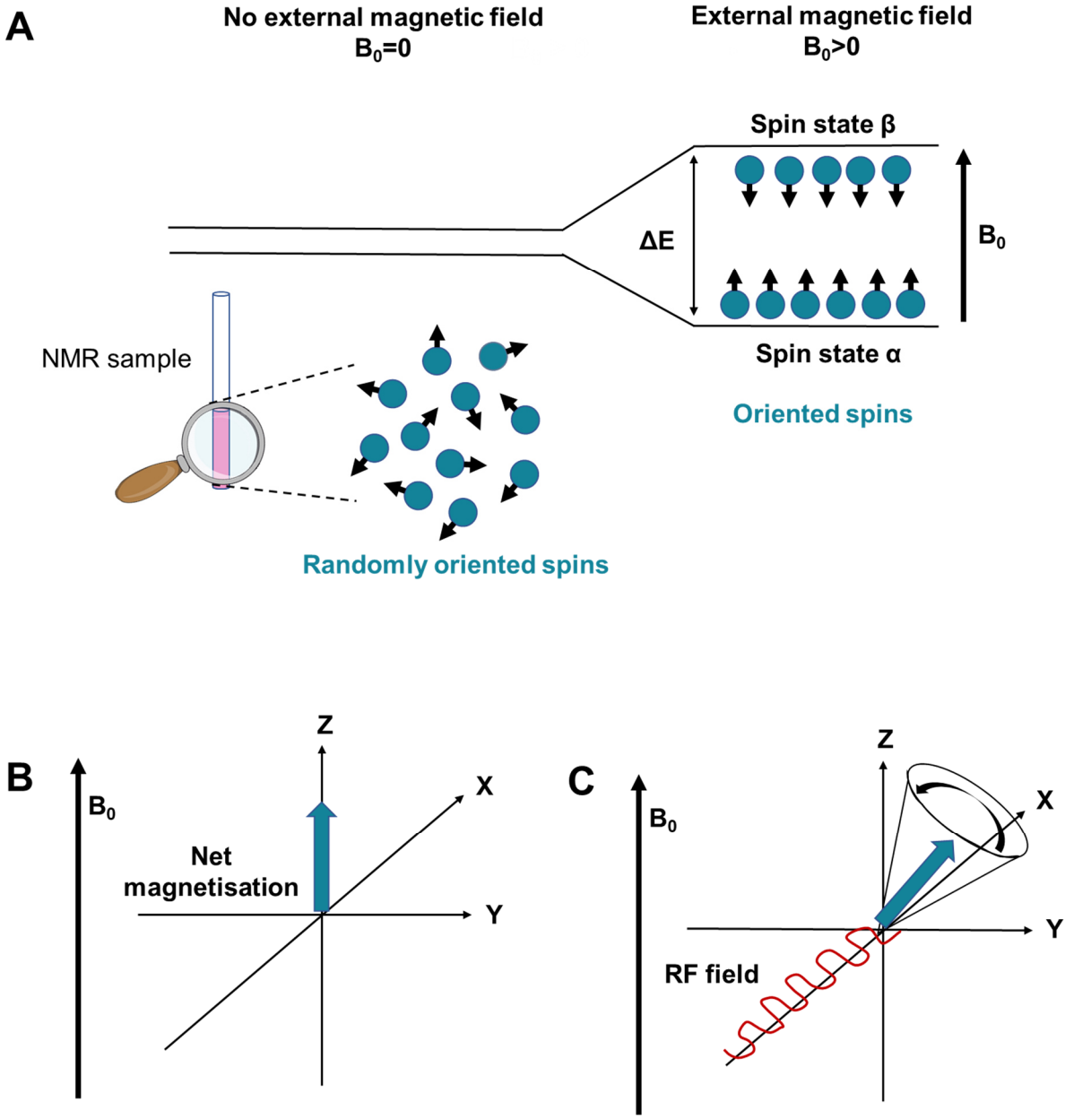

Figure 1-6: Schematic representations of the two energy states for ½ nuclear spins and the net magnetisation under a magnetic field.

A) Schematic representations of the two energy states for ½ nuclear spins and the orientation of spins in the absence or presence of an external magnetic field. Spins of ½ nuclei are oriented randomly in the absence of an external magnetic field but are oriented parallel (α) or anti-parallel (β) to the applied magnetic field. ΔE represents the differences in energy between the two states. B) Under a magnetic field B_0, the excess of spins in α state will cause the formation of a net magnetisation vector in the direction of the field. C) When a radio frequency (RF) pulse is applied, the net magnetisation moves towards the direction of the applied RF pulse and start precessing.

1.3.2. NMR signal and chemical shift

In the previous section, the physical properties at the origin of the NMR signal were briefly explained. During NMR experiments, the signal will decay and is called free induction decay (FID). This time-domain signal can be converted into a frequency-domain spectrum using a mathematical operation called Fourier transformation.

Typically, an NMR spectrum is a plot of signal intensity against chemical shift (δ). The chemical shift of a nucleus is the difference between the frequency of the nucleus and a standard compound such as trimethylsilyl propanoic acid (TMSP). To prevent the influence of the NMR instrumentation and the field strength on the chemical shift values, the chemical shift is defined as a field-independent quantity, in units of parts per million (ppm) of the applied field, calculated as followed:

Equation 1-4

$$\delta = \frac{\upsilon - \upsilon_{\text{reference}}}{\upsilon_{\text{spectrometer}}} \times 10^6$$

Where υ is the frequency of the signal of interest, $\upsilon_{\text{reference}}$ is the frequency of the reference compound and, $\upsilon_{\text{spectrometer}}$ is the frequency of the spectrometer [278,279].

The signals in NMR depend on the external magnetic field B_0 applied, but also on the chemical environment of each nucleus in a molecule. Nuclei will perceive the magnetic field strength differently, depending on their chemical bound(s) and structure. As a result, different signals will be obtained at different frequencies allowing the independent identification of multiple metabolites in a spectrum. Expected chemical shifts ranges for different functional groups in organic molecules can be seen in Figure 1-7.

The multiplicity of an NMR peak is another parameter essential to discriminate between the different metabolites. Multiplicity arises because chemical bonds connect nuclei in a molecule, and this causes *J*-couplings. Spins can take different energy levels triggering multiple resonance

lines to emerge. The number of signals will depend directly on the number of spins coupled. The distance between peaks, measured in Hz, is defined as the coupling constant and is independent on the magnetic field strength. *J*-couplings can be observed between identical or dissimilar nuclei, i.e., ^{1}H-^{1}H (J_{HH}), ^{13}C-^{13}C (J_{CC}), ^{1}H-^{13}C (J_{HC}), ^{15}N–^{13}C (J_{NC}). Suppression of determined couplings is enabled through selective radiofrequency irradiation, known as decoupling [278].

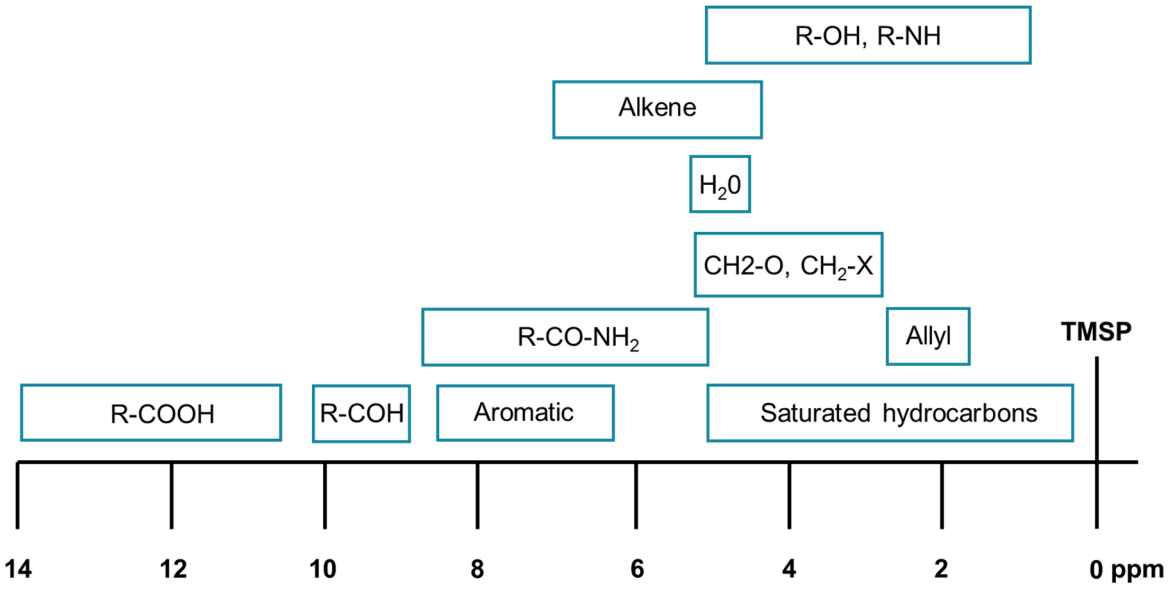

Figure 1-7: ^{1}H chemical shift ranges (in ppm) of different functional groups.

Based on Metin Balci's book [278].

1.3.3. NMR instrumentation

NMR spectrometers are devices designed for the acquisition of NMR spectra. They comprise a sample-holder inside a superconducting magnet, a probe with an RF transmitter/receiver, and a signal recorder (Figure 1-8). The superconducting magnet together with the shim coils generate the strong, stable, and homogenous external magnetic field (B_0), essential for a good NMR sensitivity and spectral resolution. It is located in an inner chamber containing liquid helium (4 K), surrounded by liquid nitrogen (77 K) as a protection from external heat and consecutive helium loss. The sample-holder is positioned vertically in the centre of the magnet and surrounded by a probe. Within the probe, the RF emitter excites nuclei by delivering short pulses at a specific frequency. The signal emitted is sent to the RF receiver [276,281,282]. Probes are tuned to the nuclei to be studied, but also on the sample size, usually between 1.7 and 10 mm [283].

The magnetic field must be steady and homogenous to obtain high-resolution NMR spectra. To compensate for the drift of the magnetic field, the probe contains a lock coil that monitors the deuterium (^{2}H) signal of a deuterated compound, often D_2O, added to the sample, which is used to control a direct current through a room temperature B_0 coil to maintain a constant magnetic field over a longer time period [284]. To guarantee the homogeneity of the external magnetic field, coils called shims generate small magnetic fields upon the external magnetic field [285]. In the modern spectrometers, lock and shimming controls are automated. However manual adjustments are sometimes needed for better spectral resolution and minimal line width of the resonances in spectra.

Finally, the signal emitted from the probe will be sent to the spectrometer console and digitised.

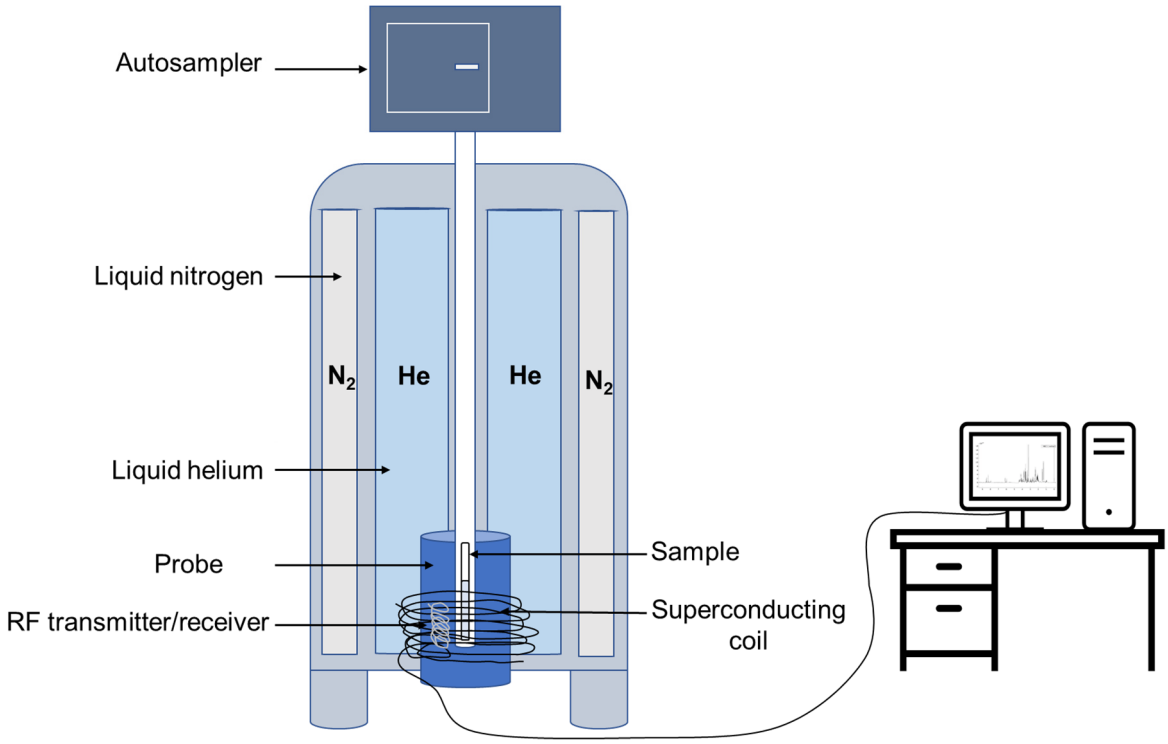

Figure 1-8: Schematic representation of an NMR spectrometer.

The NMR sample is placed in the sample holder inside a superconducting coil. The sample holder is surrounded by a probe comprising multiple coils, including an RF transmitter and receiver coil. The signal emitted can be amplified and sent to the spectrometer console.

1.3.4. 1D and 2D NMR spectroscopy

Most NMR experiments consist of the application of RF pulses, followed by delays and signal recording. The type and number of pulses and delays, along with other acquisition parameters, are identified as the pulse sequence of the NMR experiment. One- or multi-dimensional NMR experiments are used to study an individual nucleus or a system of coupled nuclei, respectively [278,279].

A one-dimensional (1D) proton (^{1}H) NMR NOESY is the most widely used experiment in metabolomics to study simultaneously multiple metabolites in samples including biofluids, cells and tissues, mainly because it offers excellent solvent suppression. Biological samples used for NMR experiments are typically prepared in aqueous solutions. Therefore, the NMR pulse sequence will have to include a pre-saturation pulse to prevent the appearance of a strong water signal shadowing the rest of the metabolites [286]. 1D ^{1}H NMR spectra allow the identification of metabolites through their chemical shifts and multiplicity and can provide information about their concentrations, given the 1D NMR signal is proportional to number of protons from which the resonance originates. Metabolites can then be correlated to specific metabolic pathways, biological processes, or response to external stimuli. Hence, depending on the type of the sample studied in NMR, it is possible to study intracellular and extra metabolite concentrations. However, given the complexity of biological samples, ^{1}H NMR spectra include many signals overlapping that can compromise metabolites assignments [287].

2D NMR experiments can help resolve peak overlap in 1D spectra and facilitate the identification of compounds in NMR spectra for complex samples. They can be used to study two nuclei and get information about their chemical bonds [288]. 2D heteronuclear single quantum coherence (HSQC) for instance, involves a transfer of the proton magnetisation to a heteronucleus (nucleus other than a proton), typically ^{15}N or ^{13}C, followed by an evolution

period, before signal detection. The 2D spectra will show the proton chemical shifts on the x-axis and the chemical shifts for the heteronucleus on the y-axis. In 2D HSQC spectra, peaks arise from protons attached to the heteronucleus. The intensities are represented by contours and the multiplicity in the ^{13}C-dimension provides information for isotopomers analysis.

1.3.5. Tracer-based NMR experiments

Tracer-based metabolism allows us to examine the fate of isotopically labelled precursors in distinct metabolic pathways and to examine the labelling incorporation at specific atomic positions in metabolic intermediates.

NMR is particularly useful to measure metabolic fluxes using isotopically labelled precursors, usually ^{13}C and ^{15}N. For instance, ^{1}H-^{13}C-HSQC experiments observe ^{1}H and ^{13}C chemical shifts and the different couplings, especially the J_{CC} in compounds with adjacent ^{13}C-nuclei [278,289]. The major challenge of ^{1}H-^{13}C-HSQC experiments results in the metabolites quantification. Indeed, the natural abundance of ^{13}C (1.1%) can cause a misreading of total ^{13}C labelling. Several methods have been proposed to obtain absolute label incorporations from HSQC spectra. As an example, simulated *J-couplings* can be combined with mass isotopologues obtained by mass spectrometry as described in [290]. Another approach used within this thesis consists of acquiring an unlabelled reference NMR spectrum together with the corresponding ^{13}C labelled sample. Given both spectra include signal intensities for natural abundant ^{13}C, the total label incorporation can be calculated by subtracting ^{13}C in the reference sample to the labelled sample [291].

1.4. Aim of this thesis

In cells, the typical DNA damage response involves the control of cell-cycle checkpoints, repair proteins or apoptosis but, alterations of the repair processes can lead to cell diseases or cancer [89,292]. The last years have seen significant improvement in the identification of genes and proteins involved in the DDR and their roles in cell physiology and pathology. Most notably, alterations of the DNA repair were shown to cause a metabolic rewiring in human cells which suppose metabolism and the DDR are intimately connected [135,185]. Therefore, this thesis aimed at investigating how faults in the DDR resulting from ATM or RNASE-H2 deficiencies or exposition to an external source of DNA damage might affect the metabolism in haematological cells.

This project, using primarily NMR spectroscopy focused on diverse objectives:

- To obtain the metabolic profiles of haematological cell lines and CLL primary cells wild-type or with a defect in ATM or RNASE-H2 to identify whether a metabolic rewiring occurred in these cells and possible metabolic biomarkers of DNA damage
- To use different models of induced DNA damage to study the consequences of such impair at the metabolic level
- To investigate whether differences in glucose and glutamine metabolism existed between WT and DDR-deficient cells using tracer-based NMR isotopic labelling HSQC experiments
- To perform 2D NMR experiments and use various inhibitors to explore further the metabolic differences observed between ATM- and RNASE-H2-deficient cells

Chapter 2 Material and method

2.1. Cell culture

2.1.1. Culture conditions

All cell lines were cultured in RPMI 1640 media (Gibco) supplemented with 10% (v/v) heat-inactivated foetal bovine serum (FBS) (Sigma) and 100 U/mL penicillin-streptomycin (Gibco), in a humidified incubator at 37 °C and 5% CO_2. All cell lines used in the project were available in our laboratory or were obtained by Prof. Malcolm Taylor's group. A list of all cell lines used, and their characteristics can be found in Table 1.

Cell cultures were maintained at a density between 0.5-2 x10^6 cells per ml and passaged every 3-4 days to preserve cells in the best conditions. Cell aliquots were harvested, counted, and centrifuged (5 min, 1200 rpm). The cell pellets were resuspended in an appropriate volume of fresh culture media.

Table 1: List of cell lines used throughout the project

Cell line	Description
MEC1 WT and ATM	CLL isogenic cell line expressing short hairpin (sh)-RNA against GFP or ATM
MEC1 WT and RNASEH2-KO	WT or CRISPR-edited RNaseH2-KO CLL cell lines
CII	CLL isogenic cell line
CII WT or ATM	CLL isogenic cell lines expressing short hairpin (sh)-RNA against GFP or ATM
Lymphoblastoid cells lines (LCLs)	Wild-type (WT) or ATM-deficient lymphoblastoid cells lines
JJN3 WT and RNASEH2-KO	WT or CRISPR-edited RNaseH2 KO multiple myeloma cell lines

2.1.2. Lymphoblastoid cells lines

LCLs were obtained from Prof. Malcolm Taylor's group. Five LCLs were derived from healthy donors, and seven were generated from B-cells presenting an ATM deficiency with or without residual AT activity. LCLs and their ATM status and activity are described in Table 2.

Table 2: LCLs used within this project and characteristics

	ATM protein	ATM activity	ATM mutations
LCLs WT 1-5	Yes	Yes	None
LCLs ATM 1	Feint presence	No	c.3695_3713del19; p.(Ser1232TyrfsTer2) (homozygous)
LCLs ATM 2	Feint presence	No	c.6047A>G; p.Asp2016Gly c.3576 G>A (p.Ser1135_Lys1192del58
LCLs ATM 3	No	No	c.7788G>A p.(Glu2596=) (homozygous)
LCLs ATM 4	No	No	c.2483delA p.(Lys828SerfsTer8) c.3802delG p.(Val1268Ter)
LCLs ATM 5	Yes	Yes	c.103CGA>TGA c.103 C>T; p.Arg35X c.7271T>G (V2424G)
LCLs ATM 6	Feint presence	Yes	c.5763-1050A>G (p. Pro1922Leufs*9) c.8418+2_5delTGAG (p.Val2757_Met2806del)
LCLs ATM 7	Yes	Yes	c.5763-1050A>G; p.(Pro1922fs)(homozygous)

2.1.3. Isotopic labelling

For isotopic labelling, cells were cultured in RPMI 1640 media (Gibco) supplemented with 10% (v/v) FBS (Sigma) and 100 U/mL penicillin-streptomycin (Gibco) with or without glucose, glutamine, cysteine, methionine and supplemented with labelled precursors. Control cells were cultured in the same culture media supplemented with natural abundant precursors (Table 3). Cells were grown for 24 hours to seven days before extraction, depending on the experiment. For labelling over more than 24 hours, media was replaced with fresh media every day. A minimum of 20 million cells was used for the labelling experiments to allow sufficient NMR signal.

Table 3: Media used in the isotopic labelling experiments

Experiment	RPMI 1640 (manufacturer, catalogue number)	Supplemented components (manufacturer)
CTL glucose	No glucose (Gibco, 11879020)	11.11 mM glucose (Sigma)
[U-^{13}C] glucose	No glucose (Gibco, 11879020)	11.11 mM [U-^{13}C] glucose (Cortecnet)
CTL glutamine	No glutamine (Gibco, 21870076)	2.05 mM glutamine (Gibco)
[3-^{13}C] glutamine	No glutamine (Gibco, 21870076)	2.05 mM [3-^{13}C] glutamine (Sigma)
CTL cysteine or methionine	Modified, with sodium bicarbonate, without methionine, cystine and glutamine (Sigma, R7513)	2.05 mM glutamine (Gibco), 0.1 mM methionine (Sigma), 0.2 mM cysteine (Sigma)
[$^{13}C_3$] cysteine	Modified, with sodium bicarbonate, without methionine, cystine and glutamine (Sigma, R7513)	0.2 mM [$^{13}C_3$] cysteine (Sigma), 0.1 mM methionine (Sigma), 2.05 mM glutamine (Gibco)
[U-^{13}C] methionine	Modified, with sodium bicarbonate, without methionine, cystine and glutamine (Sigma, R7513)	0.1 mM [U-^{13}C] methionine (Sigma), 0.2 mM cysteine (Sigma), 2.05 mM glutamine (Gibco)

2.2. Primary cells

2.2.1. Patients

Blood samples from CLL patients were obtained from Birmingham and Bournemouth Hospitals. It included a total of 8 WT CLLs and 9 CLLs with ATM dysfunction (Table 4). Patients were diagnosed with CLL according to current standard evaluation criteria. The project was covered by ethical approval from the South Birmingham Ethics Committee.

Table 4: Primary CLL patient information

CLL patient	Date	FISH - 11qdel	NGS-ATM mutation
WT 1	10-04-14	Normal	WT
WT 2	04-01-18	Normal	WT
WT 3	25-08-11	Normal	WT
WT 4	14-10-10	Normal	WT
WT 5	20-12-07	Normal	WT
WT 6	03-11-16	Normal	WT
WT 7	15-5-14	Normal	WT
WT 8	06-08-14	Normal	WT
ATM 1	03-13-13	N.A.	c.634delT, pF212fs (AF n/a)
ATM 2	18-05-11	Normal	c.5784T>A, p.F1928L, 51%
ATM 3	17-05-12	Normal	c.742C>T, p.R248X, 9%
ATM 4	01-05-14	Normal	c.998C>T, p.S333F, 40%
ATM 5	30-4-15	Normal	c.7927+6T>-, p n/a, AF n/a
ATM 6	15-05-08	Normal	c.4470_4476del, p.1490_1492del, 9% c.8089A>G, p.N2697D, 15%
ATM 7	10-12-09	88%, mono	c.3161C>G, p.P1054R, 45%
ATM 8	20-07-08	78.5%, bi	WT
ATM 9	21-10-14	63%	c.146C>G, p.S49C, 40%

2.2.2. Isolation from blood and culture conditions

CLL blood samples were collected in vacutainers coated with heparin. Peripheral blood mononuclear cells (PBMCs) were isolated from blood using Lymphoprep™ (Stemcell Technologies, Cambridge, UK) density gradient centrifugation as early as possible after the samples collection. Briefly, blood samples were transferred into 50 ml tubes. The tubes were filled to 35 ml with RPMI 1640. The tube content was slowly overlaid onto 10 ml of Lymphoprep™ to prevent mixing of the phases. The Lymphoprep™ and blood were centrifuged for 30 min at 1500 rpm without brake, at room temperature. After the centrifugation, PBMCs formed a visible white-grey layer located at the plasma:Lymphoprep™ interface. The mononuclear cells layer was collected with a Pasteur pipette and washed twice with RPMI 1640. PBMCs were either maintained in RPMI 1640 supplemented with 10% (v/v) foetal bovine serum (FBS) and 100 U/mL penicillin-streptomycin, in a humidified incubator at 37 °C and 5% CO_2 or resuspended in freezing media (FBS with 10% (v/v) DMSO) and transferred into a -80 °C freezer. Frozen primary cells were then relocated and stored in liquid nitrogen. Primary CLL cells were either studied right after their isolation from the blood ("fresh samples") or thawed and cultured in vitro ("frozen samples").

2.2.3. Thawing primary cells

Frozen primary cells were thawed by adding 10 ml of RPMI 1640 with 10% (v/v) FBS slowly to the cryovial. Cells were counted, and cell viability was assessed. Cells were then centrifuged at 1200 rpm for 5 minutes and resuspended in RPMI 1640 supplemented with 10% (v/v) FBS and 100 U/mL penicillin-streptomycin.

2.3. Cell viability

During all experiments, cells' viability was assessed using trypan blue (Sigma), a blue dye that stains dead cells. The number of living cells and dead cells coloured in blue were counted using a haemocytometer. Only cells with viability above 90% were used in this study.

When the viability was not sufficient, a dead cell removal kit (Miltenyi, Germany) was used. Briefly, cells were collected and spun at 1200 rpm for 5 minutes. The supernatant was discarded, and the cell pellet was resuspended in 100 µL of Dead Cell Removal MicroBeads® per 10^7 total cells. The same volume was used for fewer cells. Cells were incubated for 15 minutes at room temperature, placed onto an LS column, and separated in the magnetic field of a MACS® Separator. Finally, the effluent containing the live cell fraction was collected.

2.4. Cell treatments

2.4.1. Cystathionine γ-lyase inhibition

Cells were treated with DL-propargylglycine (PAG) (Sigma) to inhibit cystathionine γ-lyase. PAG was dissolved in water at 200 mM as a stock solution. Aliquots of the stock solution were kept at -20 °C. On the day of the experiment, an aliquot was thawed. PAG was added to the culture media to reach a final concentration of 1, 2 or 3 mM, as found in the literature [293,294]. Cells were incubated at 37 °C, 5% CO_2 for 48 hours. The samples were collected at 24- and 48-hours.

2.4.2. Degradation pathways inhibition

Cells were incubated with MG132 (Alta Aesar) or bafilomycin (BAF) (Sigma) to inhibit the proteasome or the autophagy, respectively. Stock solutions of 10 mM MG132 or 100 μM BAF were prepared in dimethyl sulfoxide (DMSO) (Sigma). Aliquots of the stock solutions were kept at -20 °C and thawed on the day of the experiment. Stocks were added to the cell culture medium to a final concentration of 10 μM MG132 and 10 nM BAF. Cells were incubated for 6 hours in media with 10 μM MG132 or for 24 hours in media with 10 nM BAF at 37°C, 5% CO_2. DMSO was used as a control vehicle in all experiments.

2.5. Reactive oxygen species measurements

ROS measurements were achieved by flow cytometry analysis using a CyAn ADP flow cytometer (Beckman Coulter). Data were analysed using the FlowJo software package (BD).

2.5.1. Intracellular ROS

The total intracellular ROS was measured using 2',7'-Dichlorodihydrofluorescein Diacetate (DCFH-DA) (Sigma). Two samples were analysed, each containing 0.5 x10^6 cells (DCFH-DA CTL, DCFH-DA H_2O_2). A 20 mM DCFH-DA reagent stock solution was made. Subsequently, a reagent working solution with 100 µM DCFH-DA in Hank's balanced salt solution (HBSS) was prepared from the stock. Five minutes before the DCFH-DA staining, H_2O_2/HBSS was added to the culture media of one of the samples to reach a concentration of 1mM (DCFH-DA H_2O_2). Afterwards, the DCFH-DA H_2O_2 cells and another cell aliquot (DCFH-DA CTL) were centrifuged, and supernatants were discarded. Cell pellets were resuspended in 500 µl of DCFH-DA reagent working solution. All samples were then incubated 30 minutes at 37℃, protected from light. After the incubation, cells were washed twice and resuspended in PBS with 2% (v/v) for flow cytometry analysis.

2.5.2. Mitochondrial ROS

For mitochondrial superoxide measurements, MitoSOX™ (Invitrogen) was used. Two samples were analysed, each containing 0.5 x10^6 cells (MitoSOX™ CTL, MitoSOX™ H_2O_2). A 5 mM MitoSOX™ reagent stock solution was made. Then, a reagent working solution with 5 µM MitoSOX™ in Hank's balanced salt solution (HBSS) was prepared from the stock. Five minutes before the MitoSOX™ staining, H_2O_2/HBSS was added to the culture media of one of

the samples to reach a concentration of 1mM (MitoSOX™ H_2O_2). Afterwards, the MitoSOX™ H_2O_2 cells and another cell aliquot (MitoSOX™ CTL) were centrifuged, and supernatants were discarded. Cell pellets were resuspended 1 ml of MitoSOX™ reagent working solution. All samples were then incubated 10 minutes at 37°C, protected from light. After the incubation, cells were washed twice and resuspended in PBS with 2% (v/v) FBS for flow cytometry analysis.

2.6. ATM activity, inhibition, and DDR activation

2.6.1. Western blots

Cells were cultured in fresh cell culture media for 24 hours before protein extraction. For each sample, 5 million cells were harvested and washed with PBS (Sigma). Protein extracts were obtained by sonification in UTB buffer (8 M urea, 150 mM β- mercaptoethanol, 50 mM Tris HCl, pH 7.5, all purchased from Sigma). Protein concentrations were determined using the Bradford protein assay (Bio-rad, Hercules, California, USA). Proteins samples were electrophoresed onto a 6% (v/v) sodium dodecyl sulphate (SDS) polyacrylamide gel and blotted onto a nitrocellulose membrane. Blots were probed overnight with primary antibodies against ATM (Sigma) or phospo-ATM (R&D Systems, Abingdon, UK) or anti-actin (Sigma), used as the loading control. Afterwards, blots were incubated with a suitable secondary antibody (mouse or rabbit). Proteins bands were revealed using Immobilon™ Western (Millipore, Watford, U.K.) based on horseradish peroxidase (HRP) chemiluminescent reaction.

2.6.2. DDR activation

To simulate double-strand breaks in DNA and activate DNA damage repair pathways, cells were irradiated with 10 Gy of γ-rays (Cs137) and incubated at 37 °C, 5% CO_2 for different times as indicated.

2.6.3. ATM inhibition

Cells were treated with the ATM inhibitors KU-60019 or AZD0156 (Selleckchem) to inhibit the ATM activity. Stock solutions of 1.5 mM KU-60019 or AZD0156 were prepared in DMSO. Aliquots of the stock solutions were kept at -20 °C and thawed on the day of the experiment.

KU-60019 and AZD0156 were added to the culture media to reach a final concentration of 3 µM. Control cells were incubated with 3 µM DMSO. Finally, cells were incubated at 37 °C, 5% CO_2 over 96 hours.

For isotopic labelling after ATM inhibition, the cells were cultured over 72 hours in culture media (CTL) or culture media with 3 µM KU-60019 (KU) or AZD0156 (AZ). Cells were split in two and resuspended in culture media, with or without ATM inhibitors, and supplemented with labelled precursors (labelled) or natural abundant precursors (unlabelled). Cells were cultured for 24 extra hours before metabolic extraction.

2.7. NMR spectroscopy

2.7.1. NMR samples and preparation

2.7.1.1. Intracellular metabolites extraction

Intracellular metabolites were obtained using a methanol-water-chloroform extraction adapted from Saborano *et al.* [291]. Cells in RPMI/10%(v/v) FBS were counted. A volume of cell suspension containing 10-20x10^6 cells was harvested. Cells were centrifuged at 1500 rpm for 5 minutes, and the supernatant was removed. Cell pellets were washed with 1 ml of PBS (Sigma), transferred into Eppendorfs, and centrifuged again at 1500 rpm for 5 minutes. PBS was discarded, cell pellets were resuspended in 400 µl cold HPLC methanol (Alta aesar) and transferred on dry ice. At this stage, it is possible to carry on with the extraction procedure or to transfer samples into a -80°C freezer to be extracted later. Methanol samples were transferred into glass vials where 325 µl cold H_2O and 400 µl cold HPLC chloroform (Alta aesar) were added. Vials were vortexed for 1 minute and left on wet ice for 10 minutes for phase separation. Samples were centrifuged at 4000 rpm for 15 minutes at 4 °C, brake off. There were then removed from the centrifuge and left to stand for 10 minutes at room temperature. The vials now include an upper and lower layer containing all polar and non-polar metabolites respectively, separated by a protein layer. 400 µl of the polar phase was transferred into Eppendorf tubes. 200 µl of the non-polar phase was transferred into glass vials. The last step consisted of drying samples; polar samples were transported to a vacuum dryer, and non-polar samples were left to dry overnight under a fume hood.

For NMR sample preparation, polar extracts were reconstituted in 50 µL of 0.1 M phosphate NMR buffer (100 mM sodium phosphate buffer, 0.5 mM TMSP, 3 mM sodium azide in 10% or 100% D_2O, pH 7). Nonpolar extracts were resuspended in deuterated chloroform with 0.03%

(v/v) tetramethylsilane (TMS) (Sigma). Both polar and non-polar extracts were transferred in 1.7 mm NMR tubes (CortecNet) and stored at 4 °C before the NMR acquisition. A simplified scheme of our workflow is summarised in Figure 2-1.

2.7.1.2. Extracellular metabolites

To study the extracellular metabolites, 1 ml of media samples was harvested for the time indicated for each NMR experiment. Media samples were prepared with a 10% (v/v) of 1 M deuterated NMR phosphate buffer (1 M phosphate buffer, 5 mM TMSP, 3 mM NaN3 in 100% D_2O, pH 7). Media samples were transferred in 3 mm NMR tubes (CortecNet) and kept at 4 °C prior to NMR acquisition.

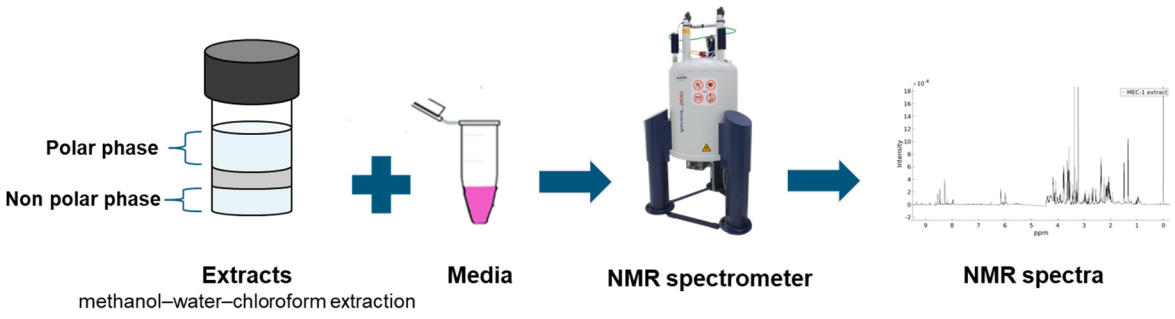

Figure 2-1: Simplified workflow of an NMR experiment

Extracellular metabolites and media samples were transferred in NMR tubes. NMR samples were placed in a spectrometer, and NMR spectra were acquired.

2.7.2. One-dimensional NMR

2.7.2.1. Spectra acquisition

All 1D ^{1}H spectra were acquired on 600 MHz Bruker Avance III spectrometers with Bruker SampleJet autosampler. Spectrometers were equipped with a 1.7 mm triple resonance cryoprobe (TCI) z-axis pulsed field gradient (PFG) for polar and non-polar samples and with a 5 mm TCI z-PFG cryogenic probe for media samples. The pulse sequence used was a standard Bruker 1D ^{1}H NOESY, noesygppr1d with pre-saturation of the water signal. The parameters for the NMR acquisition were different regarding the type of samples (Table 5).

Table 5: Parameters for 1D ^{1}H NMR spectra acquisition

Type of samples	Parameters
Polar and non-polar extracts	Spectral width: 12.15 ppm (7288.6 Hz); complex points, TD: 32768; interscan delay, d1: 4 s; short NOE mixing time, d8: 10 ms; number of scans, ns=128; dummy scans, ds=8; experimental time = 14 min
Media samples	Spectral width: 12.15ppm (7288.6Hz); complex points, TD: 32768; interscan delay, d1: 4s; short NOE mixing time, d8: 10ms; number of scans, ns=64; dummy scans, ds=8; experimental time = 7.5 min

2.7.2.2. Data processing

1D ^{1}H NMR data were processed using the *MetaboLab* [295] software in MATLAB (MathWorks, USA). The free induction decay (FID) signals were multiplied by a 0.3 Hz exponential window function and zero-filled to 131,072 data points prior to Fourier transformation. Spectra were phased manually and referenced to TMSP (0.00 ppm). Water and TMSP region were excluded. A spline-based baseline correction and total spectral area (TSA) scaling was applied to all spectra. Since the total spectral area reflects the total concentration of metabolites, this allows for correcting for differences in cell number between samples. Metabolites were assigned using the *Chenomx* software (Chenomx Inc., Canada) and the Human Metabolome Database (HMDB). Peak intensities were obtained from *MetaboLab* directly.

2.7.3. Two-dimensional NMR

2.7.3.1. Spectra acquisition

All ^{1}H-^{13}C HSQC spectra were acquired with the same 600 MHz Bruker Avance III spectrometer as for the 1D spectra and described in 2.7.2.1. The probe used was the same as for the extracts. The pulse sequence used was a modified version of Bruker's hsqcetgpsp with additional gradient pulses for better water and T1 noise suppression and soft 180°-pulses for ^{13}C. The spectral widths for ^{1}H and ^{13}C spectra were set to 7812.5 Hz/13.02 ppm or 24154.6 Hz/160.1 ppm, respectively. To sensibly reduce the acquisition time without jeopardising the resolution, ^{1}H-^{13}C HSQC spectra were recorded using a non-uniform sampling (NUS) list, calculated using Wagner's schedule generator[296] (tolerance set to 0.01 and other parameters set as default values). ^{1}H dimension was acquired using 1024 complex data points. 25% of the 8192

complex data points (2048) acquired for ^{13}C dimension were sampled using NUS. Spectra were recorded with two scans and an interscan delay of 1.5 s. The experimental time was 4 hours.

2.7.3.2. Data processing

^{1}H-^{13}C HSQC spectra were reconstructed using *NMRpipe* (National Institute of Standards and Technology of the U.S.) software with the Hyberts extension. Cosine-squared window functions were applied to ^{1}H and ^{13}C dimensions. Spectra were phased manually. Afterwards, 2D HSQC spectra were processed using *MetaboLab.* Spectra were referenced manually to the methyl group of L-lactic acid (1.31/22.9 ppm). Metabolites were assigned using the assign tool in *MetaboLab* which contain a chemical shift library for approximatively 200 metabolites, based on the HMDB. Peak intensities of the 2D spectra were obtained from signals in the spectra in *MetaboLab*.

2.7.3.3. HSQC scaling

For every HSQC spectrum, a ^{1}H-NMR spectrum was acquired. The intensities on the 2D spectra were normalised using TSA values from the corresponding 1D ^{1}H NOESY spectra to correct for the differences in cell number. The normalised peak intensities obtained from cells incubated in isotopically labelled media (Labelled HSQC) were compared to the normalised peak intensities from cells incubated in media with natural abundance isotopes (unlabelled HSQC). For a specific carbon, a ratio between $^{13}C/^{12}C$ was calculated by dividing the normalised peak intensity of this carbon in the labelled HSQC by the normalised peak intensity of the same carbon in the corresponding reference unlabelled HSQC. This ratio was then multiplied by the natural abundance for ^{13}C isotope (1.1%) to obtain the percentage of ^{13}C in a metabolite (%^{13}C).

2.8. Statistical analysis

Statistical analysis was conducted using GraphPad Prism version 8.0 for Windows (GraphPad Software, INC, La Jolla California, USA). Student's t-test was used to study the statistical significance between paired data and corrected for false discovery rate (FDR) with Benjamini, Kriger, Yekutieli method (Q value set to 5%). For multiple-group comparison, the one-way analysis of variance (ANOVA) was used and corrected for multiple comparison using statistical hypothesis testing. The level of significance was set at $p < 0.05$. The number of samples used in each experiment can be found in figures legends where p-values were indicated as follow: * $p<0.05$, ** $p<0.01$, *** $p<0.001$.

Chapter 3 Metabolic changes associated with faults in DNA repair

3.1. Overview

Human cells are confronted continuously with endogenous stress, including replication and oxidative stress or exogenous stress such as exposure to UV and ionising radiation that can ultimately damage DNA. As a result, cells have developed many mechanisms, included in the so-called DNA-damage response (DDR), to detect and promote the repair of DNA lesions. These DNA repair mechanisms are essential to maintain genome stability and prevent cellular dysfunction and diseases [1,3].

DDR pathway alterations can cause mutations in genes such as tumour suppressor genes or oncogenes and lead to carcinogenesis. DDR pathway alterations are considered as a hallmark of cancer cells and can play a role in cell survival, tumour progression, as well as in drug resistance and chemosensitivity [89,292]. For instance, in chronic lymphocytic leukaemia (CLL) TP53 and ataxia telangiectasia mutated (ATM) aberrations are among the most frequent chromosomal abnormalities. They are considered poor outcome predictors and can cause clonal evolution and chemoresistance [297,298].

Mutations in genes involved in the DNA repair pathway can also have downstream effects such as alterations in metabolic genes leading to dysregulated metabolism. Given the variety of repair mechanisms, different DDR defects will lead to distinct metabolic reprogramming in cells. Although DDR mechanisms and cancer metabolism are well-studied biology fields, it is still unclear how DNA repair can modulate cellular metabolism, especially in cancer [134].

In this chapter, NMR spectroscopy was used to study examples of DDR alterations and their consequences on the metabolism of haematological cells. The metabolic response to the accumulation of DNA damage in cells was also investigated. Metabolic profiles of cells with a defect in ATM or with a defect in RNase H2 were obtained. The ATM protein is a serine/threonine protein kinase which is activated in response to DNA double-strand breaks

(DSBs) and initiates cell cycle arrest, DNA repair or apoptosis [21]. Ribonuclease H2 (RNase H2) is an enzyme responsible for the removal of RNA from RNA–DNA hybrids formed during replication through the ribonucleotide excision repair (RER) pathway [77]. The objective was to study metabolic signatures associated with defects in the DDR, including defects in ATM and RNase H and identify the metabolic adaptations following the cellular stress caused by an inefficient DNA repair. The metabolism of CLL, multiple myeloma or normal B cell lines as well as primary CLL cells with or without DDR deficiency were studied using 1D ^{1}H NMR spectroscopy to find possible targetable DNA damage metabolic biomarkers. Besides, ^{1}H NMR metabolic profiles of WT and AT LCLs with or without ATM activity and of cell lines after *in vitro* ATM inhibition were obtained. The aim was once again to investigate the metabolic effect of ATM loss, but also to study the impact of the accumulation of endogenous damage caused by ATM inhibition. Also, by inhibiting ATM, it was possible to examine if the metabolic variations in AT-deficient cells are induced by loss of ATM kinase activity.

Finally, the metabolism of cells after *in vitro* radiation as a source of exogenous DNA damage was also examined.

3.2. Results

3.2.1. Metabolic signature of cells with a defect in ATM

To identify metabolic alterations related to defects in ATM, I decided to investigate how metabolism varies between chronic lymphocytic leukaemia and lymphoblastoid cell lines (LCLs) with and without ATM deficiencies. Given CLL cells are prone to display ATM defects, they appeared as a perfect biological material for this NMR study. Exploring ATM alterations in these cells will bring knowledge about the consequence of the loss of ATM in CLL, from a metabolic perspective. LCLs, on the other hand, were EBV-transformed lymphoblastoid B-cell lines derived from healthy donors or ATM-deficient patients with or without residual ATM activity. The objective was to identify metabolic changes between WT and AT LCLs, but also to investigate if the loss of kinase activity causes these metabolic differences. LCLs not only have the advantage of being a source of immortalised proliferating B cells, replicating spontaneously. They also represent a non-cancerous *in vitro* model of WT and ATM-deficient B cells [299]. It is noteworthy as cancer cells often, if not always, exhibit metabolic rewiring, as reviewed in [300–302]. This way, it was possible to study the consequence of loss of ATM on metabolism in cells without cancer metabolic alterations. Supplemental information about the cell lines used within this project can be found in the method section 2.1.

Metabolic profiles of cell lines were obtained using 1D ^{1}H NMR spectroscopy. Cells were cultured for 24 hours before intracellular metabolite extraction using a methanol/chloroform/water extraction, a method used to extract hydrophilic metabolites such as lactate, amino acids, TCA cycle intermediates (polar extracts) and hydrophobic metabolites such as fatty acids and cholesterol (lipid extracts) from the same sample [287,303,304]. The polar phases were studied in every cell lines. Only the lipid content of MEC1 WT and ATM, CII WT and ATM, WT and AT LCLs were analysed. Samples of media were collected at time 24 hours.

To study the metabolome in cell line with a defect in DDR, intracellular and extracellular metabolites were identified in extracts and media, respectively. 1D ^{1}H NMR spectra of CII cells allowed for the identification of 29 polar and five non-polar metabolites in extracts (Figure 3-1), and 20 metabolites in media (Figure 3-2). For the rest of this thesis, metabolites were assigned using the same chemical shifts.

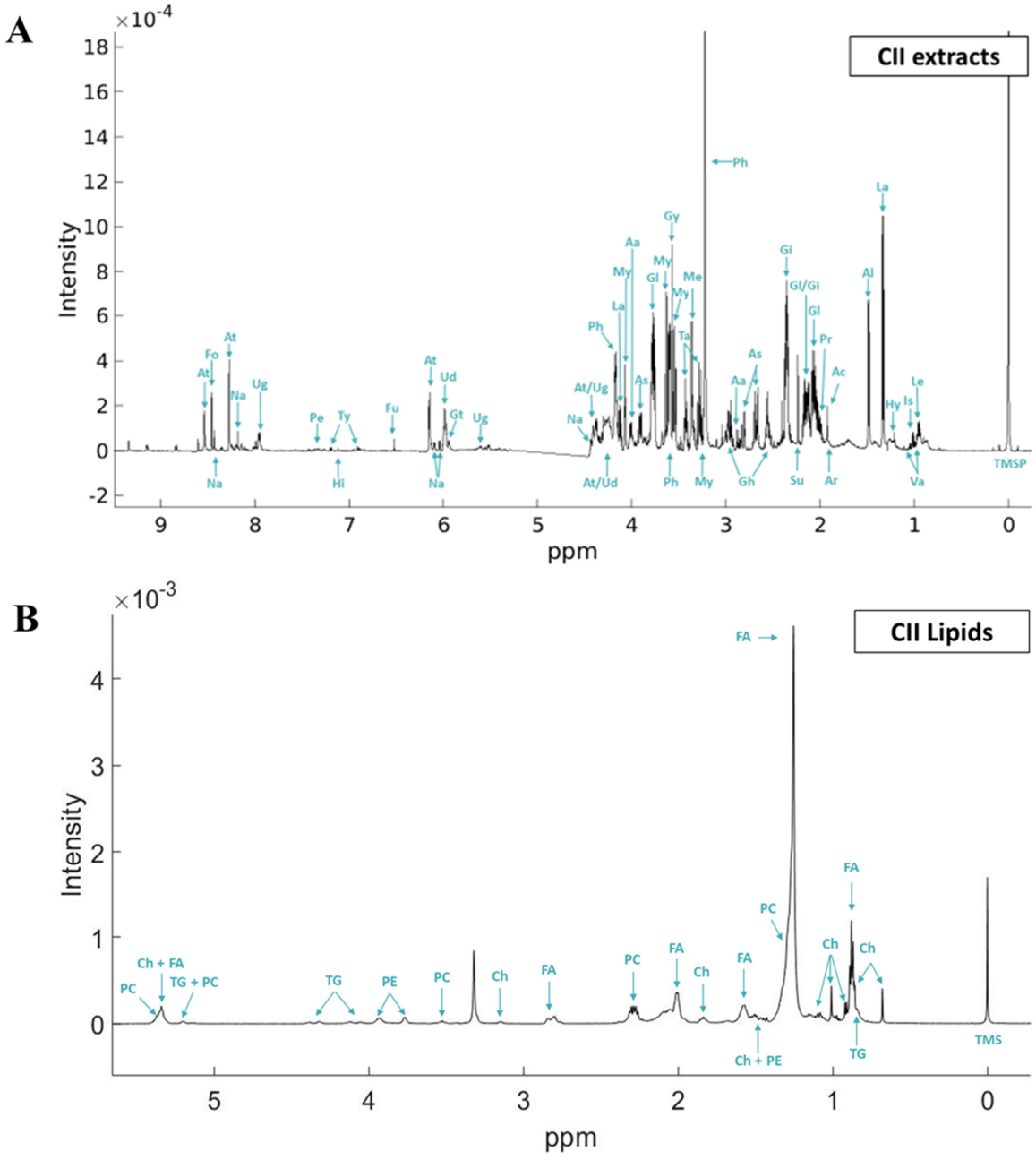

Figure 3-1: 1D ^{1}H-NMR spectrum of CII polar and non-polar extracts.

After processing of the spectra, 29 polar and five non-polar intracellular metabolites were assigned in *Metabolab*. A) Polar extracts. Metabolites identified: Le, Leucine; Va, Valine; Is, Isoleucine; Hy, 3-Hydroxybutyrate; La, Lactate; Al, Alanine; Ar, Arginine; Ac, Acetate; Pr, Proline; Gl, Glutamate; Gi, Glutamine; Su, Succinate; Gh, Glutathione; As, Aspartate; Aa, Asparagine; Ph, Phosphocholine; Ta, Taurine; Me, Methanol; My, Myo-inositol; At, ATP; Ug, UDP-glucose; Ud, UDP, Na, NAD+; GT, GTP; Fu, Fumarate; Ty, Tyrosine; Hi, Histidine; Pe, Phenylalanine; Fo, Formate. B) Non-polar extracts. Metabolites identified: Ch, Cholesterol; FA, Fatty acids/Fatty acyl chains; PC, phosphatidylcholine; PE, phosphatidylethanolamine; TG, triglycerides.

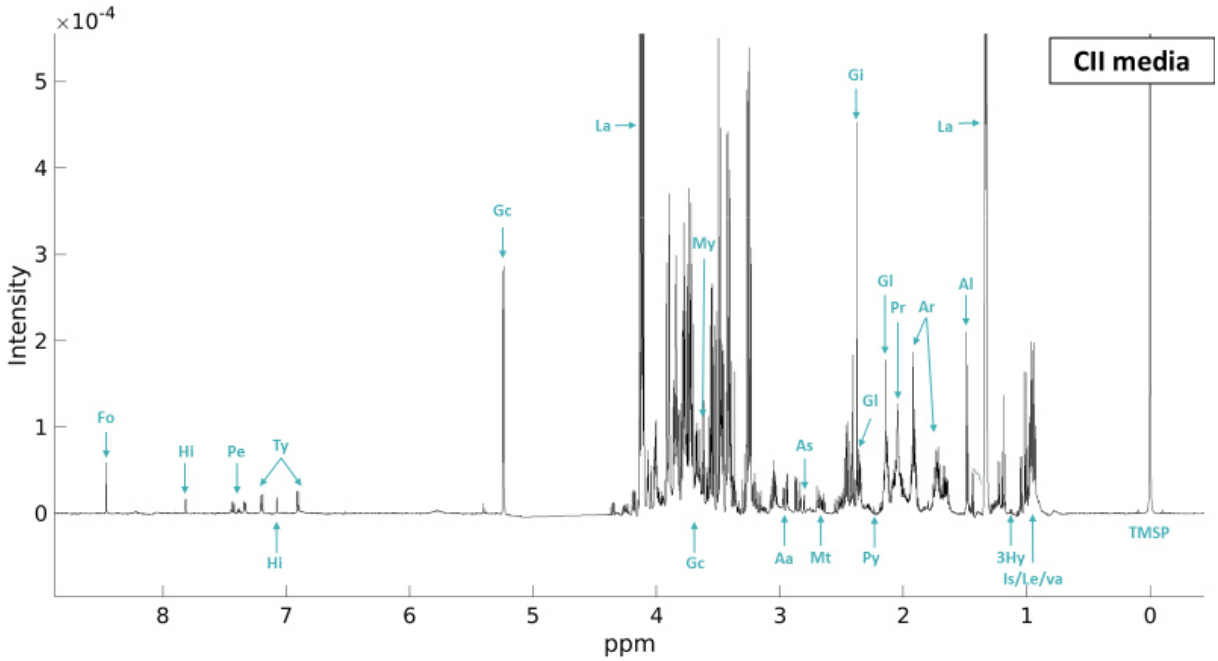

Figure 3-2: 1D ^{1}H-NMR spectrum of a CII media sample.

After processing of the spectra, 20 extracellular metabolites were assigned in *Metabolab*. Metabolites identified: Is, Isoleucine; Le, Leucine; Va, Valine; 3Hy, 3-Hydroxybutyrate; La, Lactate; Al, Alanine; Ar, Arginine; Gl, Glutamate; Pr, Proline; Py, Pyruvate; Gi, Glutamine; Mt, Methionine; As, Aspartate; Aa, Asparagine; Gc, Glucose; My, Myo-inositol; Ty, Tyrosine; Hi, Histidine; Pe, Phenylalanine; Fo, Formate.

After the 1D ^{1}H NMR spectra acquisition of the polar extracts and media samples of MEC1 and CII cells, metabolites were analysed by metabolic groups. Several metabolic differences were observed between polar extracts of WT vs ATM-deficient CLL cells. Some of these differences were common between cell lines such as higher levels of phenylalanine and taurine in both the MEC1 and CII ATM-deficient cell lines (MEC1 and CII ATM) compared to their equivalent WT cell lines (MEC1 and CII WT) (Figure 3-3). Another common alteration was the lower alanine levels in the ATM-deficient cell lines. Additionally, MEC1 ATM cells had lower *myo*-inositol intensity compared to MEC1 WT.

Nonetheless, CII ATM cells seemed to display the opposite effect, with higher *myo*-inositol intensity found in CII ATM in comparison with CII WT. After the lipid extracts analysis, no metabolic changes could be detected between MEC1 WT and MEC1 ATM. Regarding CII cells, CII ATM had higher lipid content than WT CII as demonstrated by the higher levels in cholesterol, fatty acids, phosphocholine and plasmalogen (Figure 3-4). Metabolic variations also existed in the media of WT vs ATM CLL cells, but they varied according to the type of CLL cells studied. The analysis of media samples from MEC1 cells revealed higher intensities in lactate and 3-hydroxybutyrate and lower intensities in asparagine and glucose in MEC1 ATM, which suggests more active glycolysis in MEC1 ATM cells (Figure 3-5). In CII ATM media samples, intensities in several amino acids (leucine, isoleucine, valine, arginine, glutamine, tyrosine, phenylalanine) and glucose levels were higher than in CII WT media. In contrast, glutamate, lactate, alanine, 3-hydroxybutyrate and formate intensities were lower than in the CTL (Figure 3-5).

Metabolic analysis of LCLs revealed increased levels in UDP and glutathione intracellularly and in arginine, glutamate, glutamine, aspartate, proline, succinate and formate extracellularly in ATM-deficient LCLs (AT LCLs) with remaining ATM activity compared to WT LCLs. On

the contrary, AT LCLs conserving some AT activity exhibited lower levels in intracellular leucine, isoleucine, arginine, asparagine, tyrosine, glutamine and in extracellular leucine and 3-hydroxybutyrate compared to WT LCLs. The differences in intracellular polar metabolites between WT LCLs and AT LCLs are shown in Figure 3-6 and Figure 3-7. Extracellular metabolites can be found in Figure 3-8.

AT LCLs with no ATM activity had lower intracellular intensities in amino acids such as isoleucine, glutamine, and asparagine, tyrosine, phenylalanine, in phosphocholine and *myo*-inositol and lower extracellular 3-hydroxybutyrate and formate intensities compared to their WT equivalent. On the other hand, intensities of ATP, and taurine in polar extracts and of leucine, isoleucine, glutamine, and glucose in media were higher in AT LCLs with no ATM activity compared to WT LCLs. Remarkably, AT LCLs without AT activity displayed increased taurine levels and variations in metabolites shown to be involved in the DDR, including increased intracellular intensities in fumarate and decreased intensities in glycine in comparison with both WT LCLs and AT LCLs with residual kinase activity. While the increase in fumarate in AT LCLs without AT activity might be due to its role in DNA repair [147,148], the decrease in glycine intensities might result from an increase in its consumption for nucleotide synthesis, a crucial metabolic pathway in the DDR [149].

Only the lipid content of WT and AT LCLs without residual ATM activity was investigated, but no differences could be found between WT and AT LCLs (Figure 3-7).

Overall the metabolic variations observed in AT-deficient cells suggest a role of ATM in metabolism and could be linked with the loss of ATM kinase activity.

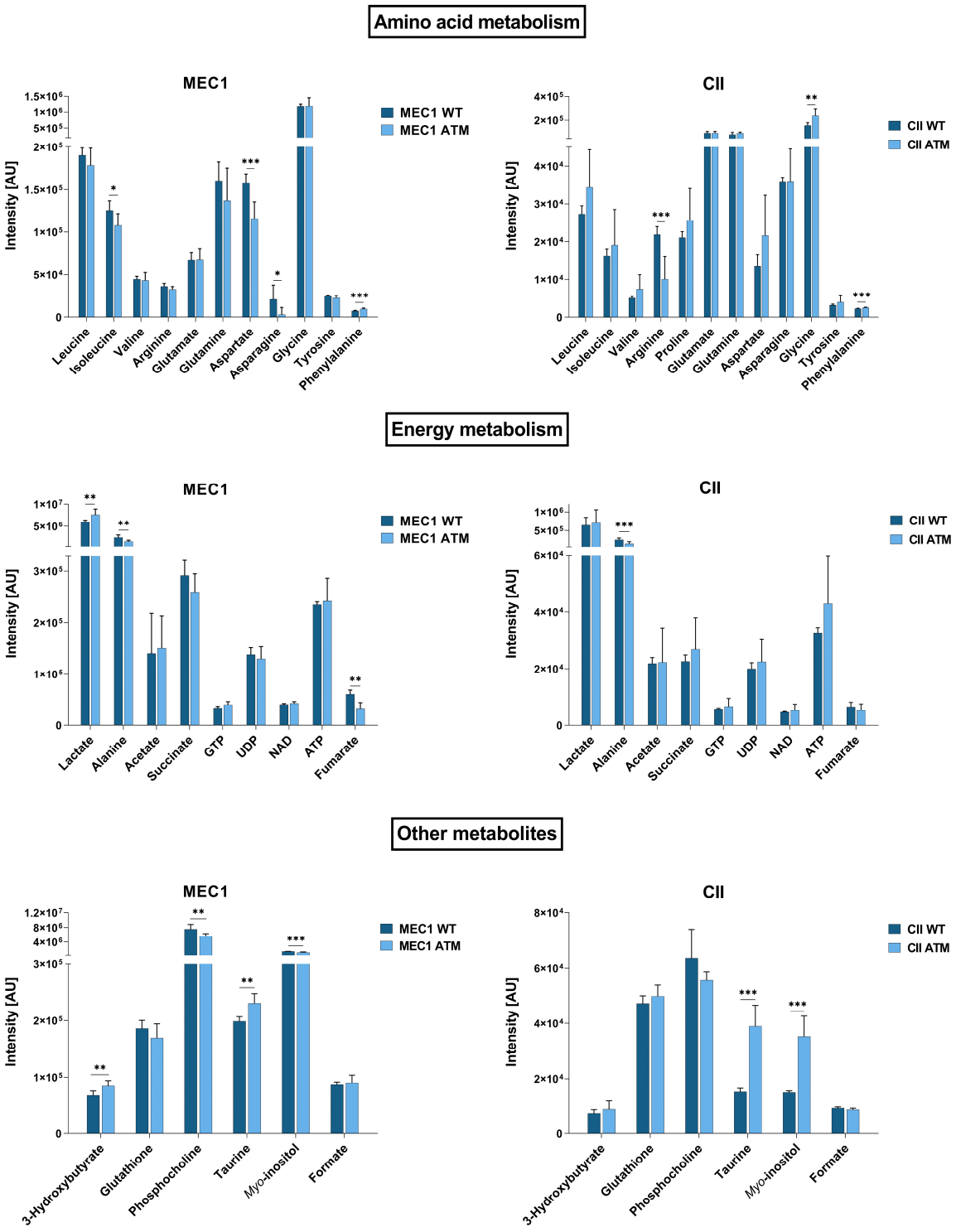

Figure 3-3: Intracellular polar metabolites levels of MEC1 and CII WT and ATM cell lines cultured for 24 hours.

Metabolites were extracted using a methanol-water-chloroform extraction. ^{1}H-NMR spectra were acquired. NMR data were processed and analysed in *Metabolab*. Data are mean of n=6 (MEC1 WT and ATM), n=9 (CII WT), n=8 (CII ATM) independent samples ± standard deviation. *, $P < 0.05$; **, $P < 0.05$; ***, $P < 0.001$ by student's t-test.

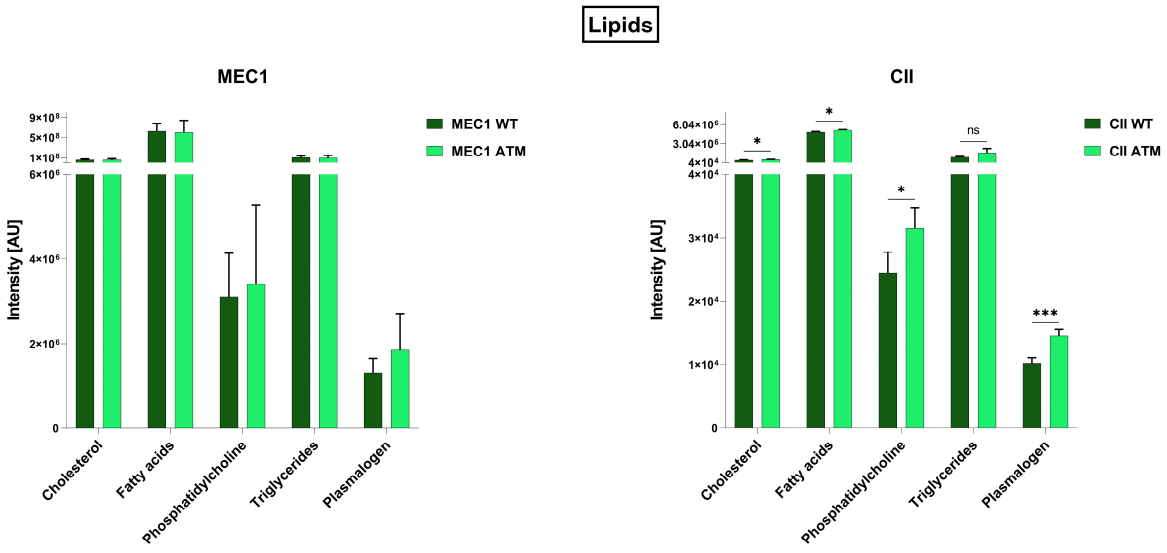

Figure 3-4: Intracellular lipids levels of MEC1 and CII WT and ATM cell lines cultured for 24 hours.

Metabolites were extracted using a methanol-water-chloroform extraction. ^{1}H-NMR spectra were acquired. NMR data were processed and analysed in *Metabolab*. Data are mean of n=6 (MEC1 WT and ATM) and n=3 (CII WT and ATM) independent samples ± standard deviation. *, $P < 0.05$; **, $P < 0.05$; ***, $P < 0.001$ by student's t-test.

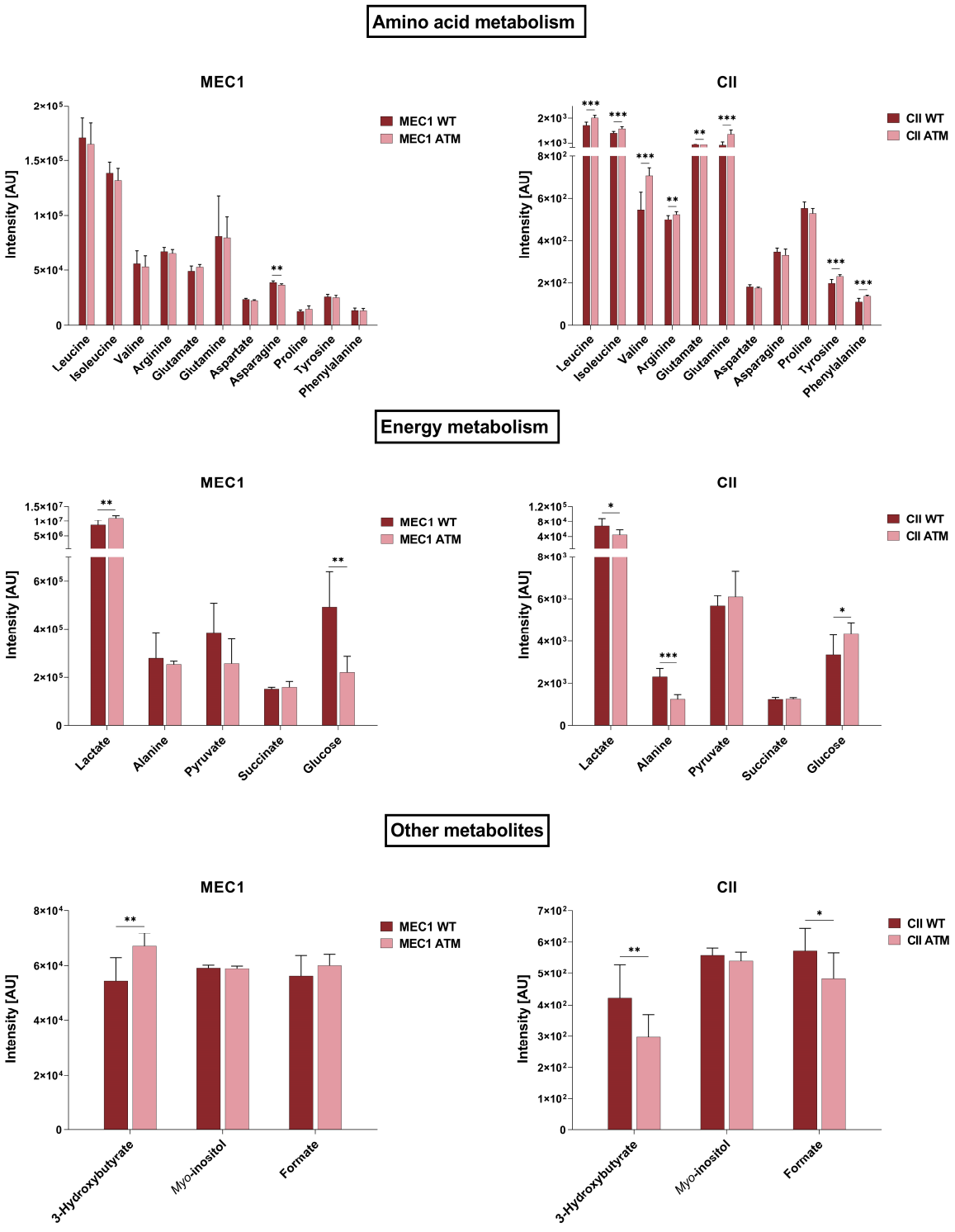

Figure 3-5: Extracellular metabolites levels of MEC1 and CII WT and ATM cell lines cultured for 24 hours.

Media samples were collected at time 24 hours and analysed by ^{1}H-NMR. NMR data were processed and analysed in Metabolab. Data are mean of n=6 (MEC1 WT and ATM), n=9 (CII WT), n=8 (CII ATM) independent samples ± standard deviation. *, $P < 0.05$; **, $P < 0.05$; ***, $P < 0.001$ by student's t-test.

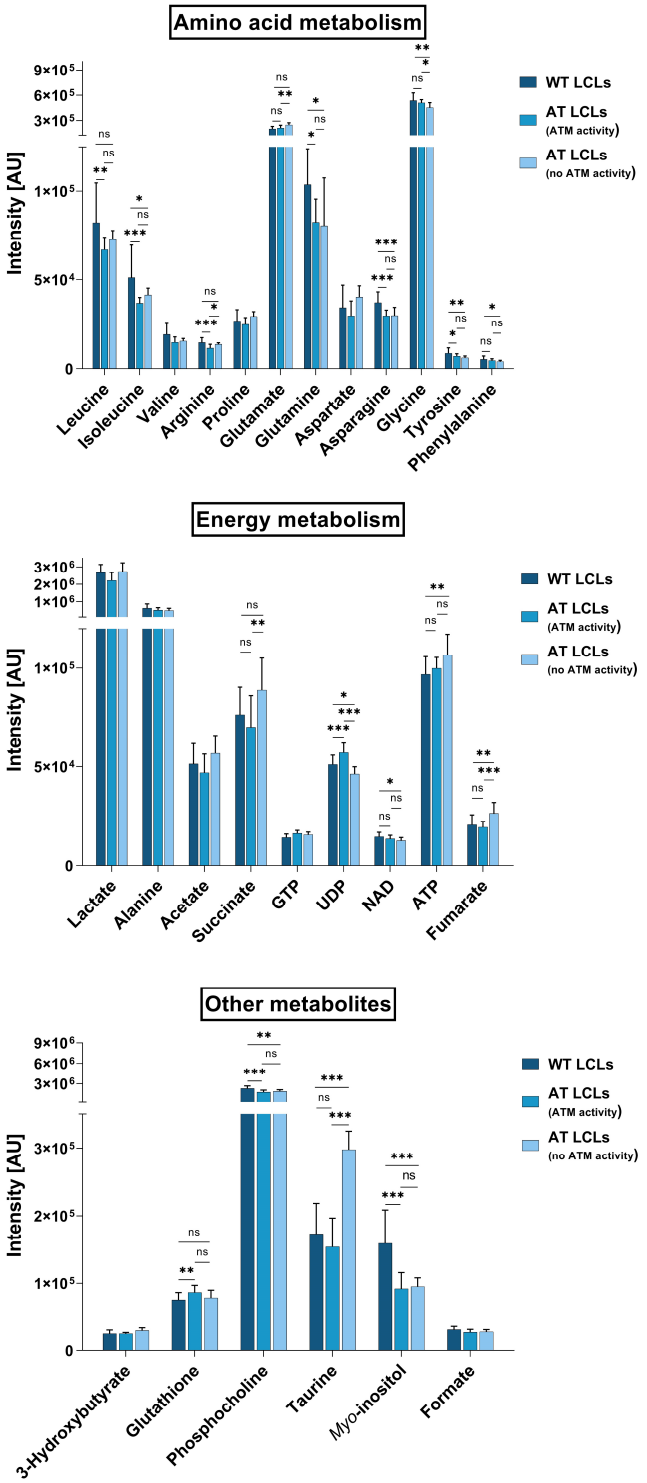

Figure 3-6: Intracellular polar metabolites levels of WT LCLs and AT LCLs with or without residual ATM activity cultured for 24 hours.

Metabolites were extracted using a methanol-water-chloroform extraction. ^{1}H-NMR spectra were acquired. NMR data were processed and analysed in *Metabolab*. Data are mean of n=15 (WT LCLs), n=9 (AT LCLs, ATM activity), n=11 (AT LCLs, no ATM activity) independent samples ± standard deviation. *, $P < 0.05$; **, $P < 0.05$; ***, $P < 0.001$ by ANOVA.

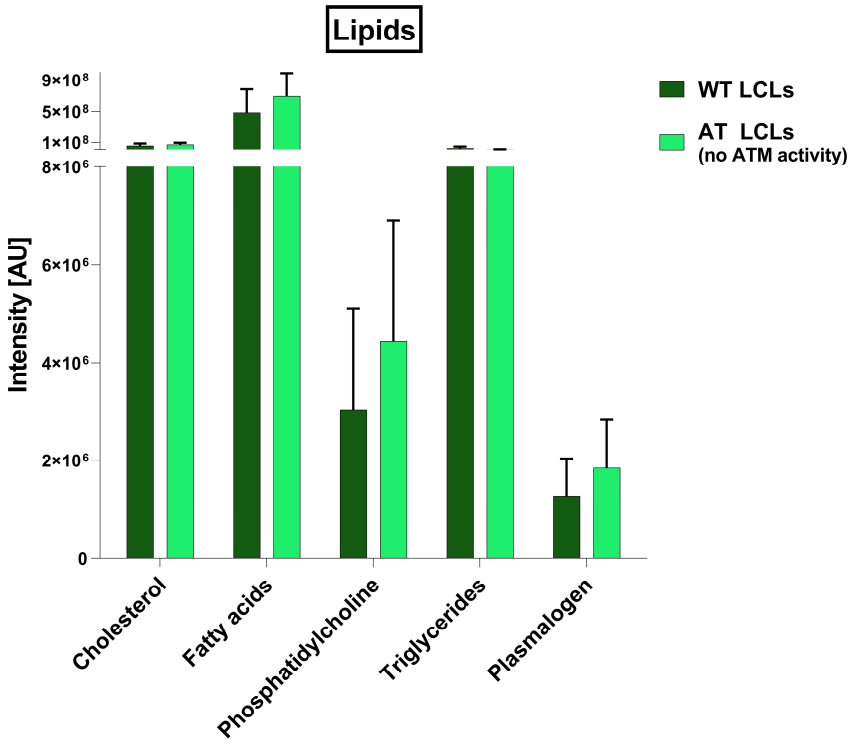

Figure 3-7: Intracellular lipids levels of WT and AT LCLs without residual ATM activity cultured for 24 hours.

Metabolites were extracted using a methanol-water-chloroform extraction. ^{1}H-NMR spectra were acquired. NMR data were processed and analysed in *Metabolab*. Data are mean of n=15 (WT LCLs), and n=11 (AT LCLs, no ATM activity) independent samples ± standard deviation. Student's t-test was used to study the statistical significance and showed no differences.

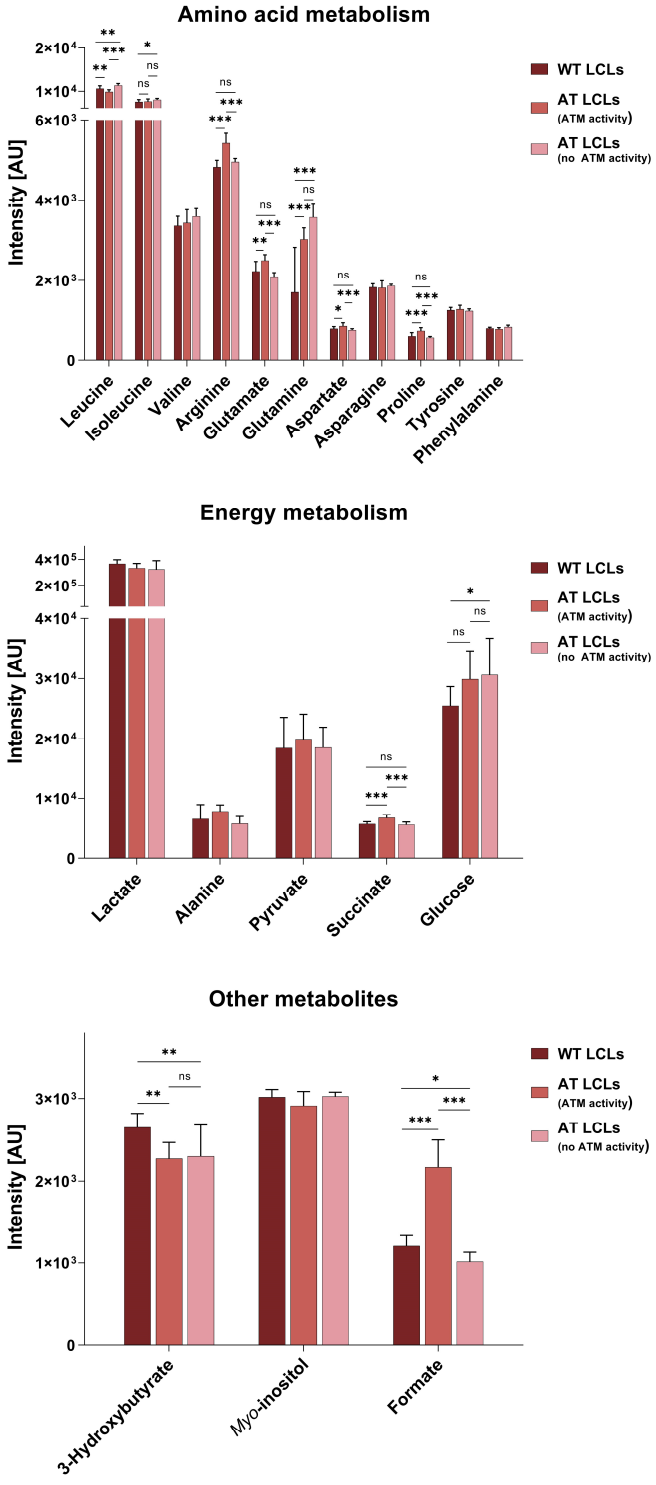

Figure 3-8: Extracellular metabolites levels of WT LCLs and AT LCLs with or without residual ATM activity cultured for 24 hours.

Media samples were collected at time 24 hours and analysed by ^{1}H-NMR. NMR data were processed and analysed in *Metabolab.* Data are mean of n=15 (WT LCLs), n=9 (AT LCLs, ATM activity), n=11 (AT LCLs, no ATM activity) independent samples ± standard deviation. *, $P < 0.05$; **, $P < 0.05$; ***, $P < 0.001$ by ANOVA.

3.2.1. Metabolic signature of cells with a defect in RNase H2

To identify metabolic modifications linked with altered repair excision pathway as an example of DDR alteration, metabolic differences between CLL and multiple myeloma cell lines with and without RNase H2 deficiencies were investigated. Decision to study RNase H2 deficiency in CLL and multiple myeloma cell lines was motivated by the high incidence of RNase H2 mutations found in haematological cancers and mostly because, despite the progress made in understanding the role of RNase H2, only a few studies have investigated alternative cellular functions of RNase H2 [86,87].

By comparing the metabolic profile of WT cells with RNase H2 cells, the aim was to explore a potential metabolic role for RNase H2. CLL and multiple myeloma cells were cultured for 24 hours before metabolite extraction. Samples of medium were collected at 24 hours. All samples were analysed by ^{1}H-NMR.

The analysis of the polar extract samples revealed that MEC1 with RNase H2 deficiencies (MEC1 RNASEH2-KO) had lower intracellular levels in several amino acids (leucine, isoleucine, proline, aspartate, asparagine, tyrosine, phenylalanine) as well as in succinate and UDP compared with MEC1 WT cells. However, MEC1 RNASEH2-KO intracellular levels in arginine, glutamine, acetate, glutathione, phosphocholine, taurine and *myo*-inositol were higher compared to MEC1 WT (Figure 3-9). In the media samples, only an increase in glutamine levels and a decrease in aspartate were observed in RNASEH2-KO vs MEC1 WT (Figure 3-10).

In JJN3 cells lacking RNase H2 (JJN3 RNASEH2-KO), most of the intracellular levels in amino acids were reduced as well as in succinate and glutathione. On the contrary, levels for phosphocholine, taurine and *myo*-inositol were higher than in JJN3 with intact RNase-H2 (Figure 3-11). Extracellular metabolite analysis in JJN3 RNASEH2-KO revealed higher levels of pyruvate, but lower levels in amino acids and glucose than in JJN3 WT (Figure 3-12).

Globally, it seems that the differences observed in RNase H2-deficient cells compared to the WT were the consequence of the loss of RNase H2 and encourage the idea of metabolic functions of RNase H2.

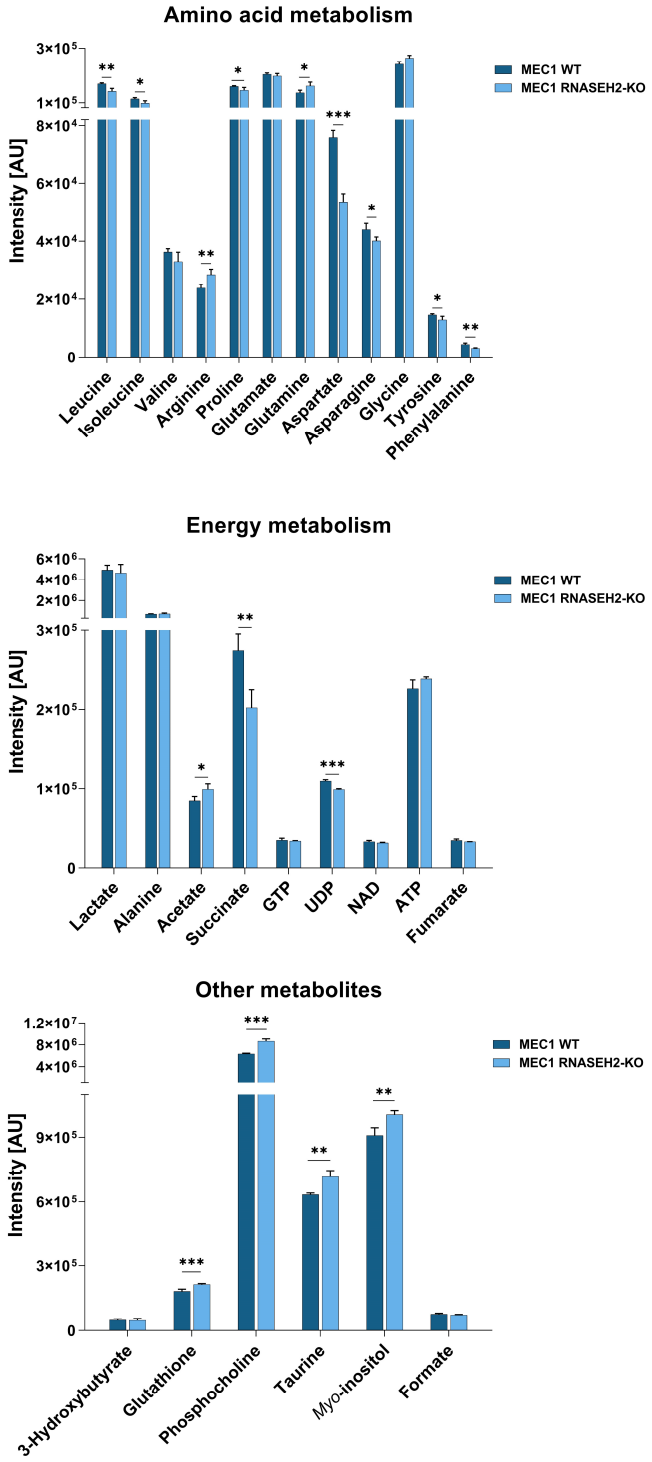

Figure 3-9: Intracellular polar metabolites levels of MEC1 WT and RNASEH2-KO cultured for 24 hours.

Metabolites were extracted using a methanol-water-chloroform extraction. ^{1}H-NMR spectra were acquired. NMR data were processed and analysed in *Metabolab*. Data are mean of n=4 independent samples ± standard deviation. *, $P < 0.05$; **, $P < 0.05$; ***, $P < 0.001$ by student's t-test.

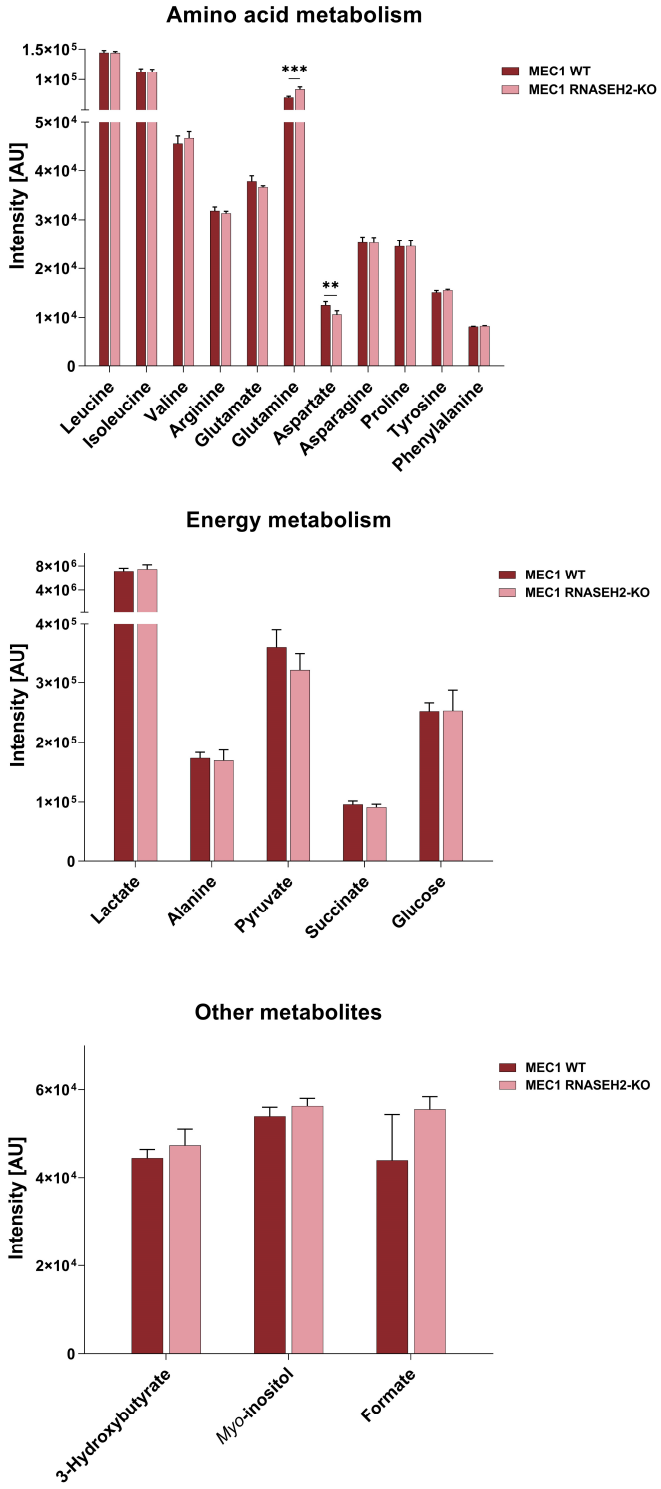

Figure 3-10: Extracellular metabolites levels of MEC1 WT and RNASEH2-KO cell lines cultured for 24 hours.

Media samples were collected at time 24 hours and analysed by ^{1}H-NMR. NMR data were processed and analysed in Metabolab. Data are mean of n=4 independent samples ± standard deviation. *, $P < 0.05$; **, $P < 0.05$; ***, $P < 0.001$ by student's t-test.

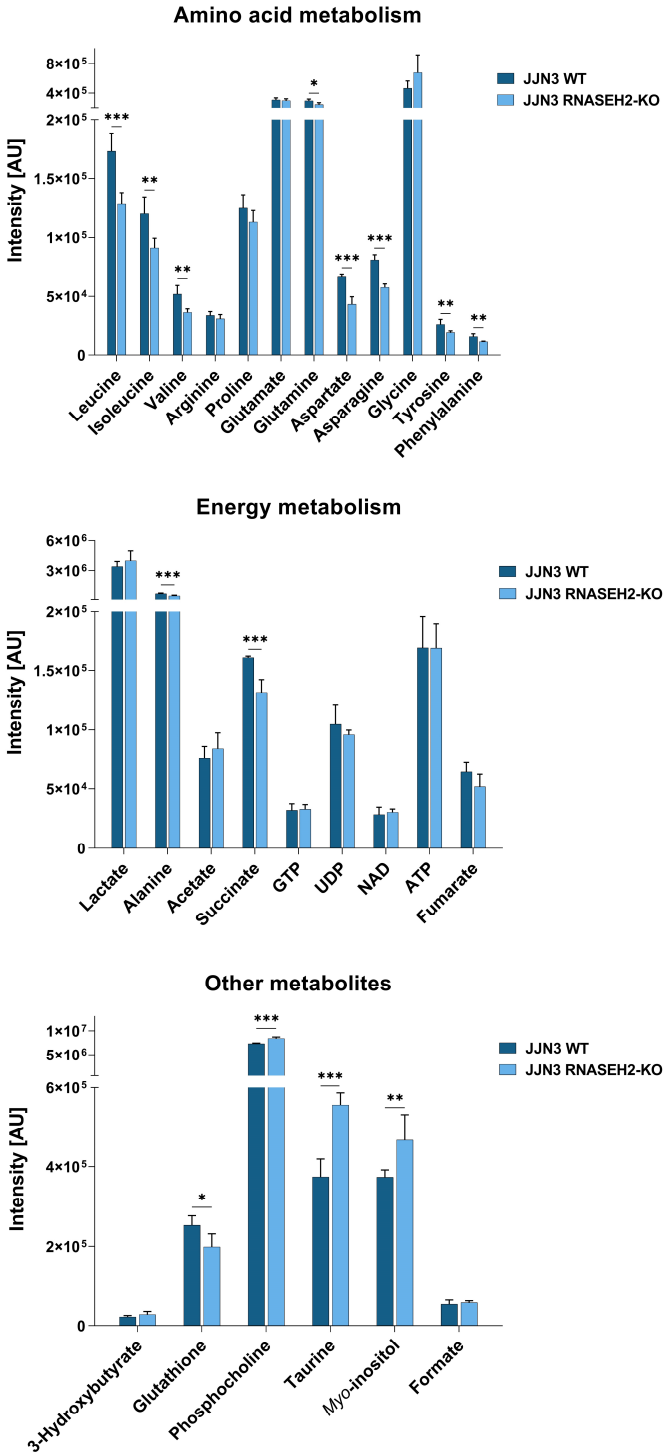

Figure 3-11: Intracellular polar metabolites levels of JJN3 WT and RNASEH2-KO cultured for 24 hours.

Metabolites were extracted using a methanol-water-chloroform extraction. ^{1}H-NMR spectra were acquired. NMR data were processed and analysed in *Metabolab*. Data are mean of n=4 independent samples ± standard deviation. *, $P < 0.05$; **, $P < 0.05$; ***, $P < 0.001$ by student's t-test.

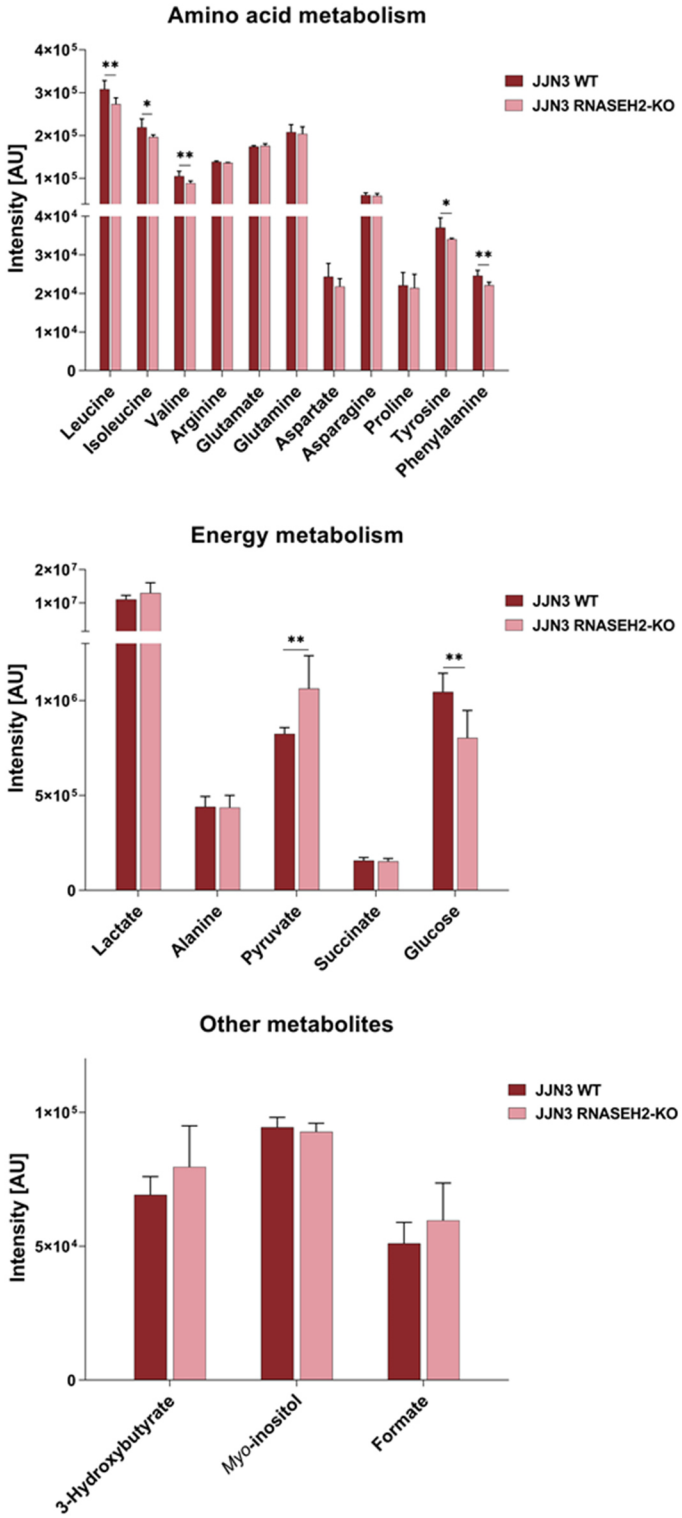

Figure 3-12: Extracellular metabolites levels of JJN3 WT and RNASEH2-KO cell lines cultured for 24 hours.

Media samples were collected at time 24 hours and analysed by ^{1}H-NMR. NMR data were processed and analysed in *Metabolab*. Data are mean of n=4 independent samples ± standard deviation. *, $P < 0.05$; **, $P < 0.05$; ***, $P < 0.001$ by student's t-test.

3.2.2. Taurine, a metabolite of interest?

Taurine is one of the four common sulphur-containing amino acids [238]. In the human body, most of the taurine present is acquired from external nutrients. Taurine can also be synthesized from methionine and cysteine [240]. Although taurine is not incorporated into proteins, is has been suggested to play a role in many biological functions such as an osmoregulator, antioxidant, neuroprotector or precursor for bile salt synthesis [240,241]. High levels of taurine have been found in some cancers and can be used as a tumour biomarker. Nonetheless, the question of the role of taurine in cancer remains unanswered today.

In the previous section, higher intracellular taurine levels were detected in all DDR-deficient cell lines in comparison with the WT cell lines (Figure 3-13). To validate the taurine assignment, an NMR spectrum of a taurine sample constituted of 50 mM taurine in dH_2O/10%(v/v) NMR buffer was acquired. With this method, it was possible to confirm taurine appeared as two triplets at 3.2 and 3.4 ppm, respectively, in the 1D ^1H NMR spectra (Figure 3-14A). Taurine peaks were also visible at 3.2 and 3.4 ppm in all DDR-deficient cell lines as confirmed by the overlapping of the NMR spectra with the taurine profile in *Chenomx* (Figure 3-14B).

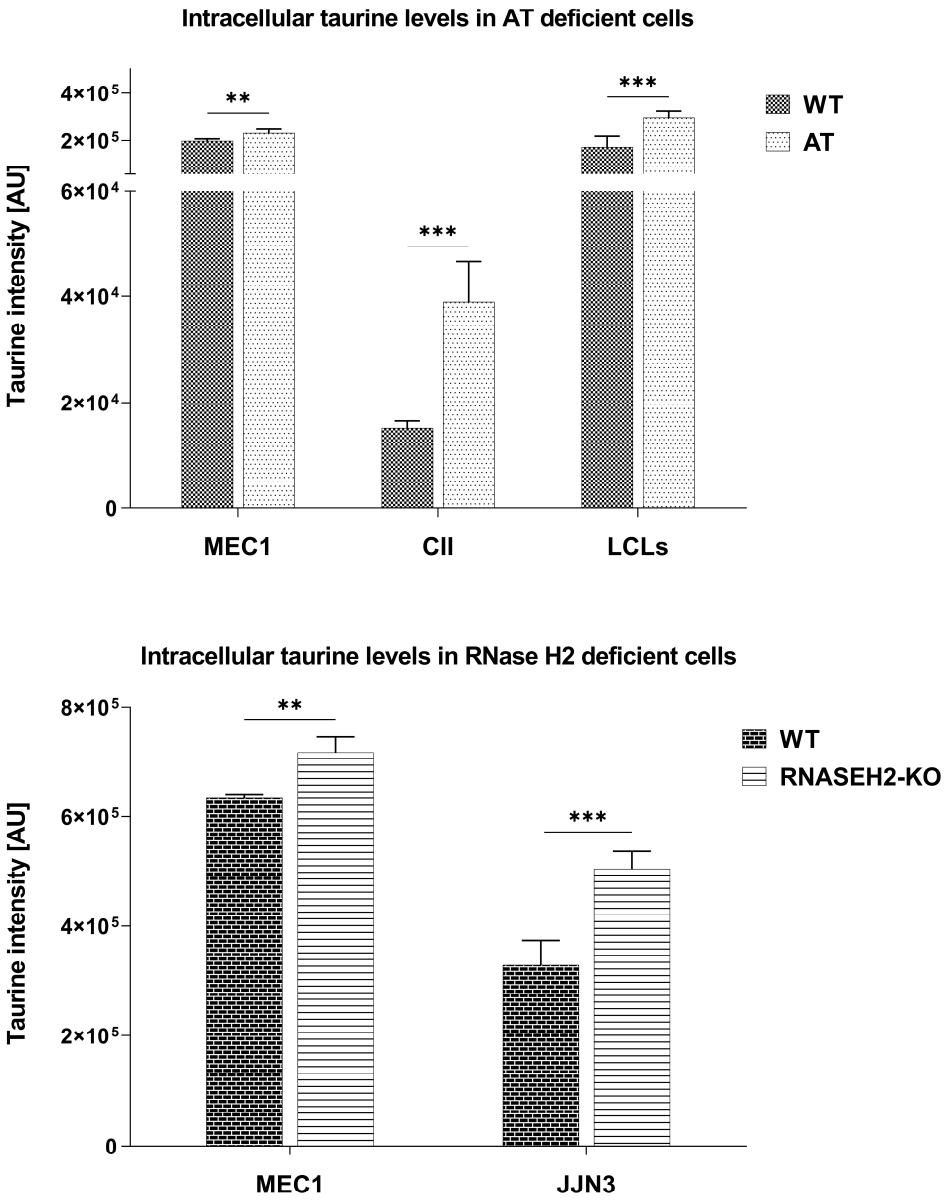

Figure 3-13: Cells with a defect in the DNA damage response exhibit higher intracellular taurine intensities.

Taurine levels were obtained from ^{1}H-NMR spectra in *Metabolab* after metabolites extraction, ^{1}H-NMR spectra acquisition and processing. Data are mean of n=6 (MEC1 WT and ATM), n=9 (CII WT), n=8 (CII ATM), n=15 (WT LCLs), n=11 (AT LCLs, no ATM activity), n=4 (MEC1 WT and RNASEH2-KO), n=4 (JJN3 WT and RNASEH2-KO) independent samples ± standard deviation. *, $P < 0.05$; **, $P < 0.05$; ***, $P < 0.001$.

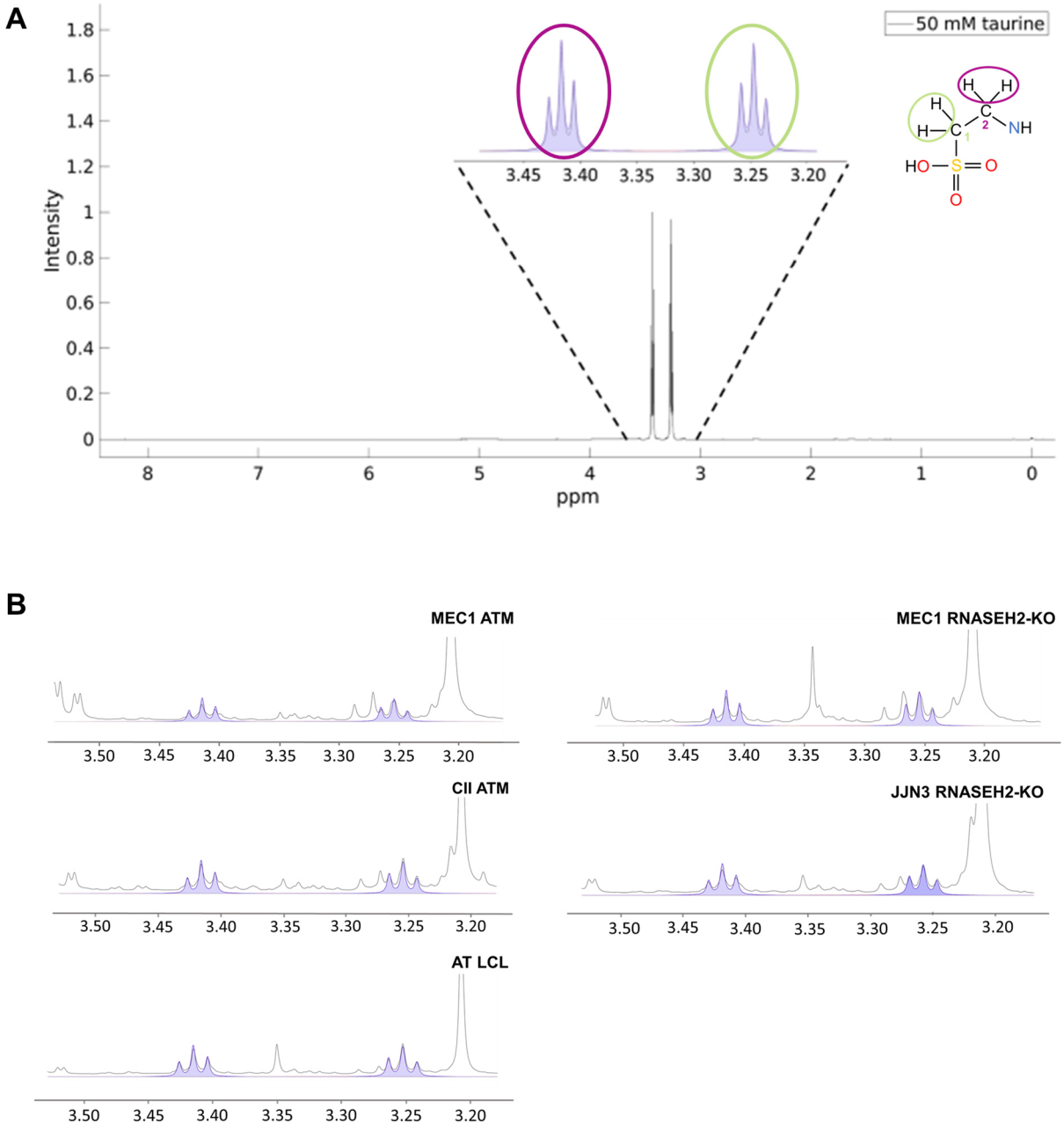

Figure 3-14: 1D ^{1}H-NMR spectra of taurine in NMR buffer and of taurine regions in cell extracts.

A) 1D ^{1}H-NMR spectrum of 50 mM taurine in dH_2O/10% NMR buffer. Two taurine triplets at 3.2 and 3.4 ppm were visible in the 1D ^{1}H NMR spectrum and corresponded to the ^{1}H signals in C1 (green) and C2 (fuchsia). B) Taurine regions in NMR spectra from polar extracts of DDR-deficient cells lines: MEC1 ATM, CII ATM, AT LCL, MEC1 RNASH2-KO, JJN3 RNASEH2-KO. After processing of the spectra in Metabolab, taurine peaks (3.4 and 3.2 ppm) were identified using the *Chenomx* assign tool. The peaks in purple represent the expected profile for taurine in *Chenomx* and were overlapped with the NMR spectra.

3.2.3. Effect of *in vitro* DNA damage exposure on metabolism

In this section, the effect of a DNA damaging agent on metabolism was studied. For this, WT and DDR-deficient cells were exposed to ionising radiation, known to induce DNA double-strand breaks. This experiment was driven by the increased taurine levels observed in DDR-deficient cells, suggesting that high levels of DNA damage is associated with an increase in taurine intensities. The aim was to examine if an exogenous source of DNA damage could affect the level of taurine in cells.

Cells were treated with 10 Gy *in vitro* radiation to study the effect of ionising radiation on the metabolism of WT and DDR-deficient cells. After the IR treatment, cells were kept in culture for 24 hours before analysing the intracellular metabolites with ^{1}H-NMR.

In both WT LCLs, taurine was increased after IR but was only found to be statistically significant for one of the WT LCLs. In JJN3 WT cells, taurine was significantly increased after the IR treatment. In cell lines with a DDR defect, there were no differences in taurine intensities before or after irradiation (Figure 3-15).

Overall, these results suggest that taurine could be increased in response to exogenous DNA damaging agents.

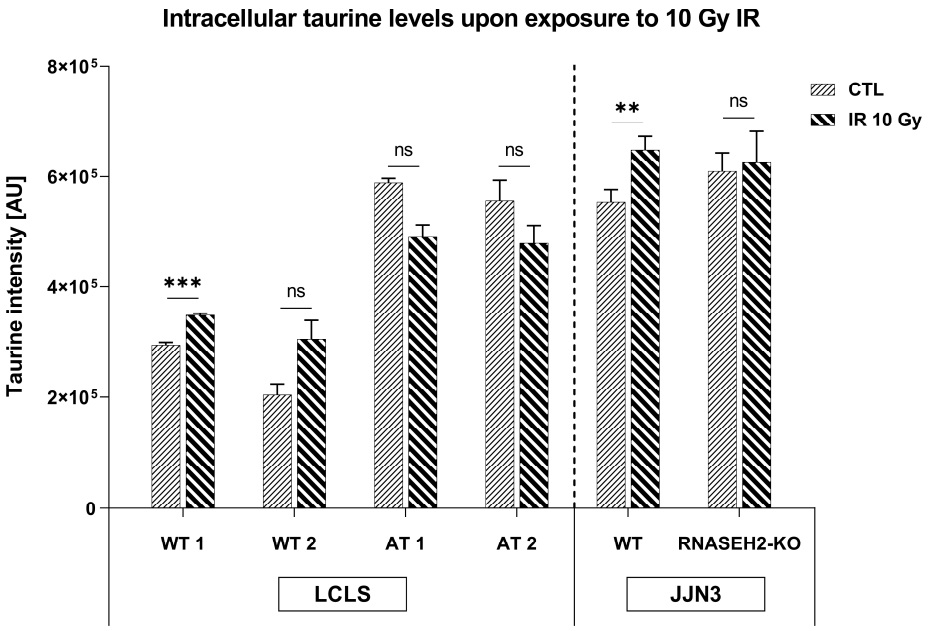

Figure 3-15: Intracellular taurine levels after inducing DDR *in vitro* in WT and ATM or RNASEH2-KO deficient cell lines.

Cells were treated with 10 Gy ionising radiation and kept cells in culture for 24 hours. The intracellular metabolic profiles were obtained by NMR spectroscopy. Taurine levels were obtained from ^{1}H-NMR spectra in *Metabolab* after metabolites extraction, ^{1}H-NMR spectra acquisition and processing. Data are mean of n=3 independent samples ± standard deviation. *, $P < 0.05$; **, $P < 0.05$; ***, $P < 0.001$ by student's t-test.

3.2.4. Metabolic changes upon ATM inhibition

Higher levels of taurine were measured in cells with a DDR defect and when DNA damage was induced using exogenous sources. Therefore, this section aimed at studying if the inhibition of the ATM repair pathway, causing accumulation of endogenous damage, would increase taurine levels. Another objective was to research a possible role for ATM kinase activity in the modulation of intracellular taurine levels.

First, I investigated the dose of inhibitors that was necessary to suppress the background signal of ATM and monitored cell growth and viability in cells incubated with ATM inhibitor KU-60019 or AZD0156. Then, the intracellular and extracellular metabolic profiles of cell lines after four days incubation with KU-60019 or AZD0156 were obtained using 1D ^{1}H NMR spectroscopy.

To verify the ability of KU-60019 or AZD0156 to inhibit irradiation-induced activation of ATM protein kinase, Western blotting was used. Western blotting of ATM in WT LCLs cell lysates after ATM inhibition using 0-3 μM KU60019 or AZD0156 resulted in 3 μM being the lower dose to inhibit the ATM kinase activity completely. Western blotting of ATM in CII WT cell lysates using 0-10 μM ATM inhibitors also revealed that 3 μM was the lowest concentration that fully inhibited ATM activity (Figure 3-16).

Following the assessment of the optimal concentration of ATM inhibitor to use, cell viability of CII WT and a WT LCL was measured over 96 hours using 3 μM of both ATM inhibitors. The goal was to ensure high cell viability was maintained throughout the experiment and find a time point where cells were proliferating. I assumed that this time point corresponds to the cellular metabolic adaptation to the loss of ATM. Results in Figure 3-16 revealed that viability was approximately 95% during the whole experiment. Cells seemed to proliferate slower than

the control over the first 48 hours. However, cells recovered proliferation rate after 48 hours. Following these results, 96 hours was chosen as the time point for the NMR experiments.

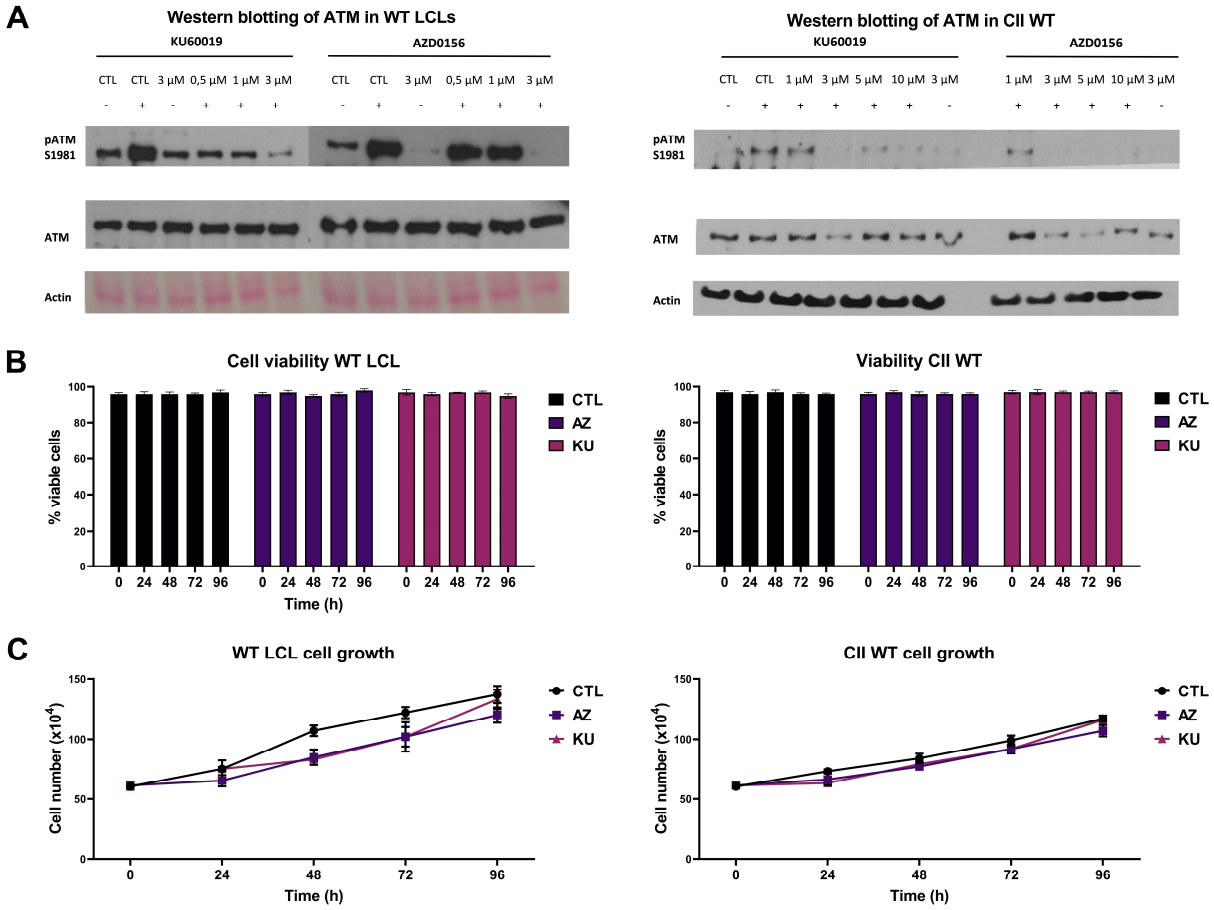

Figure 3-16: Western blot, viability and growth curve of CII WT and WT LCL after ATM inhibition.

A) Analysis of ATM protein by Western blot of WT LCL and WT CII cells. Cells were exposed to increased doses of KU60019 and AZD0156 for 1 hour followed (+) or not (-) by exposure to in *vitro* radiation (10Gy). The protein content was extracted 1 hour following irradiation, and ATM protein expression was assessed by Western blot. Actin was used as a loading control. B) Cell viability of WT CII and LCL over 96 hours treatment with ATM inhibitors. Approximatively, $6x10^5$ cells were transferred in a flask in RPMI with 3 µM DMSO (CTL), 3 µM AZD0156 or 3 µM KU60019. Results are mean of n=3 independent samples ± standard deviation. Cells were counted every day, and cell viability was assessed using trypan blue assay. C) Growth curves of WT CII and LCL over 96 hours treatment with ATM inhibitors. Growth curves were obtained by plotting the number of cells counted every day during treatment with AZD0156 or KU60019. Results are mean of n=3 independent samples ± standard deviation.

After finding an optimal dose for the inhibitors and choosing a time point where cells have adapted to the loss of ATM, ^{1}H-NMR spectra of WT and ATM-deficient CII cells and LCLs after 96 h of ATM inhibition were acquired.

The comparison of the intracellular metabolic profile of all the WT cell lines revealed an increase in intracellular taurine levels after ATM inhibition with KU60019 and AZD0156. On the contrary, ATM-deficient CII and LCL cell lines did not show any differences in taurine levels before and after ATM inhibition (Figure 3-17). These results could be suggesting that ATM deficiency is related to higher taurine levels. Besides, inhibiting ATM in already ATM-deficient cells does not yield an increase in taurine, confirming that: (i) these cells have no ATM activity; and, (ii) the rise in taurine is only caused by ATM inhibition and is not a side effect of the inhibitor.

Interestingly, the analysis of the extracellular metabolite levels revealed significantly higher glucose and lower lactate levels in CII WT cell lines upon ATM inhibition compared to the control, which indicates lower glycolytic activity. A similar tendency was observed in the two WT LCLs, although the results were not statistically significant (Figure 3-18).

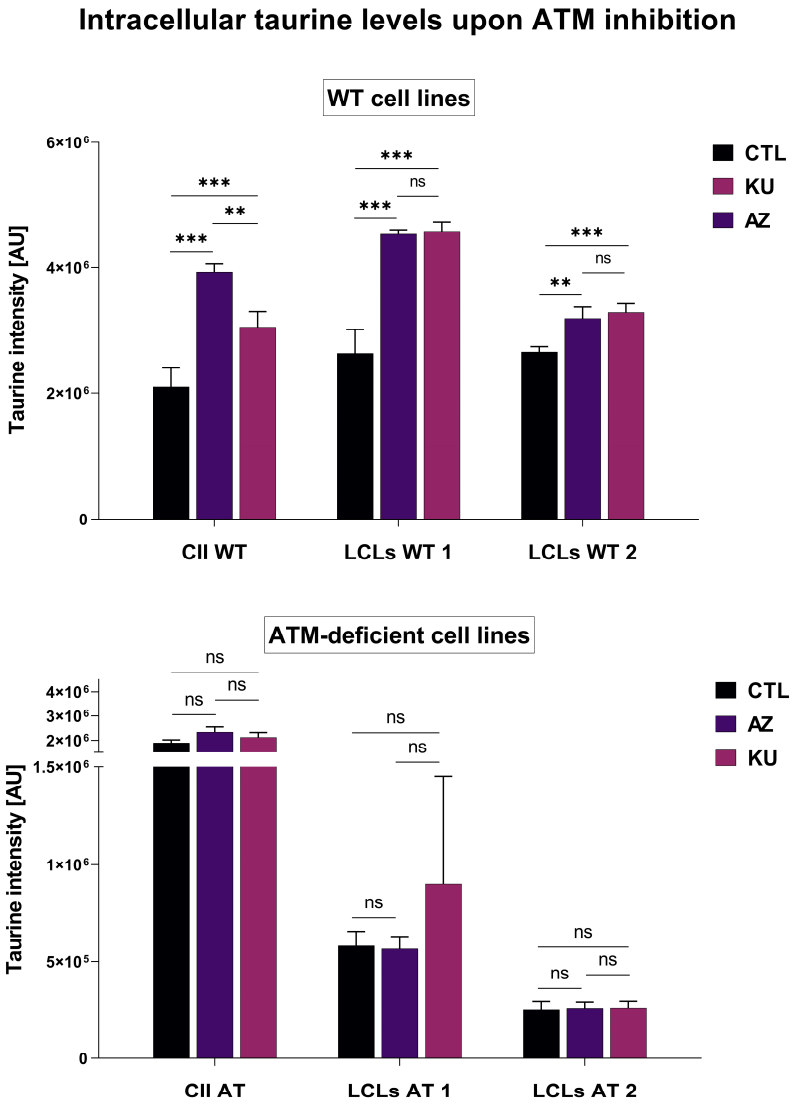

Figure 3-17: Effect of ATM inhibition on intracellular taurine levels in WT and AT-deficient cell lines.

Cells were maintained in culture in classic RPMI with 3 µM DMSO (CTL), AZD0156 (AZ) or KU60019 (KU). Metabolic content was extracted after 96 hours and analysed by 1D ^{1}H NMR. Taurine levels were obtained from ^{1}H-NMR spectra after processing in *Metabolab*. Bar graphs are mean of n=3 independent samples ± standard deviation. *, $P < 0.05$; **, $P < 0.05$; ***, $P < 0.001$ by ANOVA.

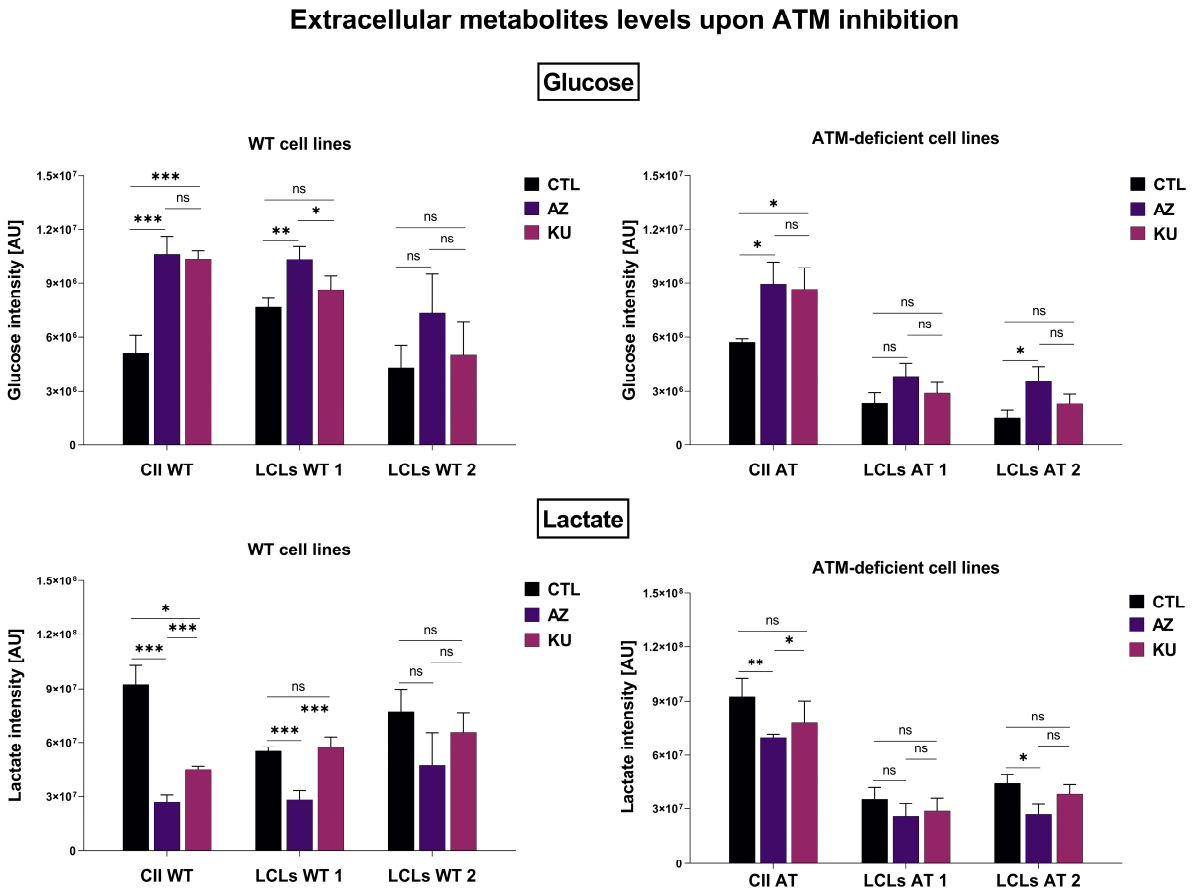

Figure 3-18: Effect of ATM inhibition on extracellular metabolites in WT and AT-deficient cell lines.

Cells were maintained in culture in classic RPMI with 3 µM DMSO (CTL), AZD0156 (AZ) or KU60019 (KU). Media samples were collected after 96 hours and analysed by 1D ^{1}H NMR. Glucose and lactate levels were obtained from ^{1}H-NMR spectra after processing in *Metabolab*. Bar graphs are mean of n=3 independent samples ± standard deviation. *, $P < 0.05$; **, $P < 0.05$; ***, $P < 0.001$ by ANOVA.

3.2.5. ATM deficiency in primary CLL cells

After having characterised the metabolic profile of CLL cell lines with a defect in DDR, I wanted to study whether similar metabolic changes could be generalised in primary ATM-deficient CLL cells. Although gene expression levels following the loss of ATM in primary CLL had already been investigated by Stankovic and co-workers [305], the metabolic profile of primary CLL upon ATM defects had not been studied before by our group.

To study the metabolic consequences of the loss of ATM in primary CLL cells, 1D ^{1}H NMR spectra of ATM-deficient and WT primary CLL samples were compared. The effect of *in vitro* radiation on the metabolism of primary CLL was also studied.

Given the importance of choosing the good cellular material for NMR experiments [289], a first experiment to decide on the type of CLL samples to use was conducted. The metabolic profiles of B-cells after 24 hours of their isolation from the blood of patients diagnosed with CLL (fresh sample) were compared with the same cells after 24 hours thawing (frozen sample). To assess whether freezing primary cells could affect their metabolism, after density gradient centrifugation, half of the mononuclear cells were kept in culture for 24 hours, and their metabolic content was extracted. The other half of the cells were frozen. Later, the frozen cells were thawed, kept in culture for 24 hours and their metabolic profile was obtained using 1D ^{1}H NMR spectroscopy. Only metabolic differences in glutamate and glutamine were observed between fresh and frozen primary CLL cells. Taurine levels did not seem to be affected by the freezing process (Figure 3-19). For this reason, and because working on frozen samples offers more logistical flexibility, I decided to use frozen primary CLL cells to investigate the differences in taurine between WT and AT primary CLL cells.

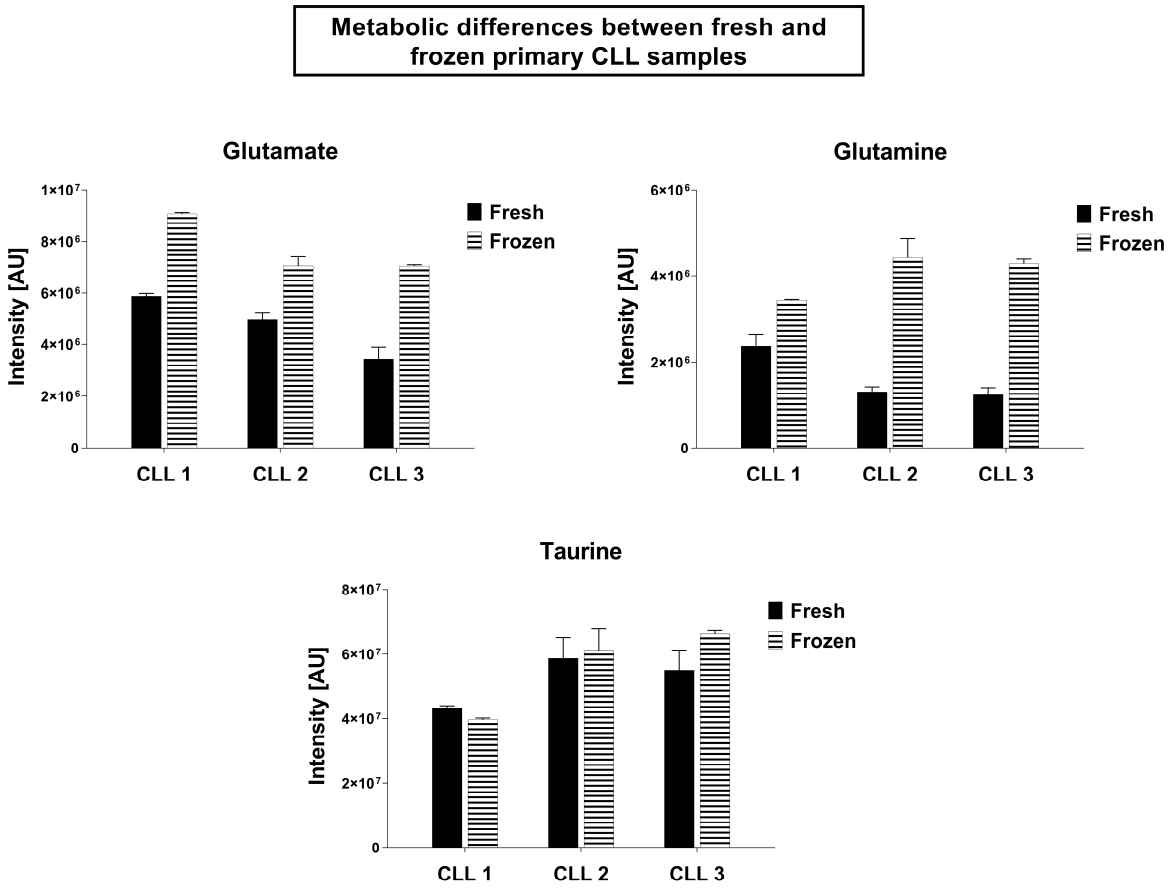

Figure 3-19: Differences in the metabolic profile of fresh and frozen primary CLL cells.

Metabolites of primary CLL B-cells were extracted after 24 hours of their isolation from the blood of patients diagnosed with CLL (fresh sample) or 24 hours after 24h thawing (frozen sample). ^{1}H-NMR spectra of fresh and frozen samples were acquired. Glutamate, glutamine, and taurine levels were obtained from ^{1}H-NMR spectra after processing in *Metabolab*. Data are mean of n=2 independent samples.

Following the experimental set up described in the previous sections, WT and ATM-deficient primary cells were cultured for 24 hours prior to polar intracellular metabolite extraction and analysis by ^{1}H-NMR. Results revealed that no significant differences could be highlighted when comparing NMR profile of WT CLL and ATM CLL cells (Figure 3-20). This result was not expected as cell lines showed an increase in taurine. However, metabolic profile analysis revealed that primary cells have high metabolic variability. The intracellular rise in taurine found in cell lines was not higher than 3-fold, thus, suggesting that it might be in the range of variation between primary cells.

To simulate DDR activation in CLL and examine the effect on taurine levels, an experiment where CLL primary cells WT or ATM-deficient were treated with 10 Gy *in vitro* radiation was conducted. After *in vitro* radiation, cells were cultured for 24 hours before polar metabolite extraction and further analysis by ^{1}H-NMR. Among the eight WT CLLs, five had higher taurine levels after IR. Higher taurine levels were also observed in five out of nine ATM-deficient CLLs analysed, although the other four samples presented a twofold decrease in taurine intensities (Figure 3-20).

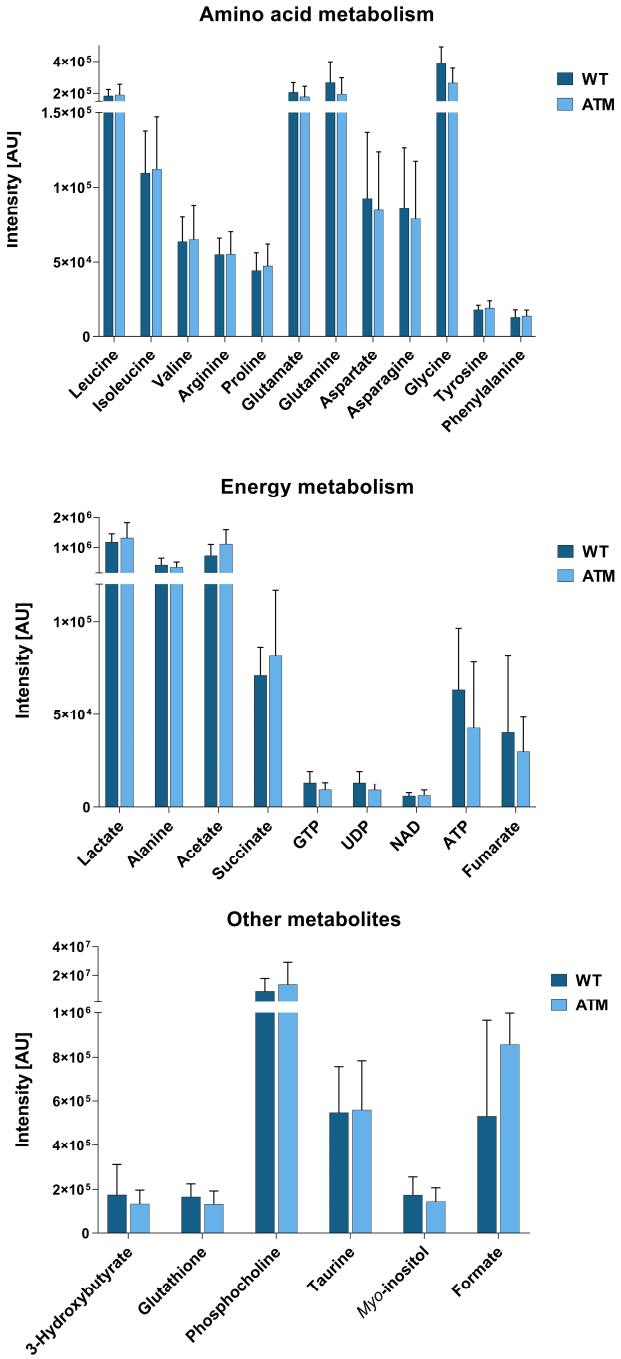

Figure 3-20: Intracellular polar metabolites levels of WT CLL and ATM primary CLL cultured for 24 hours.

Metabolites were extracted using a methanol-water-chloroform extraction. ^{1}H-NMR spectra were acquired. NMR data were processed and analysed in *Metabolab.* Data are mean of n=8 (WT CLL) and n=9 (ATM CLL) independent samples ± standard deviation. Student's t-test was used to study the statistical significance and showed no differences.

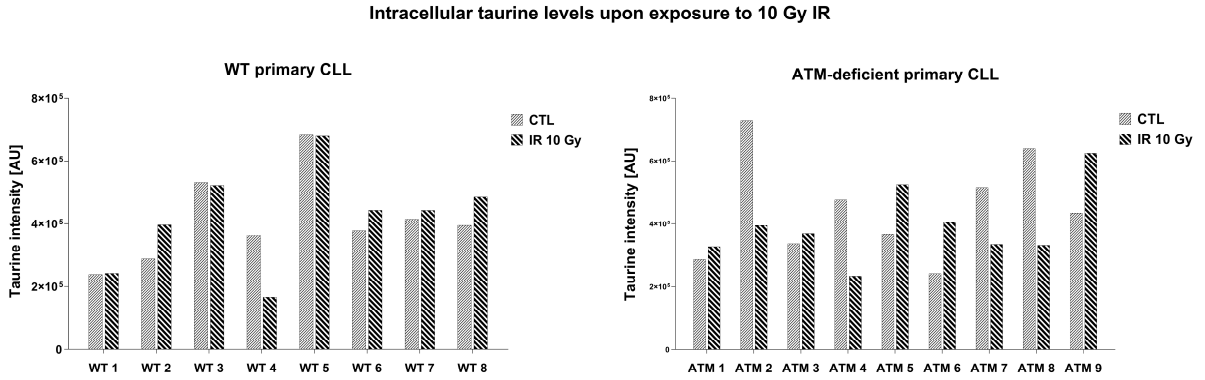

Figure 3-21: Intracellular taurine intensities after inducing DNA damage response *in vitro* in primary CLL cells.

CLL cells were treated with 10 Gy ionising radiation and kept cells in culture for 24 hours. Taurine levels were obtained from ^{1}H-NMR spectra in *Metabolab* after metabolites extraction, ^{1}H-NMR spectra acquisition and processing. Bar graphs show taurine levels for 8 independent WT (left) and 9 AT primary CLL (right).

3.3. Discussion

3.3.1. ATM and RNase H2 deficient cells exhibit higher intracellular levels of taurine

In this chapter, metabolite concentrations were analysed by NMR in extracts and media samples from ATM- and RNase H2-deficient cells to study the metabolic changes for examples of DNA damage response defects in different cell lines, including CII, multiple myeloma, and lymphoblastic cell lines. The main finding was the higher taurine levels in all DDR-defective cell lines compared to the control.

Apart from its function in DNA repair, ATM is suspected of having a role in cellular metabolism, reviewed in [153] and [306]. The suspected metabolic functions of ATM include (I) regulation of the PPP by activation of glucose-6-phosphate dehydrogenase [70]; (II) regulation of glycolysis [154], (III) glucose intolerance and insulin resistance [223], (IV) ROS sensing and activation through oxidative stress [307]. Therefore, it was expected that the absence of ATM would lead to metabolic alterations in cells. Although previous publications mostly examined a function of ATM in carbon metabolism; here, I identified for the first time a link between loss of ATM and taurine intracellular levels. Interestingly, taurine levels were also increased in cells lacking RNase H2. To my knowledge, this is the first time NMR technology was used to describe the metabolome of RNase H2 deficient cells and to study a metabolic function of RNase H2. The results in this thesis encouraged the idea that RNase H2 has a role to play in cell metabolism.

Overall, the increased intracellular levels in both ATM and RNase H2 cells indicates a link between taurine and the DDR. It suggests taurine could be used as a DDR alteration biomarker, but more model of DDR-deficient cells would need to be studied to arise to confirm this. It

could also be that the increase in taurine levels reflects the accumulation of DNA damage in DDR-deficient cells.

Interestingly, in LCLs, the increase in taurine levels was only observed in AT LCLs that had a complete loss of ATM activity. It suggests that variations in taurine levels are linked with the loss of kinase activity in ATM-deficient cells.

3.3.2. ATM inhibition causes an increase in intracellular taurine

To examine if the accumulation of DNA damage in cells induced metabolic changes, including modification of taurine levels, but also to study further the metabolic consequence of the loss of ATM kinase activity in cells, ATM inactivation was achieved in cell lines using the ATM inhibitors KU60019 and AZD0156. It was crucial to establish a dose of ATM inhibitors to use and to characterise the cell viability and growth of cells upon ATM inhibition for metabolic comparison between treated and control cells. Proliferation assays are crucial as they can influence nutrients uptake and utilisation [308]. On the other hand, viability assay is essential as apoptosis can severely alter metabolism in cells as reviewed in [309]. Cells were viable and proliferating to ensure that the metabolic changes observed could be solely attributed to ATM inhibition and not to a difference in proliferation or viability. After treatment of WT and ATM-deficient cells with 3 μm of KU60019 and AZD0156 over 96 hours, I observed an increase in intracellular taurine levels using KU60019 and AZD0156 in WT cell lines only. These results reinforced the idea that taurine is increased in response to DNA damage. On the other hand, these results support the idea that the metabolic variations in ATM-deficient cells are a consequence of the loss of ATM kinase activity.

3.3.3. Other intracellular metabolic alterations in DDR-deficient cells

Taurine was not the only metabolite affected by the loss of ATM or RNase H2. Other metabolites were found to be altered in cells with faulty DNA repair. For instance, intensities in intracellular phenylalanine were higher in extracts of CII AT and MEC1 AT, but lower in AT LCLs compared to the control. In both MEC1 and JJN3, the loss of RNase H2 seemed to induce other metabolic changes such as a decrease in several intracellular amino acid levels and an increase in phosphocholine and *myo*-inositol. These variations could be explained by the nature of these cell lines as well by the type of DDR alteration they are carrying. The cell lines used in this project had a different origin. Some were derived from CLL cells, others from B-cells and others from multiple myeloma plasma cells. Given that different cell types can exert various metabolic pathways usage [310], it is plausible that the metabolic differences observed are linked with the cell origin and not with repair pathways alterations. A possible explanation for the differences observed between the metabolic alterations induced by ATM, or RNase H2 is that, because of the numerous mechanisms underlying the DDR pathways, different DDR defects could lead to distinct metabolic reprogramming, suggested in [134].

An interesting finding was the rise in fumarate intensities and the decrease in glycine intensities found intracellularly in AT LCLs with complete loss of ATM activity compared to WT CTL cells, given these two metabolites had been shown to have a role in DNA repair [147,148] and nucleotides synthesis [149], respectively. Given it was only a feature of AT LCLs, it is possible that this metabolic rewiring only occurs in non-tumour B-cells with defective ATM repair pathway.

When analysing the lipid fractions with NMR, only CII ATM cells showed differences in lipids content which was higher than in CII WT. However, the same study conducted in ATM-deficient and WT MEC1 and LCLs cells did not reveal any metabolite of interest. As a result, the lipid metabolism in DDR-deficient cells was not further investigated.

3.3.1. Glucose metabolism in DDR-deficient cells

The collection and analysis of media samples throughout various NMR experiments gave insight into the effect of DDR pathway alterations on extracellular metabolites. Modification in glucose levels in ATM-deficient cells was expected given that ATM is considered as a regulator of glucose homeostasis and loss of ATM has been shown to induce glucose intolerance and insulin resistance in AT patients [223] and in a mouse AT animal models [224,225].

The analysis of the extracellular content revealed alteration of glucose, lactate and glutamine levels in DDR-deficient cells compared to WT cells. Still, there were a few discrepancies between the cell lines. After pharmacological ATM inhibition, the results were more consistent. They indicated reduced glycolysis upon ATM inhibition as shown by the increase in extracellular glucose levels and the decrease in lactate. However, these findings were contradictory to previous publication showing that glycolysis was increased in response to ATM inhibition in MCF7 and HepG2 cells [311]. Similarly, glucose and glutamine consumptions, as well as lactate production, were significantly increased in the media of senescent cells after ATM inhibition with KU55933 [152].

Overall, the effect of loss of ATM on glucose, glutamine and lactate levels in DDR-deficient cells was unclear and seemed to contradict results found in the literature. For these reasons, HSQC experiments using ^{13}C glucose and glutamine were performed and are presented in the next chapter. They will aim for a better comprehension of the effect of the loss of DDR in cells on glucose and glutamine metabolism.

3.3.2. Consequence of ATM loss in primary CLL cells

In this chapter, I also examined if the metabolic alterations found in the ATM-deficient cell lines could be duplicated in primary CLL cells by comparing the metabolic signature of primary WT and AT CLL cells with NMR spectroscopy. First, it was crucial to decide on the cell material to use for the metabolic studies. Comparing fresh and frozen primary cells showed that the metabolic profile of both sample types remained mostly unchanged. Although little differences were observed between the metabolome of fresh and frozen cells, there were no differences in taurine levels, which was of interest for this thesis. Additionally, assessing the metabolic profile of fresh vs frozen samples raises the importance of the choice of sample to use in NMR experiment and shows how important it is to stay consistent with the nature of the sample used throughout the experiments [289]. Despite all the care taken to choose the right NMR sample and to ensure cell viability was maintained over 90% throughout the experiment, there were no differences between the metabolome of WT and AT primary CLL. It could be explained by the high degree of genetic and clonal heterogeneity that exists within CLL [312,313]. Another reason for the absence of metabolic changes between WT and AT CLL could be that primary cells were isolated from the blood, thus are arrested in the G0/G1 cell cycle phase. Although it has been shown that quiescent CLL cells have an active metabolism, the absence of ATM function might not induce sufficient intracellular changes when the cells are not cycling [314]. Therefore, it could be interesting to increase the number of samples and conduct a metabolic study on cycling primary cells. Finally, although it was ensured that the cells were viable at the time of the experiment, it is possible that the cells, most of them having been kept for a long time were no longer metabolically active. Indeed, although our experience above indicated that the freezing process has little effect on cell metabolism, this experiment was carried out over a

short period and did not account for the impact of long-term freezing on the metabolism of primary cells.

3.3.3. Effect of *in vitro* radiation on intracellular taurine levels

The increase in taurine observed in cells with a DNA repair defect implied taurine increased in response to DNA damage. To verify this hypothesis, the metabolic response in cells and primary cells after generating DNA damage using *in vitro* radiation was investigated.

A day after the IR treatment, higher taurine levels were detected in wild-type cells lines compared to controls. In ATM and RNase H2 deficient cells, the taurine levels remained stable. The absence of modification in taurine levels in the DDR-deficient cells could be explained because these cells are known to accumulate DNA damage [1]. If taurine is increased in response to DNA damage, the main explanation would be that DDR-deficient cells always maintain high intracellular levels of taurine, to a maximum concentration. In that scenario, the intracellular levels of taurine would not be increased following DDR pathway activation. Regarding the primary cells, half of the WT and AT CLL had increased taurine intensities upon ionising radiation even though the sample size was too small to draw any conclusion.

To summarise, these results seem to indicate that taurine could be increased in response to DNA damage.

Overall, the findings in this chapter suggest that intracellular taurine is increased in cells with a defect in the DNA repair pathway. Since the same phenomenon occurred in cells lacking either ATM or RNase H2, this could be linked with genome instability in these cells and could be a marker of DNA damage. The increase in taurine after *in vitro* radiation and ATM inhibition in WT cells also supports this idea. At this stage, the sources, and the mechanisms behind taurine increase in DDR-deficient cells are unknown and will be examined in the next chapters.

DDR alterations also seemed to induce changes in the glucose and glutamine metabolism, but this question will be further explored within the next chapter using 2D NMR spectroscopy.

Chapter 4 Glucose and glutamine metabolism in DDR-deficient cells

4.1. Overview

In the previous chapter, metabolic differences were highlighted between WT and DDR-deficient cells. One of the questions left unanswered was whether the glucose and glutamine metabolism was altered in the absence of efficient DNA repair mechanisms. This chapter aimed at addressing this question using tracer-based NMR approaches.

The decision of studying glucose and glutamine metabolism in DDR-deficient cells was, in part driven by previously reported mechanisms showing that DNA damage response is linked to the regulation of metabolic homeostasis. Hence, many molecules in the DNA repair network are associated with metabolism; this has been reviewed by Shimizu *et al*. [222]. On the other hand, many studies have linked DDR impairment and accumulation of DNA damage with perturbation of energy metabolism reviewed in [315]. Studying DNA repair molecules and their association with metabolism is an area under constant investigation with most studies focusing on the link between the DNA repair network and the glucose or glutamine metabolism, two crucial metabolic fuels. Nevertheless, many roles for these repair molecules are yet unrevealed [135,169,222].

So far, the examination of the metabolism of DDR-deficient cells presented in this thesis has mainly been focused on the analysis of cellular extracts and media using 1D NMR. This chapter takes a closer look at the metabolic response to the loss of ATM or RNase H by monitoring the changes in glucose and glutamine flux in isogenic cell lines using tracer-based NMR approaches. 2D ^{13}C-^{1}H HSQC analysis of WT and DDR-deficient cells, after incubation with [U-^{13}C] glucose and [3-^{13}C] glutamine, will be presented. Overall, the objective was to assess if cells with ineffective DNA repair demonstrated different glucose or glutamine metabolism compared to WT cells.

4.2. Results

4.2.1. Incorporation of ^{13}C from [U-^{13}C] glucose in isogenic cell lines

In the previous chapter, variations in extracellular glucose levels were observed between WT and cells with defective DNA repair. However, it was unclear if the loss of ATM or RNase H was at the origin of these differences.

As mentioned before, ATM is suspected to regulate glucose homeostasis. Hence, the loss of ATM has been previously reported to alter glucose metabolism [224,225]. On the other hand, RNase H2, given its role in the removal of RNA from DNA [85], is directly involved in nucleic acid metabolism [87] which is again linked to glucose metabolism via the pentose phosphate pathway [316]. However, the effect of RNase H2 alterations on glucose metabolism is so far unknown.

This section aims at investigating further if differences in glucose utilisation exist between WT and DDR-deficient cells. CII ATM and RNASEH2-KO JJN3 cell lines were used as a model for ATM or RNase H2 deficiency, respectively, and compared to their WT equivalent.

Cells were cultured for 24 hours in cell culture media with [U-^{13}C] glucose (labelled) or in control cell culture media with natural abundance precursors (unlabelled). Cells were harvested, intracellular metabolites were extracted and analysed by ^{1}H-^{13}C HSQC NMR. The ^{1}H-^{13}C HSQC intensities in the labelled and unlabelled spectra were normalised using TSA values from the corresponding 1D ^{1}H spectrum. To obtain the ^{13}C percentages in the different carbons, the $^{13}C/^{12}C$ ratio obtained from the normalised labelled and corresponding unlabelled sample was multiplied by the natural abundance of ^{13}C (1.1%), as described in the Methods section (2.7.3.3).

Figure 4-1 shows the expected labelled metabolites after incubation with [U-^{13}C] glucose. Glucose is converted to pyruvate through glycolysis. Pyruvate can be further oxidised into acetyl-CoA by the enzyme pyruvate dehydrogenase (PDH) to enter the TCA cycle or being converted directly into oxaloacetate by pyruvate carboxylase (PC). Pyruvate can also be metabolised directly to lactate or alanine. After multiple turns of the TCA cycle, the label distribution becomes very intricate, as depicted in Figure 4-1. Also, the labelling pattern will differ depending on whether glucose is metabolised through PDH or PC (Figure 4-1). The Krebs cycle will produce energy precursors, but also metabolic intermediates used as building blocks for other metabolites such as amino acids, fatty acids, purines, and pyrimidines.

After 24 hours incubation with [U-^{13}C] glucose, many metabolic intermediates appeared to be ^{13}C labelled in the HSQC spectra of CII and JJN3 cells. An example of a ^{1}H-^{13}C HSQC spectrum and metabolite assignments obtained after incubation of CII cells with [U-^{13}C] glucose is visible in Figure 4-2.

HSQCs spectra are informative of signal intensities, but also of ^{13}C chemical shifts and coupling patterns. ^{13}C percentages were calculated for individual carbons in all cell lines. Label percentages for the metabolic intermediates of interest were plotted and organised by metabolic groups for CII (Figure 4-3) and JJN3 (Figure 4-4) cell lines. All cell lines consumed glucose, and carbons in several downstream metabolites became ^{13}C labelled. For many metabolites analysed, the percentages of ^{13}C label were similar between WT and DDR-deficient cells, although they varied between CII and JJN3 cell lines (Figure 4-3 and Figure 4-4). Among glycolysis intermediates ^{13}C labelling was observed in 3-phosphoglycerate (position C2 and C3), pyruvate (C3), lactate (C2 and C3), alanine (C2 and C3), NAD+ (C1), UDP (C2) and glycerol-3-phosphate (C1, C2, C3) (Figure 4-3 and Figure 4-4). Other ^{13}C carbons were expected to be labelled as for C1 in lactate or alanine, but because these carbons are

deprotonated, they are not directly observable in ^{1}H-^{13}C HSQC spectra. However, J_{CC} coupling can be seen, which is more precise than intensities.

Interestingly, ^{13}C percentages in C2 of glycine, a metabolite of the one-carbon metabolism and needed for purine synthesis, were lower in ATM and RNASEH2-KO compared to WT (Figure 4-3 and Figure 4-4). The incubation of DDR-deficient cells with [U-^{13}C] glucose also led to the accumulation of more ^{13}C-labeled pyruvate (C3), and lactate (C2) compared to WT, though the results were not statistically significant. On the other hand, while all cell lines exhibited the same range of ^{13}C percentages in pyruvate, higher levels of $\%^{13}C$ for lactate and alanine, were measured in JJN3, compared to CII cells. The same way, more glucose was converted in NAD+ and UDP in JJN3 vs CII cells which could suggest a more active glycolysis pathway in multiple myeloma JJN3 cells than in CII cells. Another interesting observation was the higher ^{13}C percentages in glycerol-3-phosphate in JJN3 cells compared to CII, independently of their mutation status and could reflect more lipogenesis in JJN3 than in CII cells.

Glucose was further metabolised in TCA cycle intermediates, including citrate (C2), succinate (C2 and C3), and malate (C2 and C3) as demonstrated by the ^{13}C percentages in the different carbons (Figure 4-3 and Figure 4-4). It seemed that more glucose was converted to succinate in DDR-deficient cells compared to WT, but the results were not statistically different.

In JJN3, higher percentages of ^{13}C were measured in carbons of α-ketoglutarate, succinate, and fumarate than CII cells, indicating a more active TCA cycle for the multiple myeloma cell line. However, CII cells had most of their glucose transiting to the Krebs cycle being converted into TCA cycle products, including glutamate, glutamine, glutathione, proline, aspartate, and n-acetyl aspartate compared to JJN3, as indicated by the higher percentage in ^{13}C label, and still suggests CII cells have undergone multiple TCA cycles.

Finally, the HSQC spectra also revealed that none of the glucose was metabolised into asparagine (C2, C3) in JJN3 cells. In CII cells, a small amount of glucose was converted to asparagine as shown by the low label incorporation percentages. These results could indicate an absence of asparagine synthetase (ASNS) activity, an enzyme catalysing the conversion of aspartate to asparagine.

Overall glucose metabolism was similar for DDR-deficient cells and WT. The significant differences observed in this section were the differences between leukaemia and myeloma cell lines.

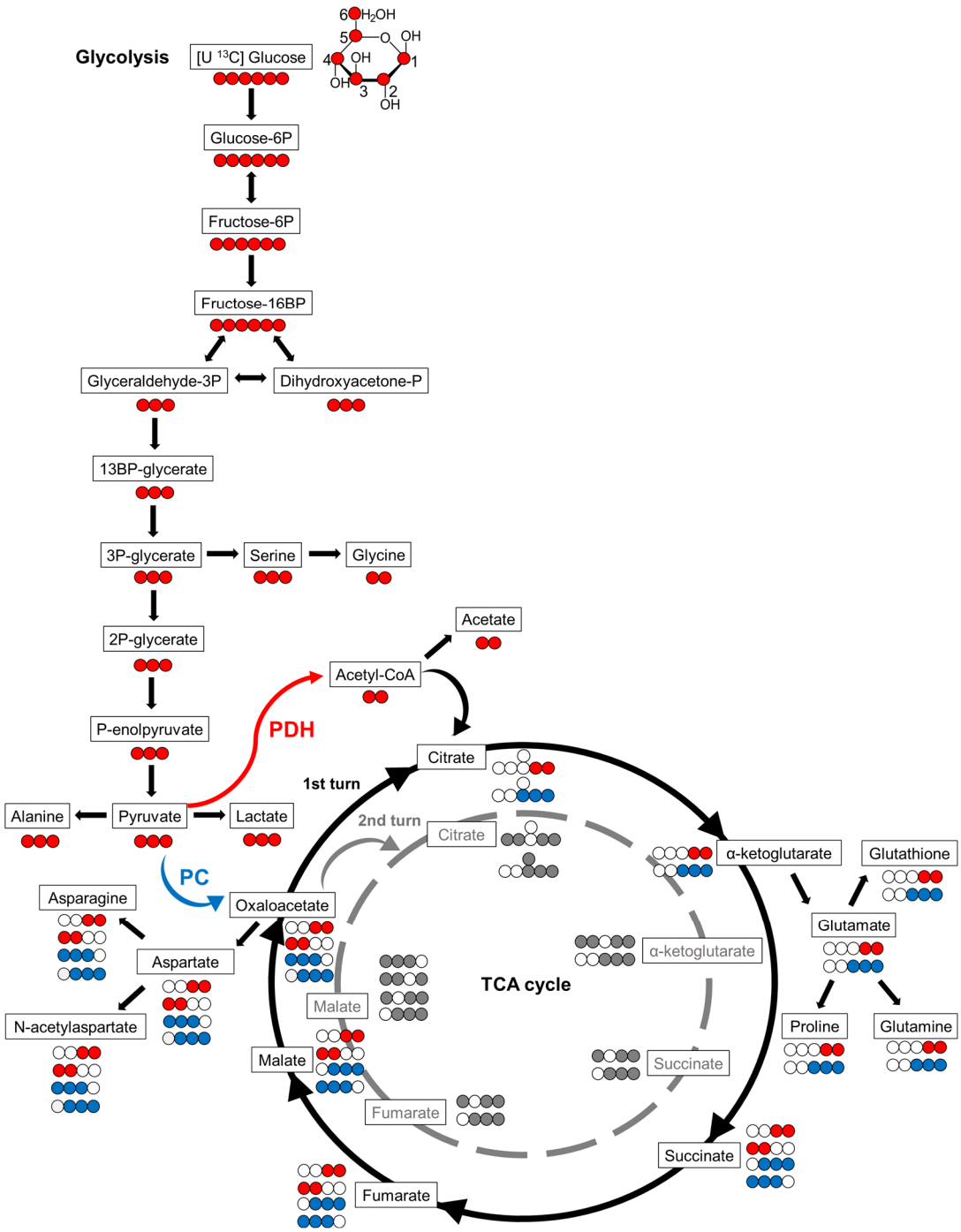

Figure 4-1: Expected label distribution in intracellular metabolites arising from [U-^{13}C] glucose

In short, [U-^{13}C] glucose is converted to $^{13}C_3$ pyruvate through glycolysis. Pyruvate can be further oxidised into acetyl-CoA by the enzyme pyruvate dehydrogenase (PDH) to enter the TCA cycle or being converted directly into oxaloacetate by pyruvate carboxylase (PC). Expected ^{13}C carbons are represented in red in the different metabolites excepted the ^{13}C carbons resulting from PC activity which are illustrated in blue. Labelling patterns arising from the second round of the TCA are shown for metabolites derived from PDH activity with ^{13}C carbons coloured in grey.

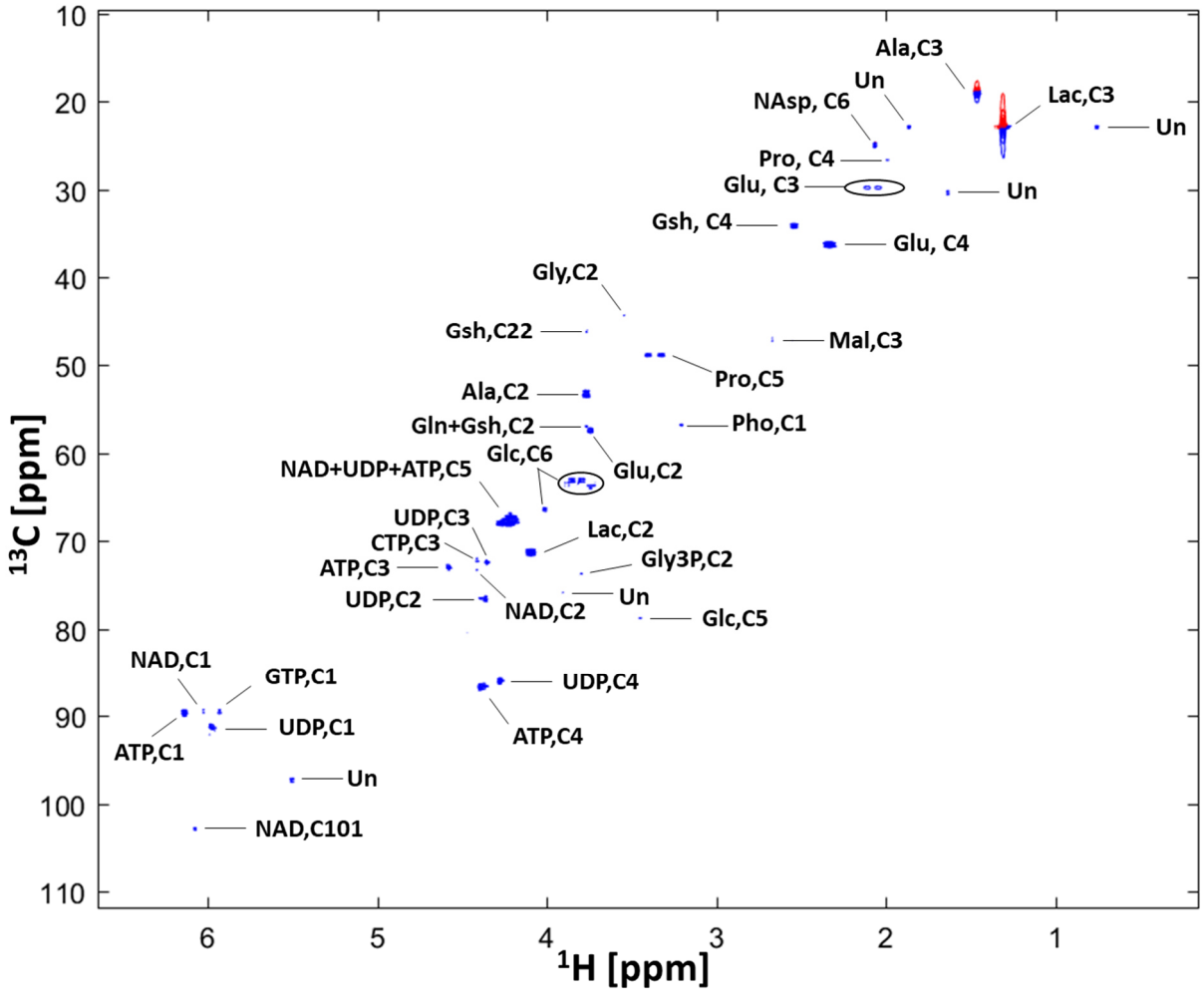

Figure 4-2: Example of a ^{1}H-^{13}C HSQC spectrum and assignments of polar cell extracts obtained after 24 hours labelling with [U-^{13}C] glucose

^{1}H-^{13}C HSQC spectra obtained from CII cell extracts after 24 hours incubation with [U-^{13}C] glucose. Metabolites assigned: Ala, alanine; Asp, asparagine; ATP, adenosine triphosphate; CTP, cytidine triphosphate; Gln, glutamine; Glc, glucose; Glu, glutamate; Gly, glycine; Gly3P, glycerol-3-phosphate; Gsh, glutathione reduced; Lac, lactate; Mal, malate; NAD, Nicotinamide adenine dinucleotide; NAsp, N-acetylaspartate; Pho, phosphocholine; Pro, proline; Pyr, pyruvate; Suc, succinate; UDP, uridine diphosphate; Un, undefined.

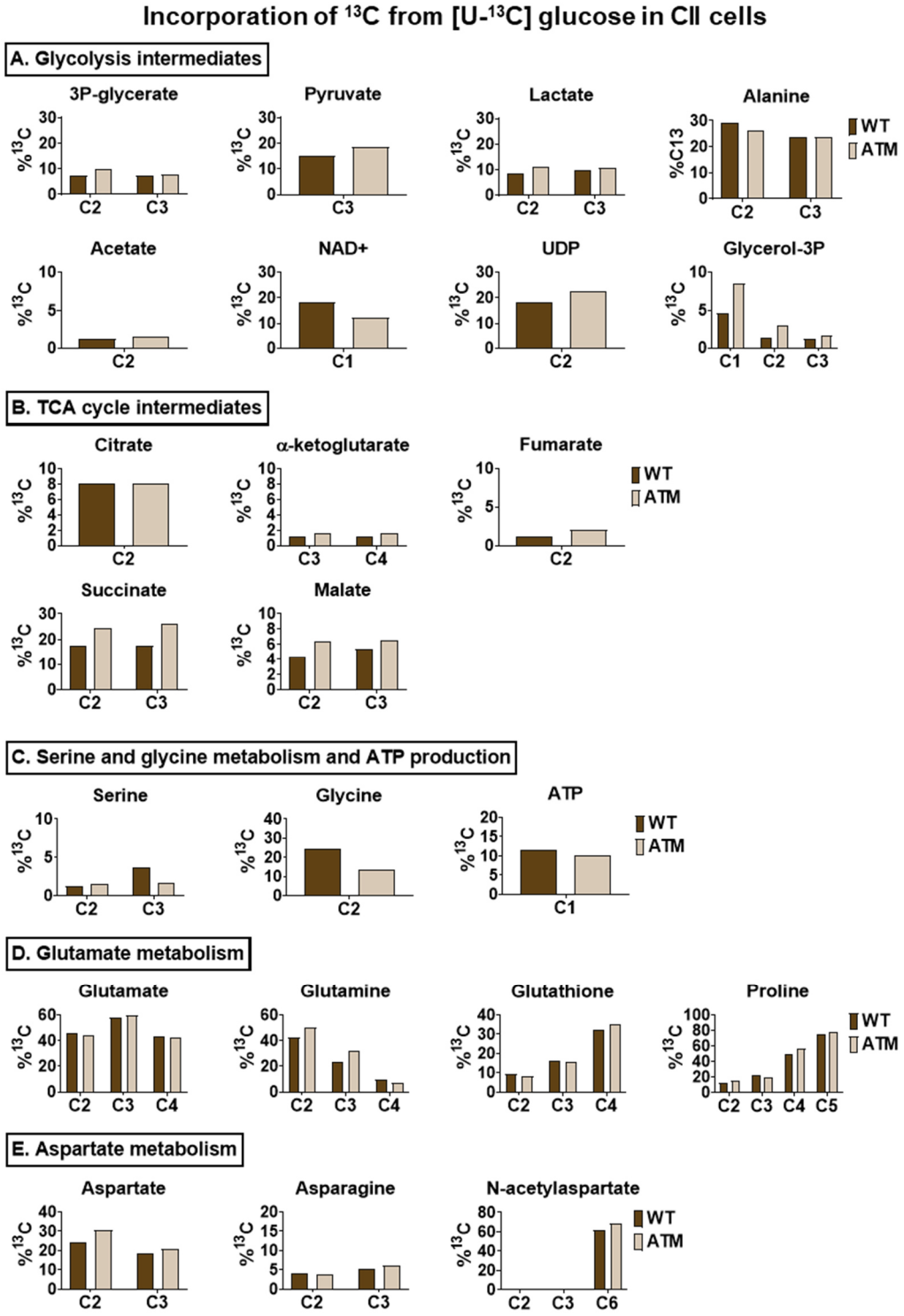

Figure 4-3: Label incorporation in metabolites arising from [U-^{13}C] glucose after 24 hours in CII cells

For each experiment, bar graphs represent the mean percentage of ^{13}C for one independent sample (n=1). ^{13}C percentages (%^{13}C) in the different carbons were calculated after multiplying the ^{13}C/^{12}C ratio obtained from the labelled and corresponding unlabelled HSQC by the natural abundance of ^{13}C (1.1%). %^{13}C for the metabolic intermediates of interest were plotted by metabolic groups**.**

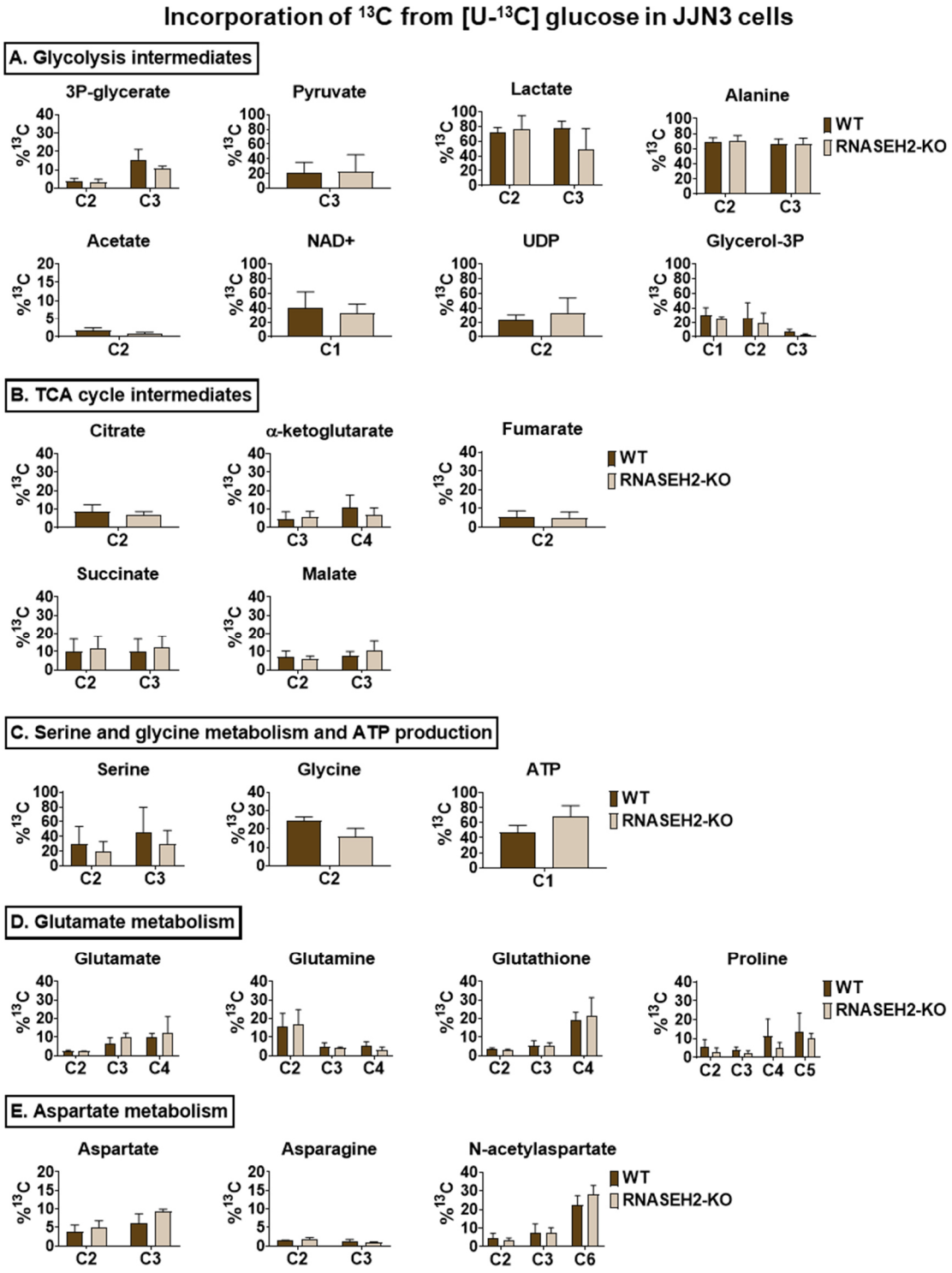

Figure 4-4: Label incorporation in metabolites arising from [U-^{13}C] glucose after 24 hours in JJN3 cells

For each experiment, bar graphs represent the mean percentage of ^{13}C for three independent samples (n=3). ^{13}C percentages (%^{13}C) in the different carbons were calculated after multiplying the ^{13}C/^{12}C ratio obtained from the labelled and corresponding unlabelled HSQC by the natural abundance of ^{13}C (1.1%). %^{13}C for the metabolic intermediates of interest were plotted by metabolic groups**.**

4.2.2. Incorporation of ^{13}C from [3-^{13}C] glutamine in isogenic cell lines

In the previous chapter, variations in intracellular and extracellular levels of glutamine were noticed in cells lacking ATM or RNaseH2 compared to wild-type cells. However, it was not clear whether defects in the DNA repair pathway caused alteration in glutamine metabolism. To answer this question, ^{13}C glutamine flux was monitored in isogenic cell lines using 2D ^{13}C-^{1}H HSQC analysis and the results are presented in this section.

Previous publications have already suggested a link between ATM and glutamine metabolism. For instance, in *Atm* $^{-/-}$ mice, blood glutamine concentration was reduced compared to control mice yet, the supplementation of glutamine restored values to near control levels. Also, gene expression analysis revealed increase glutaminase (GLS) expression in *Atm* −/− mice as well as in AT patients [234]. In another study, glutamine synthetase was shown to be expressed at higher levels in del11q than in WT CLL cells while the inhibition of the glutaminase was cytotoxic for del11q CLL lymphocytes.

On the other hand, glutamine metabolism in cells lacking RNase H2 has never been examined. However, these cells represent good candidates to investigate the effect of altered DNA repair pathway on glutamine flux given the roles of RNase H2 in nucleic acid metabolism and glutamine, involved in the biosynthesis of nucleotides.

As for the above glucose labelled experiment, isogenic cells lines with a defect in ATM or RNase H2 were used as an example for DDR deficiencies. Cells were either grown in control media or media with [3-^{13}C] glutamine at the same concentration as in the control media. After 24 hours, cells were harvested, their intracellular metabolic content was extracted, and ^{1}H-^{13}C HSQC spectra were acquired. ^{13}C percentages were calculated as for the above glucose labelled experiment (4.2.1). Expected labelled metabolites after incubation with [3-^{13}C] glutamine can

be seen in Figure 4-5. The conversion of glutamine to α-ketoglutarate is called glutaminolysis and occurs in two steps. First, [3-^{13}C] glutamine is metabolised to [3-^{13}C] glutamate through hydrolysis of its amine group by the glutaminase enzyme. Glutamate is then converted into α-ketoglutarate to feed the TCA cycle and serve as an energy source or a precursor for the synthesis of other metabolites, including amino acids, nucleotides, and lipids. The glutamate synthesised from glutamine might also be directly metabolised to glutathione or proline.

After 24 hours incubation with [3-^{13}C] glutamine, many metabolites showed isotope enrichment. Figure 4-6 depicts an example of an HSQC spectrum and metabolic assignments obtained for CII cells after 24 hours incubation with [3-^{13}C] glutamine. The calculated ^{13}C percentages for individual carbons were arranged by metabolic groups and can be seen in Figure 4-7 for CII and Figure 4-8 for JJN3 cells. Glutaminolysis was observed in CII and JJN3 cells as demonstrated by the ^{13}C label incorporation in intermediates of glutamine metabolism and TCA cycle. ^{13}C label was detected in glutamate, pyroglutamate, proline, glutathione (position C3) as well as in α-ketoglutarate (C3), succinate (C2 and C3), fumarate (C2), malate (C2 and C3), and citrate (C2). Other metabolites of the aspartate metabolism were ^{13}C labelled, including aspartate and N-acetyl aspartate (C2 or C3). Interestingly, though not significant, lower ^{13}C label percentages were observed for glutamate and glutathione in DDR-deficient cells. On the contrary, the label incorporation was higher in succinate in these cells. It could indicate that cells lacking ATM or RNase H2 are more prone to metabolised glutamine through glutaminolysis rather than using it for glutathione synthesis.

As for the previous labelling experiments, differences existed between CII and JJN3 cell lines. JJN3 had converted more glutamine into α-ketoglutarate, fumarate and malate compared to CII and could be an indicator of more TCA cycle activity in JJN3. Besides, it seemed that none of the glutamine was metabolised into N-acetylaspartate in CII cells.

A close reading of the results also showed the absence of ^{13}C asparagine in all cells and could indicate a lack of ASNS activity in both JJN3 and CII cells.

Finally, in interpreting these results, it seemed that there were no significant differences between the glutamine metabolism of WT and cells with deficient ATM or RNase H2.

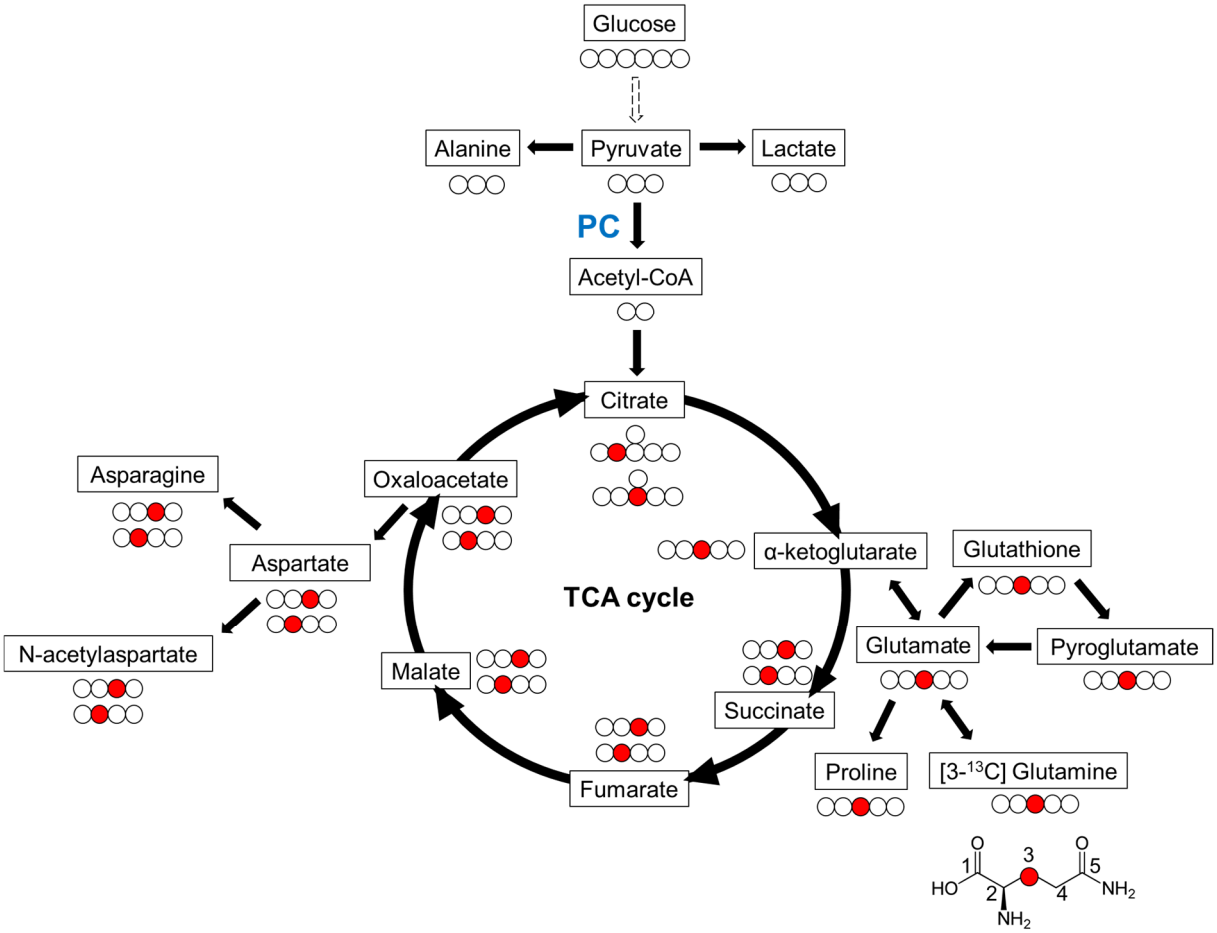

Figure 4-5: Expected label distribution in intracellular metabolites arising from [3-^{13}C] glutamine

Expected ^{13}C carbons are represented in red in the different metabolites. In brief, [3-^{13}C] glutamine is first converted to [3-^{13}C] glutamate then to α-ketoglutarate and enter the TCA cycle via glutaminolysis. PC, pyruvate carboxylase.

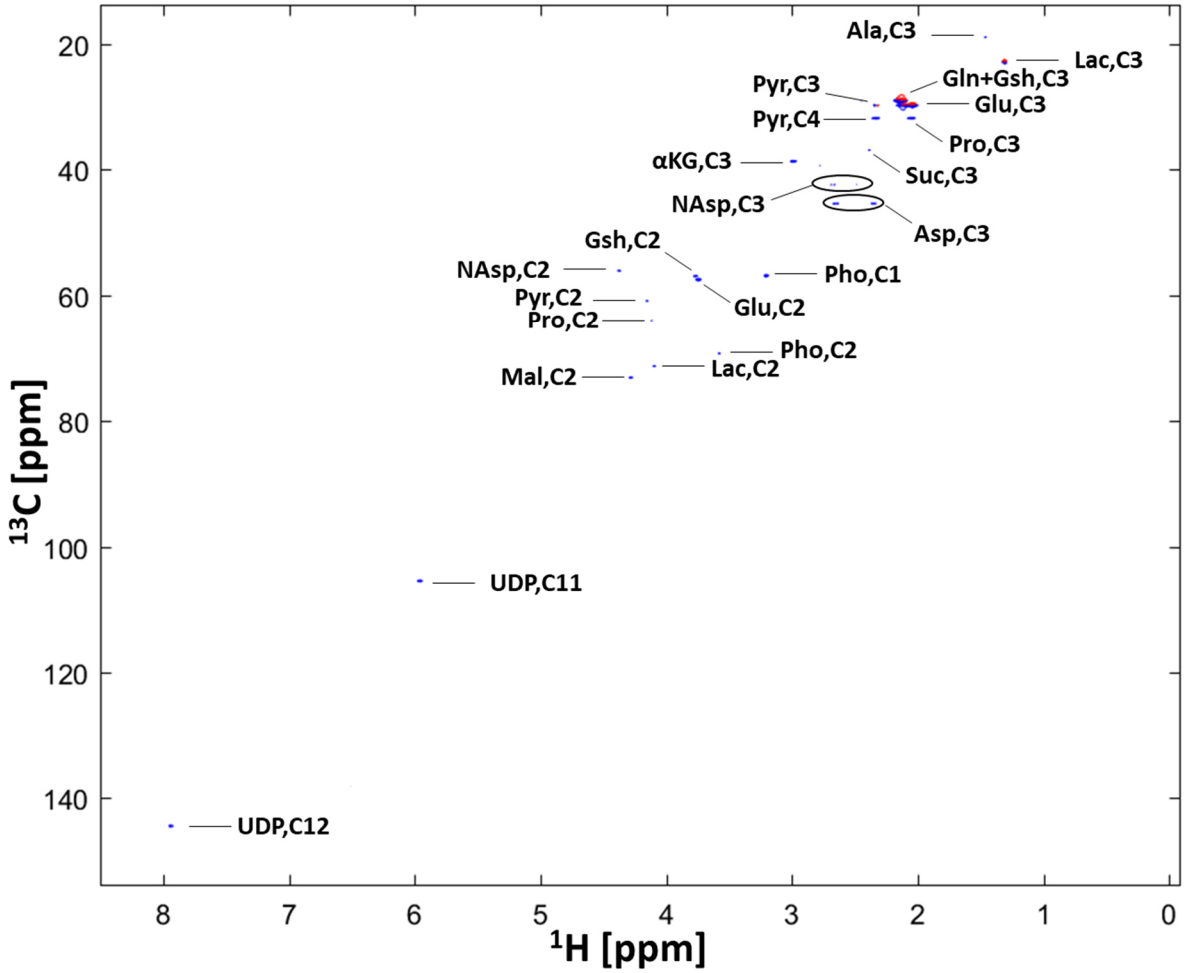

Figure 4-6: Example of ^{1}H-^{13}C HSQC spectra and assignments of polar cell extracts obtained after 24 hours labelling with [3-^{13}C] glutamine

^{1}H-^{13}C HSQC spectra obtained from CII cell extracts after 24 hours incubation with [3-C_3] glutamine. Metabolites assigned: αKG, α-ketoglutarate; Ala, alanine; Asp, asparagine; Gln, glutamine; Glu, glutamate; Gsh, glutathione reduced; Lac, lactate; Mal, Malate; NAsp, N-acetylaspartate; Pho, phosphocholine; Pro, proline; Pyr, pyruvate; Suc, succinate; UDP, uridine diphosphate.

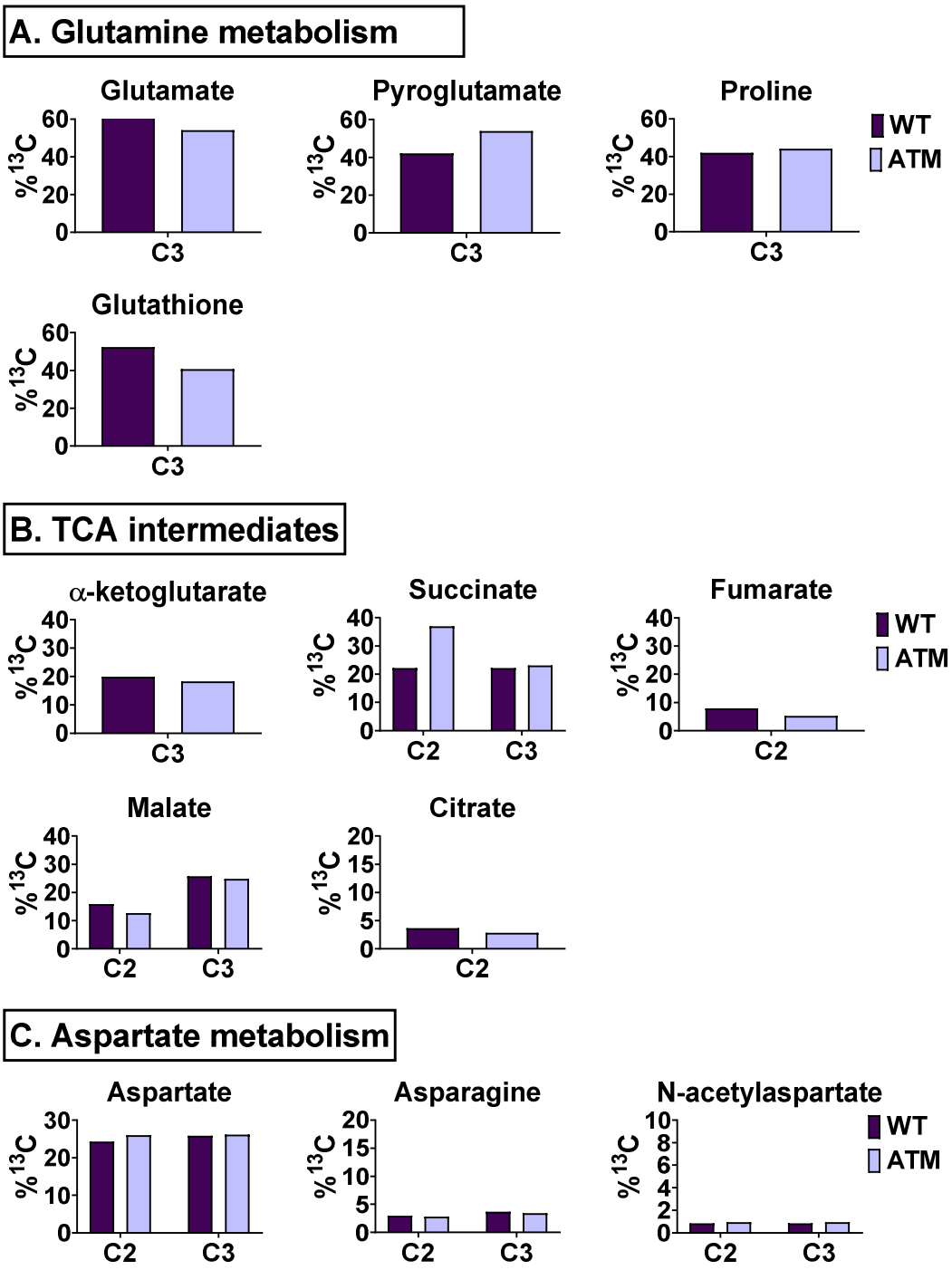

Figure 4-7: Label incorporation in metabolites arising from [3-^{13}C] glutamine after 24 hours in CII cells

For each experiment, bar graphs represent the mean percentage of ^{13}C for one independent samples (n=1). ^{13}C percentages (%^{13}C) in the different carbons were calculated after multiplying the ^{13}C/^{12}C ratio obtained from the labelled and corresponding unlabelled HSQC by the natural abundance of ^{13}C (1.1%). %^{13}C for the metabolic intermediates of interest were plotted by metabolic groups.

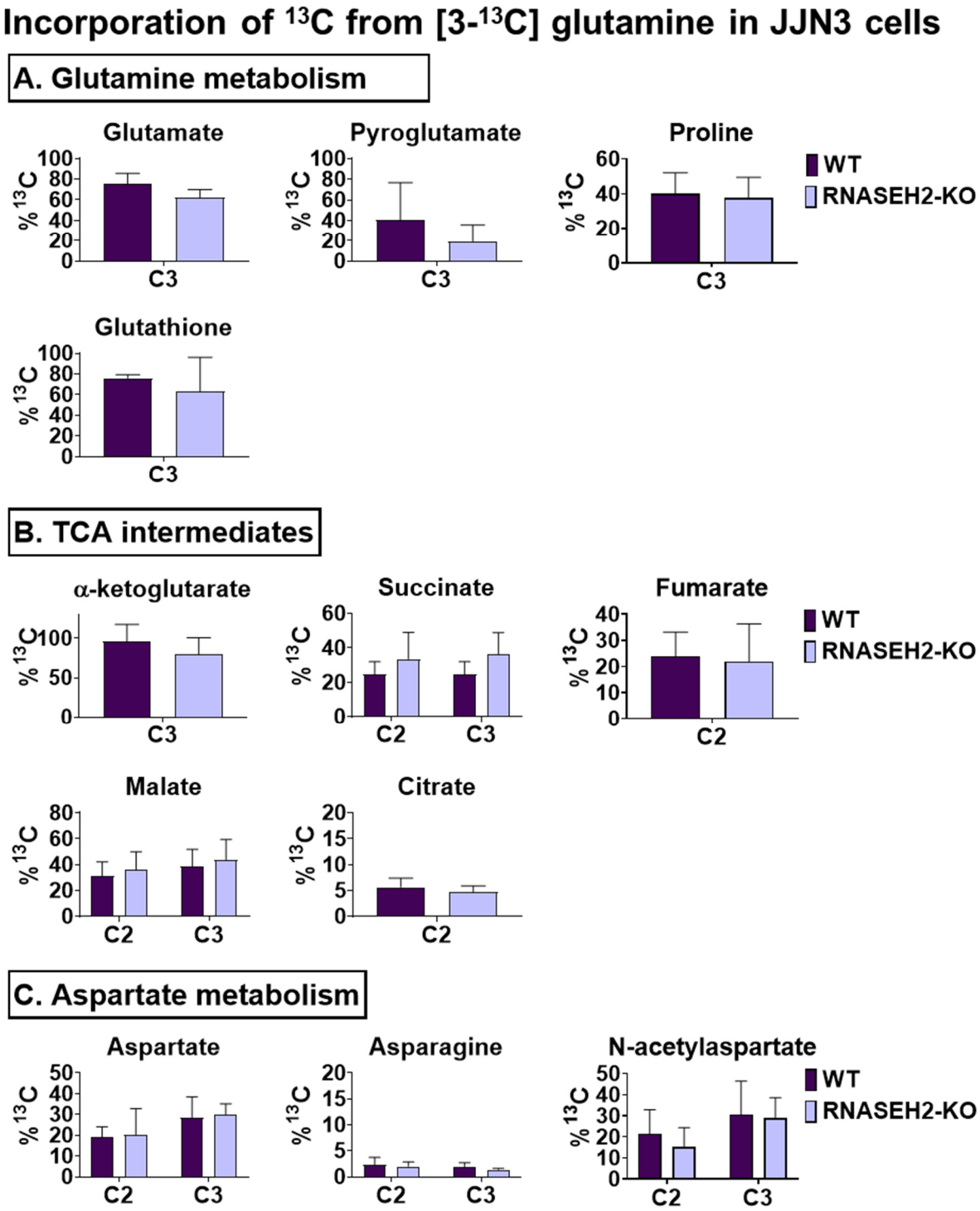

Figure 4-8: Label incorporation in metabolites arising from [3-^{13}C] glutamine after 24 hours in JJN3 cells

For each experiment, bar graphs represent the mean percentage of ^{13}C for three independent samples (n=3). ^{13}C percentages (%^{13}C) in the different carbons were calculated after multiplying the ^{13}C/^{12}C ratio obtained from the labelled and corresponding unlabelled HSQC by the natural abundance of ^{13}C (1.1%). %^{13}C for the metabolic intermediates of interest were plotted by metabolic groups.

4.3. Discussion

4.3.1. Glucose metabolism in cells defective in DNA repair pathways

The overall aim of this chapter was to determine whether cells with a defective DNA repair pathway would present different glucose or glutamine metabolism compared to their WT counterpart. For this, we used NMR-based approaches to study cells with faulty ATM (CII) or RNase H2 (JJN3). Using 2D HSQCs, it was possible to follow the glucose and glutamine consumption and the ^{13}C label distribution in the different downstream metabolites, reported in [317–321]. Depending on the cell's needs and activity, these metabolites will themselves feed other metabolic pathways and can be used for lipid, protein or nucleotide synthesis [322,323].

For the [U-^{13}C] glucose labelling experiment, the results showed all cells had consumed glucose which was metabolised through glycolysis into pyruvate. Pyruvate was then further converted into lactate or alanine or entered the Krebs cycle.

In cells with repair pathway alterations, more glucose was converted to pyruvate and lactate than in the WT. It could indicate that DDR-deficient cells have a more active glycolysis pathway than WT cells. Although not statistically significant, these results are in partial agreement with previous publications showing enhancement of glycolysis in cells lacking ATM, including castration-resistant prostate cancer cells[324] and cerebellar Purkinje cells[325]. One-carbon metabolism also seemed more active in cells lacking ATM or RNase H2 as demonstrated by the high levels of glycine labelled. Glycine is notably involved in purine synthesis [326], but these results would need further clarification.

What was most striking, however, were the differences observed between CII and JJN3 cell lines. It seemed JJN3 cells had higher glycolytic flux than CII, demonstrated by the higher ^{13}C

percentage in lactate, alanine NAD+ and UDP, and it could be directly correlated with the nature of the cells. Besides, more ^{13}C glycerol-3-phosphate was found in JJN3 cells after incubation with [U-^{13}C] glucose and could be an indicator of greater lipogenesis. Although it was not the aim of this chapter, it could be interesting to investigate further the differences in glucose metabolism between CLL and multiple myeloma cells by using other cell lines representative of these hematologic malignancies as well with healthy cells.

Finally, it seemed that all cell lines studied within this section, independently of their mutation status, lack asparagine synthetase activity. These results are in line with several studies showing low expression of ASNS in another type of lymphoid leukaemia, acute lymphocytic leukaemia and multiple myeloma [327–330]. However, experiments aiming at ASNS expression levels and activity assessment should be completed in CII and JJN3 to confirm this hypothesis.

In summary, despite the different glucose labelling experiments presented in this section, it was not sure if the lack of efficient DNA repair pathway in the CII and JJN3 cell model had caused a change in glucose metabolism.

4.3.1. Glutamine metabolism of WT and DDR-deficient cells

After incubation with [3-^{13}C] glutamine, all cells metabolised glutamine through glutaminolysis or, after conversion to glutamate, directly to glutathione and proline.

The differences in ^{13}C labelled incorporation between WT cells and cells with a defective DNA repair pathway suggested more glutamine going through TCA cycle in DDR-deficient cells. However, ^{13}C percentages in the different TCA cycle intermediates were not significantly increased to confirm this hypothesis. Also, cells lacking CII or RNase H2 had metabolised less glutamine into glutathione than their WT counteract. Although these results were not significant, they are partially supported by previous studies showing a significant reduction in glutathione synthetase, the enzyme catalysing the last step in glutathione synthesis in AT deficient cells [234].

The differences that appeared between CII and JJN3 were, as for the glucose labelling experiments, mainly variations in ^{13}C percentages in TCA cycle intermediates. This further supports more TCA cycle activity in JJN3 cells than CII, but this would need to explore in more detail. Also observed for the above glucose labelling experiments, cells incubated with [3-^{13}C] glutamine did not metabolise glutamine into asparagine. Once again, this suggests an absence of ASNS activity in the cell lines studied.

In the end, there were no evident differences in the glutamine flux between WT and cells lacking ATM or RNase H2. However, the comparison of ^{13}C percentages in metabolites from both [U-^{13}C] glucose and [3-^{13}C] glutamine labelling experiments was noteworthy because it revealed a higher rate of ^{13}C in metabolites after incubation with glutamine than glucose in all cells studied. It implies that glutamine is the primary carbon substrate for the TCA cycle in these cells and partly confirm what has been previously assessed in multiple myeloma [331]. Even

if it was not the aim of this thesis, in the future, it would be interesting to find out if the glucose and glutamine flux in MM and CLL cells differs from those of healthy cells.

To conclude this chapter, the use of ^{13}C labelled precursors revealed differences between glucose and glutamine metabolism in cells with different cell origin. However, there were no notable differences in cells in relation to their mutation status. The differences observed between CII and JJN3 cell lines demonstrated that glucose and glutamine metabolism depend on the type of cells and highlights the importance of the choice of the cell model in studying metabolism. On the other hand, although it contradicts the literature suggesting the loss of ATM cause perturbation of glucose and glutamine metabolism, they are different reasons that could explain the absence of differences between WT and DDR-deficient cells presented in this chapter. Cell lines may have adapted to the loss of ATM or RNase H2. Another reason could be the choice of labelled precursors. Other labelled precursors could have been used, including [1,2]glucose which is more precise to study glycolysis and the PPP while universally labelled glucose is more informative of the TCA cycle [332]. Also, a double labelling approach combining [U-^{13}C] glucose and [^{15}N] glutamine could have been used as it was shown to be valuable to study nucleotides synthesis [291].

Chapter 5 Defective DNA repair and taurine metabolism

5.1. Overview

In the previous chapters, the metabolic variations in several cell lines with a defect in the DNA damage response compared to control cells was investigated. The key finding was that higher intracellular taurine levels were found in all ATM- and RNase H2-deficient cells. Moreover, taurine levels were increased when inducing DNA damage *in vitro* or after inhibition of ATM-regulated DNA repair in cells without DDR deficiency.

In human cells, taurine mainly comes from dietary sources or can be synthesised from methionine or cysteine [333]. Taurine is not incorporated into proteins and is the end-product of sulphur metabolism which is essential for cell homeostasis and is involved in detoxification processes [334]. Nonetheless, taurine is suspected of having many biological functions, e.g. as an osmoregulator, neuroprotector or precursor for bile salt synthesis, as reviewed in [240,333]. In addition, the regulation of oxidative stress is another metabolic function attributed to taurine. Several publications revealed reduced ROS levels after taurine supplementation both in *in vitro* and *in vivo* models [246–249]. However, the mechanism underlying how taurine functions as an antioxidant is poorly understood.

In this chapter, the sources, and roles of taurine in DDR-deficient cells were investigated. To decipher how DDR-deficient cells obtain taurine, several experiments were performed focusing on (I) the taurine synthesis pathway in normal and DDR-deficient cells; (II) the effect of a taurine synthesis inhibitor, DL-propargylglycine on intracellular taurine levels; (II) the role of the proteasome and autophagy as possible sources of taurine; and (IV) the function of taurine as an antioxidant by measuring reactive oxygen species (ROS) levels.

5.2. Results

5.2.1. Absence of taurine from the culture media

This chapter aimed to characterise how DDR-deficient cells obtained taurine to identify the source of the increased taurine found in these cells. The first experiment was to verify if the cell culture medium or the FBS contained taurine that could be taken up by cells. Samples of RPMI medium with or without 10 % FBS and of FBS were screened for taurine by 1D ^{1}H NMR spectra. The analysis of metabolites in the RPMI medium and FBS revealed the absence of taurine from the RPMI and FBS (Figure 5-1). Based on these results, it was ruled out that taurine could be obtained from the culture medium. Other sources of taurine will be investigated in the following sections.

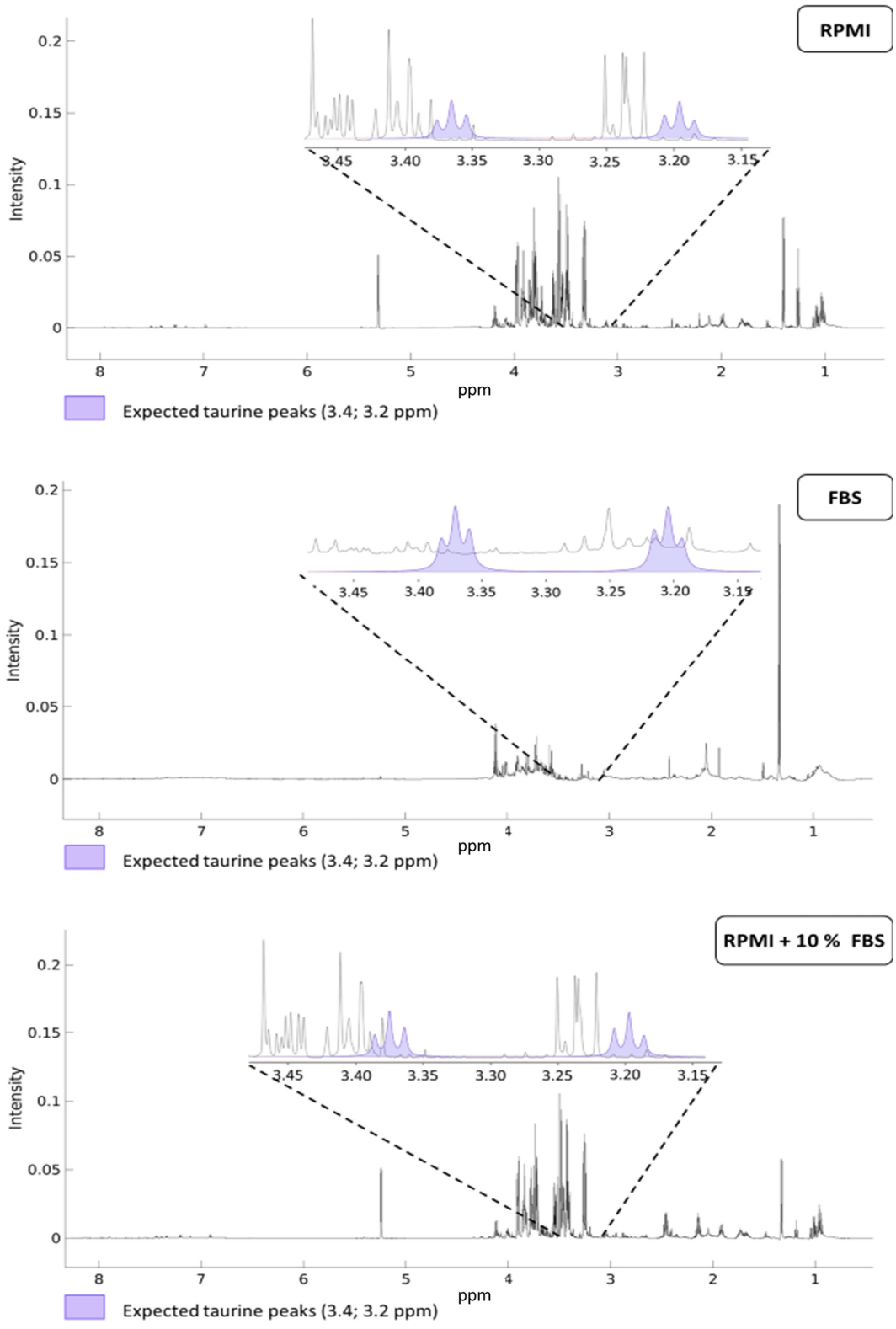

Figure 5-1: 1D ^{1}H-NMR RPMI, FBS and RPMI supplemented with 10 % FBS.

After processing of the spectra in *Metabolab*, the absence of taurine peaks (3.4 and 3.2 ppm) in RPMI, FBS and RPMI supplemented with 10 % FBS was confirmed using the *Chenomx* assign tool. The peaks in purple represent the expected profile for taurine in *Chenomx*.

5.2.2. Taurine synthesis pathway

Given that the cell culture media used in all the experiments did not contain taurine, I wanted to explore whether taurine in DDR-deficient cells could arise from the taurine synthesis pathway.

Taurine can be synthesised from methionine or cysteine via the cysteine sulfinic acid decarboxylase (CSAD) [333]. To examine whether taurine could be generated from cysteine and/or methionine in cells with or without a defective DDR, I performed tracer-based analysis using isotopically labelled precursors. CII wild-type and ATM-deficient CLL cell lines, and JJN3 WT and RNASEH2-KO multiple myeloma cell lines, were grown for 24 hours in cell culture media with [$^{13}C_3$] cysteine or [U-^{13}C] methionine (labelled). Cells grown in cell culture media with natural abundance precursors were prepared as controls. CII cells were also cultured for 7 days in media with ^{13}C labelled or natural abundant cysteine to complete a long ^{13}C labelled cysteine experiment. Cells were harvested, intracellular metabolic metabolites were extracted and analysed by ^{1}H-^{13}C HSQC NMR. An example of ^{1}H-^{13}C HSQC spectra and metabolite assignments obtained after incubation of cells with [$^{13}C_3$] cysteine or [U-^{13}C] methionine can be seen in Figure 5-2. ^{13}C label incorporations were calculated as described in the Methods section and as for the ^{13}C labelled glucose and glutamine experiment from the previous chapter (4.1).

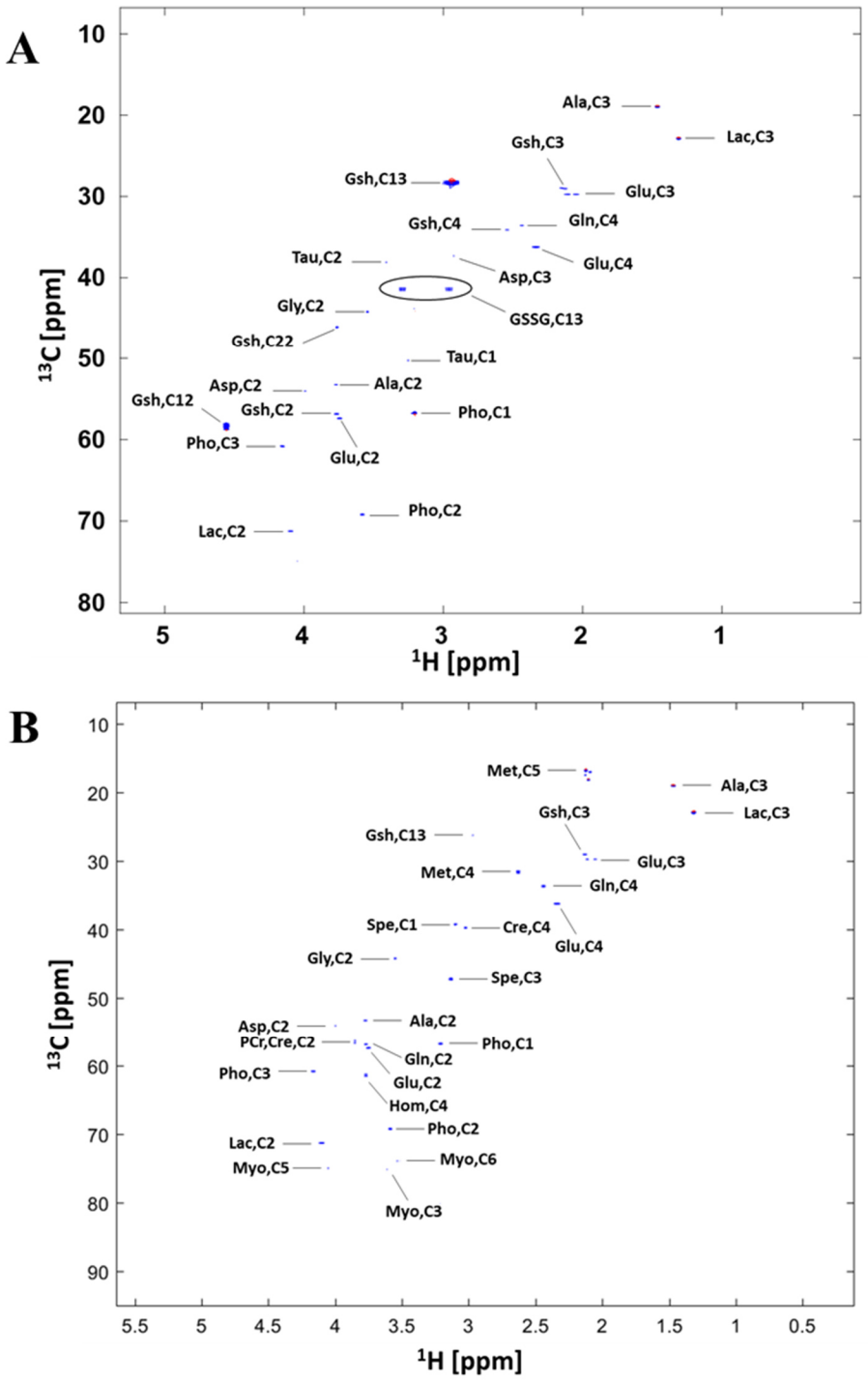

Figure 5-2: Example of ^{1}H-^{13}C HSQC spectra and assignments of polar cell extracts obtained after 24 hours labelling with [$^{13}C_3$] cysteine or [U-^{13}C] methionine.

A) ^{1}H-^{13}C HSQC spectra obtained from CII cell extracts after 24 hours incubation with [$^{13}C_3$] cysteine. B) ^{1}H-^{13}C HSQC spectra obtained from CII cell extracts after 24 hours incubation with [U-^{13}C] methionine. Metabolites assigned: Ala, alanine; Asp, asparagine; Cre, creatine; Gly, glycine; Gln, glutamine; Glu, glutamate; Gsh, glutathione reduced; GSSG, glutathione oxidised; Hom, homoserine; Lac, lactate; Met, methionine; Myo, *myo*-inositol; PCr, phosphocreatine; Pho, phosphocholine; Spe, spermidine; Tau, taurine.

After labelling CII and JJN3 cells lines with [$^{13}C_3$] cysteine, ^{13}C cysteine label incorporation was only found in carbon 12 and 13 of glutathione in either WT or DDR-deficient cells. ^{13}C label incorporation in carbon in position 1 and 2 of hypotaurine and taurine were below 3% for all cell lines (Figure 5-3 and Figure 5-4). Hence, no splitting was observed in the taurine signal after cell lines were cultured for 24 hours in media with [$^{13}C_3$] cysteine (Figure 5-5 and Figure 5-6). Incubation over seven days with [$^{13}C_3$] cysteine in CII WT and ATM showed the same labelling pattern (Figure 5-7). These results suggest that none of the cells was synthesising taurine from cysteine even over a relatively long period, independently of their DDR alteration *status*.

The taurine synthesis pathway was also explored after ATM inhibition in non-tumorous cells. For this, ^{13}C cysteine label incorporation in WT LCLs was measured five days after their incubation with the ATM inhibitor AZD0156 or KU60019 and in control cells. Cells were cultured over 72 hours in RPMI (CTL) or RPMI containing 3 μM KU-60019 (KU) or AZD0156 (AZ). Cells were then divided in two and cultured for an additional 24 hours in RPMI with or without AZD0156, or KU60019 supplemented with [$^{13}C_3$] cysteine or natural abundance cysteine for labelled and unlabelled sample, respectively. After incubating cells with the labelled and unlabelled precursors, intracellular metabolites were extracted, ^{1}H-^{13}C HSQC spectra acquired, and ^{13}C label incorporation was calculated for the different carbons. As can be seen in Figure 5-8, only carbons in position 12 and 13 in glutathione were labelled from [$^{13}C_3$] cysteine. These results suggest an absence of taurine synthesis from cysteine in LCLs same as for leukaemia and multiple myeloma cell lines.

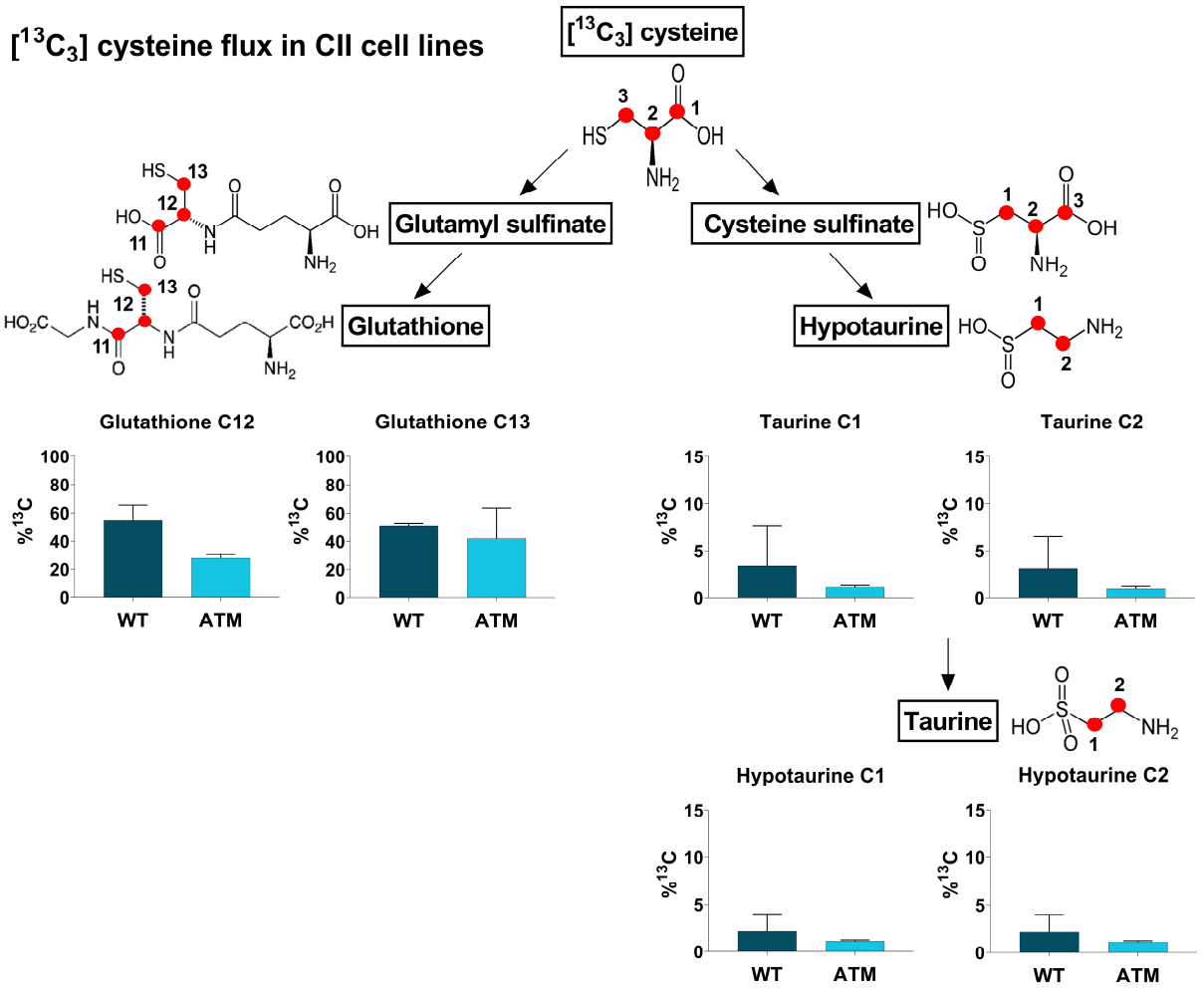

Figure 5-3: ^{13}C labelled cysteine flux to glutathione or taurine in CII cells after 24 hours.

Label incorporation in metabolites arising from [$^{13}C_3$] cysteine after 24 hours incubation in CII cells. Expected ^{13}C carbons are represented in red in the different metabolites. For each experiment, bar graphs and standard deviation represent the mean percentage of ^{13}C for three independent samples (n=3) ^{13}C percentages (%^{13}C) in the different carbons were calculated after multiplying the $^{13}C/^{12}C$ ratio obtained from the labelled and corresponding unlabelled HSQC by the natural abundance of ^{13}C (1.1%).

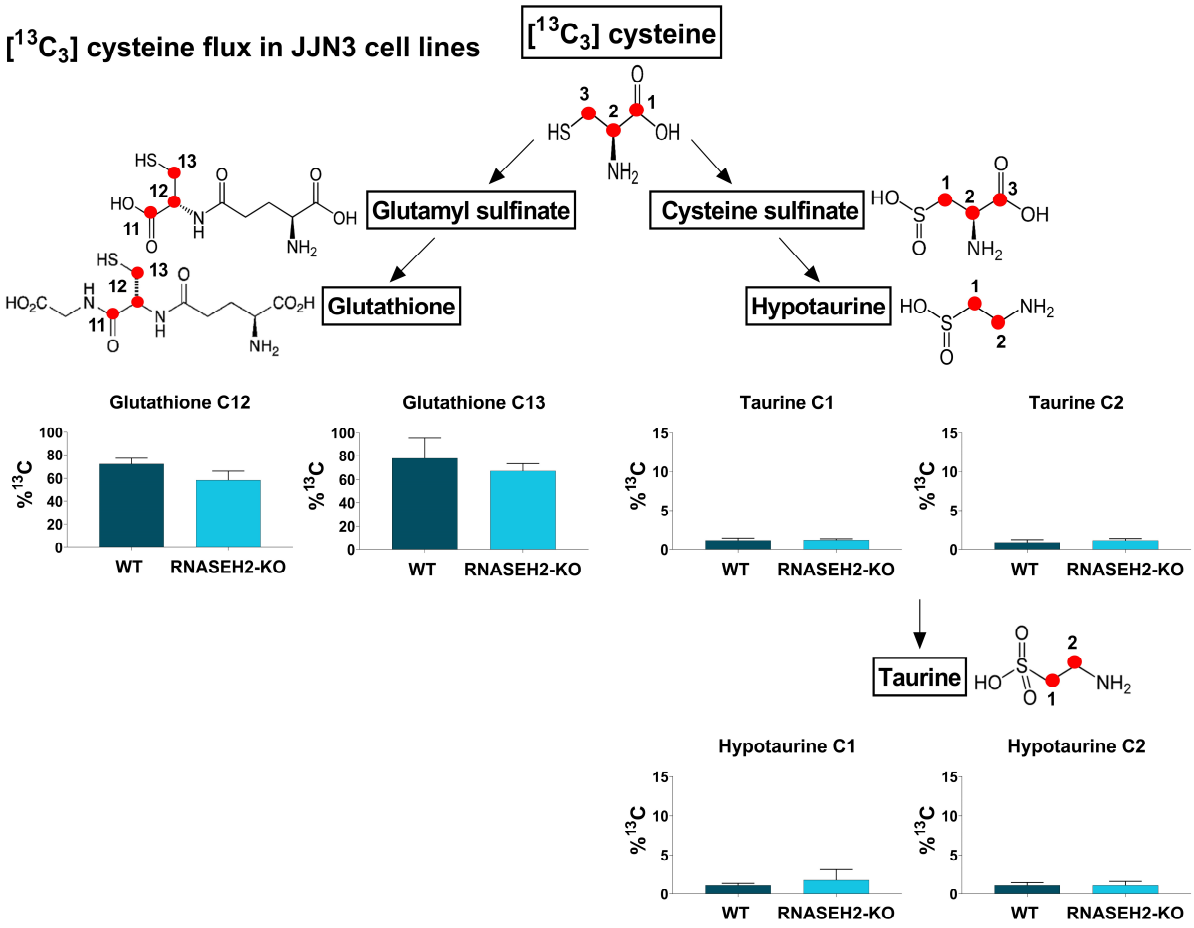

Figure 5-4: ^{13}C labelled cysteine flux to glutathione or taurine in JJN3 cells after 24 hours.

Label incorporation in metabolites arising from [$^{13}C_3$] cysteine after 24 hours incubation in JJN3 cells. Expected ^{13}C carbons are represented in red in the different metabolites. For each experiment, bar graphs and standard deviation represent the mean percentage of ^{13}C for three independent samples (n=3). ^{13}C percentages (%^{13}C) in the different carbons were calculated after multiplying the $^{13}C/^{12}C$ ratio obtained from the labelled and corresponding unlabelled HSQC by the natural abundance of ^{13}C (1.1%).

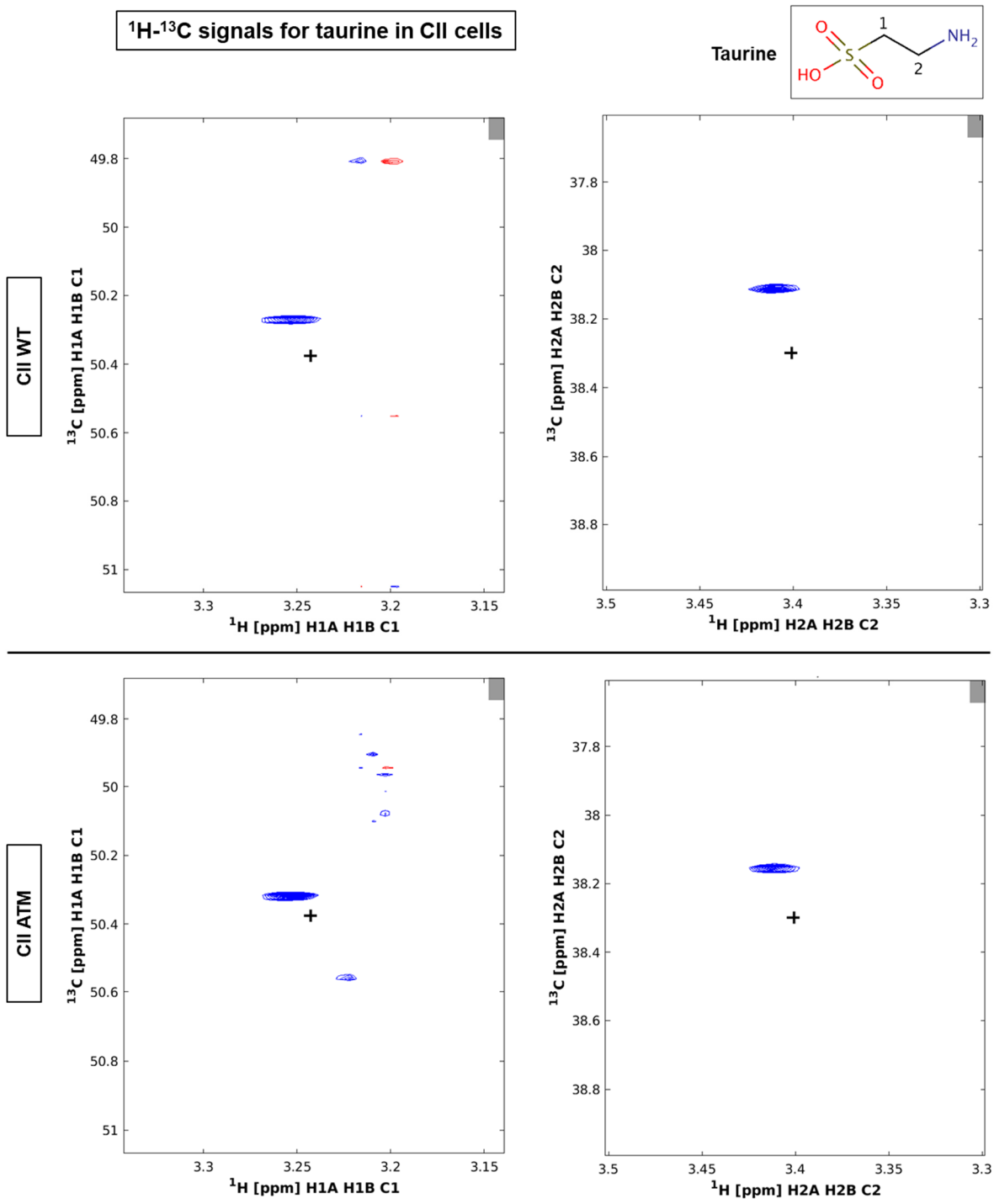

Figure 5-5: ^{1}H-^{13}C signals for taurine in CII WT and ATM cells

CII cells were cultured for 24 hours in media with [$^{13}C_3$] cysteine. ^{1}H-^{13}C HSQC spectra were acquired, and the different H-C peaks are visible for taurine in CII WT and ATM. No splitting of the taurine signal was observed in neither CII WT nor ATM. The black cross in the centre of each section of the HSQC represents the expected chemical shift for taurine.

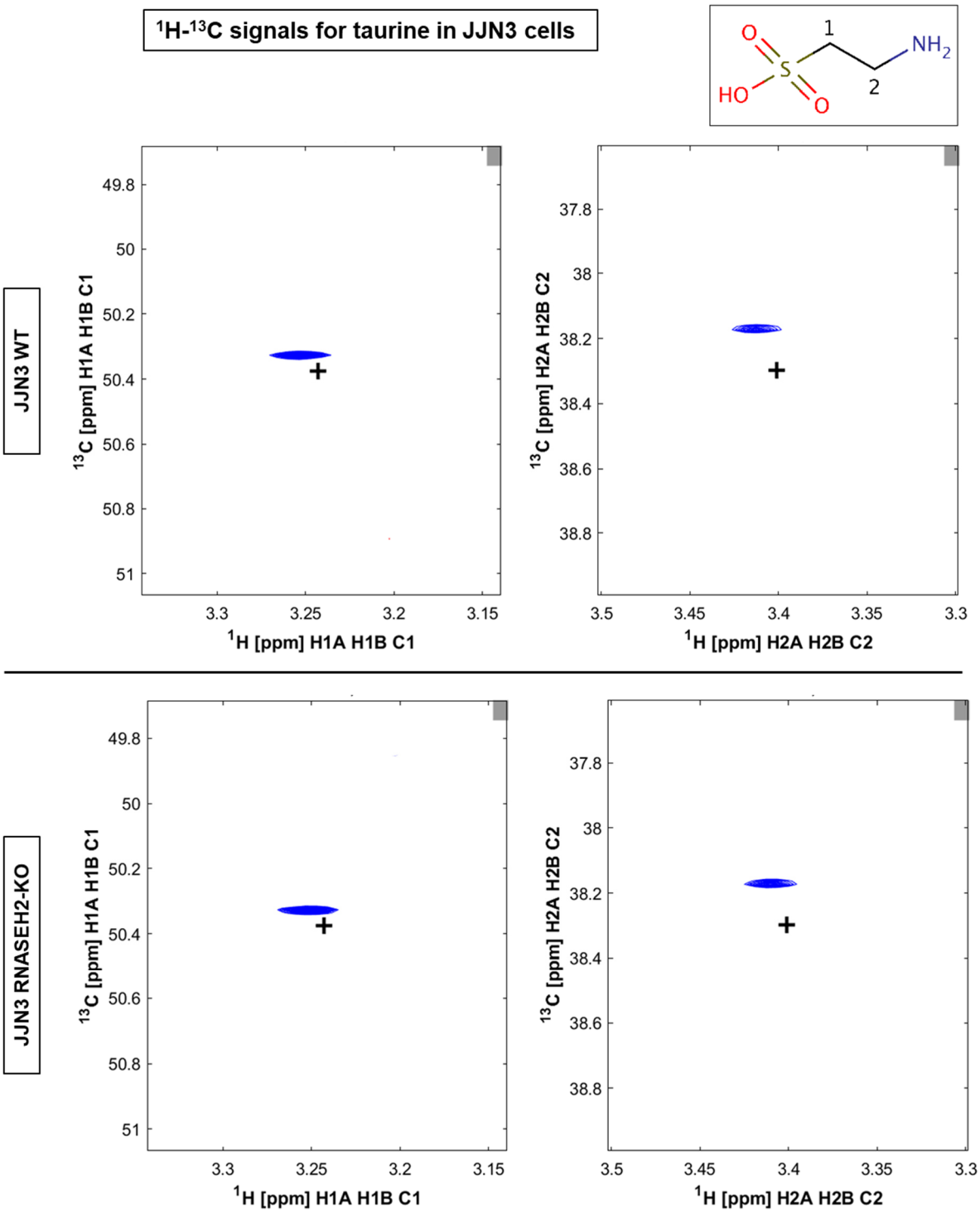

Figure 5-6: ^{1}H-^{13}C signals for taurine in JJN3 WT and RNASEH2-KO cells

CII cells were cultured for 24 hours in media with [$^{13}C_3$] cysteine. ^{1}H-^{13}C HSQC spectra were acquired, and the different H-C peaks are visible for taurine in JJN3 WT and RNASEH2-KO. No splitting of the taurine signal was observed in neither JJN3 WT nor RNASEH2-KO. The black cross in the centre of each section of the HSQC represents the expected chemical shift for taurine.

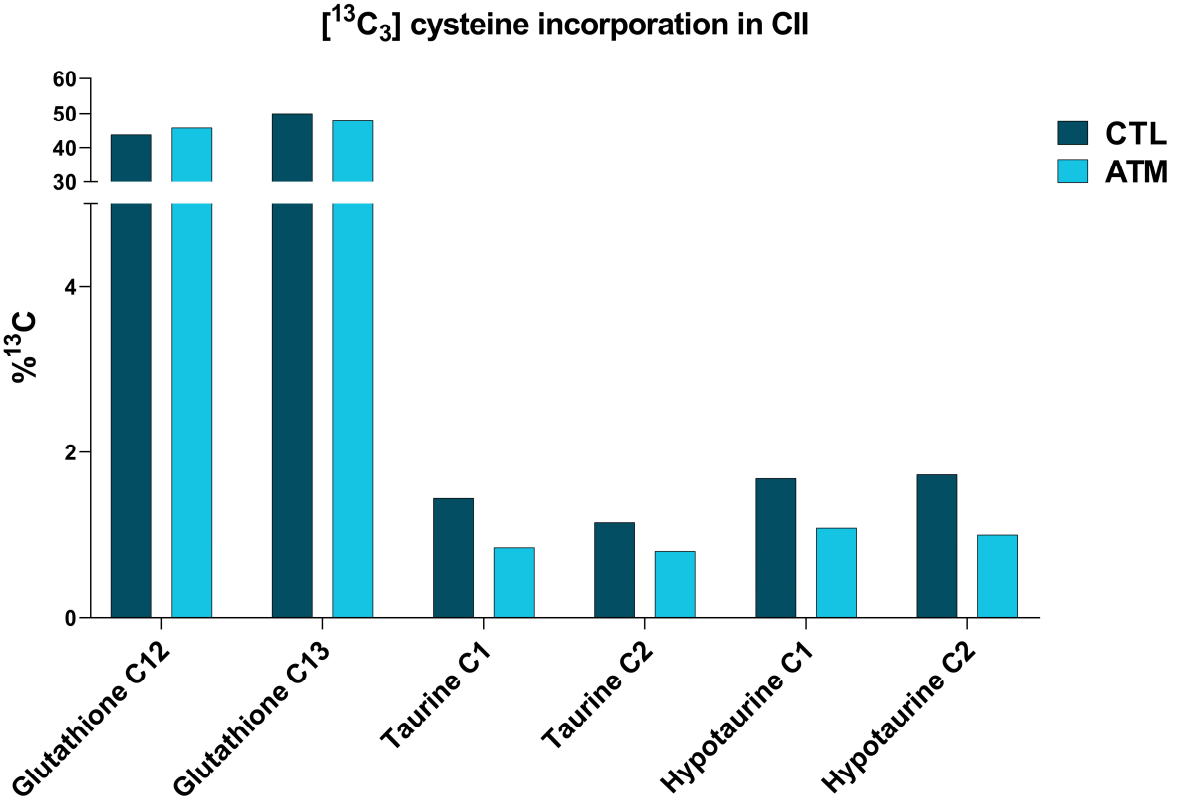

Figure 5-7: ^{13}C labelled cysteine flux to glutathione or taurine in CII cells after seven days.

Label incorporation in metabolites arising from [$^{13}C_3$] cysteine after seven days. For each experiment, bar graphs represent the percentage of ^{13}C for one independent sample (n=1). ^{13}C percentages (%^{13}C) in the different carbons were calculated after multiplying the $^{13}C/^{12}C$ ratio obtained from the labelled and corresponding unlabelled HSQC by the natural abundance of ^{13}C (1.1%).

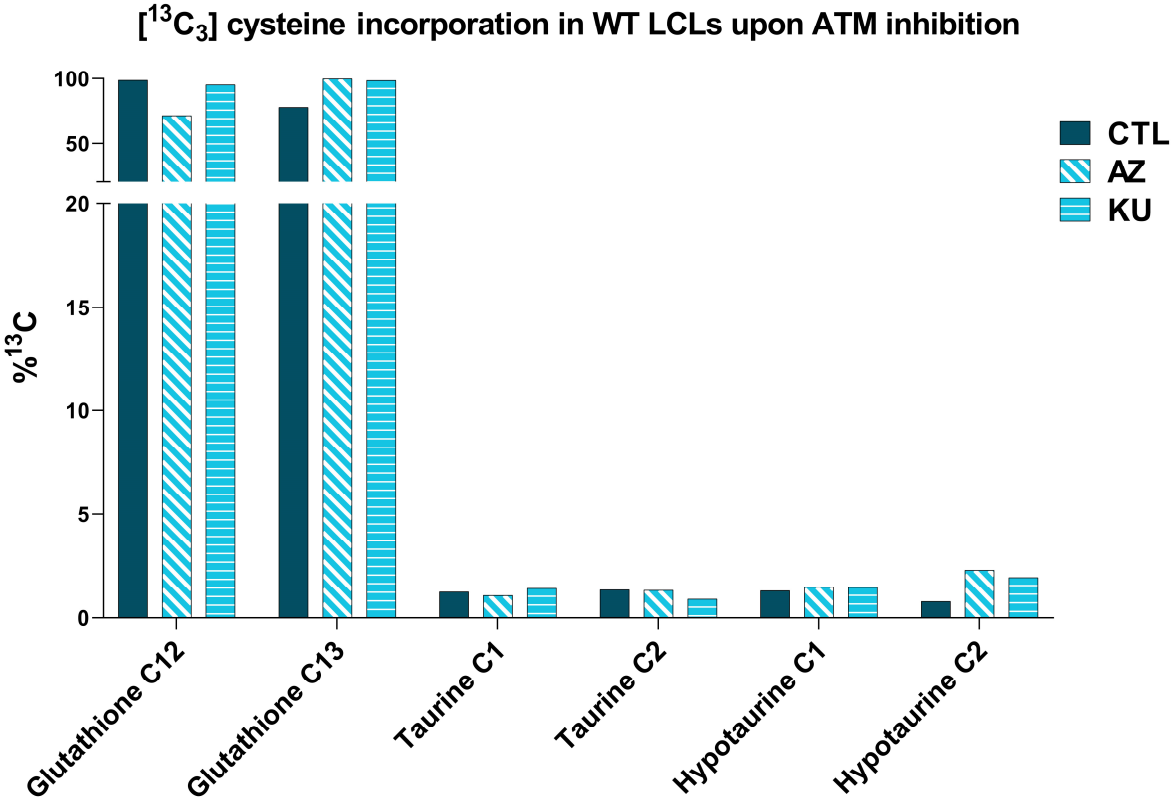

Figure 5-8: ^{13}C labelled cysteine flux to glutathione and taurine in WT LCLs upon ATM inhibition.

Label incorporation in metabolites arising from [$^{13}C_3$] cysteine in untreated WT LCLs (CTL) and WT LCLs treated with 3 μM KU-60019 (KU) or AZD0156 (AZ), cultured for 96 hours. For each experiment, bar graphs represent percentage of ^{13}C for one independent sample (n=1). ^{13}C percentages (%^{13}C) in the different carbons were calculated after multiplying the $^{13}C/^{12}C$ ratio obtained from the labelled and corresponding unlabelled HSQC by the natural abundance of ^{13}C (1.1%).

After incubation with $^{13}C^{methionine}$, the ^{13}C flux was assessed in CII and JJN3 cells. This labelling experiment was useful to evaluate a possible conversion of methionine to cysteine, precursors for taurine synthesis. ^{13}C label incorporation was only found in the fourth carbon of creatine and phosphocreatine in CII (Figure 5-9) or JJN3 cells (Figure 5-10). Although methionine can be converted in homocysteine and cystathionine in cells (Figure 5-9 and Figure 5-10), there was no ^{13}C methionine label incorporation into cystathionine and homocysteine.

Cystathionine can be further converted in cysteine or α-ketobutyric acid, with the ^{13}C from ^{13}C methionine conserved in α-ketobutyric acid only. Independently of their mutation status, all CII and JJN3 cells showed less than 5% ^{13}C label incorporation in either homocysteine, cystathionine or α-ketobutyric acid after the ^{13}C methionine label experiment and suggest an absence of cysteine synthesis from methionine. In this labelling experiment, correct assignments of the HSQC spectra were crucial to study the flux of [U-^{13}C] methionine in homocysteine and cystathionine. Given carbons are labelled in all positions in [U-^{13}C] methionine, if methionine is converted in homocysteine, the carbons in position 1, 2 and 3 of homocysteine should be labelled (Figure 5-9 and Figure 5-10). If homocysteine is then converted into cystathionine, carbons will be labelled in position 4, 5, 6 and 7. When comparing methionine, homocysteine and cystathionine peaks, it appeared that all carbons were ^{13}C labelled in methionine for all cell lines (Figure 5-11 to Figure 5-14). Not all the expected labelled carbons were observed in homocysteine or cystathionine suggesting methionine was converted into neither of these two metabolites. Indeed, a closer look to the HSQC spectra revealed that the signal for C2 in homocysteine and C4, 5 or 6 in cystathionine were those corresponding to [U-^{13}C] methionine (Figure 5-11 to Figure 5-14) and confirmed the absence of homocysteine and cystathionine synthesis from methionine in CII or JJN3 cells.

Overall, these results showed methionine being converted into creatine and phosphocreatine, but not into cystathionine, suggesting that methionine is not the precursor of cysteine and, thus, taurine synthesis in CII and JJN3 cells, independently of their DDR alteration status.

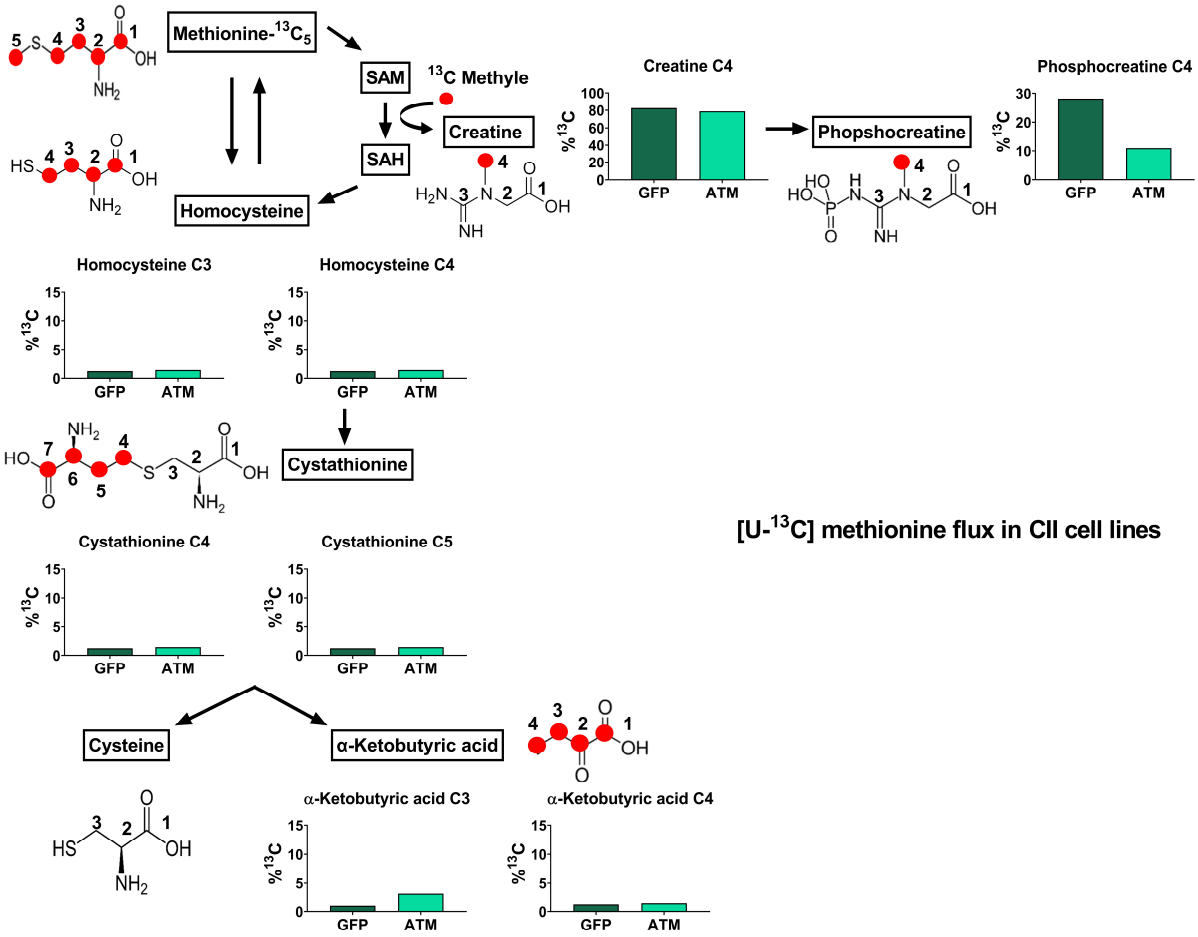

Figure 5-9: ^{13}C labelled methionine flux to phosphocreatine or α-ketobutyric acid in CII cells after 24 hours.

Label incorporation in metabolites arising from [U-^{13}C] methionine after 24 hours incubation in CII cells. Expected ^{13}C carbons are represented in red in the different metabolites. For each experiment, bar graphs represent the percentage of ^{13}C for one independent sample (n=1). ^{13}C percentages (%^{13}C) in the different carbons were calculated after multiplying the $^{13}C/^{12}C$ ratio obtained from the labelled and corresponding unlabelled HSQC by the natural abundance of ^{13}C (1.1%).

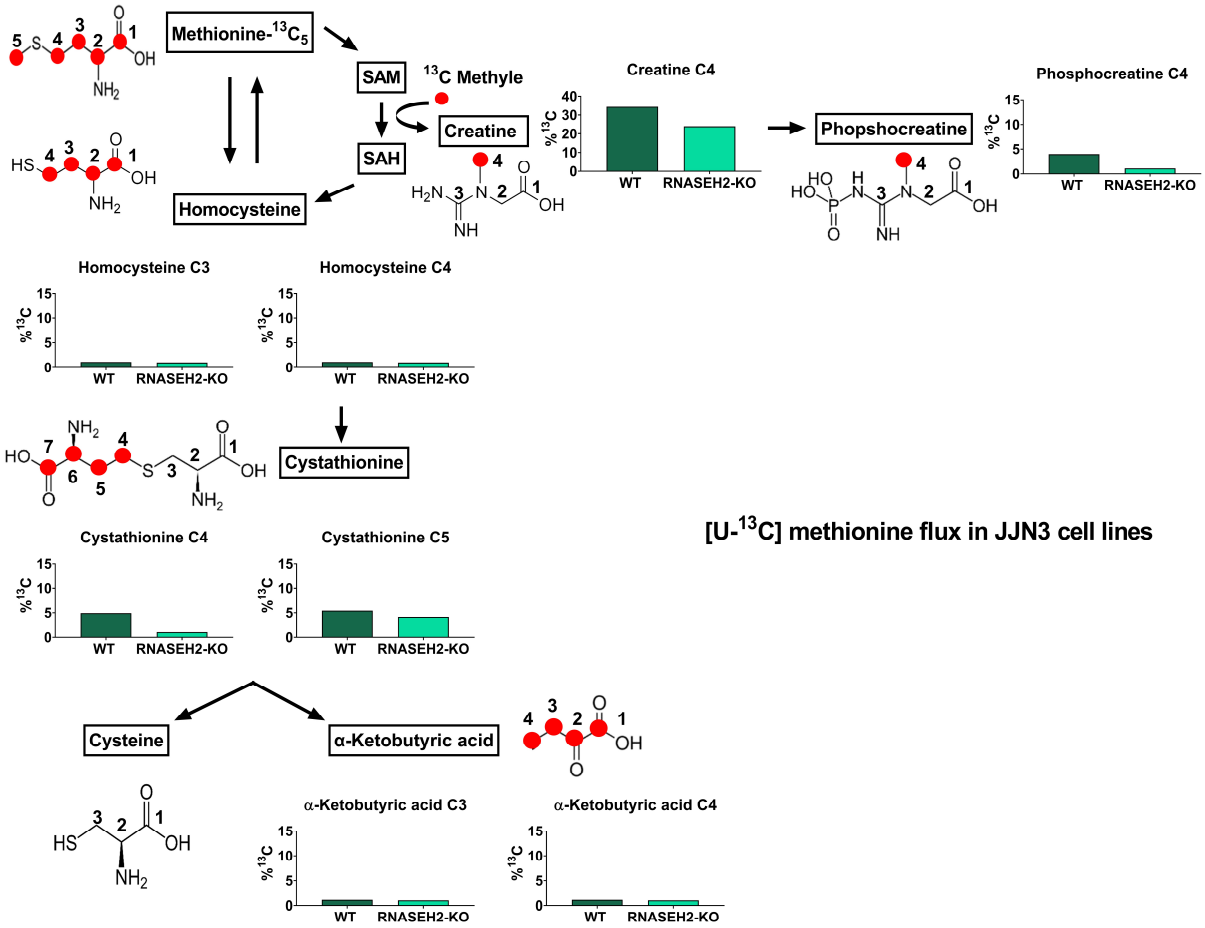

Figure 5-10: ^{13}C labelled methionine flux to phosphocreatine or α-ketobutyric acid in JJN3 cells after 24 hours.

Label incorporation in metabolites arising from [U-^{13}C] methionine after 24 hours incubation in JJN3 cells. Expected ^{13}C carbons are represented in red in the different metabolites. For each experiment, bar graphs represent the percentage of ^{13}C for one independent sample (n=1). ^{13}C percentages (%^{13}C) in the different carbons were calculated after multiplying the $^{13}C/^{12}C$ ratio obtained from the labelled and corresponding unlabelled HSQC by the natural abundance of ^{13}C (1.1%).

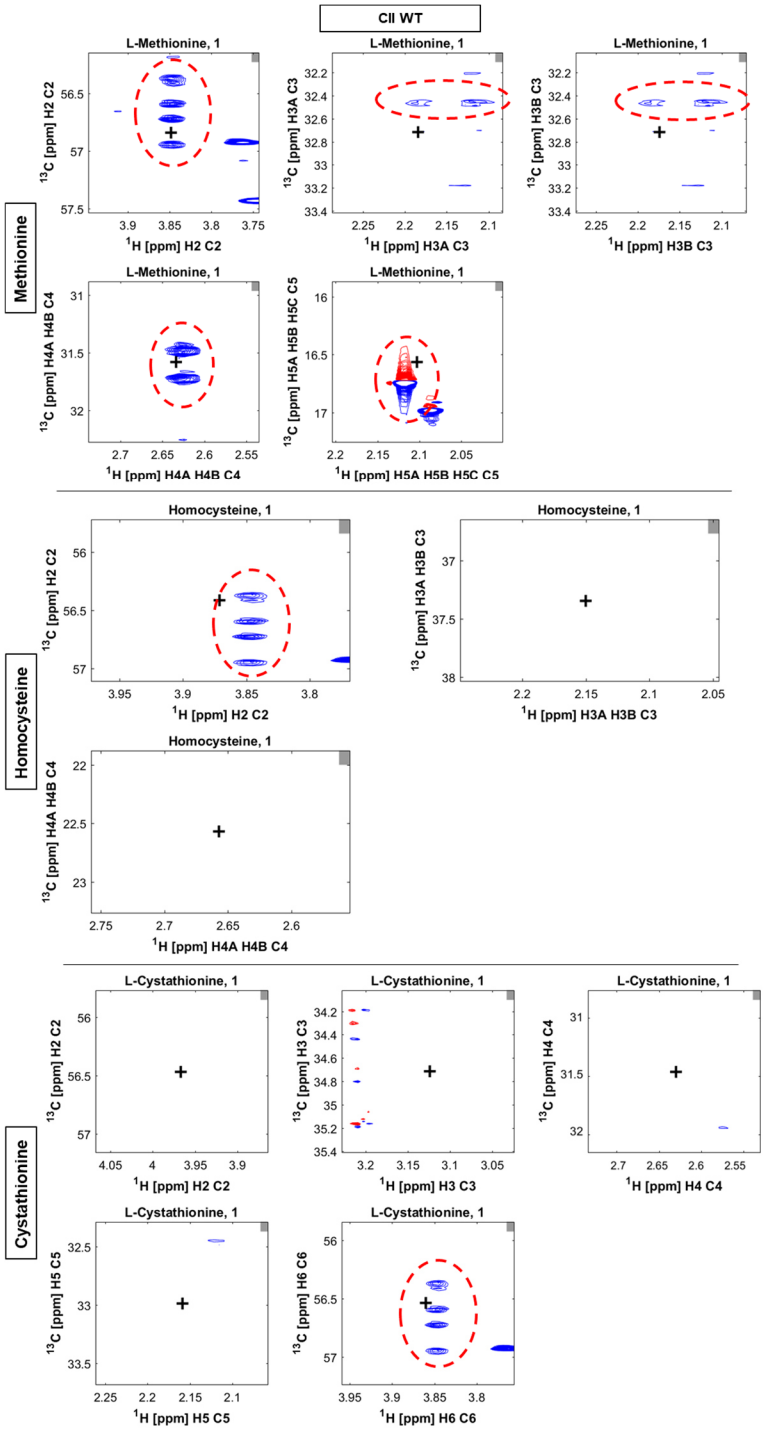

Figure 5-11: ^{1}H-^{13}C signals for methionine, homocysteine, and cystathionine in CII WT cells.

CII WT cells were cultured for 24 hours in media with [U-^{13}C] methionine. ^{1}H-^{13}C HSQC spectra were acquired, and the different H-C peaks are visible for methionine, homocysteine, and cystathionine. ^{1}H-^{13}C signals were observed for all carbons in methionine but only in C2 of homocysteine and C6 of cystathionine. The black cross in the centre of each section of the HSQC represents the expected chemical shift for each metabolite. The red circles correspond to the ^{1}H-^{13}C peaks for [U-^{13}C] methionine.

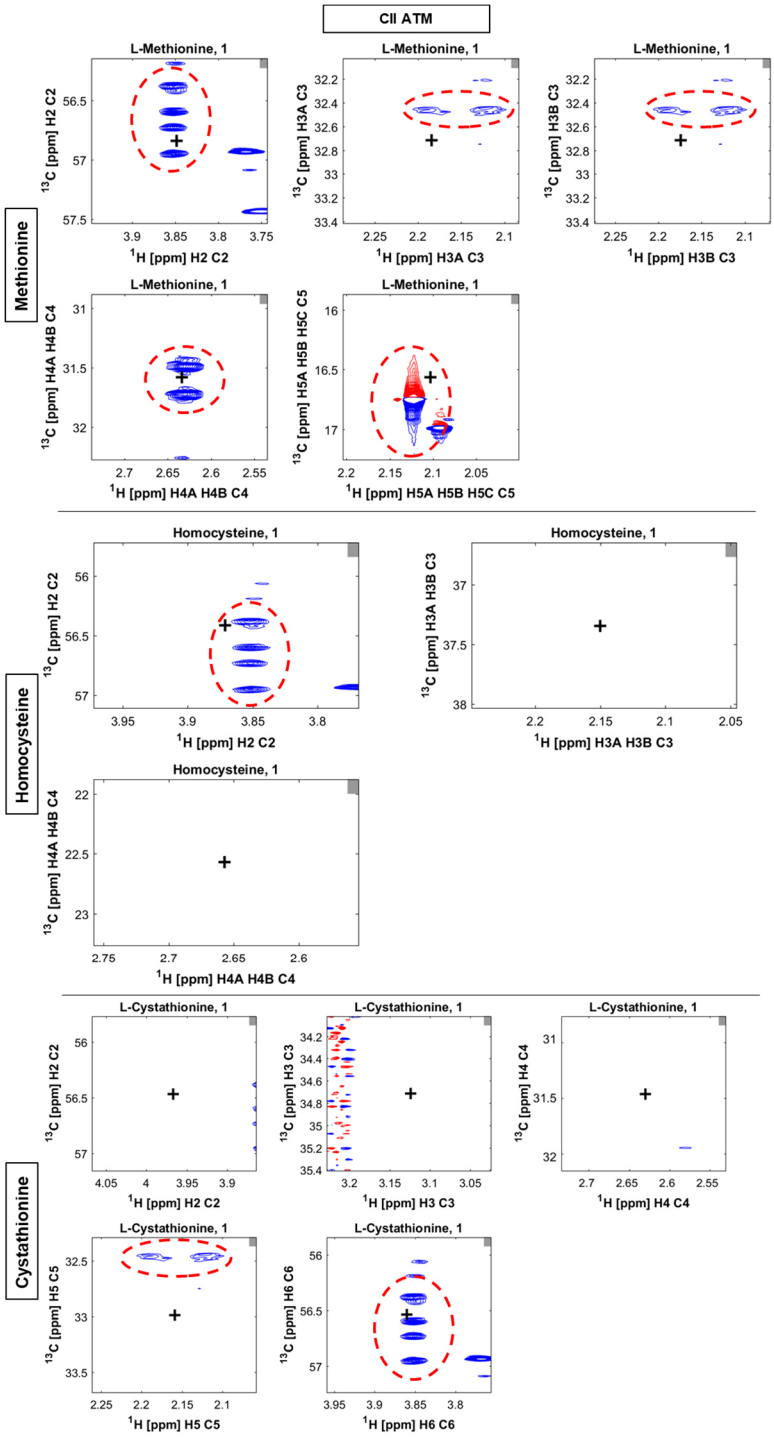

Figure 5-12: ^{1}H-^{13}C signals for methionine, homocysteine, and cystathionine in CII ATM cells.

CII ATM cells were cultured for 24 hours in media with [U-^{13}C] methionine. ^{1}H-^{13}C HSQC spectra were acquired, and the different H-C peaks are visible for methionine, homocysteine, and cystathionine. ^{1}H-^{13}C signals were observed for all carbons in methionine but only in C2 of homocysteine and C5, C6 of cystathionine. The black cross in the centre of each section of the HSQC represents the expected chemical shift for each metabolite. The red circles correspond to the ^{1}H-^{13}C peaks for [U-^{13}C] methionine.

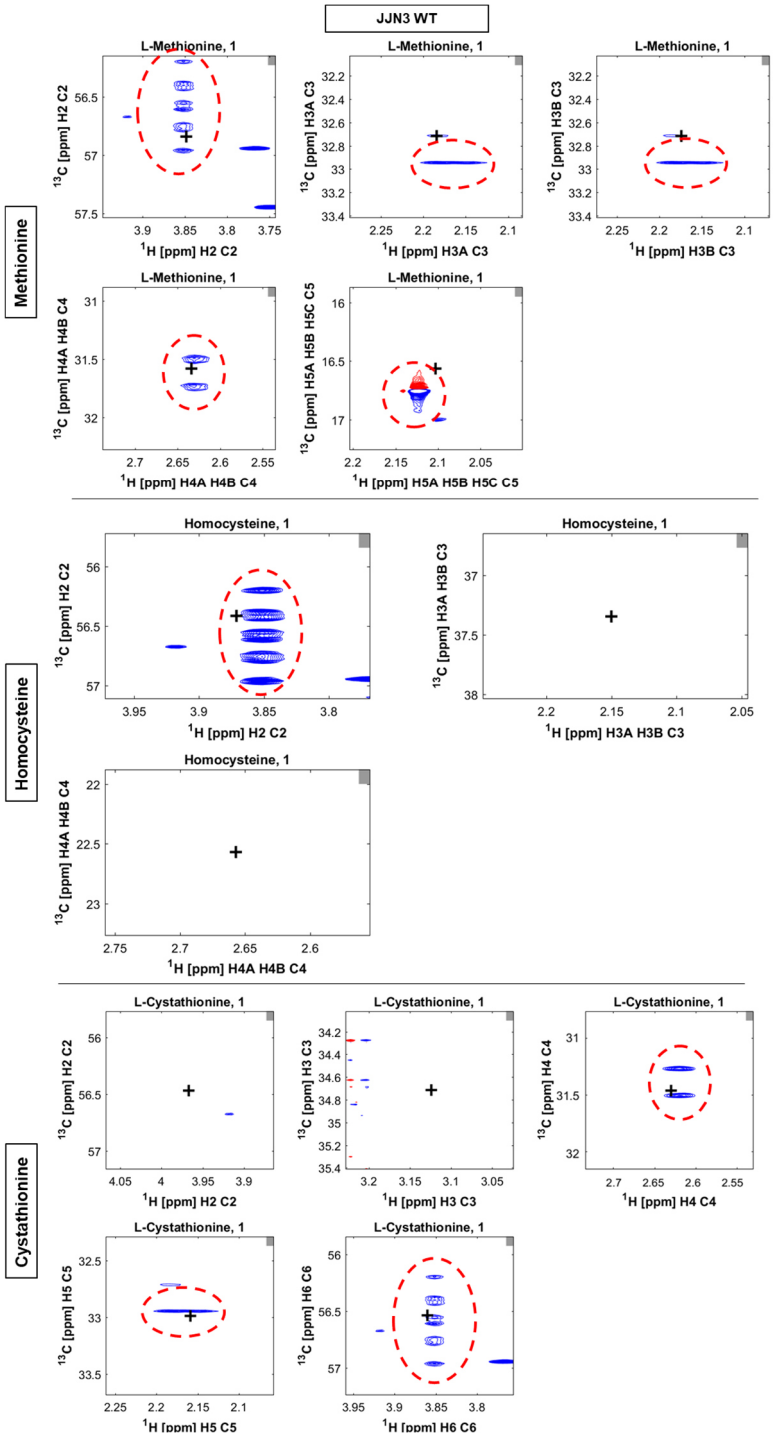

Figure 5-13: ^{1}H-^{13}C signals for methionine, homocysteine, and cystathionine in JJN3 WT cells.

JJN3 WT cells were cultured for 24 hours in media with [U-^{13}C] methionine. ^{1}H-^{13}C HSQC spectra were acquired, and the different H-C peaks are visible for methionine, homocysteine, and cystathionine. ^{1}H-^{13}C signals were observed for all carbons in methionine but only in C2 of homocysteine and C4, C5, C6 of cystathionine. The black cross in the centre of each section of the HSQC represents the expected chemical shift for each metabolite. The red circles correspond to the ^{1}H-^{13}C peaks for [U-^{13}C] methionine.

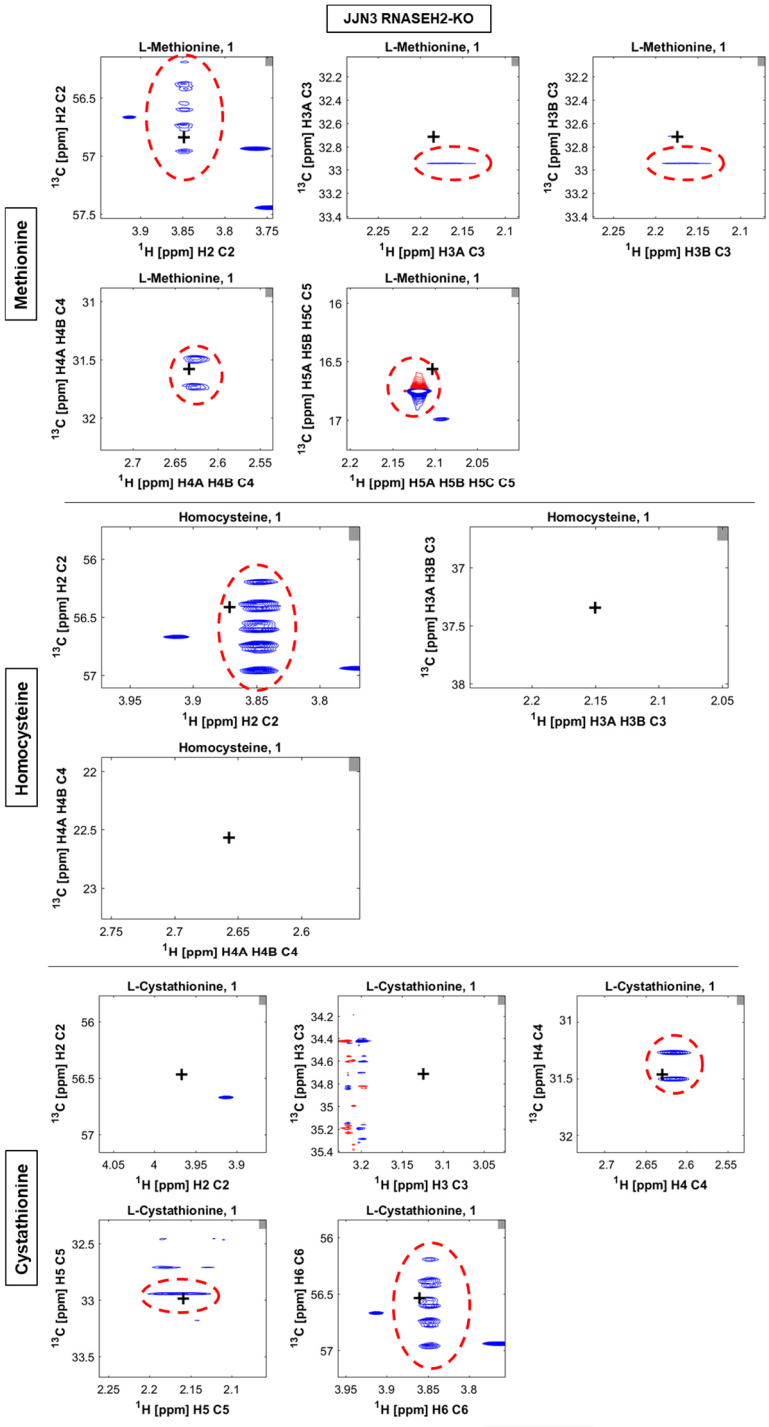

Figure 5-14: ^{1}H-^{13}C signals for methionine, homocysteine, and cystathionine in JJN3 RNASEH2-KO cells.

JJN3 RNASEH2-KO cells were cultured for 24 hours in media with [U-^{13}C] methionine. ^{1}H-^{13}C HSQC spectra were acquired, and the different H-C peaks are visible for methionine, homocysteine, and cystathionine. ^{1}H-^{13}C signals were observed for all carbons in methionine but only in C2 of homocysteine and C4, C5, C6 of cystathionine. The black cross in the centre of each section of the HSQC represents the expected chemical shift for each metabolite. The red circles correspond to the ^{1}H-^{13}C peaks for [U-^{13}C] methionine.

5.2.3. Cystathionine γ-lyase inhibition

The next experiment focused on studying the effect of a DL-propargylglycine (PAG), an inhibitor of cystathionine γ-lyase (CSD) activity on cell proliferation, viability, and intracellular taurine levels in WT and AT LCLs. The enzyme cystathionine γ-lyase (CSD) is involved in the transsulfuration pathway and glutathione synthesis. CSD catalyses the hydrolysis of cystathionine into cysteine, α-ketobutyrate and ammonia.

A previous publication suggested PAG could also inhibit taurine synthesis by blocking cysteine sulfinic acid decarboxylase (CSAD) activity [294,335]. Based on these findings, I decided to study the effect of PAG in the taurine synthesis pathway in WT and AT LCLs cells using NMR spectroscopy. The aim was to verify the results of the above tracer-based approaches (5.2.2) but also to examine the consequence of the inhibition of CSD on the intracellular taurine levels in WT and AT LCLs and to assess if it was possible to inhibit CSAD, thus taurine synthesis in cells.

First, cell growth and viability were assessed in WT and AT LCLs over 48 hours using increasing concentrations of PAG to ensure high cell viability and proliferation were maintained throughout the experiment. As shown in Figure 5-15, the viability and cell proliferation were not affected by PAG, and it was decided to extract metabolites in cells after 24- and 48-hours treatment with PAG.

For the NMR experiment, cells were maintained in RPMI with increasing concentrations of PAG (1, 2 or 3mM) for treated cells or in regular RPMI for control cells. After 24 h and 48 h incubation, the polar intracellular content was extracted and analysed by 1D ^{1}H NMR.

The comparison of the intracellular metabolic profile of all LCLs indicates stable taurine and glutathione levels over time in treated and control cells. Homocysteine and cystathionine levels

increased with increasing PAG concentrations. Alanine levels decreased in a dose-dependent manner.

These results could suggest that PAG only inhibited CSD activity, but not CSAD. Alternatively, these results could imply that taurine is not synthesised from methionine or cysteine, corroborating the previous labelled experiments. Thus, inhibiting CSAD activity would not affect taurine levels in cells.

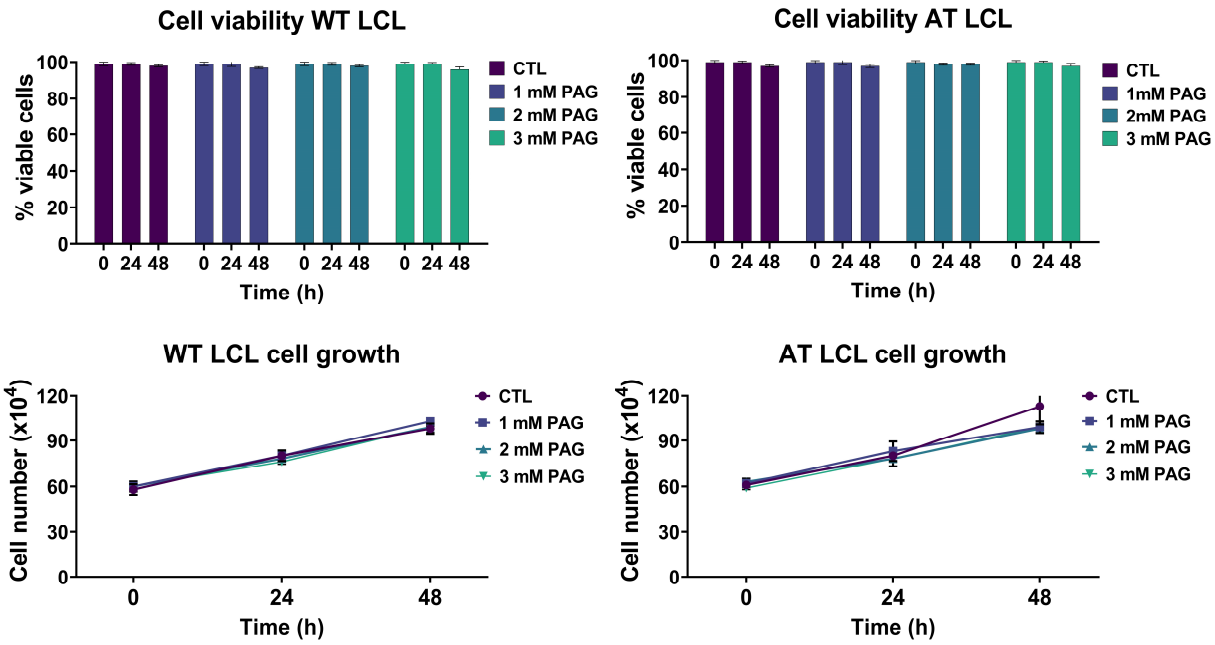

Figure 5-15: Viability and growth curve of WT and AT LCLs over 48h PAG treatment.

Approximately 60 x 10^4 cells were transferred in a flask with classic RPMI (CTL) or in RPMI containing 1, 2 or 3 mM of PAG (1 mM PAG, 2 mM PAG, 3 mM PAG). Cell growth and viability were monitored over 48 h. Viability was assessed using trypan blue assay. Results are mean of n=3 independent samples ± standard deviation.

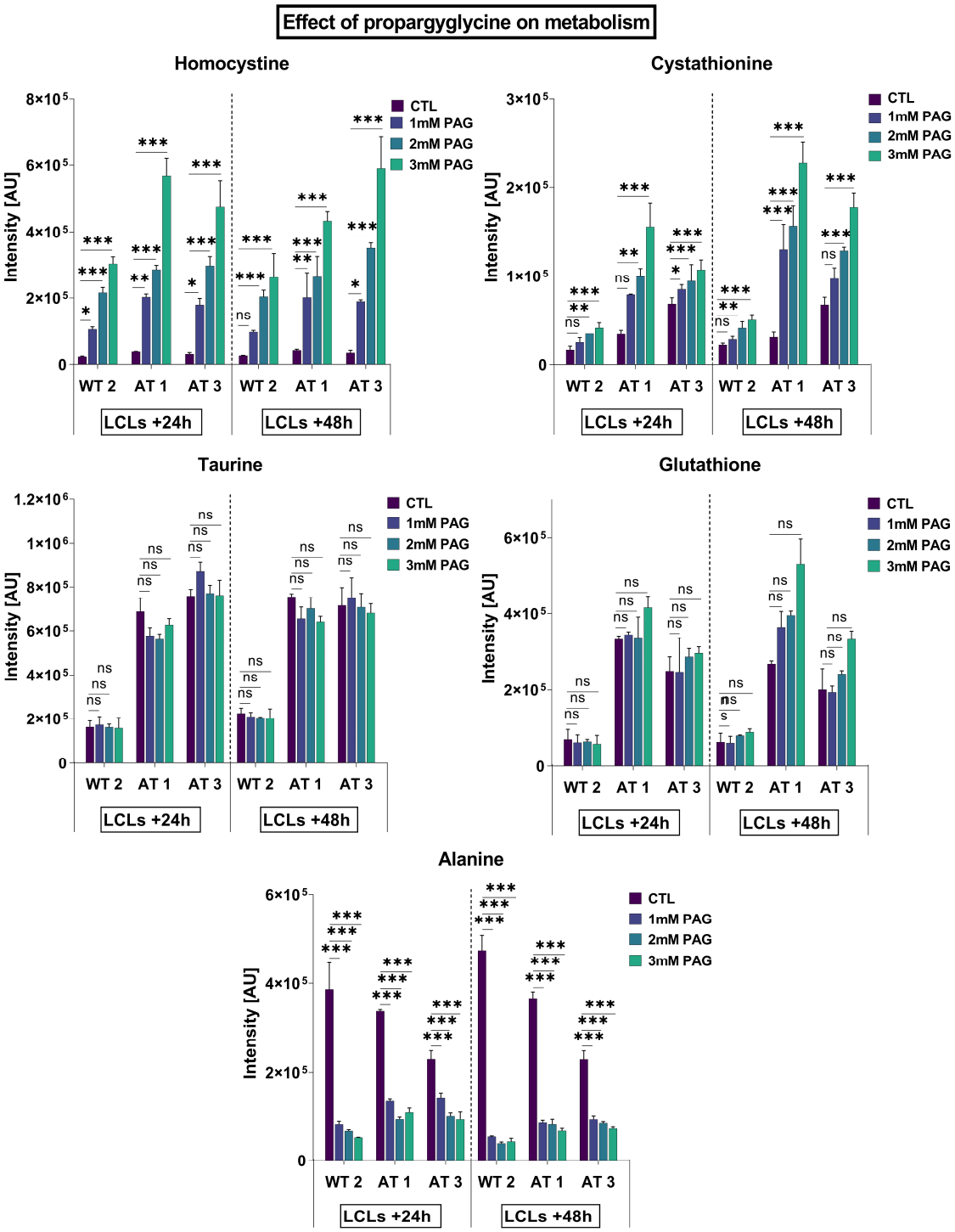

Figure 5-16: Effect of propargylglycine on intracellular metabolism of WT and AT LCLs.

Cells were maintained in culture over 48 h in classic RPMI (CTL) or RPMI containing 1, 2 or 3mM of PAG (1 mM PAG, 2 mM PAG, 3 mM PAG). Metabolic content was extracted after 24 and 48 hours and analysed by 1D ^{1}H NMR. Metabolites levels were obtained from ^{1}H-NMR spectra after processing in *Metabolab*. Bar graphs are mean of n=3 independent samples ± standard deviation. Statistical significance was calculated using ANOVA *, $P < 0.05$; **, $P < 0.05$; ***, $P < 0.001$.

5.2.4. Degradation pathways inhibition

As the source of taurine in cells was uncertain but did not appear to come from cysteine or methionine metabolism, I decided to investigate if taurine could arise from degradation processes such as autophagy or ubiquitin-proteasome pathway using inhibitors. To examine the effect of degradation pathways inhibition on intracellular taurine levels, an inhibitor of autophagy, bafilomycin (BAF), and an inhibitor of the proteasome, MG132 was used in isogenic cell lines.

The first experiment aimed at monitoring cell growth and viability in cells incubated over 24 hours with BAF or MG132 to determine the optimal time point for the NMR experiment. After incubation with both inhibitors, the intracellular metabolic profiles of WT cells and cells with defective DNA repair were obtained using 1D ^{1}H NMR spectroscopy.

Cell growth and viability were assessed in DDR-deficient cells over 24 hours. Cells were cultured in media with 10 nM BAF or 10 μM MG132. The working concentration for each inhibitor used was based on previous publications [214,336–338]. Media with 10 μM DMSO was used as a control vehicle. To choose an optimum time point for the treatments of BAF or MG132 for the NMR experiment, where metabolic changes are induced without altering cell viability or growth, both inhibitors were tested over a time course of 24 hours. Cell viability and growth curve of all cells treated with bafilomycin were similar to the control. For MG132, a decrease in cell proliferation and viability was observed after 6 hours in AT LCLs and in CII ATM cells (Figure 5-17). For JJN3 RNASEH2-KO cells, the same results were obtained after 8 hours (Figure 5-15). Based on these observations, the time of incubation chosen for the NMR experiments were 24 hours for BAF and 6 hours for MG132.

After cells were incubated 6 hours in RPMI with 10 μM of MG132 or 24 hours in RPMI with 10 nM BAF, the polar intracellular content was extracted and analysed by ^{1}H 1D NMR. DMSO was used as a control vehicle in both experiments.

After 24 hours of BAF treatment, the most interesting metabolic change was the decreased intracellular intensities in taurine in all WT and DDR-deficient cells (Figure 5-18). Interestingly the levels of *myo*-inositol were also reduced in all cell lines. Autophagy inhibition also induced a reduction in glutathione levels in cell lines except for JJN3 RNASEH2-KO but was only significant for two LCLs. Other metabolic changes included changes in intracellular leucine, alanine, glutamate, aspartate, and asparagine levels, although the results were not consistent within all the cell lines used (Figure 5-19).

After 6 hours of MG132 treatment, metabolic changes in all cell lines except WT and RNASEH2-KO JJN3 were detected. Interestingly, all LCLs and CII cells exhibited a decrease in taurine levels (Figure 5-20). LCLs and CII cells also showed a reduction in glutathione levels (Figure 5-20) and an increase in leucine, valine, arginine, glutamine, phenylalanine, and tyrosine levels following proteasome inhibition (Figure 5-21).

Altogether, the reduction of taurine levels in cells after autophagy or proteasome inhibition seemed to indicate that these degradation processes could constitute a source for taurine in cells.

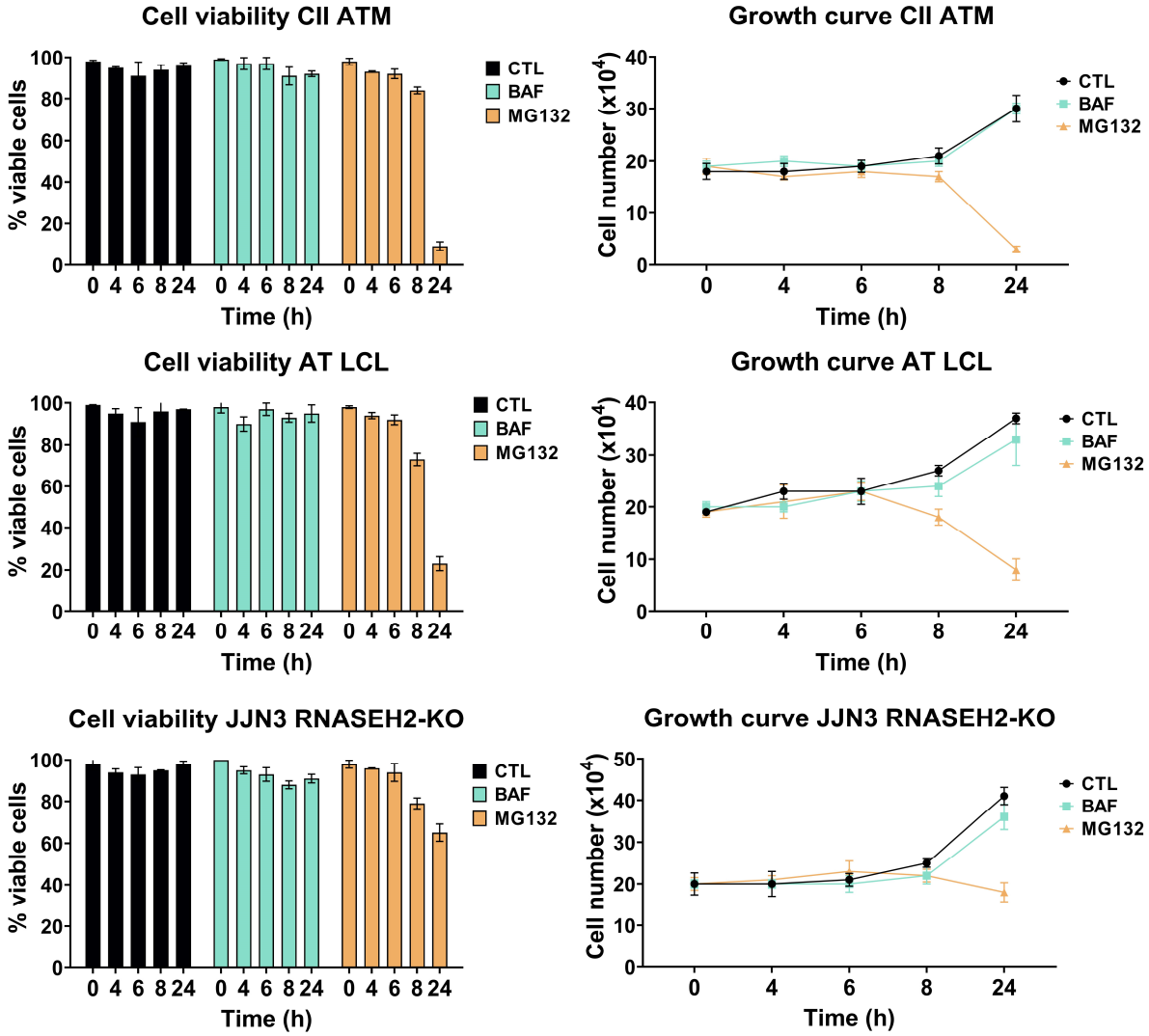

Figure 5-17: Viability and growth curve of DDR-deficient cell lines over 24 hours BAF and MG132 treatment.

Approximately 20x10^4 cells were transferred in a flask in RPMI with 10 µM DMSO (CTL), 10 nM BAF or 10 µM MG132. Cell growth and viability were monitored over 24 hours. Viability was assessed using trypan blue assay. Results are mean of n=3 independent samples ± standard deviation.

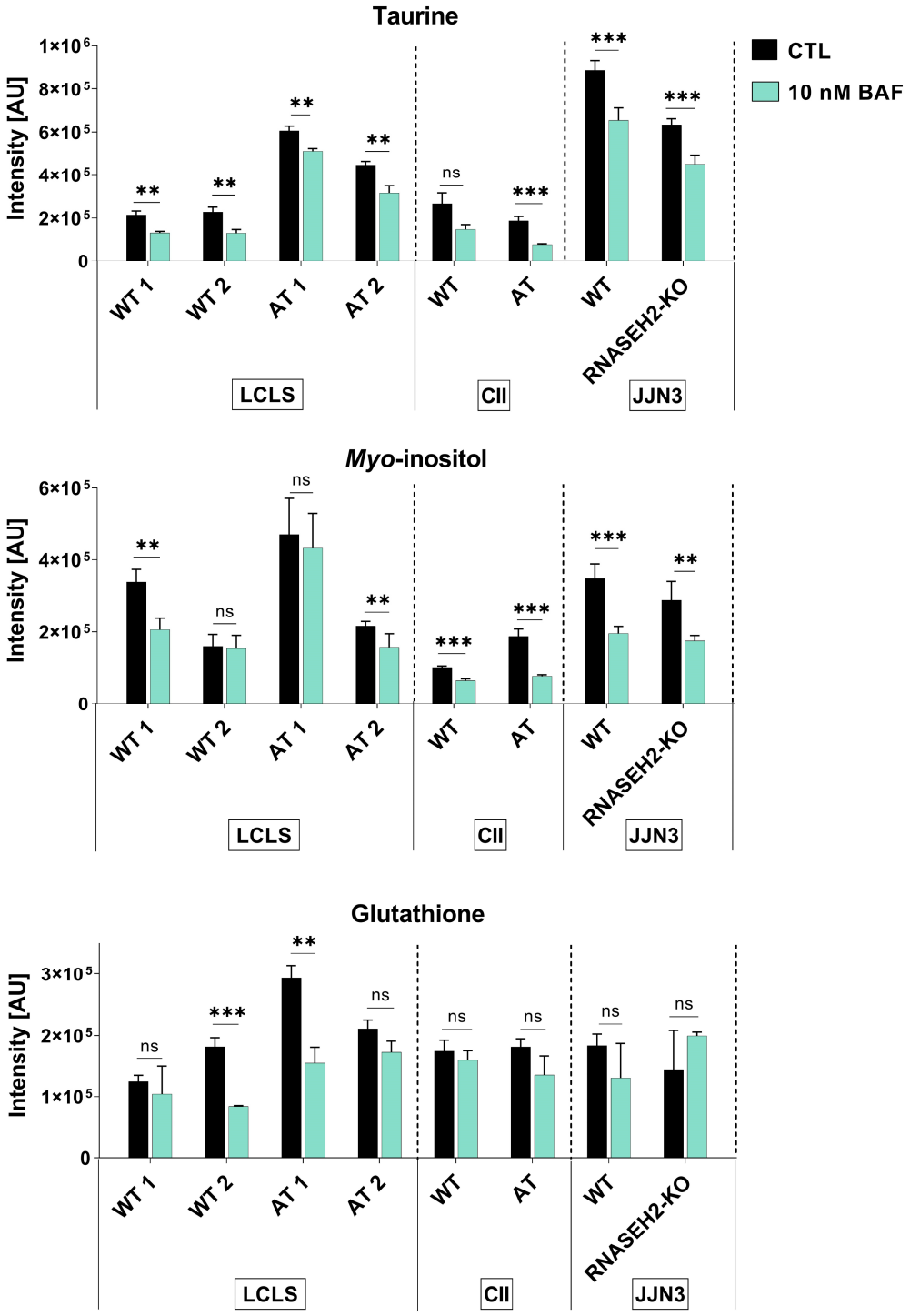

Figure 5-18: Effect of autophagy inhibition on taurine, *myo*-inositol and glutathione levels in WT and DDR-deficient cell lines.

Cells cultured over 24 hours in classic RPMI with 10 nM DMSO (CTL) or bafilomycin (BAF). The intracellular metabolic content was extracted and analysed by 1D ^{1}H NMR. Metabolites levels were obtained from ^{1}H-NMR spectra after processing in *Metabolab*. Bar graphs are mean of n=3 independent samples ± standard deviation. *, $P < 0.05$; **, $P < 0.05$; ***, $P < 0.001$ by student t-test.

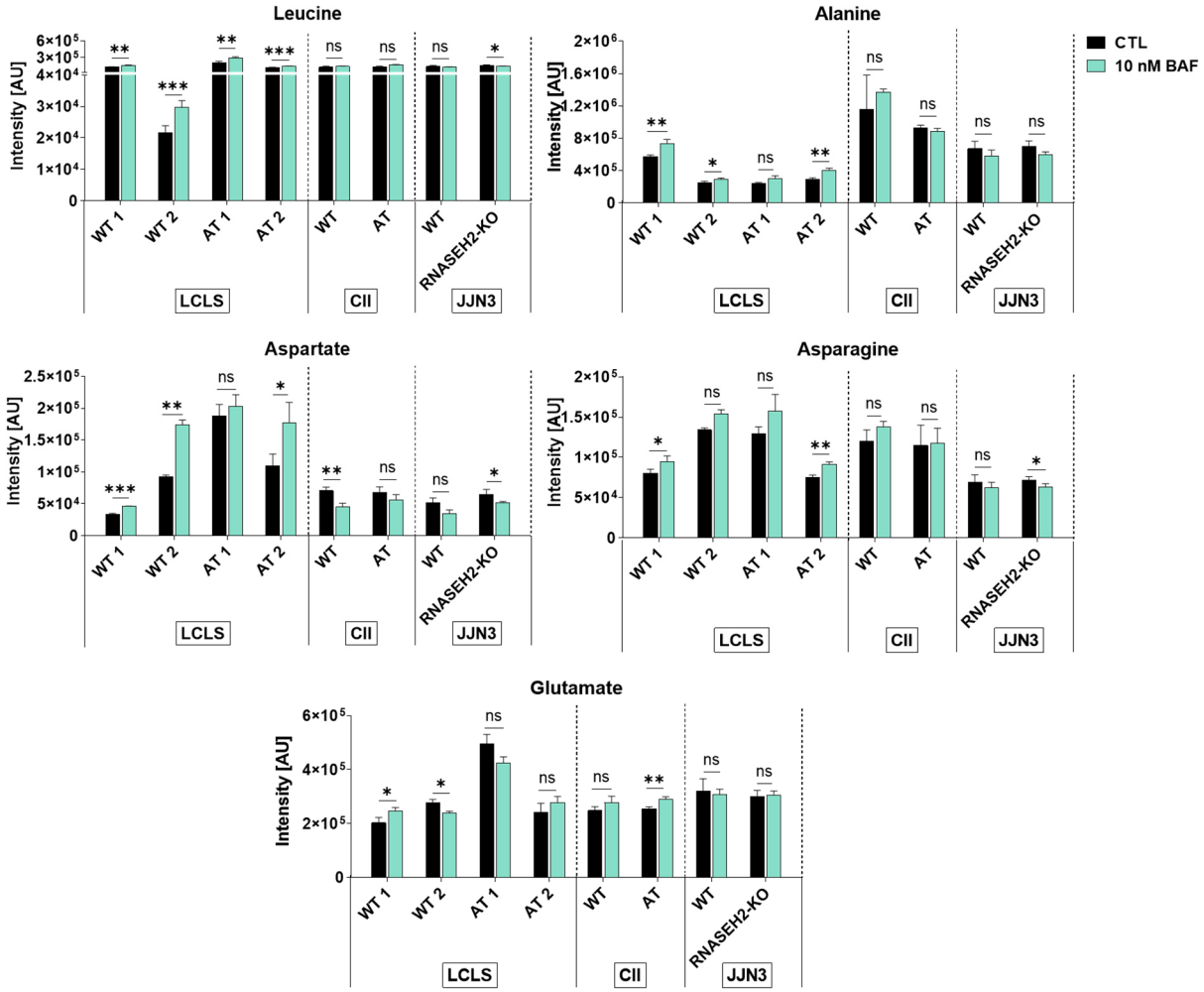

Figure 5-19: Effect of autophagy inhibition on amino acids levels in WT and DDR-deficient cell lines.

Cells cultured over 24 hours in classic RPMI with 10 nM DMSO (CTL) or bafilomycin (BAF). The intracellular metabolic content was extracted and analysed by 1D ^{1}H NMR. Metabolites levels were obtained from ^{1}H-NMR spectra after processing in *Metabolab*. Bar graphs are mean of n=3 independent samples ± standard deviation. *, $P < 0.05$; **, $P < 0.05$; ***, $P < 0.001$ by student t-test.

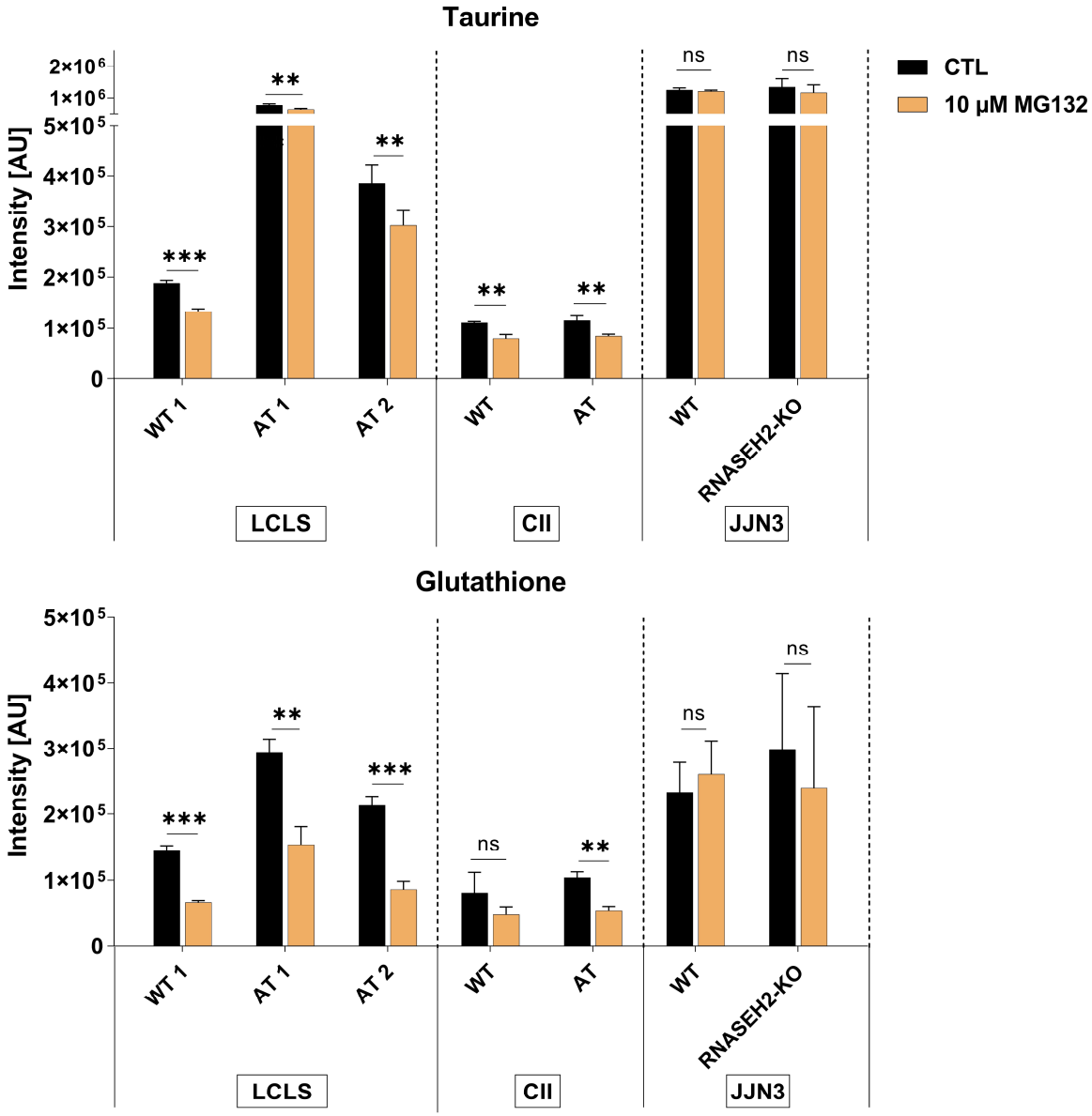

Figure 5-20: Effect of proteasome inhibition on taurine and glutathione levels in WT and DDR-deficient cell lines.

Cells were cultured over 6 hours in classic RPMI with 10 µM DMSO (CTL) or MG132. The intracellular metabolic content was extracted and analysed by 1D ^{1}H NMR. Metabolites levels were obtained from ^{1}H-NMR spectra after processing in *Metabolab*. Bar graphs are mean of n=3 independent samples ± standard deviation. *, $P < 0.05$; **, $P < 0.05$; ***, $P < 0.001$ by student t-test.

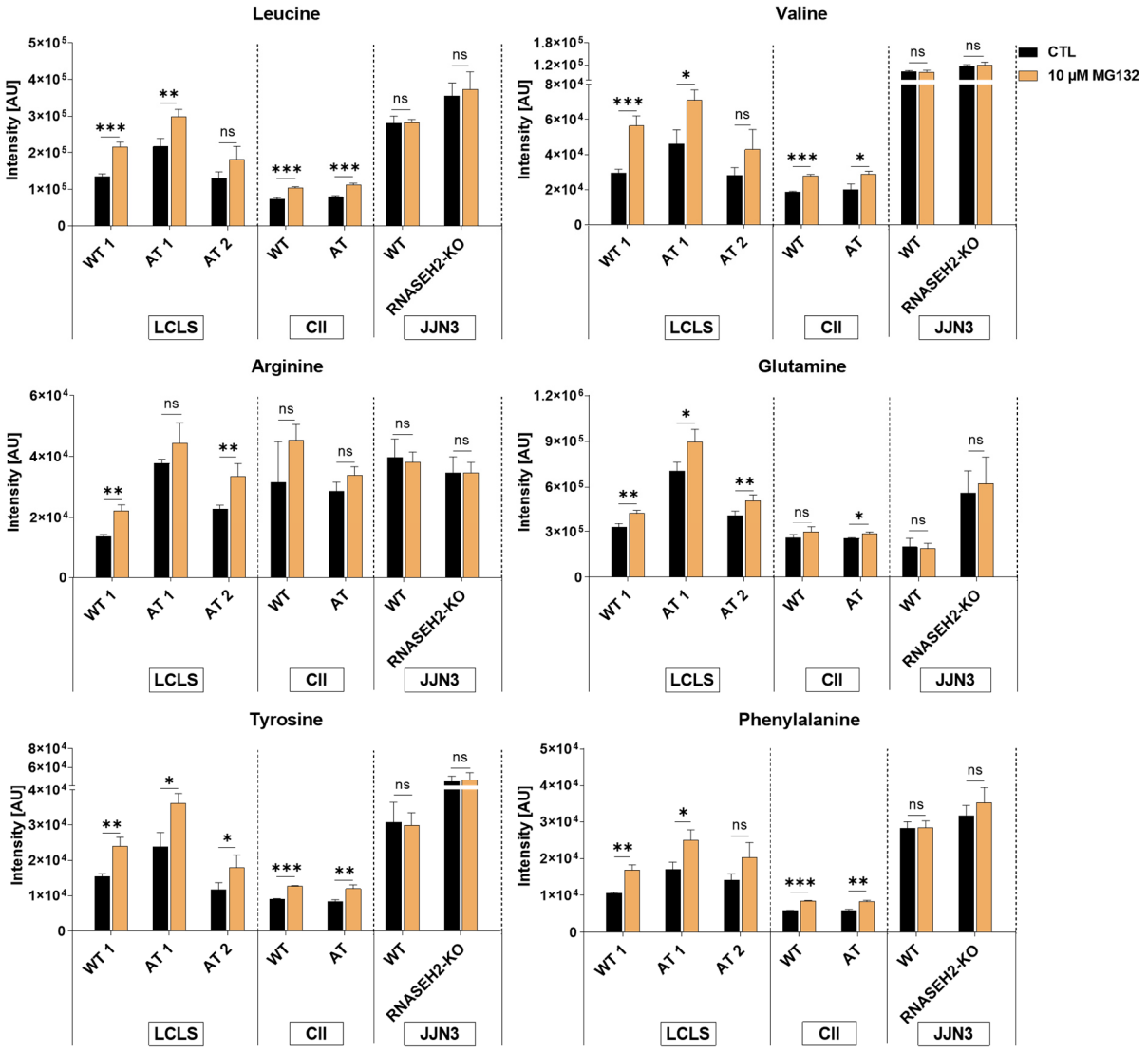

Figure 5-21: Effect of proteasome inhibition on amino acids levels in WT and DDR-deficient cell lines.

Cells were cultured over 6 hours in classic RPMI with 10 µM DMSO (CTL) or MG132. The intracellular metabolic content was extracted and analysed by 1D ^{1}H NMR. Metabolites levels were obtained from ^{1}H-NMR spectra after processing in *Metabolab*. Bar graphs are mean of n=3 independent samples ± standard deviation. *, $P < 0.05$; **, $P < 0.05$; ***, $P < 0.001$ by student t-test.

5.2.5. Measurement of oxidative stress in ATM-deficient cells

The next experiment was aimed at characterising the role of taurine in DDR-deficient cells. A link between oxidative stress and the DNA damage response has already been emphasised as reviewed in [190]. In particular, the ATM pathway is involved in redox homeostasis. Indeed, oxidative stress has been shown to lead to ATM activation and downstream activation of the DDR [69,307]. On the other hand, ATM-deficient cells were shown to display increased mitochondrial ROS levels and subsequent oxidative stress [72,339].

In this thesis, measurements of reactive oxygen species were performed in CII WT and ATM-deficient leukemic cell lines. The objective was to examine a possible correlation between ROS levels and the higher taurine levels measured in CII ATM, as taurine has been proposed to function as antioxidant.

For this experiment, total intracellular levels of ROS and mitochondrial ROS were measured in the leukemic cell lines CII WT and ATM. Cells were cultured for 24 hours in classic RPMI before staining with 2',7'-dichlorofluorescein diacetate (DCFH-DA) or MitoSOX™. Both DCFH-DA and MitoSOX turn fluorescent upon oxidation. The difference between these stains resides in their substrates, intracellular ROS and mitochondrial superoxide ($O_2^{\bullet -}$), respectively [340].

Five minutes before staining, cells were maintained in classic RPMI (control), or 1mM H_2O_2 was added to the culture media. Cell fluorescence was measured by flow cytometry.

As shown in Figure 5-22, total ROS levels were not higher in CII ATM compared to WT. After treatment with H_2O_2, CII ATM exhibited higher total ROS levels than WT cells. For mitochondrial ROS measurements, CII ATM demonstrated higher ROS levels before and after treatment with H_2O_2.

These results could suggest a link between the high levels of taurine observed in the CII ATM and the oxidative stress in these cells, but further experiments are required to corroborate this hypothesis.

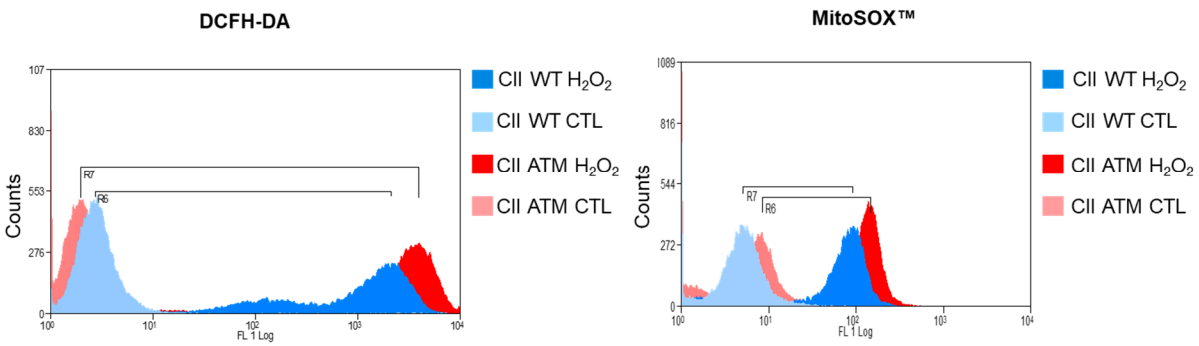

Figure 5-22: Measurement of total intracellular ROS and mitochondrial ROS in CII WT and ATM.

Intracellular and mitochondrial ROS levels were measured by flow cytometry in CII WT and ATM cell lines. Cells were cultured for 24 hours and kept in classic RPMI (CTL) or incubated in RPMI with 1mM H_2O_2 before DCFDA or MitoSox staining and fluorescence measurement by flow cytometry. The analysis was carried out with FlowJo software. Histograms are results for n=1 independent experiment.

5.3. Discussion

5.3.1. Absence of taurine synthesis

In this chapter, I explored the sources and the synthesis pathway of taurine. After verifying that the media culture did not contain taurine, I used ^{1}H-^{13}C HSQC to explore taurine synthesis pathway in WT and ATM or RNASE-H2 deficient cells and study if differences in ^{13}C labelled cysteine and methionine flux existed between these cells. In every HSQC experiment using [$^{13}C_3$] cysteine, cysteine seemed to be only metabolised into glutathione as indicated by the ^{13}C label incorporation in C12 and C13. Taurine synthesis from cysteine appeared absent as demonstrated by the absence of ^{13}C label incorporation in taurine and hypotaurine in all WT or DDR-deficient cell lines. The lack of signal splitting for taurine in the HSQC, although it could be explained the fact that the level of ^{13}C label incorporation in taurine was too low for detection, it also supports the idea of the absence of ^{13}C taurine thus its synthesis from cysteine. It is unlikely that the absence of labelling incorporation in taurine is the consequence of too short incubation time with [$^{13}C_3$] cysteine as the same labelling pattern was observed after longer incubation with ^{13}C cysteine.

Regarding the methionine labelled experiment, only phosphocreatine and creatine appeared to be labelled from [U-^{13}C] methionine. The absence of ^{13}C label incorporation in homocysteine, cystathionine and α-ketobutyric acid suggests a lack of cysteine synthesis from methionine; therefore, methionine does not seem to be a precursor of taurine in cells studied.

To my knowledge, this was the first time ^{13}C labelled methionine and cysteine were used to assess taurine synthesis in blood cells. The taurine pathway has been previously explored in other cell lines and primary cultures after incubation with labelled precursors, but the results varied between the cell type studied. For instance, taurine synthesis was investigated in primary rats astroglial cells and revealed oxidation of ^{13}C cysteine into taurine and hypotaurine [341]. On

the contrary, in HCT116 colorectal carcinoma cells, no taurine labelling was observed after incubation in media where glucose and all amino acids were ^{13}C labelled [342]. In another experiment using radioactive cysteine in cells of neural origin, incorporation of radioactivity from [^{35}S]cysteine in taurine was measured in primary murine astrocytes and neurons and C6 rat glioma cell line, but not in the other brain-derived transformed cell lines [343].

Given that taurine synthesis ability and levels depend on the cell type [239,240], the absence of taurine labelled from cysteine in the cells lines studied within this project could be explained by the inability of B-cells and plasma cells to synthesise taurine. This hypothesis is supported by the low RNA expression levels of CSAD found in blood cells compared to other cell types, as stated in the Human Protein Atlas (http://www.proteinatlas.org). To further confirm the absence of taurine synthesis in these cells, it would be interesting to perform anti-cysteine sulfinic acid decarboxylase Western Blot to study CSAD expression at protein levels.

5.3.2. Treatment with propargylglycine did not affect intracellular taurine levels

Another way to examine taurine metabolism was by using a supposed inhibitor of taurine synthesis, the propargylglycine. After 24 hours and 48 hours of incubation with PAG, higher intracellular levels of homocysteine and cystathionine were observed in a dose-dependent manner in WT and AT LCLs. It was probably a direct consequence of inhibition by PAG, which is known to inhibit the conversion of cystathionine into cysteine. Indeed, similar results were observed in primary mouse hepatocytes [294] and the plasma of rats [344] after treatment with propargylglycine. In primary hepatocytes and rats, PAG treatment did not affect intracellular glutathione levels and coincided with the observation of stable glutathione after PAG treatment in LCLs. Intracellular levels of taurine also remained stable in LCLs after PAG treatment. It was in contrast with previous findings where PAG treatment decreased the taurine levels in primary hepatocytes and rats [294,344]. A plausible reason could be that differences of CSAD expression levels, and activity exist between rat hepatocytes or tissue and the cells lines studied in this project.

Because of the limited number of publications showing a reduction of taurine levels upon PAG treatment and suggesting a dual inhibitory effect of PAG on CSD and CSAD, propargylglycine was first suspected to be able to inhibit CSD and not CSAD. Therefore, cysteine in the culture media could continue to be converted into hypotaurine and, in turn, to taurine in LCLs [294] and could explain the absence of variation in taurine levels after PAG treatment. However, a more probable explanation can be derived from the ^{13}C labelled cysteine and methionine experiments which seemed to indicate that there was no taurine synthesis from cysteine in any of the cells used in this project. Therefore, if taurine is not derived from cysteine,

blocking the conversion of cysteine sulfinate to hypotaurine with PAG would not have an impact on taurine intensities.

Finally, after PAG treatment in LCLs, a decrease in intracellular alanine intensities was also observed. This result was unexpected as the modulation of intracellular alanine levels by propargylglycine has not been reported so far. An off-target effect of the inhibitor was suspected but would need to be further investigated.

5.3.3. Degradation pathways, a source of taurine in cells?

The increased taurine found in DDR-deficient cells did not seem to be related to an increase in the taurine synthesis pathway and, moreover, the described taurine synthesis pathway did not seem to be used in the haematological cell lines studied in this project. Hence, other potential sources of taurine were explored, and the degradation pathways (autophagy and proteasome) were studied as alternatives to taurine synthesis.

After autophagy inhibition, by treating cells with bafilomycin, taurine levels were reduced in all cell lines independently of their mutation status. It could imply that autophagy is a source for taurine in cells. Interestingly, Kaneko *et al*. [250] highlighted for the first time a link between autophagy and taurine. In their publication, taurine was found to promote autophagosome formation and autophagic flux in mouse adipocytes through activation of the transcriptional factor EB (TFEB). Although the experimental approaches were different, the results of Kaneko *et al*. and those presented in this thesis, encourage the idea of crosstalk existing between taurine and autophagy in cells. Besides, autophagy was shown to facilitate the degradation of components of the repair network, demonstrating its importance in the DDR. It was further evidenced in studies revealing autophagy activation during DDR via mTORC1, reviewed in [345–347]. Most remarkably, recent studies have shown upregulation and disturbance of the autophagy in cells lacking ATM [72,209,235]. It is possible that autophagy, the DDR, and taurine are all intimately correlated, and that autophagy might be partly at the origin of the increase in taurine observed in DDR-deficient cells.

Changes in glutathione levels in cells after autophagy inhibition were anticipated as previous publications have demonstrated increased ROS production in a mouse leukemic cell line after treatment with bafilomycin [348] and after deletion of autophagy-related 7 protein in mouse skeletal muscle [349]. However, treatment with bafilomycin on WT and DDR-deficient cells

induced a contrary effect and glutathione was reduced following autophagy inhibition. A plausible reason could be a reduction of mitochondrial quality in these cells also reported in rat neurons after bafilomycin treatment. In permeabilised rat neurons, complex I, II, IV-linked respiration was reduced, measured by oxygen consumption rate (OCR) using appropriate substrates, and mitochondrial DNA damage were increased upon autophagy inhibition [214]. Similar mitochondrial OCR and damage measurements could be done in WT and DDR-deficient cells to confirm mitochondrial impairment after bafilomycin treatment.

Concerning the changes in *myo*-inositol levels, despite Criollo's [350] finding that the inositol trisphosphate receptor regulates autophagy in cells at the level of the endoplasmic reticulum and the mitochondria, it was unclear how bafilomycin had affected the inositol derivative, *myo*-inositol levels in this experiment. It possible that the decrease in *myo*-inositol is caused by the decreased activity of phosphatidylinositol signalling itself linked with autophagy. The present experiments could not assess this question, but it could be clarified in future studies.

The other degradation pathway studied was the proteasome. After the proteasome inhibition, intracellular levels of taurine and glutathione were found to be reduced in WT and AT cells. However, MG132 treatment did not induce any significant metabolic changes in JJN3 cells. The absence of metabolic variations in JJN3 cells was surprising as multiple myeloma cells are known to exert high proteasome inhibition sensitivity even exploited in clinical trials as reviewed in [351]. A probable reason could be the time point chosen in this project. Indeed, the decision on the incubation time was based on cell viability and proliferation assay. Or, in JJN3 cells, high cell viability was maintained over eight hours vs six hours for the other cell lines. It might be that JJN3 cells uptake MG132 slower than the other cells within this project; therefore, a six-hour treatment might not be sufficient to induce noticeable metabolic changes in the multiple myeloma cells. It would be interesting to repeat this experiment using more prolonged

MG132 exposure to find out if the metabolic profiles of JJN3 cells remained unchanged. The reduced taurine levels observed in WT and AT cells support once more degradation pathways, including ubiquitin-proteasome, could be a source of taurine in cells. It has not been reported before and could be the first evidence of haematological cells using degradation pathways to obtain taurine.

The proteasome is responsible for protein degradation in cells, but because taurine is not a constituent of proteins, it is unclear how proteasome inhibition could affect taurine levels. Since Suzuki *et al*. [242] demonstrated for the first time that taurine may be covalently linked to tubulin, it could be that taurine is increased following the breakdown of tubulin or, taurine may be incorporated into other proteins, still unknown to this day. It will be interesting to explore this further. Besides, according to the extent of cellular processes regulated through the ubiquitin-proteasome pathway , including cell cycle, cell metabolism, protein quality control and apoptosis reviewed in [352], it is likely that the taurine levels modulation could be an indirect consequence of proteasome inhibition.

Over the last years, the ubiquitin-proteasome system (UPS) has revealed its importance in the DNA repair processes, including in (I) interacting with DNA repair proteins through ubiquitin-like domains (II) recycling proteins in the DDR network, (III) stabilising repair factors, reviewed in [196,200,353]. The UPS is also involved in the modulation of the cellular responses to radiation [201]. It might be that the increase in intracellular taurine in DDR-deficient cells and cells after *in vitro* radiation observed in this thesis were caused by proteasome activation as a result of a high degree of DNA damage. However, this hypothesis needs corroboration.

On the other hand, the reduction in glutathione levels in WT and AT cells after proteasome inhibition was expected because it was previously reported in juxtaglomerular cells [219], in

human pulmonary fibroblast [221] and lung cancer cells [354] after treatment with MG132 although the mechanism for this reduction is yet unclear.

Other metabolic changes were observed in cell lines after autophagy or proteasome inhibition, including variable changes in amino acids levels. These results were difficult to interpret as the changes in metabolic levels were different between the cell lines, and no correlation could be found between modification of metabolic levels and cell types or their mutation status.

Overall, the reduction of taurine intracellular levels in WT and DDR-deficient cells after autophagy or proteasome inhibition suggests a role of degradation pathways in taurine homeostasis in cells. Besides, given the role of autophagy and proteasome in the DDR, these degradations pathways may be at the origin of the taurine levels elevation in cells with defective DNA repair.

5.3.4. Enhanced oxidative stress in cells defective for ATM

ROS measurements in CII cells demonstrated higher levels of mitochondrial ROS in CII ATM. After the treatment with hydrogen peroxide, CII ATM also exhibited a more pronounced increase in mitochondrial ROS levels compared to CII WT. It can be explained by the loss of ATM and its inability to act as a ROS sensor. Besides, these results were expected as Agathanggelou and co-workers showed that ATM-null primary and isogenic CLL exhibit elevated mitochondrial ROS levels and increased sensitivity to pro-oxidants [355]. Although the question of oxidative stress in ATM-deficient cells had already been addressed, it was interesting to confirm the more pronounced oxidative stress in ATM-deficient cells in the context of the taurine investigation.

Given taurine's antioxidative properties, the higher levels of taurine found in ATM-deficient CII cells could be linked with the high level of oxidative stress found in cells with a defective DNA repair pathway. However, more experiments are needed to confirm these observations. For instance, it would be interesting to measure mitochondrial ROS levels in DDR-deficient cells after taurine supplementation and see if taurine can reduce oxidative stress.

In conclusion, in this chapter, I have shown an absence of taurine synthesis from cysteine or methionine in WT and DDR-deficient cells. It seems that intracellular taurine arises, at least partially, from clearance pathways, including not only autophagy but also the ubiquitin-proteasome system. Moreover, the higher taurine levels in DDR-deficient seemed to be associated with oxidative stress.

Chapter 6 Final discussion

6.1. Major findings

The DNA damage response (DDR) supports genome stability and prevents the transmission of erroneous genetic information in cells. Hence, there are multiple consequences to alterations of these repair mechanisms, including cell malfunctioning, further triggering diseases, cancer, or ageing [1,3]. In recent years, a link between the DDR and metabolism was discovered, demonstrating that defective repair mechanisms can cause metabolic rewiring. However, given the complexity of the repair and metabolic networks, it remains to be identified whether certain enzymes or metabolites are associated with specific repair pathways or alterations [135,185]. Therefore, this thesis aimed to identify critical metabolites in association with the loss of two crucial DNA repair proteins, ATM or RNase H2, which are of particular importance in a disease context. The recognition of novel crosstalk between these two erroneous proteins and metabolism could be exploited for the design of new therapies, particularly in cells with deficient DNA repair that had evolved chemoresistance [123,134].

The approach chosen to identify metabolic markers of DDR alterations was to compare the metabolism of cells with deficient ATM or RNase H2 using an NMR methodology. Other experiments, including treatments with inhibitors and tracer-based NMR, were also performed, along with experiments to characterise the mechanism behind the metabolic changes observed.

The metabolic change that came to our attention was the increased intracellular taurine levels observed in all haematological cell models lacking ATM or RNase H2 compared to the control. An interesting metabolic change observed in all haematological cell models lacking ATM, or RNase H2 was the increased intracellular taurine levels compared to the control. In ATM-deficient cells, the variations in taurine levels were further associated with the loss and inhibition of the ATM kinase activity. On the other hand, our NMR data obtained from cells

exposed to ionising radiation, known to cause lesions in the DNA, suggested the increase in taurine might be linked with a high level of DNA damage in cells.

While the metabolic analysis of the culture media excluded an extracellular origin for taurine, it was clear from our tracer-based NMR studies that no increase of taurine biosynthesis occurred in the DDR-deficient cells from the usual metabolic precursors, cysteine, and methionine. Besides, inhibiting CSAD did not affect taurine levels in cells which had eliminated the idea of targeting taurine synthesis in cells with defective DNA repair. The absence of taurine synthesis might be explained by a lack of enzymes required for its biosynthesis but, an idea that emerges from these data was that cells might be using other pathways for their supply of taurine.

The results from the autophagy and proteasome inhibitor experiments suggested taurine could originate, at least partially from degradation pathways. This finding was of particular interest in the context of DNA repair alterations given both autophagy and proteasome have been shown to be linked with the DDR. Although not fully elucidated, the proposed mechanism for the increase in intracellular taurine in DDR-deficient cells, depicted in Figure 6-1, involved an increase in autophagic and proteolytic flux in cells lacking ATM- or RNaseH2. The increase in the activity of the degradation pathways could occur (I) through the activation of intermediate factors, so far unidentified following the loss of ATM or RNase H2, (II), as a result of increased DNA damage or (III) both. Therefore, the increase in taurine could represent a marker of DNA damage. Increasing the autophagic and the proteolytic flux might also be a strategy that DDR-deficient cells have found to maintain high intracellular levels of taurine, to fight against the oxidative stress. Although this mechanism remains elusive, it was suggested by the higher ROS levels concomitant with higher levels of taurine measured in ATM-deficient cells together with previous studies suggesting the role of taurine as an antioxidant [246–249].

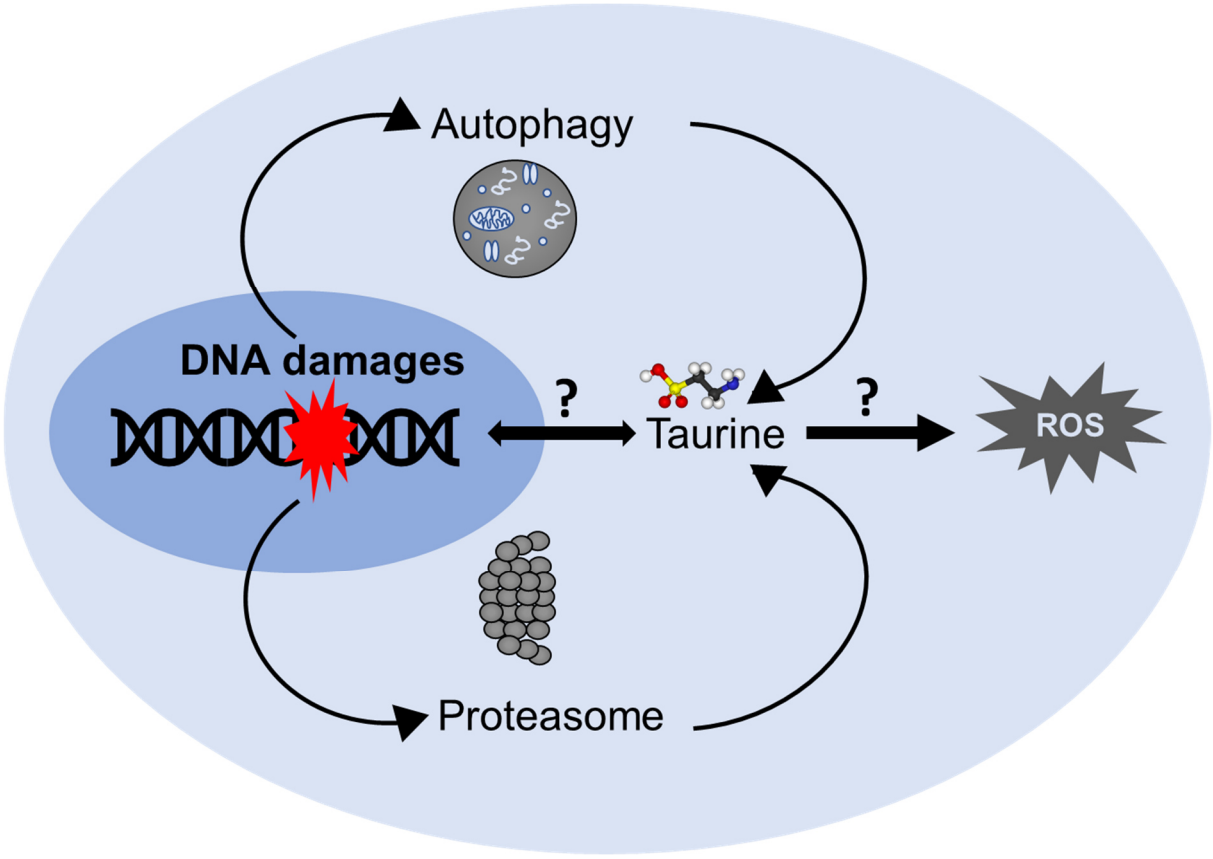

Figure 6-1: Schematic representation of the hypothetic mechanism for the increase in taurine in cells lacking ATM or RNase H2

Briefly, the accumulation of DNA damage in ATM- or RNase H2- deficient cells cause an increase in the autophagic and proteolytic fluxes that will be responsible for the increase taurine in cells. Taurine could be playing a protective role against DNA damage in the nucleus or oxidative stress.

The increase in taurine was not observed in primary CLL cells lacking ATM but, this could be explained by the high heterogeneity that characterises CLL and, the fact that the cells were arrested in G0, thus were less metabolically active. Nonetheless, an interesting finding emerged from the preliminary experiment to choose adequate samples to use for the metabolic study on primary CLLs. It appeared that differences in glutamine and glutamate existed between cells used directly after their isolation from blood or after being thawed. Not only this preliminary experiment revealed its importance in staying consistent with the type of samples used within metabolic studies but also suggested fresh primary CLL samples are more suitable when it comes to examining glutamine or glutamate metabolism.

From our results from the 1D screening of DDR-deficient cells, I suspected that the loss of ATM or RNase H2 had caused changes in the glucose and glutamine flux in cells, but the tracer-based NMR approaches did not support that hypothesis. Interesting findings though were the preferential use for glutamine of the isogenic cell lines and the absence of asparagine synthesis. Although this could be a feature of the *in vitro* models in this thesis, it showed the power of the tracer-based NMR to measure metabolic fluxes using isotopically labelled precursors.

Finally, the other metabolic differences that existed between the cell lines, or between the same cell lines but with distinct DNA repair alterations, could be explained by the various cellular origins of our in vitro models and the fact that ATM or RNase H2 are two proteins involved in separate repair mechanisms. Indeed, ATM and RNase H2 proteins have different downstream targets, plus distinct cell probably exerts differences in their basal metabolism. Nonetheless, it revealed the importance of being consistent with the type of cells and of DDR alterations to study while performing metabolic studies.

In summary, the findings in this thesis contributed to an enlarged view of ATM and RNase H2 implications in metabolism. Most importantly, it was the first time NMR-based methods

were used to investigate the metabolic role of RNase H2. Also, for the first time, a link between the degradation pathways and taurine was established, in the DDR context. These findings not only contribute towards the understanding of ATM or RNase H2 in disease and cancer but also provide opportunities for the development of therapies.

6.2. Future perspectives

Even though several aims were achieved throughout this thesis, investigating the metabolism of haematological cells with deficient ATM or RNase H2 has raised questions that were left unanswered.

First, the implication of taurine in the DDR-deficient cells should be further studied. One could consider measuring the phosphorylation of histone H2AX (γH2AX), a marker of DNA damage, after irradiation concomitant with taurine supplementation. Indeed, if the supplementation of taurine decreases the levels of γH2AX, that would confirm that taurine plays a protective role against DNA damage. Another possible diversion of this study would be to assess whether taurine localises predominantly within the nucleus, known as the site of the DDR, for instance, by comparing the metabolic profile of different cell compartment using NMR. Alternatively, measuring ROS levels in DDR-deficient cells after inducing oxidative stress using hydrogen peroxide with or without taurine supplementation to see if taurine can reduce oxidative stress would help resolve the question of the implication of taurine as an antioxidant.

Also, it could be interesting to measure CSAD expression and activity in the cell lines within this project to confirm the inability of these cells to synthesise taurine by comparing them with cells with a well-described CSAD activity.

On the other hand, the metabolic crosstalk between degradations pathways, taurine and ATM or RNase H2, should be corroborated. For example, transcriptomics analysis could improve the understanding of the mechanisms underlying the metabolic reprogramming in DDR-deficient cells and could help identify possible intermediates factors. The same way, it would be interesting to look at markers of autophagy and proteasome activation in DDR-deficient cells. Furthermore, it would be interesting to verify if the autophagy and proteasome activity increases

in response to DNA damage rather than consequently to the loss of ATM or RNase H2 in our cell models. Besides, we can imagine that in the future, the modulation of autophagy or proteasome in DDR-deficient cells could have a therapeutic potential; thus, research should be carried out in that sense. Finally, to uncover the link between the degradation pathways and taurine homeostasis, one could study if the activation of autophagy and proteasome in cells causes an increase in intracellular taurine levels.

Taurine has been shown to activate TUG1, a long non-coding RNA which is involved in metabolism and whose promoter presents a binding site for p53 [265]. Therefore, it would also be interesting to study if the increase in intracellular taurine intensities in cells with ineffective DDR is associated with an upregulation of the expression levels of TUG1 and identify which genes it regulates.

Another obvious progression of this work would be to include a larger number of primary CLL cells, this time cycling and after ensuring they are metabolically active to determine if these cells had higher levels of taurine that normal CLL cells. Also, to solve the problem of primary cell variability, genome editing method could be used to generate stable controls. Or the metabolic impact of the loss of ATM or RNase H2 in other primary cell types presenting less inter-variability and that can be more easily maintained in culture than primary CLL cells, could be studied.

It would also be interesting to complete this project by studying the metabolism of other cell types lacking ATM or RNase H2 to characterise whether an identical metabolic rewiring occurs in these other cells or if it is a feature of cells from a haematological origin. Also, this metabolic study could be extended study to other examples of DDR alterations in cell lines and primary cells to characterise whether the increase in taurine is a general feature of DDR alterations and DNA damage or only of ATM and RNase H2 deficiencies.

Finally, because of the differences that existed between the metabolism of chronic lymphocytic leukaemia and multiple myeloma cells, in a different project, the glucose and glutamine fluxes could be investigated in other cell lines and primary cells of these hematologic malignancies, as well with healthy-B and plasma cells. The interest will be to give more insight into the consequence of DDR alterations in some specific diseases. Also, together with ASNS expression levels and activity assessments, that could answer whether the lack of asparagine synthesis is a feature of CLL and multiple myeloma diseases.

6.3. Conclusion

Overall, this thesis demonstrated that defective ATM- and RNaseH2-initiated repair mechanisms caused metabolic rewiring in human haematological cells. The main finding was the higher intracellular levels of taurine found in cells lacking ATM or RNaseH2, used as models of DDR alterations, where degradations processes were likely to act as a source for taurine. Even though the increase in taurine intracellular levels could be specific to the loss of ATM and RNase H2, the same phenomenon could occur for other types of DNA repair alterations. Therefore, this study proposes new insights in the crosstalk that exists between the DDR and the metabolic networks and, further investigations should aim at researching the metabolic role of the different key proteins in the DNA repair pathways. The discovery of new associations between these two complex networks could contribute towards the development of new therapies or the enhancement of existing ones in DDR-related diseases or defective DNA repair cancers.

References

1. Jackson SP, Bartek J. The DNA-damage response in human biology and disease. *Nature*. 2009;461(7267):1071-1078. doi:10.1038/nature08467

2. Chatterjee N, Walker GC. Mechanisms of DNA damage, repair, and mutagenesis. *Environ Mol Mutagen*. 2017;58(5):235-263. doi:10.1002/em.22087

3. Giglia-Mari G, Zotter A, Vermeulen W. DNA damage response. *Cold Spring Harb Perspect Biol*. 2011;3(1):1-19. doi:10.1101/cshperspect.a000745

4. Aziz K, Nowsheen S, Pantelias G, Iliakis G, Gorgoulis VG, Georgakilas AG. Targeting DNA damage and repair: Embracing the pharmacological era for successful cancer therapy. *Pharmacol Ther*. 2012;133(3):334-350. doi:10.1016/j.pharmthera.2011.11.010

5. Blackford AN, Jackson SP. ATM, ATR, and DNA-PK: The Trinity at the Heart of the DNA Damage Response. *Mol Cell*. 2017;66(6):801-817. doi:10.1016/j.molcel.2017.05.015

6. Krokan HE, Bjoras M. Base Excision Repair. *Cold Spring Harb Perspect Biol*. 2013;5(4):a012583-a012583. doi:10.1101/cshperspect.a012583

7. Scharer OD. Nucleotide Excision Repair in Eukaryotes. *Cold Spring Harb Perspect Biol*. 2013;5(10):a012609-a012609. doi:10.1101/cshperspect.a012609

8. Kunkel TA, Erie DA. DNA MISMATCH REPAIR. *Annu Rev Biochem*. 2005;74(1):681-710. doi:10.1146/annurev.biochem.74.082803.133243

9. Shrivastav M, De Haro LP, Nickoloff JA. Regulation of DNA double-strand break repair pathway choice. *Cell Res*. 2008;18(1):134-147. doi:10.1038/cr.2007.111

10. Harper JW, Elledge SJ. The DNA Damage Response: Ten Years After. *Mol Cell*. 2007;28(5):739-745. doi:10.1016/j.molcel.2007.11.015

11. Ribezzo F, Shiloh Y, Schumacher B. Systemic DNA damage responses in aging and diseases. *Semin Cancer Biol*. 2016;37-38(Figure 1):26-35. doi:10.1016/j.semcancer.2015.12.005

12. Savitsky K, Bar-Shira A, Gilad S, et al. A single ataxia telangiectasia gene with a product similar to PI-3 kinase. *Science (80-)*. 1995;268(5218):1749-1753. doi:10.1126/science.7792600

13. Uziel T, Savitsky K, Platzer M, et al. Genomic Organization of the ATM Gene. *Genomics*. 1996;33(2):317-320. doi:10.1006/geno.1996.0201

14. Taylor AM, Byrd PJ. Molecular pathology of ataxia telangiectasia. *J Clin Pathol*. 2005;58(10):1009-1015. doi:10.1136/jcp.2005.026062

15. Gately DP, Hittle JC, Chan GKT, Yen TJ. Characterization of ATM Expression, Localization, and Associated DNA-dependent Protein Kinase Activity. Hunter T, ed.

Mol Biol Cell. 1998;9(9):2361-2374. doi:10.1091/mbc.9.9.2361

16. Rivera-Calzada A, López-Perrote A, Melero R, et al. Structure and Assembly of the PI3K-like Protein Kinases (PIKKs) Revealed by Electron Microscopy. *AIMS Biophys*. 2015;2(2):36-57. doi:10.3934/biophy.2015.2.36

17. Fernandes N, Sun Y, Chen S, et al. DNA damage-induced association of ATM with its target proteins requires a protein interaction domain in the N terminus of ATM. *J Biol Chem*. 2005;280(15):15158-15164. doi:10.1074/jbc.M412065200

18. Watters D, Khanna KK, Beamish H, et al. Cellular localisation of the ataxia-telangiectasia (ATM) gene product and discrimination between mutated and normal forms. *Oncogene*. 1997;14(16):1911-1921. doi:10.1038/sj.onc.1201037

19. Guo Z, Kozlov S, Lavin MF, Person MD, Paull TT. ATM Activation by Oxidative Stress. *Science (80-)*. 2010;6003(330):517-521. doi:10.1126/science.1192912

20. Bakkenist CJ, Kastan MB. DNA damage activates ATM through intermolecular autophosphorylation and dimer dissociation. *Nature*. 2003;421(6922):499-506. doi:10.1038/nature01368

21. Boohaker RJ, Xu B. The versatile functions of ATM kinase. *Biomed J*. 2014;37(1):3-9. doi:10.4103/2319-4170.125655

22. Lee JH, Paull TT. Activation and regulation of ATM kinase activity in response to DNA double-strand breaks. *Oncogene*. 2007;26(56):7741-7748. doi:10.1038/sj.onc.1210872

23. Mehta A, Haber JE. Sources of DNA Double-Strand Breaks and Models of Recombinational DNA Repair. *Cold Spring Harb Perspect Biol*. 2014;6(9):a016428-a016428. doi:10.1101/cshperspect.a016428

24. Yang N, Galick H, Wallace SS. Attempted base excision repair of ionizing radiation damage in human lymphoblastoid cells produces lethal and mutagenic double strand breaks. *DNA Repair (Amst)*. 2004;3(10):1323-1334. doi:10.1016/j.dnarep.2004.04.014

25. Oster S, Aqeilan RI. Programmed DNA Damage and Physiological DSBs: Mapping, Biological Significance and Perturbations in Disease States. *Cells*. 2020;9(8):1870. doi:10.3390/cells9081870

26. Vilenchik MM, Knudson AG. Endogenous DNA double-strand breaks: Production, fidelity of repair, and induction of cancer. *Proc Natl Acad Sci*. 2003;100(22):12871-12876. doi:10.1073/pnas.2135498100

27. Moynahan ME, Jasin M. Loss of heterozygosity induced by a chromosomal double-strand break. *Proc Natl Acad Sci*. 1997;94(17):8988-8993. doi:10.1073/pnas.94.17.8988

28. Khanna KK, Jackson SP. DNA double-strand breaks: signaling, repair and the cancer connection. *Nat Genet*. 2001;27(3):247-254. doi:10.1038/85798

29. Lamarche BJ, Orazio NI, Weitzman MD. The MRN complex in double-strand break

repair and telomere maintenance. *FEBS Lett*. 2010;584(17):3682-3695. doi:10.1016/j.febslet.2010.07.029

30. Uziel T, Lerenthal Y, Moyal L, Andegeko Y, Mittelman L, Shiloh Y. Requirement of the MRN complex for ATM activation by DNA damage. *EMBO J*. 2003;22(20):5612-5621. doi:10.1093/emboj/cdg541

31. Sun Y, Xu Y, Roy K, Price BD. DNA Damage-Induced Acetylation of Lysine 3016 of ATM Activates ATM Kinase Activity. *Mol Cell Biol*. 2007;27(24):8502-8509. doi:10.1128/mcb.01382-07

32. Kastan MB, Lim D. The many substrates and functions of ATM. *Nat Rev Mol Cell Biol*. 2000;1(3):179-186. doi:10.1038/35043058

33. Burma S, Chen BP, Murphy M, Kurimasa A, Chen DJ. ATM Phosphorylates Histone H2AX in Response to DNA Double-strand Breaks. *J Biol Chem*. 2001;276(45):42462-42467. doi:10.1074/jbc.C100466200

34. Xie A, Hartlerode A, Stucki M, et al. Distinct Roles of Chromatin-Associated Proteins MDC1 and 53BP1 in Mammalian Double-Strand Break Repair. *Mol Cell*. 2007;28(6):1045-1057. doi:10.1016/j.molcel.2007.12.005

35. Banin S. Enhanced Phosphorylation of p53 by ATM in Response to DNA Damage. *Science (80-)*. 1998;281(5383):1674-1677. doi:10.1126/science.281.5383.1674

36. Canman CE, Lim DS, Cimprich KA, et al. Activation of the ATM kinase by ionizing radiation and phosphorylation of p53. *Science (80-)*. 1998;281(5383):1677-1679. doi:10.1126/science.281.5383.1677

37. Michael D, Oren M. The p53–Mdm2 module and the ubiquitin system. *Semin Cancer Biol*. 2003;13(1):49-58. doi:10.1016/S1044-579X(02)00099-8

38. Craig A, Scott M, Burch L, Smith G, Ball K, Hupp T. Allosteric effects mediate CHK2 phosphorylation of the p53 transactivation domain. *EMBO Rep*. 2003;4(8):787-792. doi:10.1038/sj.embor.embor901

39. Hirao A, Kong YY, Matsuoka S, et al. DNA damage-induced activation of p53 by the checkpoint kinase Chk2. *Science*. 2000;287(5459):1824-1827. doi:10.1126/science.287.5459.1824

40. Matsuoka S. Linkage of ATM to Cell Cycle Regulation by the Chk2 Protein Kinase. *Science (80-)*. 1998;282(5395):1893-1897. doi:10.1126/science.282.5395.1893

41. Zhang X, Succi J, Feng Z, Prithivirajsingh S, Story MD, Legerski RJ. Artemis Is a Phosphorylation Target of ATM and ATR and Is Involved in the G 2 /M DNA Damage Checkpoint Response. *Mol Cell Biol*. 2004;24(20):9207-9220. doi:10.1128/MCB.24.20.9207-9220.2004

42. Karimian A, Ahmadi Y, Yousefi B. Multiple functions of p21 in cell cycle, apoptosis and transcriptional regulation after DNA damage. *DNA Repair (Amst)*. 2016;42:63-71.

doi:10.1016/j.dnarep.2016.04.008

43. Roos WP, Kaina B. DNA damage-induced cell death by apoptosis. *Trends Mol Med*. 2006;12(9):440-450. doi:10.1016/j.molmed.2006.07.007

44. Lieber MR. The Mechanism of Double-Strand DNA Break Repair by the Nonhomologous DNA End-Joining Pathway. *Annu Rev Biochem*. 2010;79(1):181-211. doi:10.1146/annurev.biochem.052308.093131

45. Bétermier M, Bertrand P, Lopez BS. Is Non-Homologous End-Joining Really an Inherently Error-Prone Process? Jinks-Robertson S, ed. *PLoS Genet*. 2014;10(1):e1004086. doi:10.1371/journal.pgen.1004086

46. Sung P, Klein H. Mechanism of homologous recombination: mediators and helicases take on regulatory functions. *Nat Rev Mol Cell Biol*. 2006;7(10):739-750. doi:10.1038/nrm2008

47. Walker JR, Corpina RA, Goldberg J. Structure of the Ku heterodimer bound to DNA and its implications for double-strand break repair. *Nature*. 2001;412(6847):607-614. doi:10.1038/35088000

48. Collis SJ, DeWeese TL, Jeggo PA, Parker AR. The life and death of DNA-PK. *Oncogene*. 2005;24(6):949-961. doi:10.1038/sj.onc.1208332

49. Goodarzi AA, Yu Y, Riballo E, et al. DNA-PK autophosphorylation facilitates Artemis endonuclease activity. *EMBO J*. 2006;25(16):3880-3889. doi:10.1038/sj.emboj.7601255

50. Pannunzio NR, Watanabe G, Lieber MR. Nonhomologous DNA end-joining for repair of DNA double-strand breaks. *J Biol Chem*. 2018;293(27):10512-10523. doi:10.1074/jbc.TM117.000374

51. Ahnesorg P, Smith P, Jackson SP. XLF Interacts with the XRCC4-DNA Ligase IV Complex to Promote DNA Nonhomologous End-Joining. *Cell*. 2006;124(2):301-313. doi:10.1016/j.cell.2005.12.031

52. Sartori AA, Lukas C, Coates J, et al. Human CtIP promotes DNA end resection. *Nature*. 2007;450(7169):509-514. doi:10.1038/nature06337

53. Ceppi I, Howard SM, Kasaciunaite K, et al. CtIP promotes the motor activity of DNA2 to accelerate long-range DNA end resection. *Proc Natl Acad Sci*. 2020;117(16):8859-8869. doi:10.1073/pnas.2001165117

54. Nimonkar A V., Genschel J, Kinoshita E, et al. BLM-DNA2-RPA-MRN and EXO1-BLM-RPA-MRN constitute two DNA end resection machineries for human DNA break repair. *Genes Dev*. 2011;25(4):350-362. doi:10.1101/gad.2003811

55. Garcia V, Phelps SEL, Gray S, Neale MJ. Bidirectional resection of DNA double-strand breaks by Mre11 and Exo1. *Nature*. 2011;479(7372):241-244. doi:10.1038/nature10515

56. Bhat KP, Cortez D. RPA and RAD51: fork reversal, fork protection, and genome

stability. *Nat Struct Mol Biol*. 2018;25(6):446-453. doi:10.1038/s41594-018-0075-z

57. Jensen RB, Carreira A, Kowalczykowski SC. Purified human BRCA2 stimulates RAD51-mediated recombination. *Nature*. 2010;467(7316):678-683. doi:10.1038/nature09399

58. Godin SK, Sullivan MR, Bernstein KA. Novel insights into RAD51 activity and regulation during homologous recombination and DNA replication. *Biochem Cell Biol*. 2016;94(5):407-418. doi:10.1139/bcb-2016-0012

59. Bizard AH, Hickson ID. The Dissolution of Double Holliday Junctions. *Cold Spring Harb Perspect Biol*. 2014;6(7):a016477-a016477. doi:10.1101/cshperspect.a016477

60. Ceccaldi R, Rondinelli B, D'Andrea AD. Repair Pathway Choices and Consequences at the Double-Strand Break. *Trends Cell Biol*. 2016;26(1):52-64. doi:10.1016/j.tcb.2015.07.009

61. Mao Z, Bozzella M, Seluanov A, Gorbunova V. Comparison of nonhomologous end joining and homologous recombination in human cells. *DNA Repair (Amst)*. 2008;7(10):1765-1771. doi:10.1016/j.dnarep.2008.06.018

62. Hustedt N, Durocher D. The control of DNA repair by the cell cycle. *Nat Cell Biol*. 2017;19(1):1-9. doi:10.1038/ncb3452

63. Reis CC, Batista S, Ferreira MG. The fission yeast MRN complex tethers dysfunctional telomeres for NHEJ repair. *EMBO J*. 2012;31(24):4576-4586. doi:10.1038/emboj.2012.313

64. Williams RS, Moncalian G, Williams JS, et al. Mre11 Dimers Coordinate DNA End Bridging and Nuclease Processing in Double-Strand-Break Repair. *Cell*. 2008;135(1):97-109. doi:10.1016/j.cell.2008.08.017

65. Symington LS. Mechanism and regulation of DNA end resection in eukaryotes. *Crit Rev Biochem Mol Biol*. 2016;51(3):195-212. doi:10.3109/10409238.2016.1172552

66. Morrison C, Sonoda E, Takao N, Shinohara A, Yamamoto K, Takeda S. The controlling role of ATM in homologous recombinational repair of DNA damage. *EMBO J*. 2000;19(3):463-471. doi:10.1093/emboj/19.3.463

67. Britton S, Chanut P, Delteil C, Barboule N, Frit P, Calsou P. ATM antagonizes NHEJ proteins assembly and DNA-ends synapsis at single-ended DNA double strand breaks. *Nucleic Acids Res*. 2020;48(17):9710-9723. doi:10.1093/nar/gkaa723

68. Guo Z, Deshpande R, Paull TT. ATM activation in the presence of oxidative stress. *Cell Cycle*. 2010;9(24):4805-4811. doi:10.4161/cc.9.24.14323

69. Zhang Y, Lee J-H, Paull TT, et al. Mitochondrial redox sensing by the kinase ATM maintains cellular antioxidant capacity. *Sci Signal*. 2018;11(538):eaaq0702. doi:10.1126/scisignal.aaq0702

70. Cosentino C, Grieco D, Costanzo V. ATM activates the pentose phosphate pathway promoting anti-oxidant defence and DNA repair. *EMBO J*. 2011;30(3):546-555. doi:10.1038/emboj.2010.330

71. Alexander A, Cai S-L, Kim J, et al. ATM signals to TSC2 in the cytoplasm to regulate mTORC1 in response to ROS. *Proc Natl Acad Sci*. 2010;107(9):4153-4158. doi:10.1073/pnas.0913860107

72. Valentin-Vega YA, MacLean KH, Tait-Mulder J, et al. Mitochondrial dysfunction in ataxia-telangiectasia. *Blood*. 2012;119(6):1490-1500. doi:10.1182/blood-2011-08-373639

73. Zhang J, Tripathi DN, Jing J, et al. ATM functions at the peroxisome to induce pexophagy in response to ROS. *Nat Cell Biol*. 2015;17(10):1259-1269. doi:10.1038/ncb3230

74. Lee J, Mand MR, Kao C, et al. ATM directs DNA damage responses and proteostasis via genetically separable pathways. *Sci Signal*. 2018;11(512):eaan5598. doi:10.1126/scisignal.aan5598

75. Brandsma I, Gent DC. Pathway choice in DNA double strand break repair: observations of a balancing act. *Genome Integr*. 2012;3(1):9. doi:10.1186/2041-9414-3-9

76. Stein H, Hausen P. Enzyme from Calf Thymus Degrading the RNA Moiety of DNA-RNA Hybrids: Effect on DNA-Dependent RNA Polymerase. *Science (80-)*. 1969;166(3903):393-395. doi:10.1126/science.166.3903.393

77. Cerritelli SM, Crouch RJ. Ribonuclease H: the enzymes in eukaryotes. *FEBS J*. 2009;276(6):1494-1505. doi:10.1111/j.1742-4658.2009.06908.x

78. Clausen AR, Zhang S, Burgers PM, Lee MY, Kunkel TA. Ribonucleotide incorporation, proofreading and bypass by human DNA polymerase δ. *DNA Repair (Amst)*. 2013;12(2):121-127. doi:10.1016/j.dnarep.2012.11.006

79. Cerritelli SM, Crouch RJ. Cloning, Expression, and Mapping of Ribonucleases H of Human and Mouse Related to Bacterial RNase HI. *Genomics*. 1998;53(3):300-307. doi:10.1006/geno.1998.5497

80. Chon H, Vassilev A, DePamphilis ML, et al. Contributions of the two accessory subunits, RNASEH2B and RNASEH2C, to the activity and properties of the human RNase H2 complex. *Nucleic Acids Res*. 2009;37(1):96-110. doi:10.1093/nar/gkn913

81. Lima WF, Rose JB, Nichols JG, et al. Human RNase H1 discriminates between subtle variations in the structure of the heteroduplex substrate. *Mol Pharmacol*. 2007;71(1):83-91. doi:10.1124/mol.106.025015

82. Lima WF, Rose JB, Nichols JG, et al. The Positional Influence of the Helical Geometry of the Heteroduplex Substrate on Human RNase H1 Catalysis. *Mol Pharmacol*. 2007;71(1):73-82. doi:10.1124/mol.106.025429

83. Sparks JL, Chon H, Cerritelli SM, et al. RNase H2-Initiated Ribonucleotide Excision Repair. *Mol Cell*. 2012;47(6):980-986. doi:10.1016/j.molcel.2012.06.035

84. Chon H, Sparks JL, Rychlik M, et al. RNase H2 roles in genome integrity revealed by unlinking its activities. *Nucleic Acids Res*. 2013;41(5):3130-3143. doi:10.1093/nar/gkt027

85. Reijns MAM, Rabe B, Rigby RE, et al. Enzymatic Removal of Ribonucleotides from DNA Is Essential for Mammalian Genome Integrity and Development. *Cell*. 2012;149(5):1008-1022. doi:10.1016/j.cell.2012.04.011

86. Kellner V, Luke B. Molecular and physiological consequences of faulty eukaryotic ribonucleotide excision repair. *EMBO J*. 2020;39(3):e102309. doi:10.15252/embj.2019102309

87. Feng S, Cao Z. Is the role of human RNase H2 restricted to its enzyme activity? *Prog Biophys Mol Biol*. 2016;121(1):66-73. doi:10.1016/j.pbiomolbio.2015.11.001

88. Machado CR, Menck CFM. Human DNA repair diseases: From genome instability to cancer. *Brazilian J Genet*. 1997;20(4):755-762. doi:10.1590/S0100-84551997000400032

89. Curtin NJ. DNA repair dysregulation from cancer driver to therapeutic target. *Nat Rev Cancer*. 2012;12(12):801-817. doi:10.1038/nrc3399

90. CLEAVER JE. Defective Repair Replication of DNA in Xeroderma Pigmentosum. *Nature*. 1968;218(5142):652-656. doi:10.1038/218652a0

91. Naegeli H, Sugasawa K. The xeroderma pigmentosum pathway: Decision tree analysis of DNA quality. *DNA Repair (Amst)*. 2011;10(7):673-683. doi:10.1016/j.dnarep.2011.04.019

92. Ahmed M, Rahman N. ATM and breast cancer susceptibility. *Oncogene*. 2006;25(43):5906-5911. doi:10.1038/sj.onc.1209873

93. Roberts NJ, Jiao Y, Yu J, et al. ATM Mutations in Patients with Hereditary Pancreatic Cancer. *Cancer Discov*. 2012;2(1):41-46. doi:10.1158/2159-8290.CD-11-0194

94. Angèle S, Falconer A, Edwards SM, et al. ATM polymorphisms as risk factors for prostate cancer development. *Br J Cancer*. 2004;91(4):783-787. doi:10.1038/sj.bjc.6602007

95. Thompson D, Duedal S, Kirner J, et al. Cancer Risks and Mortality in Heterozygous ATM Mutation Carriers. *JNCI J Natl Cancer Inst*. 2005;97(11):813-822. doi:10.1093/jnci/dji141

96. Esteller M. Promoter Hypermethylation and BRCA1 Inactivation in Sporadic Breast and Ovarian Tumors. *J Natl Cancer Inst*. 2000;92(7):564-569. doi:10.1093/jnci/92.7.564

97. Friedenson B. The BRCA1/2 pathway prevents hematologic cancers in addition to breast

and ovarian cancers. *BMC Cancer*. 2007;7(1):152. doi:10.1186/1471-2407-7-152

98. Seedhouse C. Polymorphisms in Genes Involved in Homologous Recombination Repair Interact to Increase the Risk of Developing Acute Myeloid Leukemia. *Clin Cancer Res*. 2004;10(8):2675-2680. doi:10.1158/1078-0432.CCR-03-0372

99. Voso MT, Fabiani E, D'Alo' F, et al. Increased risk of acute myeloid leukaemia due to polymorphisms in detoxification and DNA repair enzymes. *Ann Oncol*. 2007;18(9):1523-1528. doi:10.1093/annonc/mdm191

100. Pakakasama S, Sirirat T, Kanchanachumpol S, et al. Genetic polymorphisms and haplotypes of DNA repair genes in childhood acute lymphoblastic leukemia. *Pediatr Blood Cancer*. 2007;48(1):16-20. doi:10.1002/pbc.20742

101. Joseph T, Kusumakumary P, Chacko P, Abraham A, Pillai MR. DNA repair gene XRCC1 polymorphisms in childhood acute lymphoblastic leukemia. *Cancer Lett*. 2005;217(1):17-24. doi:10.1016/j.canlet.2004.06.055

102. El-Zein R, Monroy CM, Etzel CJ, et al. Genetic polymorphisms in DNA repair genes as modulators of Hodgkin disease risk. *Cancer*. 2009;115(8):1651-1659. doi:10.1002/cncr.24205

103. Economopoulou P, Pappa V, Papageorgiou S, Dervenoulas J, Economopoulos T. Abnormalities of DNA repair mechanisms in common hematological malignancies. *Leuk Lymphoma*. 2011;52(4):567-582. doi:10.3109/10428194.2010.551155

104. Lahtz C, Pfeifer GP. Epigenetic changes of DNA repair genes in cancer. *J Mol Cell Biol*. 2011;3(1):51-58. doi:10.1093/jmcb/mjq053

105. Negrini S, Gorgoulis VG, Halazonetis TD. Genomic instability — an evolving hallmark of cancer. *Nat Rev Mol Cell Biol*. 2010;11(3):220-228. doi:10.1038/nrm2858

106. O'Connor MJ. Targeting the DNA Damage Response in Cancer. *Mol Cell*. 2015;60(4):547-560. doi:10.1016/j.molcel.2015.10.040

107. Cahill DP, Kinzler KW, Vogelstein B, Lengauer C. Genetic instability and darwinian selection in tumours. *Trends Biochem Sci*. 1999;24(12):M57-M60. doi:10.1016/S0968-0004(99)01466-8

108. Klein TJ, Glazer PM. The Tumor Microenvironment and DNA Repair. *Semin Radiat Oncol*. 2010;20(4):282-287. doi:10.1016/j.semradonc.2010.05.006

109. Truini A, Germano G, Bardelli A. Inactivation of DNA repair—prospects for boosting cancer immune surveillance. *Genome Med*. 2018;10(1):91. doi:10.1186/s13073-018-0603-9

110. Loeb LA. A mutator phenotype in cancer. *Cancer Res*. 2001;61(8):3230-3239. doi:10.1038/nature11252

111. Loeb LA. Human Cancers Express a Mutator Phenotype: Hypothesis, Origin, and

Consequences. *Cancer Res*. 2016;76(8):2057-2059. doi:10.1158/0008-5472.CAN-16-0794

112. Stankovic T, Weber P, Stewart G, et al. Inactivation of ataxia telangiectasia mutated gene in B-cell chronic lymphocytic leukaemia. *Lancet*. 1999;353(9146):26-29. doi:10.1016/S0140-6736(98)10117-4

113. Stoppa-Lyonnet D, Soulier J, Laugé A, et al. Inactivation of the ATM Gene in T-Cell Prolymphocytic Leukemias. *Blood*. 1998;91(10):3920-3926. doi:10.1182/blood.V91.10.3920

114. Fang NY, Greiner TC, Weisenburger DD, et al. Oligonucleotide microarrays demonstrate the highest frequency of ATM mutations in the mantle cell subtype of lymphoma. *Proc Natl Acad Sci*. 2003;100(9):5372-5377. doi:10.1073/pnas.0831102100

115. Liberzon E, Avigad S, Yaniv I, et al. Molecular variants of the ATM gene in Hodgkin's disease in children. *Br J Cancer*. 2004;90(2):522-525. doi:10.1038/sj.bjc.6601522

116. Choi M, Kipps T, Kurzrock R. ATM mutations in cancer: Therapeutic implications. *Mol Cancer Ther*. 2016;15(8):1781-1791. doi:10.1158/1535-7163.MCT-15-0945

117. Muzny D, Bainbridge M, Chang K et al. Comprehensive molecular characterization of human colon and rectal cancer. *Nature*. 2012;487(7407):330-337. doi:10.1038/nature11252

118. Koboldt DC, Fulton RS, McLellan MD, et al. Comprehensive molecular portraits of human breast tumours. *Nature*. 2012;490(7418):61-70. doi:10.1038/nature11412

119. Shiloh Y. ATM and related protein kinases: Safeguarding genome integrity. *Nat Rev Cancer*. 2003;3(3):155-168. doi:10.1038/nrc1011

120. Stengel A, Kern W, Haferlach T, Meggendorfer M, Fasan A, Haferlach C. The impact of TP53 mutations and TP53 deletions on survival varies between AML, ALL, MDS and CLL: an analysis of 3307 cases. *Leukemia*. 2017;31(3):705-711. doi:10.1038/leu.2016.263

121. Zimmermann M, Murina O, Reijns MAM, et al. CRISPR screens identify genomic ribonucleotides as a source of PARP-trapping lesions. *Nature*. 2018;559(7713):285-289. doi:10.1038/s41586-018-0291-z

122. Bowman RL, Levine RL. TET2 in Normal and Malignant Hematopoiesis. *Cold Spring Harb Perspect Med*. 2017;7(8):a026518. doi:10.1101/cshperspect.a026518

123. Helleday T, Petermann E, Lundin C, Hodgson B, Sharma RA. DNA repair pathways as targets for cancer therapy. *Nat Rev Cancer*. 2008;8(3):193-204. doi:10.1038/nrc2342

124. Kaina B, Izzotti A, Xu J, et al. Inherent and toxicant-provoked reduction in DNA repair capacity: A key mechanism for personalized risk assessment, cancer prevention and intervention, and response to therapy. *Int J Hyg Environ Health*. 2018;221(7):993-1006. doi:10.1016/j.ijheh.2018.07.003

125. Tian H, Gao Z, Li H, et al. DNA damage response – A double-edged sword in cancer prevention and cancer therapy. *Cancer Lett*. 2015;358(1):8-16. doi:10.1016/j.canlet.2014.12.038

126. Goldstein M, Kastan MB. The DNA Damage Response: Implications for Tumor Responses to Radiation and Chemotherapy. *Annu Rev Med*. 2015;66(1):129-143. doi:10.1146/annurev-med-081313-121208

127. Taylor AMR, Harnden DG, Arlett CF, et al. Ataxia telangiectasia: a human mutation with abnormal radiation sensitivity. *Nature*. 1975;258(5534):427-429. doi:10.1038/258427a0

128. Hartwell LH, Szankasi P, Roberts CJ, Murray AW, Friend SH. Integrating Genetic Approaches into the Discovery of Anticancer Drugs. *Science (80-)*. 1997;278(5340):1064-1068. doi:10.1126/science.278.5340.1064

129. Bryant HE, Schultz N, Thomas HD, et al. Specific killing of BRCA2-deficient tumours with inhibitors of poly(ADP-ribose) polymerase. *Nature*. 2005;434(7035):913-917. doi:10.1038/nature03443

130. Farmer H, McCabe N, Lord CJ, et al. Targeting the DNA repair defect in BRCA mutant cells as a therapeutic strategy. *Nature*. 2005;434(7035):917-921. doi:10.1038/nature03445

131. Jette NR, Kumar M, Radhamani S, et al. ATM-Deficient Cancers Provide New Opportunities for Precision Oncology. Published online 2020:1-13.

132. Mccabe N, Turner NC, Lord CJ, et al. Deficiency in the Repair of DNA Damage by Homologous Recombination and Sensitivity to Poly (ADP-Ribose) Polymerase Inhibition. 2006;(16):8109-8116. doi:10.1158/0008-5472.CAN-06-0140

133. Yi M, Dong B, Qin S, Chu Q, Wu K, Luo S. Advances and perspectives of PARP inhibitors. *Exp Hematol Oncol*. 2019;8(1):29. doi:10.1186/s40164-019-0154-9

134. Turgeon M-O, Perry NJS, Poulogiannis G. DNA Damage, Repair, and Cancer Metabolism. *Front Oncol*. 2018;8(15):1-8. doi:10.3389/fonc.2018.00015

135. Chatzidoukaki O, Goulielmaki E, Schumacher B, Garinis GA. DNA Damage Response and Metabolic Reprogramming in Health and Disease. *Trends Genet*. 2020;36(10):777-791. doi:10.1016/j.tig.2020.06.018

136. Gong F, Miller KM. Histone methylation and the DNA damage response. *Mutat Res Mutat Res*. 2019;780(May 2017):37-47. doi:10.1016/j.mrrev.2017.09.003

137. Costelloe T, FitzGerald J, Murphy NJ, Flaus A, Lowndes NF. Chromatin modulation and the DNA damage response. *Exp Cell Res*. 2006;312(14):2677-2686. doi:10.1016/j.yexcr.2006.06.031

138. Chapman JR, Taylor MRG, Boulton SJ. Playing the End Game: DNA Double-Strand Break Repair Pathway Choice. *Mol Cell*. 2012;47(4):497-510.

doi:10.1016/j.molcel.2012.07.029

139. Jeggo PA, Downs JA. Roles of chromatin remodellers in DNA double strand break repair. *Exp Cell Res*. 2014;329(1):69-77. doi:10.1016/j.yexcr.2014.09.023

140. Fan J, Krautkramer KA, Feldman JL, Denu JM. Metabolic Regulation of Histone Post-Translational Modifications. *ACS Chem Biol*. 2015;10(1):95-108. doi:10.1021/cb500846u

141. Reid MA, Dai Z, Locasale JW. The impact of cellular metabolism on chromatin dynamics and epigenetics. *Nat Cell Biol*. 2017;19(11):1298-1306. doi:10.1038/ncb3629

142. Zhang N. Role of methionine on epigenetic modification of DNA methylation and gene expression in animals. *Anim Nutr*. 2018;4(1):11-16. doi:10.1016/j.aninu.2017.08.009

143. Serefidou M, Venkatasubramani AV, Imhof A. The Impact of One Carbon Metabolism on Histone Methylation. *Front Genet*. 2019;10(August):1-7. doi:10.3389/fgene.2019.00764

144. Feron O. The many metabolic sources of acetyl-CoA to support histone acetylation and influence cancer progression. *Ann Transl Med*. 2019;7(S8):S277-S277. doi:10.21037/atm.2019.11.140

145. Sidoli S, Trefely S, Garcia BA, Carrer A. Integrated Analysis of Acetyl-CoA and Histone Modification via Mass Spectrometry to Investigate Metabolically Driven Acetylation. In: Haznadar M, ed. *Physiology & Behavior*. Vol 1928. Methods in Molecular Biology. Springer New York; 2019:125-147. doi:10.1007/978-1-4939-9027-6_9

146. Mews P, Donahue G, Drake AM, Luczak V, Abel T, Berger SL. Acetyl-CoA synthetase regulates histone acetylation and hippocampal memory. *Nature*. 2017;546(7658):381-386. doi:10.1038/nature22405

147. Xiao M, Yang H, Xu W, et al. Inhibition of -KG-dependent histone and DNA demethylases by fumarate and succinate that are accumulated in mutations of FH and SDH tumor suppressors. *Genes Dev*. 2012;26(12):1326-1338. doi:10.1101/gad.191056.112

148. Jiang Y, Qian X, Shen J, et al. Local generation of fumarate promotes DNA repair through inhibition of histone H3 demethylation. *Nat Cell Biol*. 2015;17(9):1158-1168. doi:10.1038/ncb3209

149. Lane AN, Fan TWM. Regulation of mammalian nucleotide metabolism and biosynthesis. *Nucleic Acids Res*. 2015;43(4):2466-2485. doi:10.1093/nar/gkv047

150. Villa E, Ali E, Sahu U, Ben-Sahra I. Cancer Cells Tune the Signaling Pathways to Empower de Novo Synthesis of Nucleotides. *Cancers (Basel)*. 2019;11(5):688. doi:10.3390/cancers11050688

151. Fu S, Li Z, Xiao L, et al. Glutamine Synthetase Promotes Radiation Resistance via Facilitating Nucleotide Metabolism and Subsequent DNA Damage Repair. *Cell Rep*.

2019;28(5):1136-1143.e4. doi:10.1016/j.celrep.2019.07.002

152. Aird KM, Worth AJ, Snyder NW, et al. ATM Couples Replication Stress and Metabolic Reprogramming during Cellular Senescence. *Cell Rep*. 2015;11(6):893-901. doi:10.1016/j.celrep.2015.04.014

153. Dahl ES, Aird KM. Ataxia-Telangiectasia Mutated Modulation of Carbon Metabolism in Cancer. *Front Oncol*. 2017;7(291). doi:10.3389/fonc.2017.00291

154. Sun K, Tang S, Hou Y, et al. Oxidized ATM-mediated glycolysis enhancement in breast cancer-associated fibroblasts contributes to tumor invasion through lactate as metabolic coupling. *EBioMedicine*. 2019;41(1):370-383. doi:10.1016/j.ebiom.2019.02.025

155. Schwartzenberg-Bar-Yoseph F, Armoni M, Karnieli E. The Tumor Suppressor p53 Down-Regulates Glucose Transporters GLUT1 and GLUT4 Gene Expression. *Cancer Res*. 2004;64(7):2627-2633. doi:10.1158/0008-5472.CAN-03-0846

156. Watanabe M, Naraba H, Sakyo T, Kitagawa T. DNA Damage-Induced Modulation of GLUT3 Expression Is Mediated through p53-Independent Extracellular Signal-Regulated Kinase Signaling in HeLa Cells. *Mol Cancer Res*. 2010;8(11):1547-1557. doi:10.1158/1541-7786.MCR-10-0011

157. Bensaad K, Tsuruta A, Selak MA, et al. TIGAR, a p53-Inducible Regulator of Glycolysis and Apoptosis. *Cell*. 2006;126(1):107-120. doi:10.1016/j.cell.2006.05.036

158. Matoba S. p53 Regulates Mitochondrial Respiration. *Science (80-)*. 2006;312(5780):1650-1653. doi:10.1126/science.1126863

159. Green DR, Chipuk JE. p53 and Metabolism: Inside the TIGAR. *Cell*. 2006;126(1):30-32. doi:10.1016/j.cell.2006.06.032

160. Parrales A, Iwakuma T. p53 as a Regulator of Lipid Metabolism in Cancer. *Int J Mol Sci*. 2016;17(12):2074. doi:10.3390/ijms17122074

161. Lowman XH, Hanse EA, Yang Y, et al. p53 Promotes Cancer Cell Adaptation to Glutamine Deprivation by Upregulating Slc7a3 to Increase Arginine Uptake. *Cell Rep*. 2019;26(11):3051-3060.e4. doi:10.1016/j.celrep.2019.02.037

162. Tajan M, Hock AK, Blagih J, et al. A Role for p53 in the Adaptation to Glutamine Starvation through the Expression of SLC1A3. *Cell Metab*. 2018;28(5):721-736.e6. doi:10.1016/j.cmet.2018.07.005

163. Vousden KH, Ryan KM. p53 and metabolism. *Nat Rev Cancer*. 2009;9(10):691-700. doi:10.1038/nrc2715

164. Vaquero A. The conserved role of sirtuins in chromatin regulation. *Int J Dev Biol*. 2009;53(2-3):303-322. doi:10.1387/ijdb.082675av

165. Palacios JA, Herranz D, De Bonis ML, Velasco S, Serrano M, Blasco MA. SIRT1 contributes to telomere maintenance and augments global homologous recombination. *J*

Cell Biol. 2010;191(7):1299-1313. doi:10.1083/jcb.201005160

166. Ye X, Li M, Hou T, Gao T, Zhu W, Yang Y. Sirtuins in glucose and lipid metabolism. *Oncotarget*. 2017;8(1):1845-1859. doi:10.18632/oncotarget.12157

167. Jeong SM, Xiao C, Finley LWS, et al. SIRT4 Has Tumor-Suppressive Activity and Regulates the Cellular Metabolic Response to DNA Damage by Inhibiting Mitochondrial Glutamine Metabolism. *Cancer Cell*. 2013;23(4):450-463. doi:10.1016/j.ccr.2013.02.024

168. Lomb DJ, Laurent G, Haigis MC. Sirtuins regulate key aspects of lipid metabolism. *Biochim Biophys Acta - Proteins Proteomics*. 2010;1804(8):1652-1657. doi:10.1016/j.bbapap.2009.11.021

169. Choi J-E, Mostoslavsky R. Sirtuins, metabolism, and DNA repair. *Curr Opin Genet Dev*. 2014;26(2):24-32. doi:10.1016/j.gde.2014.05.005

170. Wei H, Yu X. Functions of PARylation in DNA Damage Repair Pathways. *Genomics Proteomics Bioinformatics*. 2016;14(3):131-139. doi:10.1016/j.gpb.2016.05.001

171. Walker JW, Jijon HB, Madsen KL. AMP-activated protein kinase is a positive regulator of poly(ADP-ribose) polymerase. *Biochem Biophys Res Commun*. 2006;342(1):336-341. doi:10.1016/j.bbrc.2006.01.145

172. Sanli T, Steinberg GR, Singh G, Tsakiridis T. AMP-activated protein kinase (AMPK) beyond metabolism. *Cancer Biol Ther*. 2014;15(2):156-169. doi:10.4161/cbt.26726

173. Brace LE, Vose SC, Stanya K, et al. Increased oxidative phosphorylation in response to acute and chronic DNA damage. *npj Aging Mech Dis*. 2016;2(1):16022. doi:10.1038/npjamd.2016.22

174. Lambeth JD. NOX enzymes and the biology of reactive oxygen. *Nat Rev Immunol*. 2004;4(3):181-189. doi:10.1038/nri1312

175. Forrester SJ, Kikuchi DS, Hernandes MS, Xu Q, Griendling KK. Reactive Oxygen Species in Metabolic and Inflammatory Signaling. *Circ Res*. 2018;122(6):877-902. doi:10.1161/CIRCRESAHA.117.311401

176. Cooke MS, Evans MD, Dizdaroglu M, Lunec J. Oxidative DNA damage: mechanisms, mutation, and disease. *FASEB J*. 2003;17(10):1195-1214. doi:10.1096/fj.02-0752rev

177. Hegde ML, Izumi T, Mitra S. Oxidized Base Damage and Single-Strand Break Repair in Mammalian Genomes. In: *Progress in Molecular Biology and Translational Science*. Vol 110. ; 2012:123-153. doi:10.1016/B978-0-12-387665-2.00006-7

178. Sharma V, Collins LB, Chen T, et al. Oxidative stress at low levels can induce clustered DNA lesions leading to NHEJ mediated mutations. *Oncotarget*. 2016;7(18):25377-25390. doi:10.18632/oncotarget.8298

179. Alnajjar KS, Sweasy JB. A new perspective on oxidation of DNA repair proteins and

cancer. *DNA Repair (Amst)*. 2019;76(February):60-69. doi:10.1016/j.dnarep.2019.02.006

180. Marnett LJ. Lipid peroxidation — DNA damage by malondialdehyde. *Mutat Res*. 1999;424(1-2):83-95. doi:10.1016/s0027-5107(99)00010-x.

181. Rowe LA, Degtyareva N, Doetsch PW. DNA damage-induced reactive oxygen species (ROS) stress response in Saccharomyces cerevisiae. *Free Radic Biol Med*. 2008;45(8):1167-1177. doi:10.1016/j.freeradbiomed.2008.07.018

182. Stucki M, Clapperton JA, Mohammad D, Yaffe MB, Smerdon SJ, Jackson SP. MDC1 Directly Binds Phosphorylated Histone H2AX to Regulate Cellular Responses to DNA Double-Strand Breaks. *Cell*. 2005;123(7):1213-1226. doi:10.1016/j.cell.2005.09.038

183. Paull TT, Rogakou EP, Yamazaki V, Kirchgessner CU, Gellert M, Bonner WM. A critical role for histone H2AX in recruitment of repair factors to nuclear foci after DNA damage. *Curr Biol*. 2000;10(15):886-895. doi:10.1016/S0960-9822(00)00610-2

184. Kang MA, So E-Y, Simons AL, Spitz DR, Ouchi T. DNA damage induces reactive oxygen species generation through the H2AX-Nox1/Rac1 pathway. *Cell Death Dis*. 2012;3(1):e249-e249. doi:10.1038/cddis.2011.134

185. Moretton A, Loizou JI. Interplay between Cellular Metabolism and the DNA Damage Response in Cancer. *Cancers (Basel)*. 2020;12(8):2051. doi:10.3390/cancers12082051

186. Lu SC. Regulation of glutathione synthesis. *Mol Aspects Med*. 2009;30(1-2):42-59. doi:10.1016/j.mam.2008.05.005

187. Moreno-Sánchez R, Marín-Hernández Á, Gallardo-Pérez JC, Vázquez C, Rodríguez-Enríquez S, Saavedra E. Control of the NADPH supply and GSH recycling for oxidative stress management in hepatoma and liver mitochondria. *Biochim Biophys Acta - Bioenerg*. 2018;1859(10):1138-1150. doi:10.1016/j.bbabio.2018.07.008

188. Gorrini C, Baniasadi PS, Harris IS, et al. BRCA1 interacts with Nrf2 to regulate antioxidant signaling and cell survival. *J Exp Med*. 2013;210(8):1529-1544. doi:10.1084/jem.20121337

189. Steele ML, Fuller S, Patel M, Kersaitis C, Ooi L, Münch G. Effect of Nrf2 activators on release of glutathione, cysteinylglycine and homocysteine by human U373 astroglial cells. *Redox Biol*. 2013;1(1):441-445. doi:10.1016/j.redox.2013.08.006

190. Srinivas US, Tan BWQ, Vellayappan BA, Jeyasekharan AD. ROS and the DNA damage response in cancer. *Redox Biol*. 2019;25:101084. doi:10.1016/j.redox.2018.101084

191. Hassa PO. The molecular "Jekyll and Hyde" duality of PARP1 in cell death and cell survival. *Front Biosci*. 2009;Volume(14):72. doi:10.2741/3232

192. Catalgol B, Wendt B, Grimm S, Breusing N, Özer NK, Grune T. Chromatin repair after oxidative stress: Role of PARP-mediated proteasome activation. *Free Radic Biol Med*. 2010;48(5):673-680. doi:10.1016/j.freeradbiomed.2009.12.010

193. Singh CK, Chhabra G, Ndiaye MA, Garcia-Peterson LM, Mack NJ, Ahmad N. The Role of Sirtuins in Antioxidant and Redox Signaling. *Antioxid Redox Signal*. 2018;28(8):643-661. doi:10.1089/ars.2017.7290

194. Schieber M, Chandel NS. ROS Function in Redox Signaling and Oxidative Stress. *Curr Biol*. 2014;24(10):R453-R462. doi:10.1016/j.cub.2014.03.034

195. DeMartino GN, Gillette TG. Proteasomes: Machines for All Reasons. *Cell*. 2007;129(4):659-662. doi:10.1016/j.cell.2007.05.007

196. Motegi A, Murakawa Y, Takeda S. The vital link between the ubiquitin–proteasome pathway and DNA repair: Impact on cancer therapy. *Cancer Lett*. 2009;283(1):1-9. doi:10.1016/j.canlet.2008.12.030

197. Sweder K, Madura K. Regulation of repair by the 26 S proteasome. *J Biomed Biotechnol*. 2002;2(2):94-105. doi:10.1155/S1110724302205033

198. Brooks CL, Gu W. p53 regulation by ubiquitin. *FEBS Lett*. 2011;585(18):2803-2809. doi:10.1016/j.febslet.2011.05.022

199. Brooks CL, Gu W. p53 Ubiquitination: Mdm2 and Beyond. *Mol Cell*. 2006;21(3):307-315. doi:10.1016/j.molcel.2006.01.020

200. Schwertman P, Bekker-Jensen S, Mailand N. Regulation of DNA double-strand break repair by ubiquitin and ubiquitin-like modifiers. *Nat Rev Mol Cell Biol*. 2016;17(6):379-394. doi:10.1038/nrm.2016.58

201. McBride WH, Iwamoto KS, Syljuasen R, Pervan M, Pajonk F. The role of the ubiquitin/proteasome system in cellular responses to radiation. *Oncogene*. 2003;22(37):5755-5773. doi:10.1038/sj.onc.1206676

202. Pervan M. Proteasome Structures Affected by Ionizing Radiation. *Mol Cancer Res*. 2005;3(7):381-390. doi:10.1158/1541-7786.MCR-05-0032

203. Dikic I, Elazar Z. Mechanism and medical implications of mammalian autophagy. *Nat Rev Mol Cell Biol*. 2018;19(6):349-364. doi:10.1038/s41580-018-0003-4

204. Parzych KR, Klionsky DJ. An Overview of Autophagy: Morphology, Mechanism, and Regulation. *Antioxid Redox Signal*. 2014;20(3):460-473. doi:10.1089/ars.2013.5371

205. Vessoni AT, Filippi-Chiela EC, Menck CFM, Lenz G. Autophagy and genomic integrity. *Cell Death Differ*. 2013;20(11):1444-1454. doi:10.1038/cdd.2013.103

206. Maiuri MC, Galluzzi L, Morselli E, Kepp O, Malik SA, Kroemer G. Autophagy regulation by p53. *Curr Opin Cell Biol*. 2010;22(2):181-185. doi:10.1016/j.ceb.2009.12.001

207. Rodríguez-Vargas JM, Oliver-Pozo FJ, Dantzer F. PARP1 and Poly(ADP-ribosyl)ation Signaling during Autophagy in Response to Nutrient Deprivation. *Oxid Med Cell Longev*. 2019;2019:1-15. doi:10.1155/2019/2641712

208. Robert T, Vanoli F, Chiolo I, et al. HDACs link the DNA damage response, processing of double-strand breaks and autophagy. *Nature*. 2011;471(7336):74-79. doi:10.1038/nature09803

209. Cheng A, Tse K-H, Chow H-M, et al. ATM loss disrupts the autophagy-lysosomal pathway. *Autophagy*. 2020;0(0):1-13. doi:10.1080/15548627.2020.1805860

210. Alexander A, Kim J, Walker CL. ATM engages the TSC2/mTORC1 signaling node to regulate autophagy. *Autophagy*. 2010;6(5):672-673. doi:10.4161/auto.6.5.12509

211. Tripathi DN, Chowdhury R, Trudel LJ, et al. Reactive nitrogen species regulate autophagy through ATM-AMPK-TSC2-mediated suppression of mTORC1. *Proc Natl Acad Sci*. 2013;110(32):E2950-E2957. doi:10.1073/pnas.1307736110

212. Liu M, Zeng T, Zhang X, et al. ATR/Chk1 signaling induces autophagy through sumoylated RhoB-mediated lysosomal translocation of TSC2 after DNA damage. *Nat Commun*. 2018;9(1):4139. doi:10.1038/s41467-018-06556-9

213. Fang EF, Scheibye-Knudsen M, Chua KF, Mattson MP, Croteau DL, Bohr VA. Nuclear DNA damage signalling to mitochondria in ageing. *Nat Rev Mol Cell Biol*. 2016;17(5):308-321. doi:10.1038/nrm.2016.14

214. Redmann M, Benavides GA, Berryhill TF, et al. Inhibition of autophagy with bafilomycin and chloroquine decreases mitochondrial quality and bioenergetic function in primary neurons. *Redox Biol*. 2017;11:73-81. doi:10.1016/j.redox.2016.11.004

215. Ciechanover A. The ubiquitin-proteasome proteolytic pathway. *Cell*. 1994;79(1):13-21. doi:10.1016/0092-8674(94)90396-4

216. Myung J, Kim KB, Crews CM. The ubiquitin-proteasome pathway and proteasome inhibitors. *Med Res Rev*. 2001;21(4):245-273. doi:10.1002/med.1009

217. Zhang S, Shi Y, Jin H, Liu Z, Zhang L, Zhang L. Covalent complexes of proteasome model with peptide aldehyde inhibitors MG132 and MG101: docking and molecular dynamics study. *J Mol Model*. 2009;15(12):1481-1490. doi:10.1007/s00894-009-0515-0

218. Robak P, Robak T. Bortezomib for the Treatment of Hematologic Malignancies: 15 Years Later. *Drugs R D*. 2019;19(2):73-92. doi:10.1007/s40268-019-0269-9

219. Han YH, Park WH. The changes of reactive oxygen species and glutathione by MG132 , a proteasome inhibitor affect As4 . juxtaglomerular cell growth and death. *Chem Biol Interact*. 2010;184(3):319-327. doi:10.1016/j.cbi.2010.01.033

220. GUO N, PENG Z. MG132, a proteasome inhibitor, induces apoptosis in tumor cells. *Asia Pac J Clin Oncol*. 2013;9(1):6-11. doi:10.1111/j.1743-7563.2012.01535.x

221. Park WH, Kim SH. MG132, a proteasome inhibitor, induces human pulmonary fibroblast cell death via increasing ROS levels and GSH depletion. *Oncol Rep*. 2012;27(4):1284-1291. doi:10.3892/or.2012.1642

222. Shimizu I, Yoshida Y, Suda M, Minamino T. DNA damage response and metabolic disease. *Cell Metab*. 2014;20(6):967-977. doi:10.1016/j.cmet.2014.10.008

223. Bar RS, Levis WR, Rechler MM, et al. Extreme Insulin Resistance in Ataxia Telangiectasia. *N Engl J Med*. 1978;298(21):1164-1171. doi:10.1056/NEJM197805252982103

224. Ching JK, Spears LD, Armon JL, et al. Impaired insulin-stimulated glucose transport in ATM-deficient mouse skeletal muscle. *Appl Physiol Nutr Metab*. 2013;38(6):589-596. doi:10.1139/apnm-2012-0175

225. Armata HL, Golebiowski D, Jung DY, Ko HJ, Kim JK, Sluss HK. Requirement of the ATM/p53 Tumor Suppressor Pathway for Glucose Homeostasis. *Mol Cell Biol*. 2010;30(24):5787-5794. doi:10.1128/MCB.00347-10

226. Halaby M-J, Hibma JC, He J, Yang D-Q. ATM protein kinase mediates full activation of Akt and regulates glucose transporter 4 translocation by insulin in muscle cells. *Cell Signal*. 2008;20(8):1555-1563. doi:10.1016/j.cellsig.2008.04.011

227. Barlow C, Dennery PA, Shigenaga MK, et al. Loss of the ataxia-telangiectasia gene product causes oxidative damage in target organs. *Proc Natl Acad Sci*. 1999;96(17):9915-9919. doi:10.1073/pnas.96.17.9915

228. Gatei M, Shkedy D, Khanna KK, et al. Ataxia-telangiectasia: chronic activation of damage-responsive functions is reduced by α-lipoic acid. *Oncogene*. 2001;20(3):289-294. doi:10.1038/sj.onc.1204111

229. Kamsler A, Daily D, Hochman A, et al. Increased oxidative stress in ataxia telangiectasia evidenced by alterations in redox state of brains from Atm-deficient mice. *Cancer Res*. 2001;61(5):1849-1854. http://www.ncbi.nlm.nih.gov/pubmed/11280737

230. Agathanggelou A, Weston VJ, Perry T, et al. Targeting the Ataxia Telangiectasia Mutated-null phenotype in chronic lymphocytic leukemia with pro-oxidants. *Haematologica*. 2015;100(8):1076-1085. doi:10.3324/haematol.2014.115170

231. Barzilai A. ATM deficiency and oxidative stress: a new dimension of defective response to DNA damage. *DNA Repair (Amst)*. 2002;1(1):3-25. doi:10.1016/S1568-7864(01)00007-6

232. Ambrose M, Goldstine J V., Gatti RA. Intrinsic mitochondrial dysfunction in ATM-deficient lymphoblastoid cells. *Hum Mol Genet*. 2007;16(18):2154-2164. doi:10.1093/hmg/ddm166

233. Eaton JS, Lin ZP, Sartorelli AC, Bonawitz ND, Shadel GS. Ataxia-telangiectasia mutated kinase regulates ribonucleotide reductase and mitochondrial homeostasis. *J Clin Invest*. 2007;117(9):2723-2734. doi:10.1172/JCI31604

234. Chen J, Chen Y, Vail G, et al. The impact of glutamine supplementation on the symptoms of ataxia-telangiectasia: a preclinical assessment. *Mol Neurodegener*. 2016;11(1):60. doi:10.1186/s13024-016-0127-y

235. Desai SD, Reed RE, Babu S, Lorio EA. ISG15 deregulates autophagy in genotoxin-treated ataxia telangiectasia cells. *J Biol Chem*. 2013;288(4):2388-2402. doi:10.1074/jbc.M112.403832

236. Galicia-Vázquez G, Smith S, Aloyz R. Del11q-positive CLL lymphocytes exhibit altered glutamine metabolism and differential response to GLS1 and glucose metabolism inhibition. *Blood Cancer J*. 2018;8(1). doi:10.1038/s41408-017-0039-2

237. Shoelson SE. Banking on ATM as a new target in metabolic syndrome. *Cell Metab*. 2006;4(5):337-338. doi:10.1016/j.cmet.2006.10.009

238. Brosnan JT, Brosnan ME. The Sulfur-Containing Amino Acids: An Overview. *J Nutr*. 2006;136(6):1660S-1665S.

239. Seidel U, Huebbe P, Rimbach G. Taurine: A Regulator of Cellular Redox Homeostasis and Skeletal Muscle Function. *Mol Nutr Food Res*. 2019;63(16):1-58. doi:10.1002/mnfr.201800569

240. Lourenço R, Camilo ME. Taurine: A conditionally essential amino acid in humans? An overview in health and disease. *Nutr Hosp*. 2002;17(6):262-270.

241. Bouckenooghe T, Remacle C, Reusens B. Is taurine a functional nutrient? *Curr Opin Clin Nutr Metab Care*. 2006;9(6):728-733. doi:10.1097/01.mco.0000247469.26414.55

242. Suzuki T. Taurine as a constituent of mitochondrial tRNAs: new insights into the functions of taurine and human mitochondrial diseases. *EMBO J*. 2002;21(23):6581-6589. doi:10.1093/emboj/cdf656

243. Olson MT, Yergey AL, Mukherjee K, et al. Taurine Is Covalently Incorporated into Alpha-Tubulin. *J Proteome Res*. 2020;19(8):3184-3190. doi:10.1021/acs.jproteome.0c00147

244. Han X, Patters AB, Jones DP, Zelikovic I, Chesney RW. The taurine transporter: mechanisms of regulation. *Acta Physiol*. 2006;187(1-2):61-73. doi:10.1111/j.1748-1716.2006.01573.x

245. Guizouarn H, Motais R, Garcia-Romeu F, Borgese F. Cell volume regulation: the role of taurine loss in maintaining membrane potential and cell pH. *J Physiol*. 2000;523(1):147-154. doi:10.1111/j.1469-7793.2000.t01-1-00147.x

246. ZHANG Z, LIU D, YI B, et al. Taurine supplementation reduces oxidative stress and protects the liver in an iron-overload murine model. *Mol Med Rep*. 2014;10(5):2255-2262. doi:10.3892/mmr.2014.2544

247. Thirupathi A, Freitas S, Sorato HR, et al. Modulatory effects of taurine on metabolic and oxidative stress parameters in a mice model of muscle overuse. *Nutrition*. 2018;54:158-164. doi:10.1016/j.nut.2018.03.058

248. Niu X, Zheng S, Liu H, Li S. Protective effects of taurine against inflammation, apoptosis, and oxidative stress in brain injury. *Mol Med Rep*. 2018;18(5):4516-4522.

doi:10.3892/mmr.2018.9465

249. Silva LA, Silveira PCL, Ronsani MM, et al. Taurine supplementation decreases oxidative stress in skeletal muscle after eccentric exercise. *Cell Biochem Funct*. 2011;29(1):43-49. doi:10.1002/cbf.1716

250. Kaneko H, Kobayashi M, Mizunoe Y, et al. Taurine is an amino acid with the ability to activate autophagy in adipocytes. *Amino Acids*. 2018;50(5):527-535. doi:10.1007/s00726-018-2550-6

251. Yahyavy S, Valizadeh A, Saki G, Khorsandi L. Taurine induces autophagy and inhibits oxidative stress in mice Leydig cells. *JBRA Assist Reprod*. 2020;24(3):250-256. doi:10.5935/1518-0557.20190079

252. Richer BC, Salei N, Laskay T, Seeger K. Changes in Neutrophil Metabolism upon Activation and Aging. *Inflammation*. 2018;41(2):710-721. doi:10.1007/s10753-017-0725-z

253. Srivastava S, Roy R, Singh S, et al. Taurine - A possible fingerprint biomarker in non-muscle invasive bladder cancer: A pilot study by 1H NMR spectroscopy. *Cancer Biomarkers*. 2009;6(1):11-20. doi:10.3233/CBM-2009-0115

254. Piotto M, Moussallieh FM, Dillmann B, et al. Metabolic characterization of primary human colorectal cancers using high resolution magic angle spinning 1H magnetic resonance spectroscopy. *Metabolomics*. 2009;5(3):292-301. doi:10.1007/s11306-008-0151-1

255. Taherizadeh M, Khoshnia M, Shams S, Joshaghani H. Plasma Taurine Levels between Patients with Esophageal Cancer and Healthy Controls. *mljgoums*. 2017;11(2):1-4. doi:10.18869/acadpub.mlj.11.2.1

256. Beckonert O, Monnerjahn J, Bonk U, Leibfritz D. Visualizing metabolic changes in breast-cancer tissue using 1H-NMR spectroscopy and self-organizing maps. *NMR Biomed*. 2003;16(1):1-11. doi:10.1002/nbm.797

257. Swanson MG, Vigneron DB, Tabatabai ZL, et al. Proton HR-MAS Spectroscopy and Quantitative Pathologic Analysis of MRI/3D-MRSI-Targeted Postsurgical Prostate Tissues. *Magn Reson Med*. 2003;50(5):944-954. doi:10.1002/mrm.10614

258. Zhou H, Sun L, Wan F. Molecular mechanisms of TUG1 in the proliferation, apoptosis, migration and invasion of cancer cells (Review). *Oncol Lett*. 2019;18(5):4393-4402. doi:10.3892/ol.2019.10848

259. Young TL, Matsuda T, Cepko CL. The Noncoding RNA Taurine Upregulated Gene 1 Is Required for Differentiation of the Murine Retina. *Curr Biol*. 2005;15(6):501-512. doi:10.1016/j.cub.2005.02.027

260. Cai H, Xue Y, Wang P, et al. The long noncoding RNA TUG1 regulates blood-tumor barrier permeability by targeting miR-144. *Oncotarget*. 2015;6(23):19759-19779. doi:10.18632/oncotarget.4331

261. Li J, Zhang M, An G, Ma Q. LncRNA TUG1 acts as a tumor suppressor in human glioma by promoting cell apoptosis. *Exp Biol Med*. 2016;241(6):644-649. doi:10.1177/1535370215622708

262. Jiang L, Wang W, Li G, et al. High TUG1 expression is associated with chemotherapy resistance and poor prognosis in esophageal squamous cell carcinoma. *Cancer Chemother Pharmacol*. 2016;78(2):333-339. doi:10.1007/s00280-016-3066-y

263. Li C, Gao Y, Li Y, Ding D. TUG1 mediates methotrexate resistance in colorectal cancer via miR-186/CPEB2 axis. *Biochem Biophys Res Commun*. 2017;491(2):552-557. doi:10.1016/j.bbrc.2017.03.042

264. Xie D, Zhang H, Hu X, Shang C. Knockdown of long non-coding RNA Taurine Up-Regulated 1 inhibited doxorubicin resistance of bladder urothelial carcinoma via Wnt/β-catenin pathway. *Oncotarget*. 2017;8(51):88689-88696. doi:10.18632/oncotarget.20927

265. Baliou S, Kyriakopoulos A, Spandidos D, Zoumpourlis V. Role of taurine, its haloamines and its lncRNA TUG1 in both inflammation and cancer progression. On the road to therapeutics? (Review). *Int J Oncol*. 2020;57(3):631-664. doi:10.3892/ijo.2020.5100

266. Long J, Badal SS, Ye Z, et al. Long noncoding RNA Tug1 regulates mitochondrial bioenergetics in diabetic nephropathy. *J Clin Invest*. 2016;126(11):4205-4218. doi:10.1172/JCI87927

267. Lin Y-H, Wu M-H, Huang Y-H, et al. Taurine up-regulated gene 1 functions as a master regulator to coordinate glycolysis and metastasis in hepatocellular carcinoma. *Hepatology*. 2018;67(1):188-203. doi:10.1002/hep.29462

268. Yin D, Zhang E, You L, et al. Downregulation of lncRNA TUG1 Affects Apoptosis and Insulin Secretion in Mouse Pancreatic β Cells. *Cell Physiol Biochem*. 2015;35(5):1892-1904. doi:10.1159/000373999

269. Zhang E, Yin D, Sun M, et al. P53-regulated long non-coding RNA TUG1 affects cell proliferation in human non-small cell lung cancer, partly through epigenetically regulating HOXB7 expression. *Cell Death Dis*. 2014;5(5):e1243-e1243. doi:10.1038/cddis.2014.201

270. Johnson CH, Gonzalez FJ. Challenges and opportunities of metabolomics. *J Cell Physiol*. 2012;227(8):2975-2981. doi:10.1002/jcp.24002

271. Johnson CH, Patterson AD, Idle JR, Gonzalez FJ. Xenobiotic Metabolomics: Major Impact on the Metabolome. *Annu Rev Pharmacol Toxicol*. 2012;52(1):37-56. doi:10.1146/annurev-pharmtox-010611-134748

272. DeBerardinis RJ, Thompson CB. Cellular Metabolism and Disease: What Do Metabolic Outliers Teach Us? *Cell*. 2012;148(6):1132-1144. doi:10.1016/j.cell.2012.02.032

273. Markley JL, Brüschweiler R, Edison AS, et al. The future of NMR-based metabolomics. *Curr Opin Biotechnol*. 2017;43:34-40. doi:10.1016/j.copbio.2016.08.001

274. Gowda GAN, Raftery D. Can NMR solve some significant challenges in metabolomics? *J Magn Reson*. 2016;260:144-160. doi:10.1016/j.jmr.2015.07.014.Can

275. de Graaf RA. *In Vivo NMR Spectroscopy : Principles and Techniques*. 2nd ed. (Sons JW&, ed.).; 2007.

276. Shoolery JN. *A Basic Guide to NMR, 3rd Edition*.; 2008. doi:10.3247/sl2nmr08.012

277. Levitt MH. *Spin Dynamics : Basics of Nuclear Magnetic Resonance*. John Wiley and Sons

278. Balci M. *Basic 1H- and 13C-NMR Spectroscopy*. Elsevier; 2005.

279. Keeler J. *Understanding NMR Spectroscopy*. John Wiley and Sons; 2010.

280. Lindon, J. C.; Nicholson, J. K.; Holmes E. *Handbook of Metabonomics and Metabolomics*. Elsevier; 2011.

281. Roberts JD. *Nuclear Magnetic Resonance: Applications to Organic Chemistry*.; 1959.

282. Styles P, Soffe NF, Scott CA, et al. A high-resolution NMR probe in which the coil and preamplifier are cooled with liquid helium. *J Magn Reson*. 1984;60:397-404. doi:10.1016/j.jmr.2011.09.002

283. Reynolds WF, Enríquez RG. Choosing the best pulse sequences, acquisition parameters, postacquisition processing strategies, and probes for natural product structure elucidation by NMR spectroscopy. *J Nat Prod*. 2002;65(2):221-244. doi:10.1021/np010444o

284. van Zijl PC. The use of deuterium as a nucleus for locking, shimming, and measuring NMR at high magnetic fields. *J Magn Reson*. 1987;75(2):335-344. doi:10.1016/0022-2364(87)90039-4

285. Topgaard D, Martin RW, Sakellariou D, Meriles CA, Pines A. “Shim pulses” for NMR spectroscopy and imaging. *Proc Natl Acad Sci*. 2004;101(51):17576-17581. doi:10.1073/pnas.0408296102

286. Giraudeau P, Silvestre V, Akoka S. Optimizing water suppression for quantitative NMR-based metabolomics: a tutorial review. *Metabolomics*. 2015;11(5):1041-1055. doi:10.1007/s11306-015-0794-7

287. Beckonert O, Keun HC, Ebbels TMD, et al. Metabolic profiling, metabolomic and metabonomic procedures for NMR spectroscopy of urine, plasma, serum and tissue extracts. *Nat Protoc*. 2007;2(11):2692-2703. doi:10.1038/nprot.2007.376

288. Van QN, Issaq HJ, Jiang Q, et al. Comparison of 1D and 2D NMR Spectroscopy for Metabolic Profiling. *J Proteome Res*. 2008;7(2):630-639. doi:10.1021/pr700594s

289. Heude C, Nath J, Carrigan JB, Ludwig C. Nuclear Magnetic Resonance Strategies for Metabolic Analysis. *Adv Exp Med Biol*. 2017;965:45-76. doi:10.1007/978-3-319-47656-8_3

290. Chong M, Jayaraman A, Marin S, et al. Combined Analysis of NMR and MS Spectra (CANMS). *Angew Chemie Int Ed*. 2017;56(15):4140-4144. doi:10.1002/anie.201611634

291. Saborano R, Eraslan Z, Roberts J, et al. A framework for tracer-based metabolism in mammalian cells by NMR. *Sci Rep*. 2019;9(1):2520. doi:10.1038/s41598-018-37525-3

292. Van Gent DC, Kanaar R. Exploiting DNA repair defects for novel cancer therapies. *Mol Biol Cell*. 2016;27(14):2145-2148. doi:10.1091/mbc.E15-10-0698

293. Stipanuk MH, Beck PW. Characterization of the enzymic capacity for cysteine desulphhydration in liver and kidney of the rat. *Biochem J*. 1982;206(2):267-277. doi:10.1042/bj2060267

294. Jurkowska H, Stipanuk MH, Hirschberger LL, Roman HB. Propargylglycine inhibits hypotaurine/taurine synthesis and elevates cystathionine and homocysteine concentrations in primary mouse hepatocytes. *Amino Acids*. 2015;47(6):1215-1223. doi:10.1007/s00726-015-1948-7

295. Ludwig C, Günther UL. MetaboLab - advanced NMR data processing and analysis for metabolomics. *BMC Bioinformatics*. 2011;12(1):366. doi:10.1186/1471-2105-12-366

296. Hyberts SG, Milbradt AG, Wagner AB, Arthanari H, Wagner G. Application of iterative soft thresholding for fast reconstruction of NMR data non-uniformly sampled with multidimensional Poisson Gap scheduling. *J Biomol NMR*. 2012;52(4):315-327. doi:10.1007/s10858-012-9611-z

297. Kwok M, Davies N, Agathanggelou A, et al. ATR inhibition induces synthetic lethality and overcomes chemoresistance in TP53 or ATM defective chronic lymphocytic leukemia cells. *Blood*. 2016;127(5):582-595. doi:10.1182/blood-2015-05-644872

298. te Raa GD, Moerland PD, Leeksma AC, et al. Assessment of p53 and ATM functionality in chronic lymphocytic leukemia by multiplex ligation-dependent probe amplification. *Cell Death Dis*. 2015;6(8):e1852-e1852. doi:10.1038/cddis.2015.223

299. Hussain T, Mulherkar R. Lymphoblastoid Cell lines: a Continuous in Vitro Source of Cells to Study Carcinogen Sensitivity and DNA Repair. *Int J Mol Cell Med*. 2012;1(2):75-87. http://www.ncbi.nlm.nih.gov/pubmed/24551762

300. DeBerardinis RJ, Chandel NS. Fundamentals of cancer metabolism. *Sci Adv*. 2016;2(5):e1600200. doi:10.1126/sciadv.1600200

301. Martinez-Outschoorn UE, Peiris-Pagés M, Pestell RG, Sotgia F, Lisanti MP. Cancer metabolism: a therapeutic perspective. *Nat Rev Clin Oncol*. 2017;14(1):11-31. doi:10.1038/nrclinonc.2016.60

302. Pavlova NN, Thompson CB. The Emerging Hallmarks of Cancer Metabolism. *Cell Metab*. 2016;23(1):27-47. doi:10.1016/j.cmet.2015.12.006

303. Dietmair S, Timmins NE, Gray PP, Nielsen LK, Krömer JO. Towards quantitative

metabolomics of mammalian cells: Development of a metabolite extraction protocol. *Anal Biochem*. 2010;404(2):155-164. doi:10.1016/j.ab.2010.04.031

304. Belle JE Le, Harris NG, Williams SR, Bhakoo KK. A comparison of cell and tissue extraction techniques using high-resolution1H-NMR spectroscopy. *NMR Biomed*. 2002;15(1):37-44. doi:10.1002/nbm.740

305. Stankovic T, Hubank M, Cronin D, et al. Microarray analysis reveals that TP53- and ATM-mutant B-CLLs share a defect in activating proapoptotic responses after DNA damage but are distinguished by major differences in activating prosurvival responses. *Blood*. 2004;103(1):291-300. doi:10.1182/blood-2003-04-1161

306. Guleria A, Chandna S. ATM kinase: Much more than a DNA damage responsive protein. *DNA Repair (Amst)*. 2016;39:1-20. doi:10.1016/j.dnarep.2015.12.009

307. Kozlov S V, Waardenberg AJ, Engholm-Keller K, Arthur JW, Graham ME, Lavin M. Reactive Oxygen Species (ROS)-Activated ATM-Dependent Phosphorylation of Cytoplasmic Substrates Identified by Large-Scale Phosphoproteomics Screen. *Mol Cell Proteomics*. 2016;15(3):1032-1047. doi:10.1074/mcp.M115.055723

308. Zhu J, Thompson CB. Metabolic regulation of cell growth and proliferation. *Nat Rev Mol Cell Biol*. 2019;20(7):436-450. doi:10.1038/s41580-019-0123-5

309. Mason EF, Rathmell JC. Cell metabolism: An essential link between cell growth and apoptosis. *Biochim Biophys Acta - Mol Cell Res*. 2011;1813(4):645-654. doi:10.1016/j.bbamcr.2010.08.011

310. Cliff TS, Dalton S. Metabolic switching and cell fate decisions: implications for pluripotency, reprogramming and development. *Curr Opin Genet Dev*. 2017;46:44-49. doi:10.1016/j.gde.2017.06.008

311. Zakikhani M, Bazile M, Hashemi S, et al. Alterations in Cellular Energy Metabolism Associated with the Antiproliferative Effects of the ATM Inhibitor KU-55933 and with Metformin. 2012;7(11):1-12. doi:10.1371/journal.pone.0049513

312. Guièze R, Wu CJ. Genomic and epigenomic heterogeneity in chronic lymphocytic leukemia. *Blood*. 2015;126(4):445-453. doi:10.1182/blood-2015-02-585042

313. Gutierrez C, Wu CJ. Clonal dynamics in chronic lymphocytic leukemia. *Blood Adv*. 2019;3(22):3759-3769. doi:10.1182/bloodadvances.2019000367

314. Koczula KM, Ludwig C, Hayden R, et al. Metabolic plasticity in CLL: adaptation to the hypoxic niche. *Leukemia*. 2016;30(1):65-73. doi:10.1038/leu.2015.187

315. Vose S, Mitchell J. Relationship Between DNA Damage and Energy Metabolism: Evidence from DNA Repair Deficiency Syndromes. In: *DNA Repair and Human Health*. InTechOpen; 2011. doi:10.5772/25053

316. Beaconsfield P, Reading HW. Pathways of Glucose Metabolism and Nucleic Acid Synthesis. *Nature*. 1964;202(4931):464-466. doi:10.1038/202464a0

317. Carrigan JB, Reed MAC, Ludwig C, Khanim FL, Bunce CM, Günther UL. Tracer-Based Metabolic NMR-Based Flux Analysis in a Leukaemia Cell Line. *Chempluschem*. 2016;81(5):453-459. doi:10.1002/cplu.201500549

318. Nath J, Smith T, Hollis A, et al. 13C glucose labelling studies using 2D NMR are a useful tool for determining ex vivo whole organ metabolism during hypothermic machine perfusion of kidneys. *Transplant Res*. 2016;5(1):7. doi:10.1186/s13737-016-0037-0

319. Reed MAC, Roberts J, Gierth P, Kupče Ē, Günther UL. Quantitative Isotopomer Rates in Real-Time Metabolism of Cells Determined by NMR Methods. *ChemBioChem*. 2019;20(17):2207-2211. doi:10.1002/cbic.201900084

320. Maher EA, Marin-Valencia I, Bachoo RM, et al. Metabolism of [U- 13 C]glucose in human brain tumors in vivo. *NMR Biomed*. 2012;25(11):1234-1244. doi:10.1002/nbm.2794

321. LaMonte G, Tang X, Chen JL-Y, et al. Acidosis induces reprogramming of cellular metabolism to mitigate oxidative stress. *Cancer Metab*. 2013;1(1):23. doi:10.1186/2049-3002-1-23

322. Palm W, Thompson CB. Nutrient acquisition strategies of mammalian cells. *Nature*. 2017;546(7657):234-242. doi:10.1038/nature22379

323. Metallo CM, Vander Heiden MG. Understanding Metabolic Regulation and Its Influence on Cell Physiology. *Mol Cell*. 2013;49(3):388-398. doi:10.1016/j.molcel.2013.01.018

324. Xu L, Ma E, Zeng T, et al. ATM deficiency promotes progression of CRPC by enhancing Warburg effect. *Endocr Relat Cancer*. 2019;26(1):59-71. doi:10.1530/ERC-18-0196

325. Chow HM, Cheng A, Song X, Swerdel MR, Hart RP, Herrup K. ATM is activated by ATP depletion and modulates mitochondrial function through NRF1. *J Cell Biol*. 2019;218(3):909-928. doi:10.1083/jcb.201806197

326. Lepage GA. In vitro incorporation of glycine-2-C14 into purines and proteins. *Cancer Res*. 1953;13(2):178-185. http://www.ncbi.nlm.nih.gov/pubmed/13042806

327. Su N, Pan Y-X, Zhou M, Harvey RC, Hunger SP, Kilberg MS. Correlation between asparaginase sensitivity and asparagine synthetase protein content, but not mRNA, in acute lymphoblastic leukemia cell lines. *Pediatr Blood Cancer*. 2008;50(2):274-279. doi:10.1002/pbc.21213

328. Leslie M, Case MC, Hall AG, Coulthard SA. Expression levels of asparagine synthetase in blasts from children and adults with acute lymphoblastic leukaemia. *Br J Haematol*. 2006;132(6):740-742. doi:10.1111/j.1365-2141.2005.05945.x

329. Hermanova I, Zaliova M, Trka J, Starkova J. Low expression of asparagine synthetase in lymphoid blasts precludes its role in sensitivity to L-asparaginase. *Exp Hematol*. 2012;40(8):657-665. doi:10.1016/j.exphem.2012.04.005

330. Bolzoni M, Chiu M, Accardi F, et al. Dependence on glutamine uptake and glutamine

addiction characterize myeloma cells: a new attractive target. *Blood*. 2016;128(5):667-679. doi:10.1182/blood-2016-01-690743

331. Gonsalves WI, Ramakrishnan V, Hitosugi T, et al. Glutamine-derived 2-hydroxyglutarate is associated with disease progression in plasma cell malignancies. *JCI insight*. 2018;3(1):1-16. doi:10.1172/jci.insight.94543

332. Metallo CM, Walther JL, Stephanopoulos G. Evaluation of 13C isotopic tracers for metabolic flux analysis in mammalian cells. *J Biotechnol*. 2009;144(3):167-174. doi:10.1016/j.jbiotec.2009.07.010

333. Huxtable R. Physiological Actions of Taurine. *Physiol Rev*. 1992;72(1):101-163. doi:10.1152/physrev.1992.72.1.101

334. Palego L, Betti L, Giannaccini G. Sulfur Metabolism and Sulfur-Containing Amino Acids: I- Molecular Effectors. *Biochem Pharmacol*. 2015;04(7). doi:10.4172/2167-0501.1000158

335. Belalcázar AD, Ball JG, Frost LM, Valentovic MA, Wilkinson J. Transsulfuration Is a Significant Source of Sulfur for Glutathione Production in Human Mammary Epithelial Cells. *ISRN Biochem*. 2013;2013:1-7. doi:10.1155/2013/637897

336. Yan Y, Jiang K, Liu P, et al. Bafilomycin A1 induces caspase-independent cell death in hepatocellular carcinoma cells via targeting of autophagy and MAPK pathways. *Sci Rep*. 2016;6(1):37052. doi:10.1038/srep37052

337. Meiners S, Heyken D, Weller A, et al. Inhibition of proteasome activity induces concerted expression of proteasome genes and de novo formation of mammalian proteasomes. *J Biol Chem*. 2003;278(24):21517-21525. doi:10.1074/jbc.M301032200

338. Dang L, Wen F, Yang Y, et al. Proteasome inhibitor MG132 inhibits the proliferation and promotes the cisplatin-induced apoptosis of human esophageal squamous cell carcinoma cells. *Int J Mol Med*. 2014;33(5):1083-1088. doi:10.3892/ijmm.2014.1678

339. Sullivan KD, Palaniappan V V, Espinosa JM. ATM regulates cell fate choice upon p53 activation by modulating mitochondrial turnover and ROS levels. *Cell Cycle*. 2015;14(1):56-63. doi:10.4161/15384101.2014.973330

340. Dikalov SI, Harrison DG. Methods for detection of mitochondrial and cellular reactive oxygen species. *Antioxidants Redox Signal*. 2014;20(2):372-382. doi:10.1089/ars.2012.4886

341. Brand A, Leibfritz D, Hamprecht B, Dringen R. Metabolism of cysteine in astroglial cells: Synthesis of hypotaurine and taurine. *J Neurochem*. 1998;71(2):827-832. doi:10.1046/j.1471-4159.1998.71020827.x

342. Grankvist N, Watrous JD, Lagerborg KA, Lyutvinskiy Y, Jain M, Nilsson R. Profiling the Metabolism of Human Cells by Deep 13C Labeling. *Cell Chem Biol*. 2018;25(11):1419-1427.e4. doi:10.1016/j.chembiol.2018.09.004

343. Vitvitsky V, Garg SK, Banerjee R. Taurine biosynthesis by neurons and astrocytes. *J Biol Chem*. 2011;286(37):32002-32010. doi:10.1074/jbc.M111.253344

344. Cho ES, Hovanec-Brown J, Tomanek RJ, Stegink LD. Propargylglycine Infusion Effects on Tissue Glutathione Levels, Plasma Amino Acid Concentrations and Tissue Morphology in Parenterally-Fed Growing Rats. *J Nutr*. 1991;121(6):785-794. doi:10.1093/jn/121.6.785

345. Czarny P, Pawlowska E, Bialkowska-Warzecha J, Kaarniranta K, Blasiak J. Autophagy in DNA Damage Response. *Int J Mol Sci*. 2015;16(2):2641-2662. doi:10.3390/ijms16022641

346. Jung CH, Ro S-H, Cao J, Otto NM, Kim D-H. mTOR regulation of autophagy. *FEBS Lett*. 2010;584(7):1287-1295. doi:10.1016/j.febslet.2010.01.017

347. Ma Y, Vassetzky Y, Dokudovskaya S. mTORC1 pathway in DNA damage response. *Biochim Biophys Acta - Mol Cell Res*. 2018;1865(9):1293-1311. doi:10.1016/j.bbamcr.2018.06.011

348. Yokomakura A, Hong J, Ohuchi K, et al. Increased production of reactive oxygen species by the vacuolar-type (H+)-ATPase inhibitors bafilomycin A1 and concanamycin A in RAW 264 cells. *J Toxicol Sci*. 2012;37(5):1045-1048. doi:10.2131/jts.37.1045

349. Wu JJ, Quijano C, Chen E, et al. Mitochondrial dysfunction and oxidative stress mediate the physiological impairment induced by the disruption of autophagy. *Aging (Albany NY)*. 2009;1(4):425-437. doi:10.18632/aging.100038

350. Criollo A, Vicencio JM, Tasdemir E, et al. The Inositol Trisphosphate Receptor in the Control of Autophagy. *Autophagy*. 2007;3(4):350-353. doi:10.4161/auto.4077

351. Moreau P, Richardson PG, Cavo M, et al. Proteasome inhibitors in multiple myeloma: 10 years later. *Blood*. 2012;120(5):947-959. doi:10.1182/blood-2012-04-403733

352. Rousseau A, Bertolotti A. Regulation of proteasome assembly and activity in health and disease. *Nat Rev Mol Cell Biol*. 2018;19(11):697-712. doi:10.1038/s41580-018-0040-z

353. Daulny A, Tansey WP. Damage control: DNA repair, transcription, and the ubiquitin–proteasome system. *DNA Repair (Amst)*. 2009;8(4):444-448. doi:10.1016/j.dnarep.2009.01.017

354. Han YH, Park WH. MG132, a proteasome inhibitor decreased the growth of Calu-6 lung cancer cells via apoptosis and GSH depletion. *Toxicol Vitr*. 2010;24(4):1237-1242. doi:10.1016/j.tiv.2010.02.005

355. Agathanggelou A, Weston VJ, Perry T, et al. Targeting the ataxia telangiectasia mutated-null phenotype in chronic lymphocytic leukemia with pro-oxidants. *Haematologica*. 2015;100(8):1076-1085. doi:10.3324/haematol.2014.115170